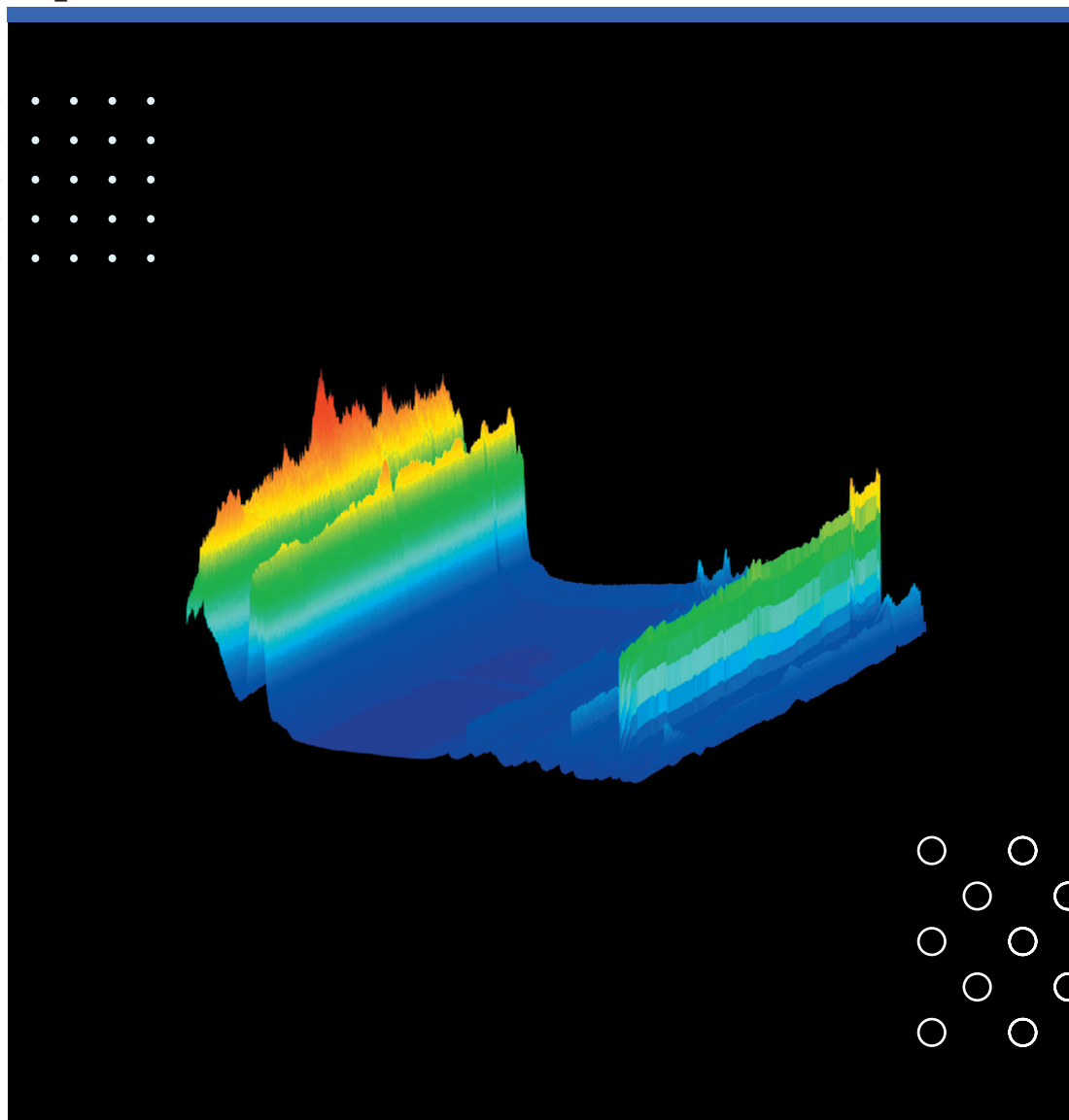M.H. Wathsala N. Jinadasa

Process analytical technology for real-time quantitative speciation of aqueous phase CO_2 capture solvents

USN

M.H. Wathsala N. Jinadasa

Process analytical technology for real-time quantitative speciation of aqueous phase CO_2 capture solvents

A PhD dissertation in
Process, Energy and Automation Engineering

Dedicated to them who defined me "love" & "care"

To my parents, sister, husband and two kids !!!

II

Preface

This thesis is submitted for the partial fulfilment of the degree of Doctor of Philosophy to the Department of Electrical Engineering, Information Technology and Cybernetics, Faculty of Technology, Natural Sciences and Maritime Sciences at University of South-Eastern Norway (USN). The research work was funded by the Ministry of Education and Research of the Norwegian Government for a period of four years including 25% teaching duties starting from February 2014. The research described herein was conducted under the supervision of Associate Professor Maths Halstensen (Applied Chemometrics and Research Group, USN), and with the guidance from co-supervisor professor Klaus-Joachim Jens (Head, Institute of Process, Energy and Environmental Technology, USN).

The research was application oriented addressing an overwhelming urge in in-situ liquid phase speciation in solvent based CO_2 capture process. Although the main focus of the research was developing such a method which could give fast and reliable complete speciation data using a spectroscopic method, the thesis presented here was compiled addressing the general concepts of implementation of Process Analytical Technology (PAT) to the CO_2 capture process providing the reader as a guideline to implement such PAT based approaches for other applicable areas in the industry. The study comprised Raman spectroscopy based model development and validation based on experimental data. Laboratory experiments were carried out at the CO_2 laboratories at Porsgrunn campus, USN and reference analysis by NMR spectroscopy was carried out by SINTEF Laboratory, Oslo. Mini pilot scale tests were performed at CO_2 rig, Process Hall, USN under the supervision and guidance of Professor Lars Erik Øi, USN. Model demonstration in continuous CO_2 absorption and desorption process was conducted at PACT Facility at Sheffield, UK under the guidance and supervision of Associate Professor Mathieu Lucquiaud, The University of Edinburgh, UK. Chemometric models were developed in Matlab PLS toolbox and the online monitoring graphical user interface was developed in Labview platform.

The thesis is structured in three parts:
Part 1 – gives the background information related to the application and focus of the thesis which are, role of fossil fuels in present and future energy systems, carbon dioxide capture, storage and sequestration (CCS) and its role in 2DS climate change mitigation scenario, CO_2 capture technologies, process analytical technology, chemometrics, Raman spectroscopy and liquid phase speciation in amine based capture processes.
Part 2 – consists of the description of initial model development using chemometrics based regression modelling. Model demonstration in continuous CO_2 capture process is described, a road map for calibration model maintenance is provided and model update procedures to specific capture scenarios are explained.
Part 3 – consists of the collection of publications (published and submitted) under this research.

Having completed a four-year bachelor degree in Chemical and Process Engineering and a two-year master degree in Energy and Environmental Technology, I could start this PhD research with confidence and I found myself enthusiastic with research activities. I am proud of being a minute contributor among thousands of those in the scientific community who have made efforts to mitigate global warming. With this research experience, I am looking forward for an exciting career in future !

Porsgrunn
20th of March 2019

Acknowledgement

It is a great pleasure to use this opportunity to express my gratitude to all the people who have been supporting me during the course of this thesis work and to the people who have made me who I am today. First and foremost, I am grateful to my main supervisor Associate Professor Maths Halstensen for his guidance and knowledge sharing. I always admire the way he supervised me to conduct this research in a less stressful manner, encouraging me during ups and downs, being patient and calm. He allowed me to be an independent researcher, but always assured if I was driving to the right target at right pace. I am proud to be a student of him. I also like to thank my co-supervisor Professor Klaus-Joachim Jens specially helping me with laboratory work and providing me the opportunity to conduct plant trials at PACT Facility, UK. He showed enthusiasm with the research outcomes and always found time to discuss my research status amidst of his busy schedule. The success of this research was built up on the perfect blend of chemometric knowledge of my main supervisor and the chemistry knowledge of my co-supervisor. I also appreciate Professor Kim Esbensen for sharing his profound knowledge on PAT and TOS which laid a strong foundation to achieve reliable results from my research.

My special thank goes to all who helped me during the laboratory experiments and plant trials. Thank you Gamunu Samarakoon, Zul Idris and Ying Jiru for your advices during laboratory experiments and giving me an excellent training in research work at CO_2 laboratory. Without the help of Associate Professor Lars Erik Øi, Per Morten Hansen, Mathias Henriksen and Sara Zarsav CO_2 rig experiments would not be successful. It was a privilege for me to meet and work with researchers with similar passion during PACT test campaign at Sheffield. I am grateful to Associate Professor Mathieu Lucquiaud from the University of Edinburgh for leading this project and Bill Buschle for coordinating to plan the test. I appreciate kindness and hard work by Muhammad Akram, Paul Tait and Kris Milkowski spending all hours at the plant during my research work supporting in numerous ways both technically and personally during PACT campaign.

The inspiration from my sincere teachers at USN during various stages of my postgraduate studies is unforgettable and please accept my gratitude to you all - Rune Bakke, Dag Eimer, Britt Moldestad, Carlos Pfeiffer, Bernt Lie, Lars Andre Tokheim, Dag Bjerketvedt and Finn Haugen. Thank you Randi Toreskås Holta, Vice Dean, Faculty of Technology, USN for your support to make my research a success while you were serving as the head of EIK department. I acknowledge Svein Thore Hagen, present Head of the TNM, USN, for his kind and fast mentoring to provide me necessary infrastructures to conduct my research in a hassle-free way. I enjoyed working at Norner AS using Raman spectrometer in their lab, and thank you Sara Ronasi, Carlos Barreto and Siw Bodil for making me a member of you research team in 'CO₂ utilization'. I am deeply indebted to Prof. P.G. Rathnasiri for initiating UoM-USN partnership, which opened opportunities for students like me to study at USN and develop their engineering career in Norway. I am always thankful to all my dedicated teachers from University of Moratuwa, Sri Lanka specially, Prof. A.D.U.S. Amarasinghe, Prof. S.

Abstract

Dependency on fossil fuel energy systems is unavoidable until there is a complete shift to alternative energy systems which have no/less impact for global warming. Rapid deployment of carbon capture and sequestration (CCS) projects for large scale power plants and industrial sectors is a timely need to follow climate change mitigation action by reduced CO_2 gas emission. It is logically and scientifically understood that more amine based CO_2 capture plants should be implemented and the existing facilities should be scaled up. A properly established reliable in-situ solvent analysis system can speed up this movement. From laboratory to industrial scale, process analytical tools have replaced most of traditional chemical analysis methods because of their massive chemical information packed in a single measurement, fast response, real- time / in-situ use, time saving, minimal errors in sample handing and quick identification of process related problems and ability to integrate with process control. Raman spectroscopy combined with multivariate analysis is a proven methodology for the determination of various chemical concentration profiles in chemical solvents for CO_2 capture.

Seven multivariate regression models were developed under this study to predict species concentrations of carbonate, bicarbonate, sum of carbonate and bicarbonate, carbamate, protonated amine, free amine and CO_2 loading in an MEA-CO_2-H_2O system based on their Raman spectra. Reference measurements were collected from ^{13}C NMR spectroscopy for individual chemical analysis which were used for the regression. The model performance was demonstrated in continuous operation at USN CO_2 rig and PACT Facility in Sheffield and the initial laboratory based model methodology was further updated to yield better predictability for each plant. The reliability of the predicted speciation were assessed in several ways both theoretically and experimentally. In addition, Raman spectroscopic measurements acquired during PACT campaign and the corresponding offline titration measurements were used to develop a new calibration model to predict amine weight percentage and sum of protonated amine and free amine in the chemical system. A graphical user interface was built in Labview to make a user friendly environment for monitoring in-situ speciation. CO_2 loading was determined when 3-amino-1-propanol, 3-dimethylamino-1-propanol and methyl diethanolamine were used as CO_2 capture solvents using Raman spectroscopy with multivariate modelling to show the method applicability in other solvents except MEA. The combination of Raman spectroscopy, chemometrics use for data treatment and variable selection, PLSR regression, reference analysis by ^{13}C NMR spectroscopy, and test set validation were the key contributors to obtain reliable regression models in this study. In addition, concepts of process analytical technology such as elements of PAT implementation, design of experiments, process sampling and calibration transfer procedures were adhered throughout the plant campaigns and they contributed to achieve higher accuracy and precision from the developed methods.

List of papers

Paper A - Jinadasa, M. H. W. N., Jens, K.-J., & Halstensen, M. (2019). In-situ Monitoring Method for CO_2 Capture Process - Complete Liquid Speciation, paper accepted in Journal of Raman Spectroscopy

Paper B - Jinadasa, M. H. W. N., Jens, K.-J., Øi, L. E., & Halstensen, M. (2017). Raman Spectroscopy as an Online Monitoring Tool for CO_2 Capture Process: Demonstration Using a Laboratory Rig. Energy Procedia, 114, 1179-1194. doi: 10.1016/j.egypro.2017.03.1282

Paper C (book chapter) - Jinadasa, M. H. W. N., Jens, K.-J., & Halstensen, M. (2018). Process Analytical Technology for CO_2 Capture. In Karamé, I., Shaya, J., & Srour, H. (Eds.), Carbon Dioxide Chemistry, Capture and Oil Recovery: IntechOpen. doi: 10.5772/intechopen.76176

Paper D - Jinadasa, W. N., Jens, K.-J., Pfeifer, C., Ronasi, S., Solar, C. B., & Halstensen, M. (2016). Principal Component Analysis Applied to CO_2 Absorption by Propylene Oxide and Amines. Linkoping Conference Proceedings, 9th EUROSIM Congress on Modelling and Simulation, Oulu, Finland. doi: 10.3384/ecp17142207

Paper E - Jinadasa, M. H. W. N., Jens, K.-J., & Halstensen, M. (2019). PCA Coupled Raman Spectroscopy as a Rapid Simple Approach for Screening CO_2 Absorption. Applied Chemometrics and Research Group (ACRG). University of South-Eastern Norway. – Manuscript submitted

Paper F - Jinadasa, M. H. W. N., Chandra, K. A., & Halstensen, M. (2018). System Development for On-line Monitoring using Raman Spectroscopy for CO_2 Absorption by MEA. Linkoping Conference Proceedings, 59th Conference on Simulation and Modelling (SIMS 59), Oslo Metropolitan University, Norway. doi: 10.3384/ecp18153328

Paper G (co-author) **-** Halstensen, M., Jilvero, H., Jinadasa, W. N., & Jens, K.-J. (2017). Equilibrium Measurements of the NH_3-CO_2-H_2O System: Speciation Based on Raman Spectroscopy and Multivariate Modeling. Journal of Chemistry, 2017, 13. doi:10.1155/2017/7590506

x

List of conference contributions

PLSR and Raman Spectroscopy for Speciation of MEA+CO$_2$+H$_2$O Systems in Post-Combustion CO$_2$ Capture - Oral presentation delivered at **SSC14** Scandinavian Symposium on Chemometrics, Sardinia, Italy, June 2015

Raman Spectroscopy Study for Speciation of MEA-CO$_2$-H$_2$O System – Poster presentation at **TCCS-8** Trondheim Conference on CO$_2$ Capture, Transport and Storage, Trondheim, Norway, June 2015

Principal Component Analysis Applied to CO$_2$ Absorption by Propylene Oxide and Amines - oral presentation at **EUROSIM 2016**, 9th EUROSIM Congress on Modelling and Simulation, Oulu, Finland, September 2016

Raman Spectroscopy as an Online Monitoring Tool for CO$_2$ Capture Process: Demonstration Using a Laboratory Rig - Poster presentation at **GHGT-13** Greenhouse Gas Control Technologies Conference Lausanne, Switzerland, November 2016

Multivariate Calibration in Real Time Process Monitoring at UKCCSRC PACT Amine Pilot Facility - Poster presentation at **TCCS-9** Trondheim Conference on CO$_2$ Capture, Transport and Storage, Trondheim, Norway, June 2017

Real Time Monitoring of Absorption and Desorption Process at The UKCCSRC PACT Amine Pilot Facility Using Raman Spectroscopy - Poster presentation at **TCCS-9**, Trondheim Conference on CO$_2$ Capture, Transport and Storage, Trondheim, Norway, June 2017

System Development for On-line Monitoring using Raman Spectroscopy for CO$_2$ Absorption by MEA – Oral presentation at **SIMS 59**, 59th Conference on Simulation and Modelling, Oslo, Norway, September 2018

Papers summary

Paper A presents the development of seven multivariate calibration models to determine chemical composition (carbonate, bicarbonate, carbamate, sum of carbonate and bicarbonate, protonated amine, free amine and total CO_2 loading) in a CO_2 absorbed monoethanolamine solution. Models were calibrated and validated using laboratory samples. It is a novel approach where ^{13}C NMR spectroscopy was used to produce reliable speciation values to use as reference measurements in PLSR regression; included maximum chemical information from the process analyzer (Raman spectrometer) for model development by using a range of wavenumbers and validated using adequate number of test set samples.

Paper B shows the demonstration of the seven chemometric models in continuous absorption and desorption process using experiments performed at USN CO_2 rig. Model predictivity was assessed for steady state operation and dynamic conditions covering reasonably different combinations of process conditions, plant start-up, plant shut down and absence of reboiler duty. Model predictivity was compared with offline measurements and models were updated to be harmonious with the plant operations (Jinadasa *et al.*, 2017).

Paper C is a book chapter written to describe how process analytical technology is imbedded to a carbon capture technology. It gives examples of implementation of a process analyzer to CO_2 capture by alkanolamine absorption process. Five elements of a PAT implementation process are described which are, selecting an appropriate process analyzer, integration the analyzer to process, model development to enable the analyzer to predict a process-related chemical or physical attribute, use of the developed model in real-time application and use of the data obtained from the analyzer as an input to a process control unit. In this chapter, four calibration models were prepared to predict CO_2 loading concentration in CO_2 absorbed two primary amines (monoethanolamine and 3-amino-1-propanol) and two tertiary amines (3-dimethylamino-1-propanol and methyl diethanolamine). The objective of the model development was to show the feasibility of Raman spectroscopic based multivariate calibration to evaluate chemical characteristics in amines other than monoethanolamine (Jinadasa *et al.*, 2018b).

Paper D shows the use of principal component analysis and Raman spectroscopy to monitor dissolved CO_2 in a mixture of propylene oxide / polypropylene carbonate and to monitor absorbed CO_2 in four alkanolamine solutions (monoethanolamine, 3-Amino-1-propanol, 3-dimethylamino-1-Propanol and Methyl diethanolamine). Raman active bands in these chemical systems were identified and PCA plots were used to characterize CO_2 composition, process dynamics and equilibrium conditions in these two chemical systems (Jinadasa *et al.*, 2016).

Paper E is a continuation of paper D where the application of PCA to assess the level of species concentration in an MEA-CO_2-H_2O system is described using score plots. Hoteling T^2 and residual Q values were used as multivariate statistical process control

to quick identification of abnormalities in continuous CO_2 absorption process by amine (CO_2 rig experiments).

Paper F – Typical procedure for acquiring measurements from RXN2 Kaiser Raman Analyzer is performed in iC Raman 4.1 software and the PLS model prediction is performed in PLS toolbox in Matlab. iC Raman 4.1 software has the facility to run in continuous mode to collect Raman measurements in a given frequency, but the measurements are required to transfer by an operator to PLS toolbox for determining speciation (by models developed in Paper A). As a result, this system does not give concentration value at the same time as the measurement is taken. It takes time to import the data from iC Raman software to Matlab and follow the preprocessing steps. There should be always an operator to carry out these steps and he needs to have knowledge and experience in use of the mentioned software. The objective of Paper F is to remove this barrier by merging these two software platforms and make a fully automated system to predict real time speciation. A graphical user interface was built in Matlab/Labview to make this system more user friendly and facilitate to use speciation for process control applications (Jinadasa *et al.*, 2018a).

Paper G reports on the development of a method for speciation of the CO_2-NH_3-H_2O equilibrium system using Raman spectroscopy and PLS-R modeling (Halstensen *et al.*, 2017). It is a novel approach to provide rapid and reliable predictions of the carbon distribution in a mixture of CO_2-NH_3-H_2O. Three calibration models were prepared by different concentrations of Na_2CO_3, $NaHCO_3$, and $NH_4NH_2CO_2$ solutions. Three models developed in this study were used by (Henrik *et al.*, 2015) in a VLE study of chilled ammonia system and showed good agreement with the offline measurements ($BaCl_2$ precipitation-titration method).

List of tables

List of figures

Abbreviations

ACRG	Applied Chemometrics and Research Group
AMP	2-amino-2-methyl-a-propanol
ANN	Artificial neural network
3-AP	3-amino-1-propanol
ATR	Attenuated total reflectance
FTIR	Fourier transform infrared
B2DS	Beyond 2 °C scenario
BECCS	Bioenergy carbon capture and sequestration
BCCS	Biomass carbon capture and sequestration
CCD	Charge-coupled device
CCS	Carbon capture and sequestration
CCUS	Carbon capture utilization and storage
CF4	Carbon tetrafluoride
CLC	Chemical looping capture
DEA	Diethanolamine
DGA	Diglycolamine
DIPA	Diisopropanolamine
DoE	Design of Experiment
DS	Direct standardization
EJ	Exajoules
EOR	Enhanced oil recovery
ET	Evolving transition
ETP	Energy technology perspectives
FDA	Food and Drug Administration
FMEA	Failure mode and effect analysis
FT	Fourier transform
GHG	Greenhouse gas
GLS	Generalized least squares
HSS	Heat stable salts
IEA	International Energy Agency
IPCC	The Intergovernmental Panel on Climate Change
IUPAC	The International Union of Pure and Applied Chemistry
LC-MS	Liquid chromatography–mass spectrometry
MDEA	Methyl diethanolamine
MEA	monoethanolamine
MIR	Mid- Infrared
MLR	Multiple linear regression
MSPC	Multivariate statistical process control
MVC	Multivariate calibration
MVDA	Multivariate data analysis
NGCC	Natural gas combined cycle

NIR	Near infrared
NMR	Nulclear magnetic resonance
OCS	Orthogonal signal correction
OECD	Organisation for Economic Co-operation and Development
OZD	2-Oxazolidinone
PAC	Process analytical chemistry
PAT	Process analytical technology
PACT	Pilot-scale Advanced CO_2 Capture Technology
PC	Pulverized coal
PCA	Principal component analysis
PCC	Post-combustion capture
PCR	Principal component regression
PDS	Piece-wise direct standardization
PLS	Partial least squares
PLSR	Partial least square regression
Poly-PLS	Polynomial partial least square
PZ	Piperazine
QdD	Quality by Design
R&D	Research and Development
RMSEP	Root mean square error of prediction
RTS	Reference technology scenario
SIC	simple interval calculation
SNR	Signal to noise ratio
SST	Spectral space transformation
TCM	Technology Centre Mongstad
TOS	Theory of sampling
SF6	Sulphur hexafluoride
UNIQUAC	universal quasichemical
USN	University of South-Eastern Norway
UV-Vis	Ultra violet - visible
VOC	Volatile organic carbon
V&V	Validation and verification
2DS	2 °C scenario

Table of contents

PART 1
Overview

1 Introduction

1.1 Motivation

The most popular method for determining CO_2 removal efficiency in CO_2 capture plants is gas phase analysis using gas analyzers such as Fourier transform infrared instrument. Liquid phase analysis in practice is mostly offline and laboratory-based but is one of the routine tasks in any CO_2 capture related R&D work and pilot plant trials. Depending on the requirement, the frequency of this offline analysis varies.

CO_2 loading and MEA concentration are the most common analysis typically determined by titration, but this method has several drawbacks that make it not attractive for plant operations such as the time required for titration. For instance, the $BaCl_2$-titration precipitation method which is used to determine CO_2 loading and MEA concentration, demands approximately two hours for analysis per sample with three replicates. In offline methods, a sample is collected from the process streams, transported to the laboratory and preserved until analysis. During the analysis, chemicals are prepared, a portion from the primary sample is extracted, and titration is performed. All these steps must be carried out cautiously to reduce sampling errors. These errors make the final result to be less representative of the actual value. The ideal investigation for a continuous plant operation is in-situ analysis for all (or at least leading) chemical compositions. Although several methods have been proposed, they are still being tested in pilot plant trials for validation in different process conditions. No reliable methods have yet been recommended/accepted for standard use in CO_2 capture plants among the research community. Liquid analysis using vibrational or absorption spectroscopic methods such as IR, NIR, and Raman have an immerging interest due to their low acquisition times, ability to reveal complete chemical information and applicability for in-situ monitoring.

In general, Raman spectroscopy can identify many organic and inorganic substances from their specific spectral patterns, and it shows weak scattering for water. It can be used for remote sensing as the Raman light can be transmitted via fibre optic cables over long distances. It is a non-destructive investigation; no sample preparation is needed, and a small volume for analysis is enough. Several studies have been done analyzing Raman spectra both univariately and multivariately to quantify concentration profiles in CO_2 capture plants. The Applied Chemometrics and Research Group (ACRG) at University of South-Eastern Norway (USN) has experience working with Raman spectroscopy to analyse liquid phase speciation in CO_2 capture solvents (Halstensen *et al.*, 2017; Henrik *et al.*, 2015; Idris *et al.*, 2014; Samarakoon *et al.*, 2013). Raman spectroscopy is a process analyzer and converting the instrument to predict in-situ speciation involves calibration model development, which is based on theories and concepts in Process Analytical Technology (PAT). CO_2 capture processes (R&D, pilot scale and commercial scale) are still not effectively benefited with PAT tools such as

multivariate data analysis, chemometrics and 'Theory of Sampling' and this research aims to make these concepts prevalent in the CO_2 capture nomenclature.

1.2 Objectives of the thesis

The objectives of the present study are fourfold.
1. Explain the necessity of using Process Analytical Technology tools, concepts and approaches for commercial deployment of amine-based CO_2 capture plants
2. Development of speciation models to completely characterize the chemical composition of CO_2 capture by aqueous monoethanolamine solution
3. Demonstration of the model validity for in-situ monitoring of CO_2 absorption-desorption process
4. Provide a roadmap for continuous improvement of Raman process analyzer to an amine-based CO_2 capture process

1.3 Structure of the thesis

The thesis is presented in three parts.

Part 1 gives the background information related to the application and focus of the thesis which are, role of fossil fuels in present and future energy systems, carbon capture and sequestration (CCS) and its role in 2DS climate change mitigation scenario, CO_2 capture technologies, CO_2 capture by chemical absorption using monoethanolamine solution, liquid phase speciation in amine-based capture processes, process analytical technology, chemometrics and Raman spectroscopy.

Part 2 consists of multivariate model development using partial least squares regression modelling and shows results on model implementation in two demonstration plants for in-situ speciation. It presents methods for model updating and improvement.

Part 3 consists of published and submitted collection of papers connected to this research.

1.4 Main contributions

Following contributions were made during experimental and theoretical work carried out under this study. They can be found either in the context of this thesis or in published and submitted manuscripts (refer Fig. 1:1) which are attached to this thesis. Results from the PACT campaign, and Raman study on amine degradation and some of their highlights are presented in chapter 7 and 8 of the thesis. Three papers will be published in journals related to these findings during 2019.

Main contributions are;
- Introduce process analytical technology to CO_2 capture process and highlight the advantages of having PAT concepts embedded in CO_2 capture framework
- Development of a novel and reliable method (real-time/in-situ) for liquid speciation in CO_2 capture process by monoethanolamine solvent

- Demonstration of the developed method in continuous CO_2 capture process and their relationship with process trends
- Development of multivariate calibration models to determine CO_2 loading in three other alkanolamine systems
- Present a user-friendly software environment for real-time conversion of raw Raman signals to chemical concentrations in the CO_2 capture process by monoethanolamine solvent
- Understanding the presence of heat stable salts/degradation through Raman spectroscopic measurements
- Highlight the importance of the use of multivariate data analysis methods and chemometrics to extract hidden chemical information from a process analyser
- Application of multivariate techniques such as PCA for screening chemical equilibrium, composition and abnormal behaviours
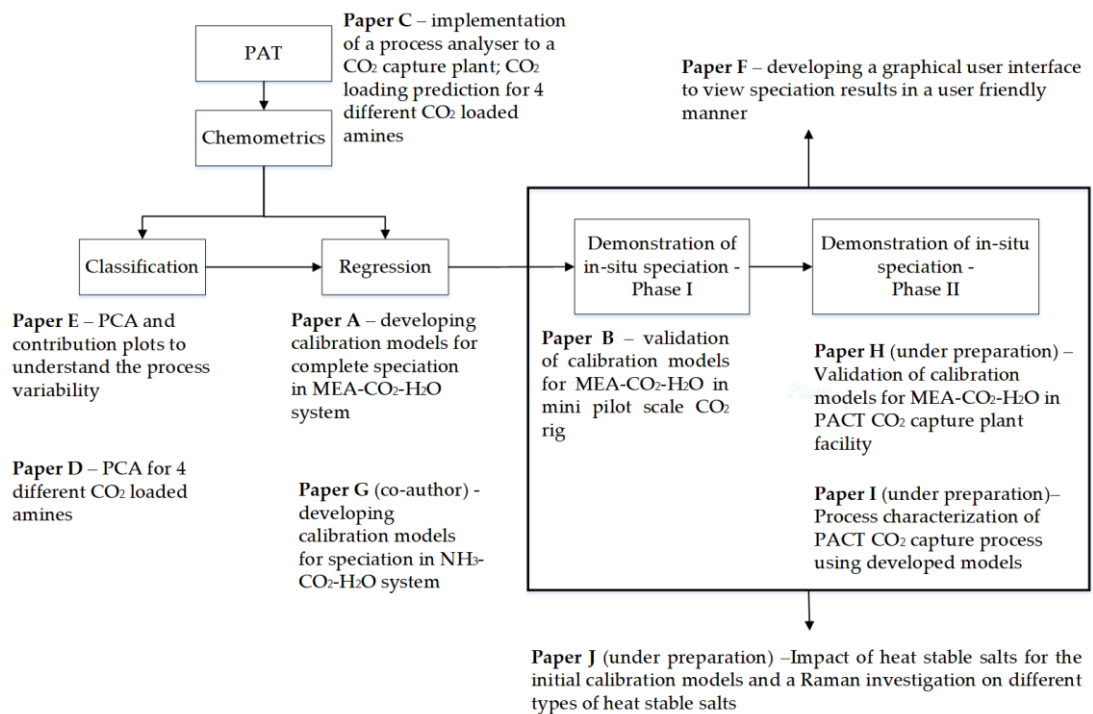
Fig. 1:1. Structure of main elements and publications of the research

2 CCS – a 'must' or a 'choice'?

Key

> *The relationship between greenhouse gases, global warming and climate change is almost known and live. The unusual rapid increase in Earth's average surface temperature (global warming) causes long term changes in the natural climate in a geographical area, including seasonal variability of temperature and precipitation. This phenomenon is referred as climate change. Human activities such as the burning of fossil fuels, deforestation, livestock farming and fertilizer usage unnecessarily increase the concentration of heat-trapping gases in the atmosphere such as carbon dioxide, methane and nitrous oxides. These gases act as a blanket between sun and earth, trapping heat and are given the name greenhouse gases (GHGs). Saturation of GHGs in the atmosphere leads to global warming, attacks to the natural balance of earth and accelerates climate changes such as extreme weather conditions, rising sea levels, extinction of living species and ocean acidification. Unless otherwise there is a mechanism to control the atmospherics GHGs well below to a level that the earth can naturally balance them, no guarantee can be provided that the living beings can protect themselves from the adverse effects of climate change.*

2.1 Global energy supply and greenhouse gas emissions

Energy fulfils our demands for daily routine activities such as cooking and residential heating. Without energy, we are unable to activate transportation mediums, energy-driven appliances, and manufacturing operations. After about 12000 years from civilization, today, it is hard to imagine a world without energy. Major power cuts in the world which have made interruptions in hospital services, water supplies, industrial sector railway and airline operations (Duddu, 2015) are more than enough evidence to prove this statement. Fig. 2:1 shows that the global energy demand in 2017 reached more than 13 gigatonnes of oil equivalent (Gtoe), compared with 10 Gtoe in 2000 (BP, 2019). In 2017 petroleum oil made up of over a third of all energy consumed, coal covered a market share of 27.6%; natural gas recorded a 23.4% share while renewables recorded a market share of 3.65% (Fig. 2:2). This energy distribution based on the source proves that fossil fuels (oil, coal and natural gas) have been playing the leading role representing 81% of global energy supply in 2017, over hydroelectricity, nuclear energy and renewable and a similar trend has been followed over several years. The energy demand for fossil fuels rose mainly due to oil use in transportation and petrochemical sector, relatively low-cost supplies in natural gas and the demand for coal-fired electricity generation especially in Asia (IEA, 2017b).
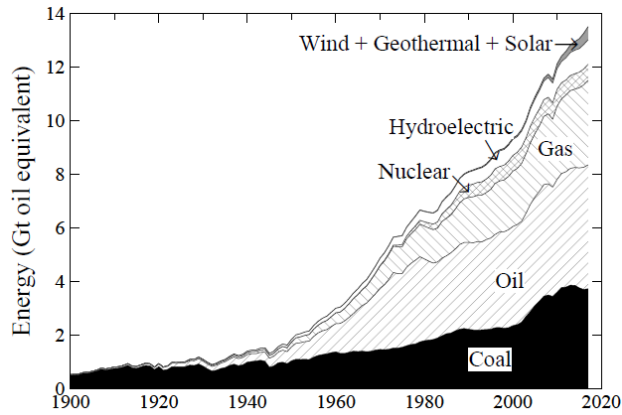
Fig. 2:1. Global energy consumption (in Gtoe) by different sources (With courtesy BP p.l.c, London (Sato *et al.*, 2019))
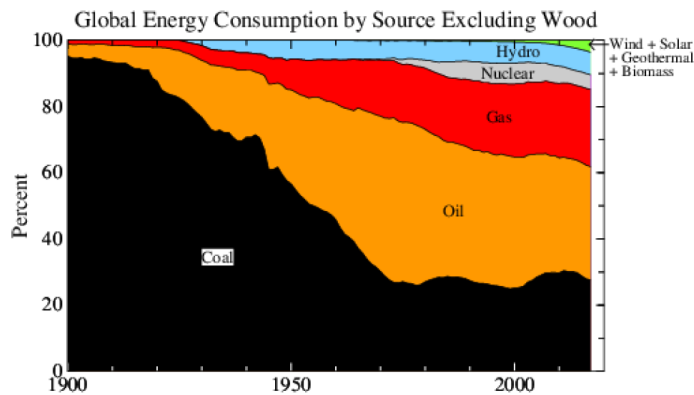
Fig. 2:2. The share of world energy consumption from 1900 to 2017 by different sources (Sato *et al.*, 2019)

According to (BP, 2018b) in 2017 global oil consumption rose by 96 billion cubic meters and coal production grew by 105 Mtoe. Supplying the energy that the world needs to develop, is necessary but the climate change experts have alarmed the future of global natural systems if the dependencies of energy supply on fossil fuels are further continued.

IPCC report (IPCC, 2014) says that by the end of 2010, the highest share of total annual anthropogenic GHG Emissions originated from CO_2. This share was 76%, and methane recorded the second largest GHG emission with a share of 16%. Contribution from nitrous oxide was 6% and from F-gases (HFC, CF4, and SF6) was 2% (Fig. 2:3). Key drivers for CO_2 gas emissions in 2017 were identified as 40% from coal combustion, 31% from oil combustion, 18% from natural gas combustion and 4% from cement clinker production (Olivier *et al.*, 2018).
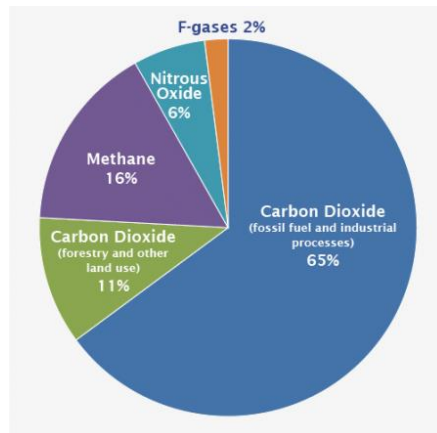
Fig. 2:3. Greenhouse gas emissions by group of gases (IPCC, 2014)

The long-term trend of production growth in energy-intensive industrial processes is continuing and the industrial sector accounted for 154 exajoules (EJ), or 36% of global total energy consumption in 2014 (IEA, 2017c). Out of this, 10.8 EJ was consumed by the cement industry. The energy demand for these industries are covered mainly by fossil fuel combustion, and therefore their contribution to global CO_2 emissions is considerable. Iron, steel, cement, chemicals, petrochemicals, pulp, paper and aluminium, are the largest CO_2 industrial emitters as shown in Fig. 2:4.
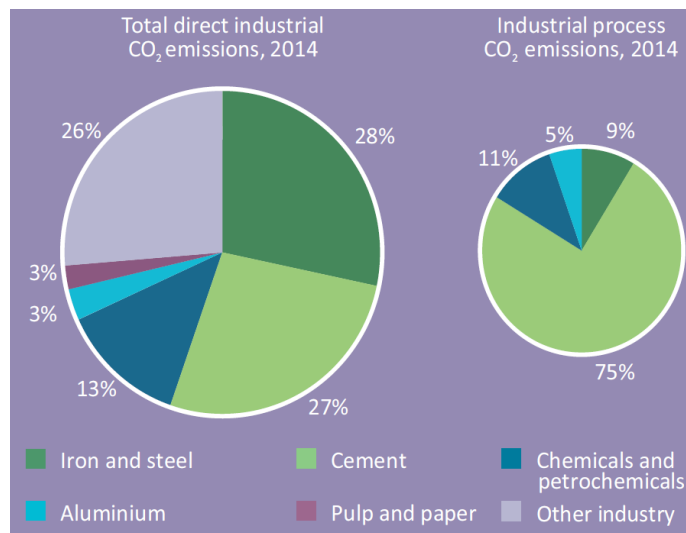
Fig. 2:4. Global direct CO_2 emissions by industrial sector in 2014 (IEA, 2017c)

Historical emission records reveal that the atmospheric CO_2 emissions were stable between 270-285 ppm until the 18th century, but the industrial revolution triggered this value rapidly (Fig. 2:5 (a)). Fig. 2:5(b) illustrates the change in global surface temperature relative to 1951-1980 average temperatures which indicate 0.8 °C of an average annual anomaly in 2018.

(a)   (b)
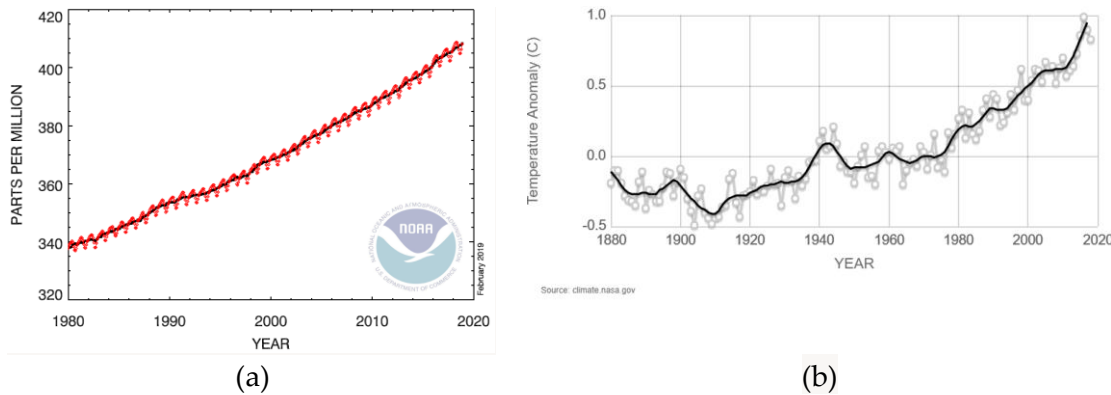
Fig. 2:5. (a) Global average atmospheric CO_2 concentration (Source: (NOAA/ESRL, 2019)) ; (b) change in global surface temperature relative to 1951-1980 average temperatures (Source :(NASA/GISS, 2018))

Recent studies have used a number of diverse independent approaches to conclude the contributions of natural and human effects on global warming. (IPCC, 2007) claims that most of the observed increase in global average temperatures since mid-20th century is very likely due to the observed increase in anthropogenic greenhouse gas concentrations. Discernible human influences now extend to other aspects of climate, including ocean warming, continental-average temperatures, temperature extremes and wind patterns Lean and the co-authors found that natural changes cannot account for significant long-term warming in the historical global surface temperature anomalies (Lean *et al.*, 2008). Human influences have been detected in changes in local temperatures, precipitation changes, atmospheric humidity, drought, Arctic ice decline, extreme heat events, ocean heat and salinity changes, and a number of other regional climate impacts (Stott, 2016). GHGs, followed by human aerosol emissions were the two largest factors influencing global temperatures in every study over every timeframe.

2.2 Trends in future energy

How far can the world sustain with the current energy systems remaining within the boundaries of greenhouse gas emissions? The BP Energy Outlook 2018, considers the energy transition from three different viewpoints (sectors, regions and fuels) and by exploring a number of different scenarios. In their predictions based on evolving transition (ET) scenario, a continuation of the recent progress and momentum in policies and technologies are assumed. Evolution on fuel consumption by region, by fuel type and total CO_2 emissions is graphed in Fig. 2:6 based on these assumptions. According to ET scenario, energy consumption in all the regions except OECD countries increase gradually in the coming years. Oil (27%), gas (26%), coal (21%), nuclear (5%), hydro (7%) and renewables (14%) will share the world's energy consumption in 2040. The market share by total fossil fuels will drop from 74% to 58% from 2016 to 2040, but this shows that more than half of the energy demand will be further supplied by fossil fuels in 2040. This will lift the CO_2 emissions to 36.8 (in 2040) billion tons.
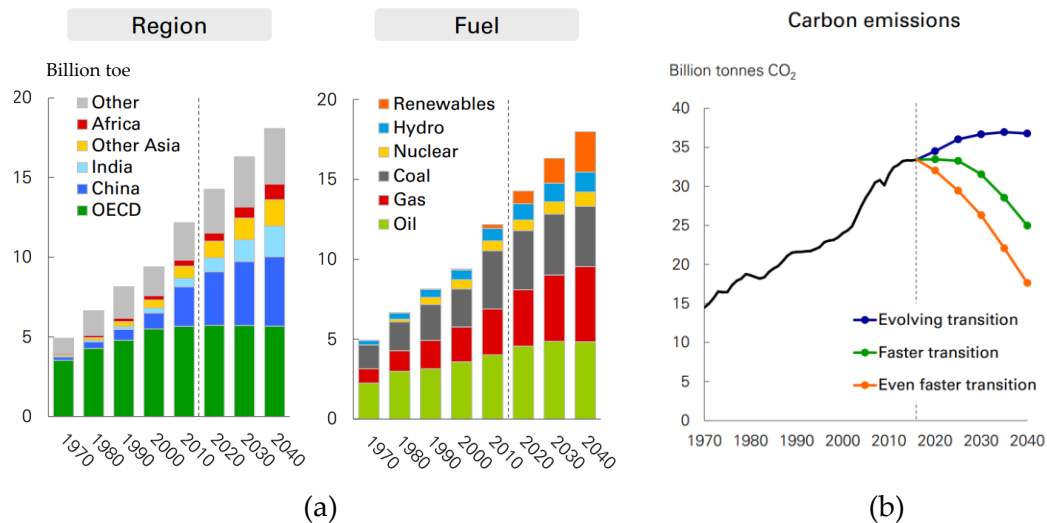
Fig. 2:6. Prediction of (a) fuel consumption based on the region and source ; (b) CO_2 emissions based on three transitions (evolving, faster and even faster) (Source :(BP, 2018a))

2.3   CCS role in reducing GHG emissions

Increased need to control global warming will have a huge impact on the use of fossil fuels in future. A global agreement to maintain global warming less than 2°C was adopted by consensus on the 12th of December 2015 at the United Nations Climate Change Conference. International Energy Agency (IEA) launched Energy Technology Perspectives (ETP) models in 2001 to analyse how the deployment of new greenhouse gas mitigation technologies can affect to the fuel market, energy security and greenhouse gas emissions and since then these models have evolved over time. In these models, carbon capture and sequestration (CCS) is shown as a mandatory requirement for GHG emission reduction. In ETP models, the Reference Technology Scenario (RTS) takes into account today's commitments by countries to limit emissions and improve energy efficiency. It will result in an average temperature increase of 2.7°C by 2100. The 2°C Scenario (2DS) lays out an energy system pathway and a CO_2 emissions trajectory consistent with at least a 50% chance of limiting the average global temperature increase to 2°C by 2100. Annual energy-related CO_2 emissions are reduced by 70% from today's levels by 2060. To stay within this range, CO_2 emissions from fuel combustion and industrial processes must continue their decline after 2060, and carbon neutrality in the energy systems must be reached before 2100. The Beyond 2°C Scenario (B2DS) explores to achieve net-zero emissions by 2060 and to stay net zero or below after that. According to (IEA, 2013a), if no action is taken to reduce GHG emission, the forecasted temperature in 2100 will be 4.5°C.
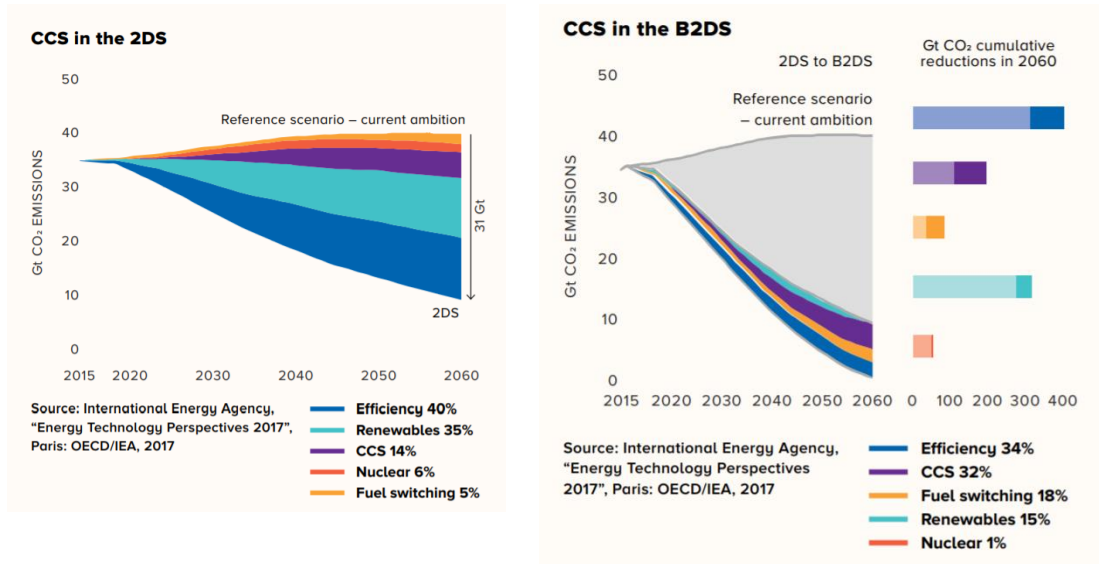
Fig. 2:7. Comparison of RTS with 2DS and B2DS ((IEA, 2017a))

Fig. 2:7 shows a comparison between RTS with 2DS and B2DS which explains the role of CCS for future CO_2 reduction. It declares a 'do-list' for movements to low emission levels which includes energy efficiency in energy systems, use of renewable energy, CCS, nuclear and fuel switching. Renewable energy which is the most sustainable option for reaching climate change goals cannot handle alone the trajectory to 2DS and B2DS limits without CCS. According to ETP models, CCS must store over 400 Mt CO_2 per year by 2025 and 142 Gt CO_2 per year by 2060 to reach 2DS goals. Within the power sector and industry CCS should contribute for 48% and 26% reduction respectively to in-line with 2DS. CCS contribution is much higher in B2DS (32%) where more CO_2 should be captured than under the 2DS by 2060. CCS complements renewables by reducing emissions in industries that renewable energy cannot penetrate – notably, steel, cement, chemicals, fertilisers, petrochemicals, paper and pulp with more than 28 Gt of emissions captured cumulatively in 2DS before 2060 (GCCSI, 2018). World Health Organization shows the threat climate change poses to health, equity, and development and immediate public health benefits by reducing the upward trajectory of greenhouse gas emissions (Hosking *et al.*, 2011). IEA in their CCS roadmap (IEA, 2013b) states seven key actions to meet 2°C goal, which are 1). Introduce financial support mechanisms for demonstration and early deployment of CCS, 2). Implement policies that encourage storage exploration, characterisation and development for CCS projects 3). Develop national laws and regulations for fossil-fuel power generation capacity to be CCS-ready, 4). Prove capture systems at pilot scales in industrial applications where CO_2 capture has not yet been demonstrated, 5). Improve understanding among public and stakeholders, 6). Reduce the cost of electricity in capture plant integrated power plants and 7). Develop CO_2 transport infrastructure. This report highlights that 100 CCS projects need to be established between 2010 -2020 storing 300 Mt CO_2 per year.

In conclusion, the world has now reached a critical juncture to accept that CCS is not a 'choice' anymore but a 'must'. The world is entirely dependent on fossil fuels and it will

take several decades to switch entirely to alternatives. Climate change will not wait until then and it is hard to see any effective solution than CCS as long as the dependencies of fossil fuel power generation exist.

2.4 CCS technology overview

CCS technology comprises three main steps, CO_2 capture from fuel combustion or industrial processes, transport of CO_2 via ships or pipelines and store in geological sites. The term "carbon capture utilization and storage," or CCUS, is also used in cases where utilization of CO_2, such as for enhanced oil recovery (EOR), can reduce the overall cost of capture and storage. The term BECCS (also abbreviated as BCCS or biomass CCS) refers to the concept of combining bioenergy applications (including all forms of power, heat, and fuel production) with CCS. BECCS projects have the potential to be negative emissions technologies, but still there is limited practical and research experience of dedicated BECCS.

Over the other CO_2 emission reduction options such as improving energy efficiency, shift to renewable energy and use of low carbon fuels, CCS is prominent as it can reduce a vast amount of CO_2 from emission sources such as power plants or cement factories with capture efficiency greater than 80%. Several types of capture technologies are available but their selection is based on the type of combustion process which produces CO_2. In general, CO_2 capture represents 75-80% of the cost of CCS where the balance is the transport and storage cost (Davidson, 2007). Post-combustion, pre-combustion and oxyfuel combustion processes are associated with capture mechanisms in combustion processes (Section 2.6). CO_2 captured from these processes are then separated from the rest of components in the captured stream via different mechanisms which are also common to other chemical gas processing applications such as absorption (chemical or physical), adsorption, chemical looping, membrane separation, hydrate-based separation and cryogenic distillation.

After the separation, CO_2 is compressed to a dense phase and transported to the storage facilities or industrial sites for utilization. Transportation will be taken by road tankers, ships or pipelines and it depends on the CO_2 volume and available infrastructure facilities (Norişor *et al.*, 2012; Svensson *et al.*, 2004). CO_2 injection to depleted oil and gas reservoirs to extract residual oil left has been in practice over several decades because of its economical advantage. However, they should be injected into geological formations such as saline aquifers when large quantities of CO_2 are captured. According to the report by (Hosking *et al.*, 2011), the United States, Canada, and Australia likely have more than enough theoretical CO_2 storage capacity to meet their needs for this century and perhaps beyond. This report says that the estimated CO_2 storage capacity is nearly 11,000 Gt CO_2 worldwide and for CO_2 stabilization from 450 to 750 ppm, the demand for CO_2 storage space does not exceed 2,220 Gt CO_2 throughout this century which further adds confidence on CCS as a doable option for emission reduction. After storage, long-

term post-injection monitoring phase begins for potential leakages. Current CO_2 storage facilities such as Sleipner – Norway, Frio - US, Nagaoka – Japan, Ketzin - Germany and Weyburn - Canada frequently monitor for CO_2 leaks using different monitoring tools such as 3D seismic, microseismic and geochemical sampling (Leung *et al.*, 2014). Captured CO_2 can be utilized in industry, agriculture and energy production. In industry, CO_2 can be used as a raw material in the synthesis of chemicals such as carboxylates, carbonates and carbamates.

2.5 CCS facilities

Information about the current status of CCS facilities is reported in (GCCSI, 2018). It says that there are now 23 commercial large-scale global CCS facilities; 18 in operation and 5 in construction. The total capture rate from them is close to 40 million tons of CO_2 per annum (Mtpa). Further 28 pilot and demonstration-scale facilities are in operation or under construction which collectively, will capture more than 3 Mtpa of CO_2. Most of the facilities capture CO_2 from natural gas processing and store for enhanced oil recovery. The earliest large scale CCS facility started in 1972 in the US connected to Val Verde Natural Gas Plants. Shute Creek Gas Processing Plant and Enid Fertilizer were retrofitted to CO_2-EOR operation in 1986 and 1982 respectively. Enid plant captures 7 Mtpa of CO_2.

Four large-scale CCS facilities which commenced operations after 2009 in the US are Century Plant (8.4 Mtpa, natural gas processing), Air Products Steam Methane Reformer (1.0 Mtpa, hydrogen production), Coffeyville Gasification Plant (1.0 Mtpa, fertiliser production) and Lost Cabin Gas Plant (0.9 Mtpa, natural gas processing). In the rest of the world, Great Plains Synfuels Plant & Weyburn-midale (Canada, 1.4 Mtpa, synthetic gas), Quest (Canada, 1 Mtpa, hydrogen production), Sleipner (Norway, 0.9 Mtpa, natural gas processing), Snøhvit (Norway, 0.7 Mtpa, natural gas processing), Abu Dhabi CCS (UAE, 0.8 Mtpa, iron and steel production), Petrobras Pre-salt (Brazil, 0.7 Mtpa, natural gas processing), Uthmaniyah (Saudi Arabia, 0.8 Mtpa, natural gas processing), Gorgon CO_2 injection project (Australia, 3.4-4 Mtpa natural gas processing) and CNPC Jilin (China, 0.6 Mtpa, natural gas processing) are remarkable CCS deployments. A detailed overview of the global CCS facilities under operation, evaluation and planned to commence can be found in Global CCS Institute's website (https://www.globalccsinstitute.com/) which is summarized in (Luis, 2016) and in the database of (OpenDataSoft). Upto date, there are only two large-scale CCS facilities connected to power generation sites in the world which are Boundary Dam Unit 3 in Saskatchewan, Canada and Petra Nova, US. Since start-up Boundary Dam capture plant, reported over 2 Mt of CO_2 captured by March 2018. Petra Nova has the capture facility of 1.4 million tonnes per annum.

2.6 CO₂ capture technologies

CO₂ capture is classified according to the type of combustion process as post combustion, pre-combustion, oxy-fuel combustion and chemical looping system which is shown in Fig. 2:8.

Post- combustion capture (PCC) -
In post combustion capture process CO₂ comes out from the flue gas stream from boilers, heaters or turbines, passes through the gas purification process such as NO_x, SO_x, particulate removal and then enters the capture process. This technology has been demonstrated in several natural gas-fired and coal-fired power plants in small scales and is the most suitable technology for retrofitting the existing combustion technology (Wang *et al.*, 2015). The CO₂ concentration which enters the capture plant by this combustion process is very low and it affects the plant efficiency.
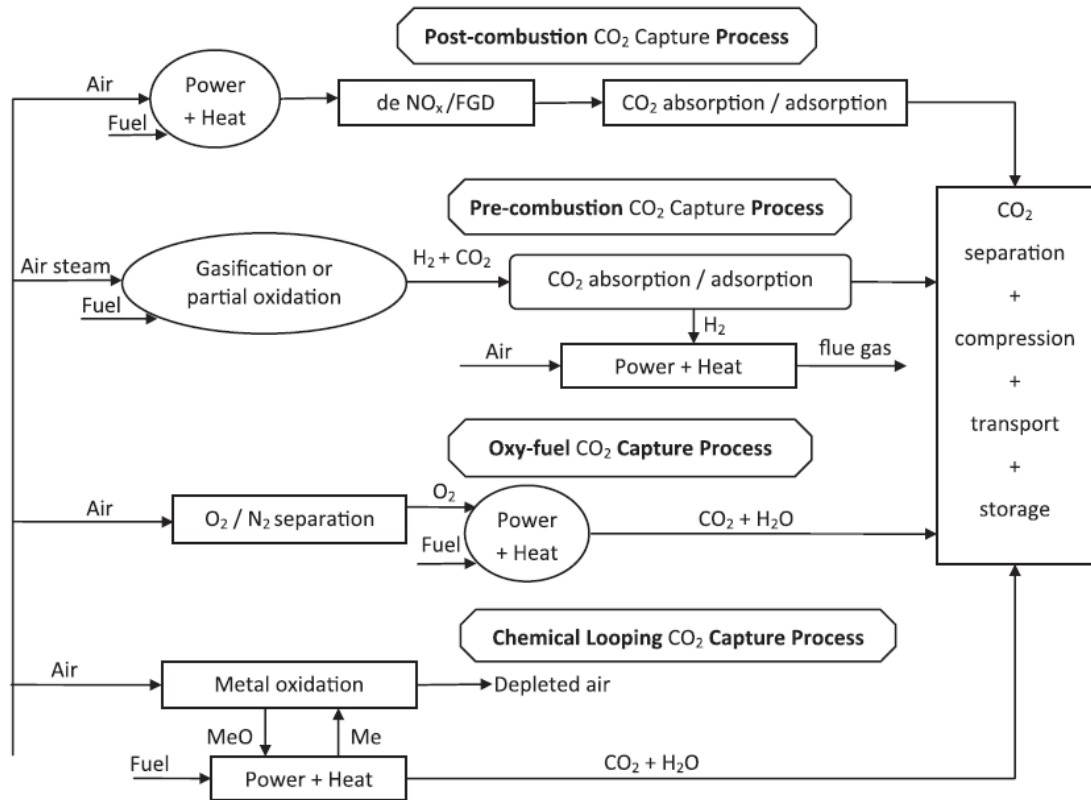
Fig. 2:8. Different CO₂ capture technologies; Source : (Leung *et al.*, 2014)

Pre- combustion capture -
Fuel is first reacted with an air/oxygen stream to produce syngas which is composed of H₂ and CO in pre-combustion capture. The syngas stream is then sent to a catalytic reactor also known as a shift converter where CO is reacted with steam to produce CO₂. After separating CO₂ chemically or physically, the remaining stream is rich in hydrogen which can be used as a fuel for many applications such as in boilers, furnaces, engines

and fuel cells. The advantage of pre-combustion capture is that it produces higher CO_2 concentration to feed to the capture plant increasing the CO_2 removal efficiency than in the post-combustion process. Examples of commercial scale pre-combustion capture plants are Uthmaniyah, Weyburn, Val Verde, Snøhvit, In Salah, Petrobras and Sleipner. The pre-combustion capture process is a highly developed technology and is most suitable for new plants.

Oxyfuel combustion capture –
In the oxyfuel combustion, oxygen in the air is separated using a cryogenic air separation unit, and fuel is combusted with a nearly pure oxygen environment. Combustion generates a stream mainly with higher CO_2 concentration and water. The water can be easily separated, and the remaining CO_2 is ready for sequestration. This method reduces the volume of exhaust gas after the combustion which affects the subsequent separation and has low NO_x emissions. Oxy-fuel combustion applies to both coal fired, and gas-fired plants, but the corrosion problems and the cost of cryogenic separation are main disadvantages.

Chemical looping capture (CLC) -
Chemical looping combustion consists of two steps, where in the first step O_2 is separated from N_2 and transferring oxygen from the air to the fuel in the second step. This process can separate both CO_2 and H_2O from the N_2 gas stream and therefore results in a higher efficiency in the capture process (Li *et al.*, 2017). CLC is a diversified process to post-combustion, pre-combustion and oxyfuel combustion CO_2 capture process. Calcium sorbent-based looping process is a chemical looping based process, where CaO is used as the regenerable sorbent for CO_2.

2.7 CO_2 separation technologies

According to Fig. 2:8, CO_2 comes with flue gas stream in post-combustion, oxy-fuel combustion and chemical looping while it comes with fuel gas stream in pre-combustion process. A number of technologies are available to separate this CO_2 from the rest of the components before it is compressed for transportation.
In the report of (IEAGHG, 2014) a list of different technologies used to separate CO_2 from combustion processes are given and they have been ranked by their technology readiness level (as '*demonstrated, developed or research*'). Ethanolamine based CO_2 absorption process has the highest readiness level which has passed research, development and demonstration levels and now fully prepared for full-scale commercial deployment. This technology is used as the benchmark to compare the other separation technologies. Improved conventional solvents, polymeric membranes, precipitating solvents and biphasic solvents are in the development stage. For pre-combustion, physical absorption of CO_2 by Selexol is at the highest readiness level for commercial scale. Other pre-combustion technologies are hydrogen separation membrane, low temperature separation, sorption enhanced water gas shift. Unlike post-combustion,

pre-combustion CO_2 capture technologies are difficult to demonstrate in full scale with existing power plants because of complexity in process integration. Fig. 2:9 outlines the available CO_2 capture technologies in all states of readiness level (screening, research, development and demonstration).
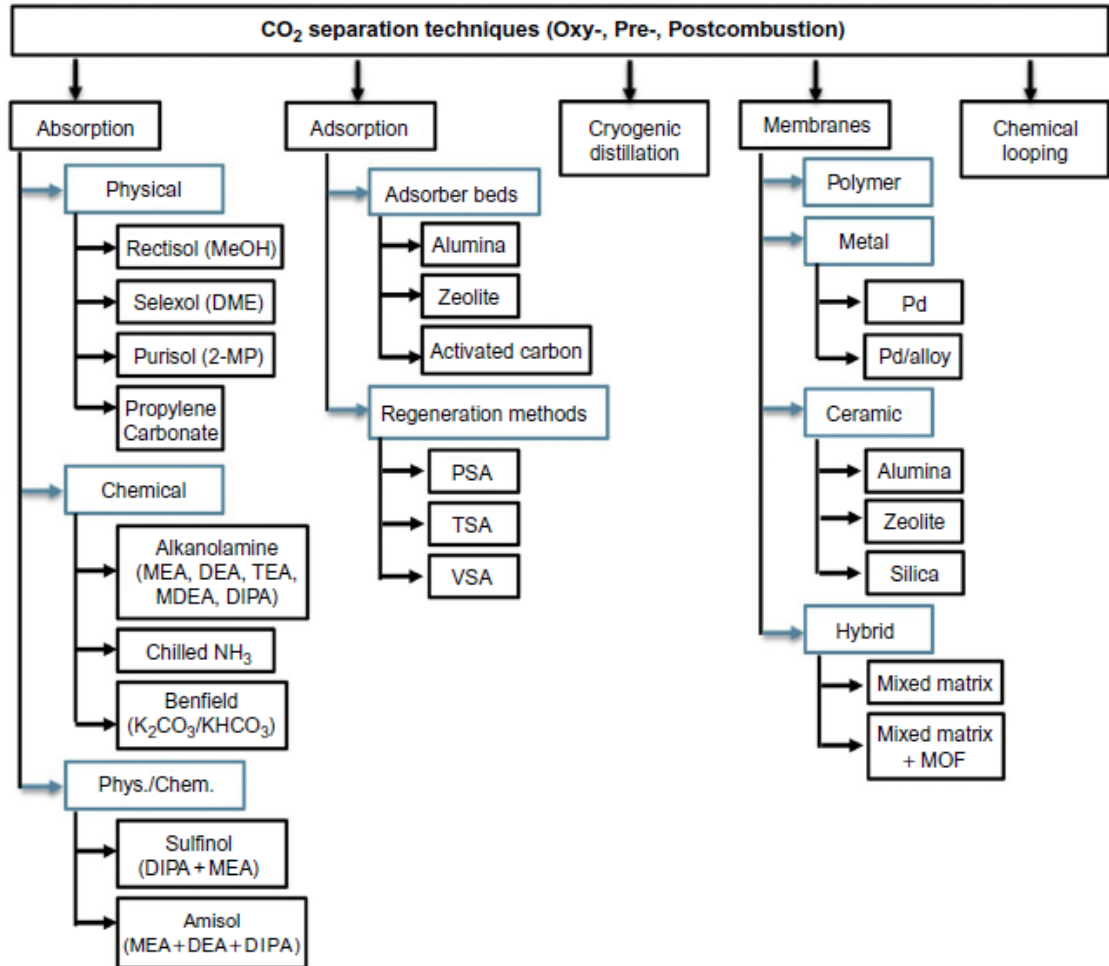
Fig. 2:9. CO_2 separation technologies (Liguori *et al.*, 2017)

2.8 Post-combustion MEA based CO₂ capture

The historical origination of the CO_2 capture facilities in the world implies that the idea of CO_2 captured from power plants started not with the climate change concern but as an economical value addition to the oil production by enhanced oil recovery (Herzog *et al.*, 1997) and to take advantage of some of the economic incentives from the governments. Such a CO_2 capture plant is North American Chemical Plant in Trona, California (started in 1978). Post combustion CO_2 capture technology has been widely used in refining and gas processing since many years giving experience to consider this process as 'commercially available'. Pre- and oxy-combustion technologies are considered to be 'emerging technologies' in contrast. Of all the post-combustion

technologies, chemical absorption is considered so far the most suitable one, and among many solvents tested for chemical absorption process, monoethanolamine (MEA) is undoubtedly the most extended solvent (Luis, 2016).
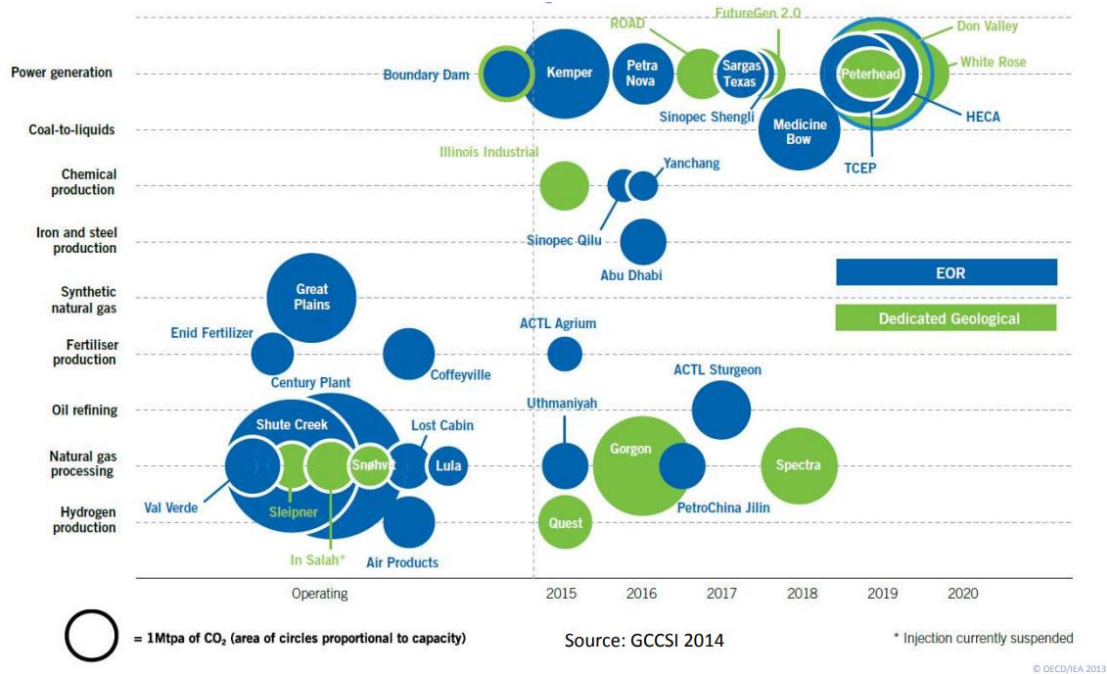
Fig. 2:10. Global CCS status around the world; source : (GCCSI, 2014)

State of the-art of CCS development projects around the world with its application area, is shown in Fig. 2:10. With the lessons learned from Boundary Dam 3 project and Petra Nova, a number of plants are in the queue and at their earlier stage of development related to power generation. The preferred solvent is amine for most of these facilities. Amines can react with CO_2 to form water-soluble components at a low CO_2 partial pressure, have reversible reactions with CO_2 and therefore fulfil the primary requirement for separation of CO_2 from many CO_2 containing gas mixture. The performance of the CO_2 absorption system by amines are dictated by properties such as solvent working capacity, solvent concentration, the heat of reaction, absorption rate and solvent stability (Raksajati *et al.*, 2018).

Although there is a momentous research focus on more advanced ways of capturing CO_2 from combustion flue gas, it is expected that amine solvents will remain the dominant large-scale technology for power plant retrofits for at least the next decade. The most likely approach to retrofitting CCS is post-combustion CO_2 capture using an amine solvent-based system in the timeframe to 2050 (IEA, 2015). Most existing power plants in China, are recently built (since 2005) and will be 20 to 30 years old if retrofit between 2025 and 2035, making the need for upgrades less acute than at Boundary Dam

experiences (IEA, 2016). Solvent based CO_2 capture systems are generally considered to be more flexible as they can be fully or partially bypassed to allow the plant to operate in a non-CCS mode even after CCS retrofit. So, the amine technology for post combustion capture becomes the dominant technology considering the balance between technology know-how, economics, political constraints and time frame.

2.8.1 Process description of CO_2 capture by amine

Cyclic CO_2 absorption-desorption mechanism by amine is the current industry standard for separating CO_2 from a flue gas stream. A simplified schematic representation of this technology is shown in Fig. 2:11. The process starts with introducing flue gas to the absorber after desulfurization, denitrification and particulate removal processes. It goes from absorber bottom to the top while amine flows counter-currently from absorber top to bottom. During the process CO_2 in the flue gas is absorbed by the amine, the clean flue gas is vented from absorber top and CO_2 absorbed amine (rich amine) is sent through a cross flow heat exchanger. Rich amine then enters to the CO_2 stripper where by the heat supplied from steam CO_2 is liberated in a pure form. The solvent which is lean in CO_2 concentration (lean amine) is then recycled to the CO_2 absorber via the cross flow heat exchanger where its temperature is reduced. The base case conditions for an amine capture plant is considered as 30 w/w% MEA (MEA weight per sum of MEA and water weight), lean amine absorber inlet at 40 °C, CO_2 concentration in the flue gas between 10-12 v/v% and stripper bottom temperature of 115-120 °C. The CO_2 liberated from stripper top, is compressed to pipeline pressure and piped offsite to be transported for use or storage.
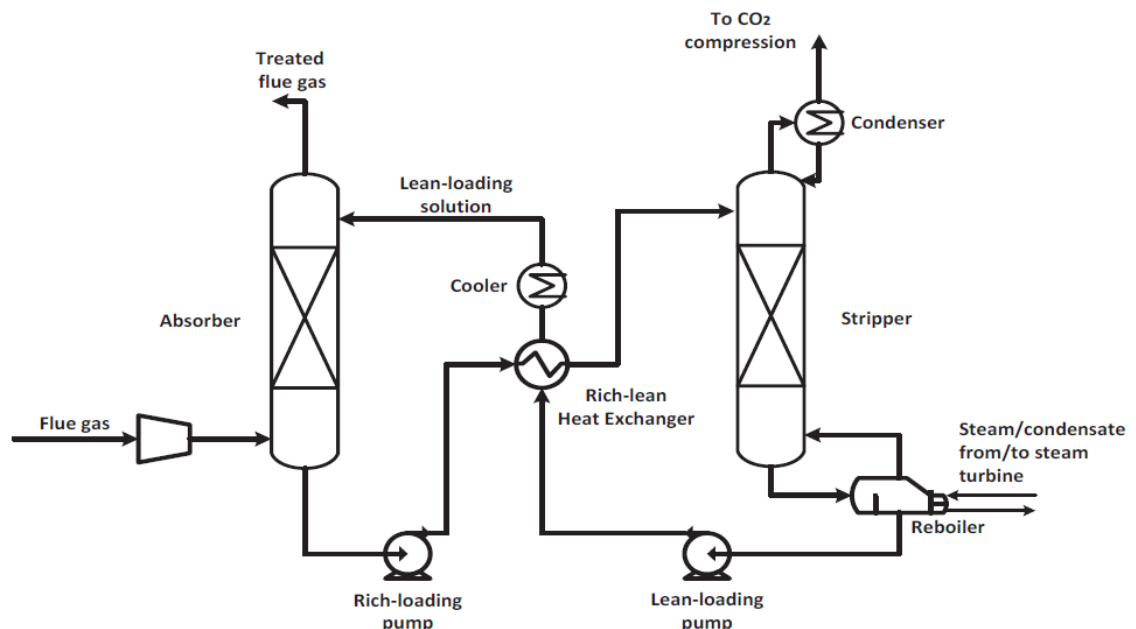
Fig. 2:11. Process flow of a post-combustion CO_2 capture facility (Wang *et al.*, 2017)

The energy required for heating such as the reboiler in the stripper is typically taken from the power plant. (Lucquiaud et al, 2009) mentions a steam pressure of around 4.5 bar as ideal for today's solvents in order to minimise energy losses. Electricity from the power plant generators is used to run compressors, fans and pumps. Cooling is supplied by cooling water and is used for cooling the flue gas feed to the absorber, condense out any remaining solvent from the CO_2 stripped before compression, and cooling CO_2 during compression. The capture plant process remains almost untouched from the power plant giving the advantage for easy retrofitting.

3 Process Analytical Technology

Chemical processes such as pharmaceutical manufacturing, food & beverage production, mining process and biogas production have gained the advantage of Process Analytical Technology (PAT) and its concepts to increase efficiency, reduce time-consuming activities and facilitate intelligent decisions. PAT helps to make the right solution at the right time at the right place. It is interesting to explore how PAT can be applied to the CO_2 capture process.

PAT was initially defined by the Food and Drug Administration (FDA) for the pharmaceutical industry, as *a system for designing, analysing, and controlling manufacturing through timely measurements (i.e., during processing) of critical quality and performance attributes of raw and in-process materials and processes, with the goal of ensuring final product quality* (FDA, 2004). *Process analysis* is the chemical or physical analysis of materials in a process stream through an in-line or on-line analyzer (Guenard *et al.*, 2010). P*rocess analyzers* measure directly physical or chemical attributes in a system and supply data which are then directly or indirectly used to map with attributes related to the process. Some key features of process analysis concerning the laboratory analysis are the speed of the analysis, fewer sample errors and the ability to integrate real-time data with process control. A typical PAT framework consists of 4 parts, as 1). Process monitoring using modern process analyzers, 2). Process analysis using multivariate data analysis (MVDA) and chemometrics, 3). Process design with concepts from Quality by Design (QbD) and Design of Experiments (DoE) and 4). Process control.

PAT tools are used to enable scientific and risk managed manufacture and quality assurance. They are categorized as 1). Multivariate data acquisition and analysis tools, 2). Modern process analyzers or process analytical chemistry tools, 3). Process and endpoint monitoring and control tools and 4). Continuous improvement and knowledge management tools. Implementation of PAT to a particular application composes an appropriate combination of some, or all, of these tools and the boundary, can be a single-unit operation, or to an entire manufacturing process. By integrating these categories, a platform is built to make a communication between the process (or single process equipment) and the process analyzers harmonizing the real-time data and offline data which are ultimately used for real-time trending, process control and quality control. By storing the real-time data during a long run, it provides ample opportunities to take suggestions to improve the process which would otherwise not perfectly successful with frequent process monitoring. To turn data into knowledge, a specific mathematical tool is used which is called *multivariate data analysis* (MVDA).

PAT is the sub-discipline under Process Analytical Chemistry (PAC). If PAT is excluded from PAC, then PAC consists time-consuming manual off-line sampling analysed in laboratories. The measured properties of process analyzers, can be univariate (scalar) quantities such as process flowrate, temperature, pH, or multivariate such as chromatogram, vibrational spectra and acoustic signals. Modern process analyzers

include UV-Visible (UV-Vis), near and mid-infrared (NIR and MIR), Raman spectroscopy, hyperspectral image sensors, tomography, NMR spectroscopy, acoustic and tetrahertz spectroscopies. The choice of process analyser to a particular application is highly specific. Several factors should be optimized such as the quality of the analyser response (depends on the complexity of raw data obtained from the analyser and the effort needed to turn data into information), required precision, accuracy, project time, budget and flexibility of the instrument for a given application (Robert Guenard, 2010). (Lyndgaard, 2013) used the following criteria to conclude which spectroscopic method is more appropriate out of five spectroscopies for a multivariate calibration process. They are, resolution, sensitivity, selectivity, interference, sample preparation, sampling flexibility, analysis time, and prize and stability. The comparison is presented in Table 3.1.

Table 3.1. Comparison of multivariate use of five spectroscopic methods (Lyndgaard, 2013)

	NIR absorption	Raman scattering	IR absorption	UV-VIS absorption	Fluorescence emission
Resolution	Low	Medium	Medium	Low	Medium
Sensitivity	Low	Medium	Medium	High	High
Selectivity	Medium	High	High	Low	Very high
'Main Interferences'	Water	Fluorescence	Water	Scattering	Quenching
Sample preparation	None	None	None	None	None
Sampling flexibility	High	High	Low	Medium	Medium
Typical analysis time	Seconds	Seconds	Minutes	Seconds	Minutes
Prize of a robust instrument	++	++++	++	+	+++
Molecular phenomena	Combination- and overtones of molecular vibrations	Fundamental molecular vibrations	Fundamental molecular vibrations	Valence electron transitions	Electron transitions
Other characteristics	–Nearly all molecules absorb –Quartz transparent	–Nearly all molecules scatter –Quartz transparent	–Nearly all molecules absorb –Quartz absorb	–Few molecules absorb –Quartz transparent	–Few all molecules fluoresce –Quartz transparent

Multivariate analysis refers to all statistical techniques that simultaneously analyze multiple measurements. Data are said to be multivariate when each observation has values for two or more random variables such as a spectroscopic signal. Multivariate statistics are used in several disciplines; some examples are in 1). Psychology – called psychometrics, 2). Taxonomy – called taxometrics, 3). Biology – called biometrics, 3). Engineering – called technometrics 4). Chemistry – called chemometrics.

3.1 Chemometrics

Chemometrics is the related discipline to this study where statistics and mathematics in chemical sciences are used to measure and interpret chemical data. "Chemometrics'' was initially coined by the Swedish chemist Svante Wold for his research grant application in 1971 (Wold, 2015). Fig. 3: shows different chemometrics methods which are used to plan experiments, exploratory (qualitative) analysis, classification, process control, quantitative analysis and multi-way analysis. DoE -Design of Experiments, (Deming *et al.*, 1991) provides methods to obtain data sets which are more likely to contain the desired information with a reduced number of trials at less cost and time. PCA (Principal Component Analysis) is a dimension-reduction technique which is used to reduce a large set of independent variables to a small set and describe the variation and structure of the data using principal components. MSPC (Multivariate Statistical Process Control) uses techniques to monitor and control the operating performance of batch and continuous processes. MCR (Multivariate Curve Resolution) can be used to resolve mixtures by determining the number of constituents and their response profiles even when no prior information is available about the nature and composition of the mixture. [MLR, PCR, PLS] consist of algorithms to build regression models to predict properties such as concentrations based on multivariate measurements. Mathematical outline under these chemometric methods with examples of analysis data sets can be found in (Esbensen *et al.*, 2010b).
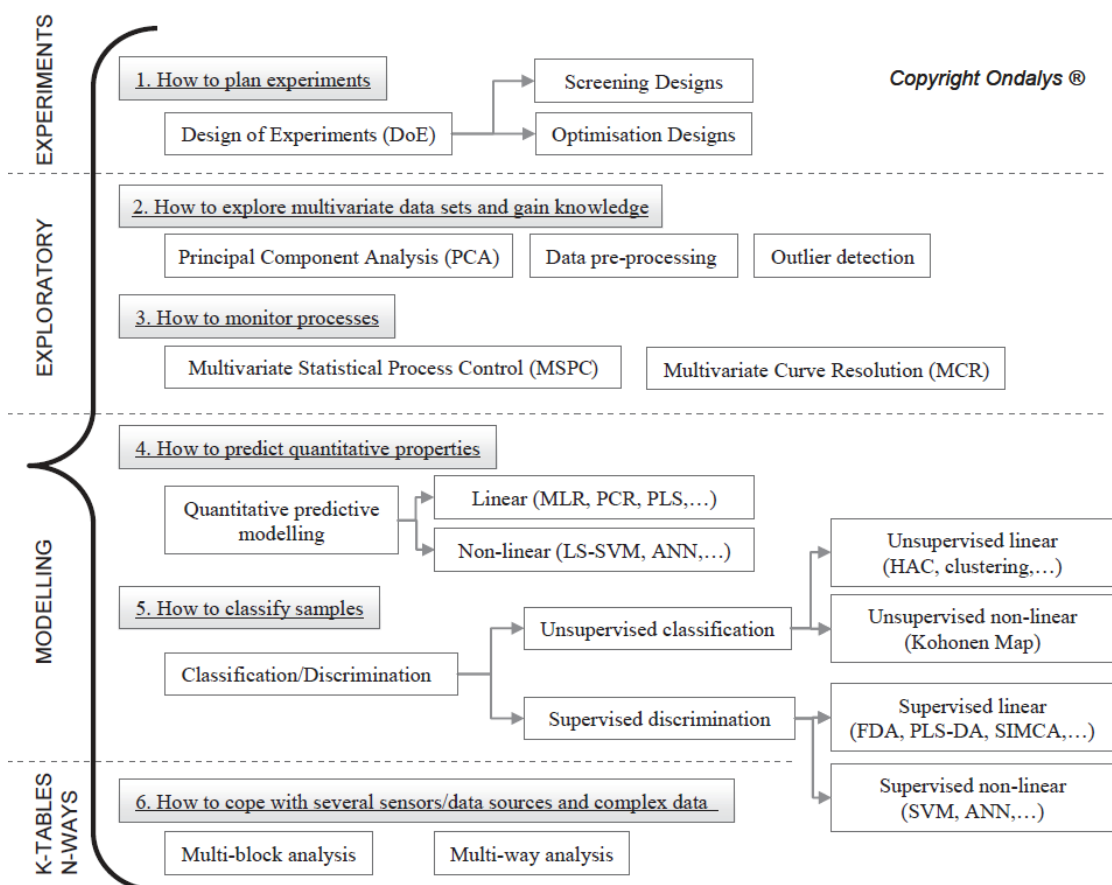
Fig. 3: 1. Different chemometric methods to analyse multivariate data; Source :
(Roussel *et al.*, 2014)

3.2 Raman spectroscopy

Raman scattering was first observed by Sir Chandrasekhara Venkata from his naked eyes where he used sunlight as the source and a telescope as the collector. Later quantitative results were published in 1928 after using a quartz spectrograph to photograph the spectrum of scattered light (Bohning *et al.*, 1998). Since then gradual progress in the physical units such as detection systems, light sources and monochromators, development of Fourier transformation techniques and use of computers for data handling have brought the present state of the art of the commercial Raman instrument.

Either dispersive Raman or Fourier transform Raman technologies are used in commercially available Raman spectrometers. In dispersive Raman instruments, separation of the collected Raman scattered light into its composite wavelengths is accomplished by focusing the Raman scattered light onto a diffraction grating (Fig. 3:1). It splits the beam into its relevant wavelengths and directs onto a charge-coupled device (CCD detector). Wavelengths 780 nm, 633 nm, 532 nm, and 473 nm are typically used for laser radiation. Shorter excitation wavelengths give stronger Raman signals nevertheless fluorescence is also much more likely to occur under these conditions (Li *et al.*, 2014).

Non-dispersive Fourier transform (FT) Raman spectroscopy (Fig. 3:2) uses IR excitation sources and has three main advantages than dispersive Raman spectroscopy by having a higher spectral resolution, less laser-induced fluorescence and ease of operation.
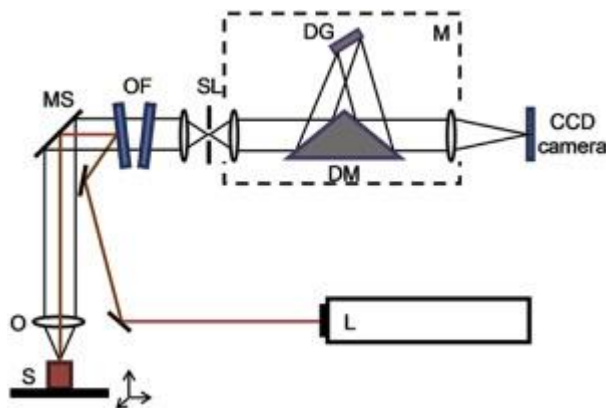
Fig. 3:1. Schematic layout of a typical dispersive micro-Raman spectrometer. CCD = charge coupled device; DG = diffraction grating; DM = dichroic mirror; L = laser; M = monochromator; MS = microscope; O = objective lens; OF = optical filters; S = sample; SL = slits. Source : (Li *et al.,* 2014)
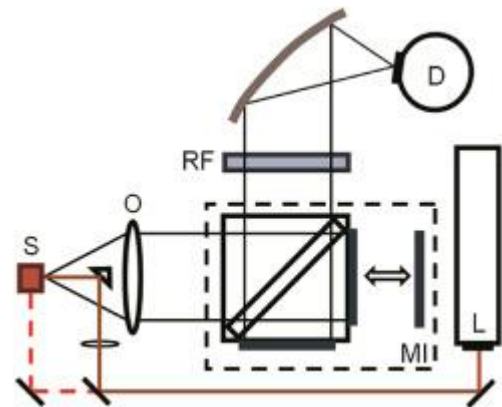
Fig. 3:2. Schematic layout of a typical Fourier transform (FT) - Raman spectrometer. D = detector; L = laser; MI = Michelson interferometer; O = objective lens; RF = Rayleigh filter; S = sample. Source : (Li *et al.,* 2014)

3.2.1 Light scattering and Raman effect

When light interacts with a matter, it can be either transmitted, absorbed or scattered. Rayleigh (elastic) scattering occurs when the scattered light has the same energy as the incident light it is. If the scattered photons have a different energy than the incident photon, it is called Raman or (inelastic) scattering which is two-fold as Stokes Raman scattering and Anti-Stokes Raman scattering. Fig. 3:3 shows the Jablonski diagram which illustrates the difference between Rayleigh and Raman scattering. This diagram is used to understand the photon scattering process where photons are assumed to move to a virtual state during an excitation but immediately transit back to a vibrational level of the ground state. Stokes Raman scattering happens when an atom or molecule absorbs energy and creates the scattered photon to have less energy than the incident photon. Anti-Stokes Raman scattering happens when an atom or molecule loses energy resulting in the scattered photon has more energy than the incident photon.
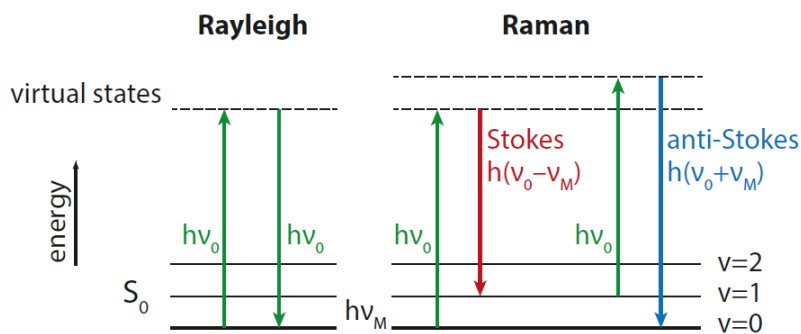
Fig. 3:3. Representation of Rayleigh, Stokes and anti-Stokes scattering by Jablonski diagrams

The classical theory and the quantum theory are used to describe the Raman effect where the first theory explains the polarizability concept of molecules and the latter one explains the photon transfer phenomena related to Raman effect. According to the classical theory, Raman scattering depends on the change in polarizability of the molecule when it vibrates due to incident radiation. The magnitude of the induced dipole moment depends both on the magnitude of the intensity of laser light and the ability to change the electron cloud in the molecule. In Raman spectroscopy, the change in polarizability (α) is measured and presented as a function of Raman intensity vs wavenumber. There is no Raman band if a molecular vibration does not change the molecular polarizability. Strong Raman scattering typically arises from double bonds (eg: C=C) than from highly polar bands because the electron cloud can be easily changed in double bonds. There are different types; stretching or bonding vibrations alter the bond length, bending or deformation vibrations alter the bond angles (in-plane and out-of-plane twisting, wagging and rocking) whereas torsion vibrations alter the torsion angle. Fig. 3:4 shows three types of vibrations for a linear ABA molecule and the rationale behind a Raman active vibration and infrared active vibration. The first vibration mode is Raman active because it makes the polarizability derivative at equilibrium coordinate to be non-zero. The second and third vibrations are infrared active because they make dipole moment derivative at equilibrium position to be non-zero.

Fig. 3:4. Polarizability and dipole moment variations in the neighbourhood of the equilibrium position and vibrational Raman and infrared activities for a linear ABA molecule (Long, 2002)

4 Speciation in CO₂ Capture Solvents

Amines, carbonates and aqueous ammonia are typical systems for chemical absorption in CO₂ capture (Fig. 2:9). Among amine based systems, monoethanolamine (MEA), diethanolamine (DEA), methyl diethanolamine (MDEA), diglycolamine (DGA), diisopropanolamine (DIPA), piperazine (PZ), sterically hindered amines such as 2-amino-2-methyl-1-propanol (AMP) or a mixture of amines are popular CO₂ absorbing solvents. According to the IUPAC definition (Templeton *et al.*, 2000) a *chemical specie* is a specific form of an element defined as to isotopic composition, electronic or oxidation state, and/or complex or molecular structure. *Speciation analysis* is referred to analytical activities of identifying and/or measuring the quantities of one or more individual chemical species in a sample; and *speciation* is referred to the distribution of an element amongst defined chemical species in a system. Understanding a liquid-gas absorption system is started by investigating the chemical reactions where speciation details are important.

4.1 Reaction of CO₂ with aqueous amine solutions

The chemical behaviour between primary amines such as MEA with CO₂ has been reviewed several times in recent and past literature (Crooks *et al.*, 1989). As shown in equation 1 and 2 (Versteeg *et al.*, 1988) two step Zwitterion mechanism describes the reaction between a primary/secondary amine R_1R_2NH and CO₂ (R_1, R_2 are organic radicals; for primary amines $R_2 = H$). This mechanism was first introduced by (Caplow, 1968) and reintroduced by (Danckwerts, 1979).

$$CO_{2(aq)} + R_1R_2NH \leftrightarrow R_1R_2NH^+COO^- \tag{1}$$
$$R_1R_2N^+HCOO^- + B \leftrightarrow R_1R_2NCOO^- + BH^+ \tag{2}$$
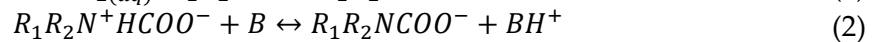
Here CO₂ reacts with an amine to form an intermediate and this intermediate immediately reacts with another molecule (B), usually a second amine molecule, to form a carbamate and a protonated amine. This reaction describes the carbamate formation. Bicarbonate/carbonate formation, and protonation/deprotonation of amine are described by (Nichola McCann, 2009) using a set of reaction schemes given from equation (3) to (6) for primary and secondary amines.

$$CO_{2(aq)} + H_2O \leftrightarrow H_2CO_3 \leftrightarrow HCO_3^- + H^+ \leftrightarrow CO_3^{2-} + 2H^+ \tag{3}$$
$$R_1R_2NH + H_2O \leftrightarrow R_1R_2NH_2^+ + OH^- \tag{4}$$
$$CO_{2(aq)} + OH^- \leftrightarrow HCO_3^- \tag{5}$$
$$CO_2 + 2R_1R_2NH \leftrightarrow R_1R_2NH + R_1R_2NCOOH \leftrightarrow R_1R_2NH_2^+ + R_1R_2NCOO^- \tag{6}$$
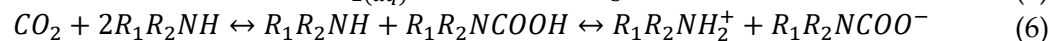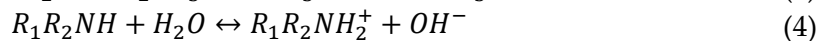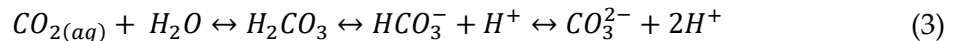
Tertiary amines do not form carbamate and their reaction with CO₂ leads to form bicarbonate and protonated amine as given in equation (7) where R_3 is an organic radical.

$$CO_2 + R_1R_2NR_3 + H_2O \leftrightarrow R_1R_2NR_3H^+ + HCO_3^- \tag{7}$$
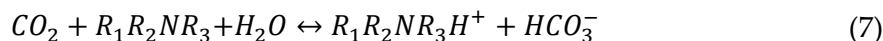
MEA contains one amine functional group and one alcohol functional group. For primary amines, the reactions showing water dissociation, carbon dioxide hydrolysis, carbonate/bicarbonate formation, amine protonation, carbamation and decarbamation generate a pool of cations and anions which include $OH^-, H^+, HCO_3^-, CO_3^{2-}, RNHCO_2^-$ and RNH_3^+. These reactions include instantaneous equilibria, quantitatively defined by equilibrium constants, and kinetically observable reactions, defined by rate constants (Nichola McCann, 2009). They explain that the carbamate is much more stable with a half-life of about 2.5 h at 30 °C whereas carbamic acid is very labile. The graphical representation of these reactions (Nichola McCann, 2009) which is presented in Fig. 4:1 shows that there are three parallel, reversible reactions of the free amine with CO₂, carbonic acid, and the bicarbonate ion. The relative importance of the three paths is strongly pH dependent.

.
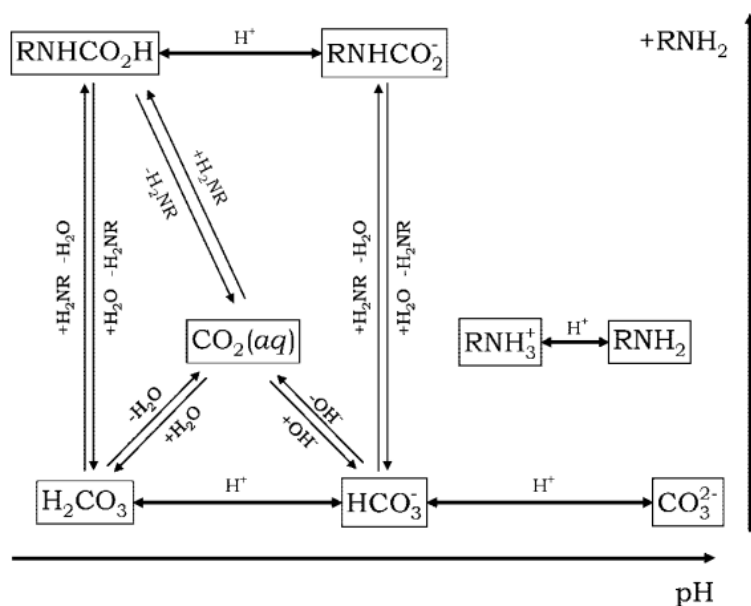
Fig. 4:1. General reaction scheme including all reactions between a primary amine, the CO₂ /carbonate group and protons. Single line/double arrow represent instantaneous protonation equilibria, double lines represent kinetically observable reactions for which rate constants are known in literature (Adapted with permission from (Nichola McCann, 2009). Copyright (2009) American Chemical Society

4.2 Recent developments in speciation of amine-CO₂-H₂O systems

The chemical analysis for amine-CO_2-H_2O systems is typically expressed in terms of CO_2 loading (mol CO_2 / mol MEA) and amine concentration. Among these analysis, barium chloride ($BaCl_2$) titration-precipitation method (Idris *et al.*, 2014; Weiland *et al.*, 1969), analysis via acidic evolution (Hilliard, 2008), $BaCl_2$ - sulfuric acid method (Hilliard, 2008) and phosphoric acid - UOP Method 826-81 (ASTM, 2010) have been used in practice from lab to industry as offline measurements techniques. (Knudsen *et al.*, 2014) used LC-MS to determining total amine concentration and (Morton *et al.*, 2013) have used automatic titration for CO_2 loading analysis. (Masohan *et al.*, 2009) suggested a method using a pH graph to calculate CO_2 content in amine. (Montañés *et al.*, 2017) used correlation from direct measurements such as pH, density, viscosity, conductivity and temperature of the solvent streams to determine CO_2 loading during TCM Mongstad Plant campaigns. Most of these analyses give only the total CO_2 loading and the MEA concentration in the system although a complete speciation details are required to understand the system in broader context.

Table 4.1 shows research attempts where Fourier transform infrared (FTIR), near-infrared (NIR), attenuated total reflectance-FTIR (ATR-FTIR), Uv-vis and Raman spectrometers have been used in qualitative and quantitative analysis of CO_2 loaded amine solutions. They have used different approaches to derive chemical data from raw spectroscopic measurements. They are univariate analysis method where peak intensity or area is used for calibration; using internal standards such as ClO_4^- for normalizing data; data preprocessing using baseline correction; PLS approach using a variable range and calibration model development based on thermodynamic model data or chemical equilibrium constants. Absorption and vibrational spectra of the CO_2 loaded amine solutions contain overlapping peaks. Some peaks are related to chemical vibrations and some are related to noise (see Fig. 5:8). A logical approach to understand which of these bands are chemically significant is observing peaks, which appear in a pure carbonate, bicarbonate, carbamate, amine or protonated amine in an aqueous medium. Isolating those individual peaks is challenging and tedious in CO_2 loaded amine spectra (see from Fig. 5:3 to Fig. 5:5). (Samarakoon *et al.*, 2013) fitted Raman active bands, to an area-normalized Gauss-Lorentzian peak function along with a polynomial baseline where they stated that the accuracy of the method would be dependent on sufficient resolution to clearly distinguish the bands to be analyzed. (Wong *et al.*, 2016) used curve-fitting to resolve complex experimental band envelopes and deconvolution method for band resolution. Using calibration curves, which are obtained from pure chemical spectra, for speciation analysis of the amine-CO_2-H_2O system, is questionable because of the shifts in Raman wavenumbers that were observed in our previous study (Table 5.3). Use of an internal standard and concentration determination based on scattering molar intensity factor also have provided promising results in literature but they cannot be used in in-situ analysis. Thermodynamic models are based on assumptions and limited for pre-defined conditions. Therefore developing calibration models using the thermodynamic

model data is also not always reliable. For spectroscopic data, PLS calibration with test set validation, adequate number of calibration and validation data and reliable reference analysis method generates more reliable quantitative results because it is built on realistic data. This approach has more representation of the actual chemical data without losing important information and it allows updating the calibration model for changes in the measured system (see section 8.2.2).

Table 4.1. Spectroscopic methods in analyzing CO_2 absorbed amine solutions

Reference	Instrument	Solvents analyzed	What were analyzed by spectrometers?	Description
(Robinson *et al.*, 2011)	ATR- FTIR	piperidine	Qualitative analysis of carbamate and bicarbonate	Analysis by peak intensity variation. The chemical reactions between CO_2 and the functionalized piperidines were followed in-situ.
(Archane *et al.*, 2011)	FTIR	Water- DEA-polyethylene oxide 400 system	Concentration of the molecular form of absorbed CO_2 and the evolution of the carbamate species	Calibration based on peak intensity variation
(Richner *et al.*, 2012)	ATR-FTIR	MEA, DEA, and AMP	Bicarbonate, carbamate, protonated amine, free amine and total CO_2	The method is based on a mathematical hard modeling. Equilibrium constants were fitted from the absorbance at different peaks
(van der Ham *et al.*, 2014)	UV-vis	MEA	-	For all measured wavelengths, UV-vis measurements was not successful for pilot scale samples and therefore MEA wt% and CO_2 wt% were determined based on correlation from conductivity, pH, density and refractive index.
(van Eckeveld *et al.*, 2014)	NIR UV−vis	MEA	MEA wt% CO_2 wt%	Density, conductivity, pH, viscosity, sonic speed, refractive index, NIR spectra, and UV−vis spectra were assessed when solvent composition was changed and in the presence of contamination. Density, conductivity, pH, refractive index, sonic speed, and NIR were included to prepare calibration model.
(Kachko *et al.*, 2016a).	NIR, ATR-FTIR	MDEA, PZ	MDEA, PZ CO_2 in mol/L	A chemometric model was built using measurements of density, pH, conductivity, sound velocity, refractive index, and NIR spectra. In-line PLS model was validated using ATR FTIR measurements
(Rogers *et al.*, 1997).	FTIR	DEA	CO_2 H₂S	The spectral area over a variable range was used to prepare the calibration model
(Diab *et al.*, 2012)	FTIR	DEA	DEA, DEAH⁺, DEACOO⁻, HCO₃⁻, molecular CO_2 in mol/m³	Based on peak intensity
(Archane *et al.*, 2008)	FTIR- ATR	Water-DEA-CO_2-methanol system	Molecular CO_2, carbamate and bicarbonate	Determination based on peak area
(Einbu *et al.*, 2012)	ATR	MEA	MEA (mol/kg) CO_2 (mol/kg)	PLS regression on selected variable ranges

(Geers *et al.*, 2011).	FTIR- ATR	equimolar solution of β-alanine and potassium hydroxide	CO_2 SO_x, β-alanine	PLS regression on selected variable ranges
(Derks *et al.*, 2011)	FTIR	MDEA	$MDEAH^+$ HCO_3^- MDEA in $kmol/m^3$	Calibration curves were constructed for molecular MDEA, protonated MDEA and bicarbonate ions using peak absorbance at a certain wavenumber
(Jackson *et al.*, 2009)	ATR-FTIR	MEA AMP MDEA	Qualitative analysis of carbamate and carbonate	Demonstrated that both carbamate and carbonate formation can be monitored
(Beumers *et al.*, 2016)	Raman	MEA	MEA $MEAH^+$ HCO_3^- $MEACOO^-$ in mol/L	Calculated the concentration of all components from the areas of all components. To determine the areas, Indirect Hard Modeling was used
(Puxty *et al.*, 2016)	IR-ATR and Raman	MEA and 3-piperidinemethanol	MEA and 3-piperidinemethanol, CO_2 in mol/L	Compared IR-ATR and Raman spectroscopy by developing PLS models to predict amine and CO_2 concentrations. They experienced that fluorescence disturbed the Raman measurement acquisition in pilot plant data while IR-ATR was successful.
(Ohno *et al.*, 1999)	Raman	2-(N-methylamino)ethanol	-	Vibrational assignments to carbonate, bicarbonate and amine carbamate of the system
(Kachko *et al.*, 2016b)	Raman, NIR, ATR-FTIR	MEA	CO_2 loading	They claim that all three spectroscopies well suit for CO_2 loading analysis
(Souchon *et al.*, 2011)	Raman	MEA, DEA, MDEA	free amine, protonated amine, bicarbonate and carbonate anions are determined for MDEA in mol/L	Reference spectra were recorded from pure CO_3^{2-}, HCO_3^- and protonated amine solutions, which were used to quantify species in MDEA by Direct Classical Least Squares algorithm. ^{13}C NMR spectroscopy was used to compare the Raman speciation.
(Wong *et al.*, 2015; Wong *et al.*, 2016)	Raman	MEA systems	Complete speciation	Based on calibration by peak area with the use of an internal calibration standard
(Samarakoon *et al.*, 2013)	Raman	MEA, DEA	HCO_3^-, CO_3^{2-}, carbamate	Speciation using molar scattering factor and ClO_4^- internal standard
(Idris *et al.*, 2014)	Raman	MEA	Bicarbonate, carbonate, carbamate	Calibration plots for bicarbonate, carbonate and carbamate species based on peak areas of various concentration of individual species
(Vogt *et al.*, 2011)	Raman	MEA, diglycolamine and MDEA	CO_2 loading analysis and qualitatively reaction monitoring	PLS calibration

(Perinu *et al.*, 2014) showed NMR spectroscopy as a potential candidate for speciation in CO_2 loaded alkanolamine systems reviewing approximately 50 published work such as the work by (Böttinger *et al.*, 2008), (Jakobsen *et al.*, 2005) and (Hilliard, 2008). The time

spend for NMR analysis has the limitation of its use in in-situ applications. Real-time process analyzers are demanded, which allow investigating compositions and structures of matters in molecular scale to replace time-consuming laboratory methods. Complete speciation, which can give fast and accurate data independent of process conditions, is a timely need from lab to industry in the field of CO_2 capture by alkanolamine solutions.

4.3 Multivariate calibration

Multivariate calibration (MVC) is the methodology for using multiple signals to determine property/s of interest and six steps are declared to perform a complete multivariate calibration in determining a concentration of an analyte (Wold *et al.*, 2006).

1. Specification of the analytes with concentration ranges and selection of the instrumental method
2. Selection of a representative set of calibration samples
3. Data pre-processing and transformation to make it suitable for the subsequent data analysis
4. Recording the multivariate signal; and measuring the sample concentration by a reference method
5. Developing the calibration model
6. Use the model to estimate the analyte concentrations in new samples (prediction set)

Out of these six steps, the first five belong to the training phase, and the last belongs to the prediction phase. Most of the process analyzers are multivariate-calibrated using PLS regression which is the most popular application in chemometrics.

4.4 Speciation from Raman spectra

The relationship between Raman intensity and the concentration can be explained by the equation 8 presented by (Larkin, 2011) which says that the Raman scattered light I_R is a function of the incident laser intensity I_0, number of scattering molecules N, frequency of exciting laser v and the squared term of $\left(\frac{\partial \alpha}{\partial Q}\right)$ where α is the polarizability of the molecule and Q is the vibrational amplitude.

$$I_R \propto v^4 I_0 N \left(\frac{\partial \alpha}{\partial Q}\right)^2 \tag{8}$$

Two important conclusions can be derived from this equation. The quantification is possible from a Raman signal since the peak intensity is concentration dependent ($I_R \propto N$), and Raman intensity can be increased by using shorter excitation wavelength or increased laser flux. (Ni *et al.*, 1985) pointed out the incorrect use of peak height to be proportional to peak intensity. They say that spectral intensity is always proportional to the area under a peak and only when two peaks have the same half-widths, peak heights can be used to compare relative intensities. Area under the Raman band is dependent

on temperature. For instance, in the Raman spectral analysis in the C-H stretching region of proteins and amino Acids by (Howell *et al.*, 1999), they have noticed a change in spectral band area with temperature. Since more photons are measured when determining peak area and inclusion of band width and shape changes, this method has been proven to be more accurate than peak height method (Pelletier, 1999).

4.5 Speciation and thermodynamic models

Thermodynamic modelling of CO_2-H_2O-alkanolamine systems provide a theoretical approach for speciation even though it has still many unresolved issues (Hessen *et al.*, 2009). These models, which are important in design, and optimization of the CO_2 capture processes, have been widely used is modelling and simulation software packages for amine-CO_2-H_2O systems. The Kent-Eisenberg model (Kent *et al.*, 1976) is an example which has a simple approach where the equilibrium constants of carbamate formation and dissociation of proton are developed only as a function of temperature. Desmukh Mather model (Deshmukh *et al.*, 1981) utilizes the extended Debye-Hückel expression to represent activity coefficients. The Electrolyte NRTL model (Chen *et al.*, 1986) examines the behaviour of aqueous multicomponent electrolyte systems to predict excess Gibbs energy. This model was chosen by (Austgen *et al.*, 1989) and (Posey *et al.*, 1997) to describe speciation in amine- CO_2 -H_2O systems. (Hilliard, 2008) updated these models using speciation data from NMR spectra. The extended UNIQUAC model was developed by (Thomsen *et al.*, 1999) and this model requires binary interaction parameters and UNIQUAC volume, surface area parameters and standard thermodynamic properties for calculations. (Faramarzi *et al.,* 2009) applied the extended UNIQUAC model to represent carbon dioxide absorption in aqueous monoethanolamine (MEA), methyldiethanolamine (MDEA) and their mixtures. Accurate modelling of thermodynamic properties requires the availability of reliable experimental speciation data and their dependence on thermodynamic state (eg: temperature, pressure). Thermodynamic models should be updated with speciation data to make them representative to real data.

PART 2
Model Calibration, Validation and Demonstration

5 Multivariate Model Development
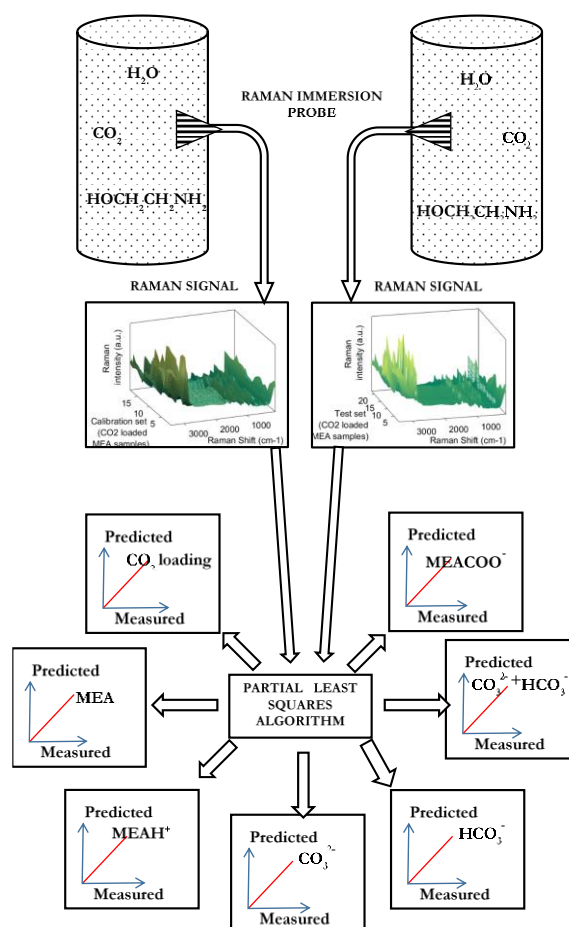
Graphical Abstract

In chemometrics knowledge, information, data and measurements are combined together using a set of mathematical tools to describe science based on the experimental results. A calibration model in chemometrics deviates far more than traditional modelling which are based on assumptions or theories because it is built on an experimental investigation.

5.1 Seven chemometric calibration models for complete speciation

The overall objective of this chapter is to provide the underlying concept of model calibration while presenting the methodology and results of the seven chemometrics models developed for complete speciation in an amine-based CO_2 capture process.

MEA-CO_2-H_2O system is converted into a pool of multiple cations, free molecules and anions after they have reached their chemical and vapour-liquid equilibrium. For instance, some part of the CO_2 is converted into carbonate and bicarbonate while the amine is converted into protonated amine and carbamate. A small proportion of water is also protonated. These conversions eventually result in ionic and neutral species in the solution as shown in Fig. 5:1. The concentrations of these species are constrained on the mass balance and the reaction equilibrium which are again dependent on several factors such as temperature, pressure and pH. When the reaction is taken place in a continuous process such as in packed columns then several other factors also govern the specie concentrations such as gas and liquid flow rates, packing type and their physical properties. Determining these specie concentrations is important in lab experiments as well as in industry because these values describe the fate of solvent and solute in the solution. For R&D people working with solvent development, reaction kinetics, and thermodynamic model development each of these species concentration are important and for people working in the plant, plant design and scale up the total CO_2 loading and the MEA concentration are important values. Considering the requirements of all these groups, the complete speciation in the MEA-CO_2-H_2O system can be segregated into seven parts (models) as shown in Fig. 5:1 and Table 5.1. For a given temperature and pressure condition, the complete speciation results in an MEA-CO_2-H_2O system can be adequately described by model number 2,3,4,6 and 7. The total CO_2 and amine concentrations can be obtained from the sum of values of models [2+3+4] or and [2+6+7] respectively but for easiness a unique model was developed as CO_2 loading model which can directly give the value (model 1). Formation of carbonate and bicarbonate in the system is comparatively very low and hence some are interested in the total of carbonate and bicarbonate concentration. This can be satisfied as the summation of models [3+4] but a unique model was developed to determine the total of carbonate and bicarbonate (model 5) directly from the Raman measurements.

Table 5.1. Seven Raman spectroscopy based calibration models
(* considering C specie balance; **considering amine specie balance)

Model no:	Model name
1	CO_2 loading
2	Carbamate ions
3	Carbonate ions
4	Bicarbonate ions
5	Total carbonate and bicarbonate ions
6	Unreacted amines (free amines)
7	Protonated amines

=CO_2 loading*

=CO_2 loading*

=total MEA**
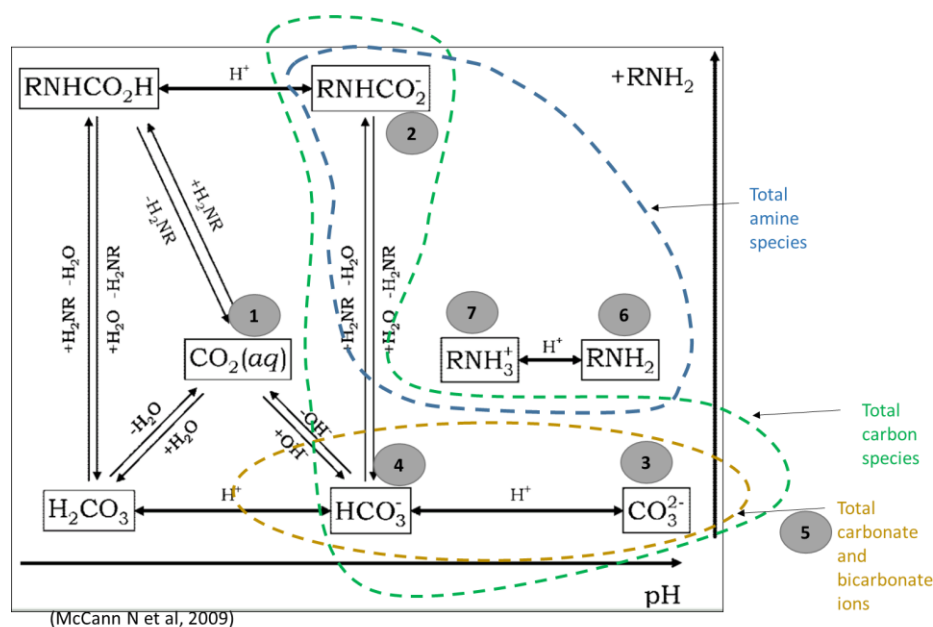
Fig. 5:1. Seven models developed in this study (modified diagram with permission from (Nichola McCann, 2009). Copyright (2009) American Chemical Society

X data which are the measurements from the Raman spectrometer was common for all the models (prior to preprocessing, variable selection and outlier removal). Y data which consisted of individual speciation results from reference analysis (NMR - Bruker Avance III 400 MHz spectrometer) were used for each respective model. The basic definitions of abbreviations which are written throughout this chapter can be found in Table 5.2.

Table 5.2: Basic definitions of abbreviated terms related to model development

An *i* PLSR model predicts specie *i* concentration using,
> X data → Raman spectroscopy measurements for a set of CO_2 loaded amine samples and
> Y_i data → concentration of specie *i* in a set of CO_2 loaded amine samples as determined by the reference analysis (NMR spectroscopy)

Two unloaded (without CO_2) and loaded (with CO_2) amine stock solutions were used to prepare a series of samples having different total CO_2 absorbed. The term "CO_2 loading" is expressed in units of mol CO_2 per mol amine (if not explicitly stated otherwise) to indicate the absorbed CO_2 in the solution. A complete description of sample preparation, methodology and laboratory measurements related to calibration model development is presented in Paper A. For the preparation of validation series, the same procedure was followed at same environmental conditions to that of calibration series (room temperature and pressure) but different stock solutions were used to make the validation set (test set) to realistically represent inherent variations in a new data set which could contribute to validate the models sucessfully (Esbensen *et al.*, 2010a).

5.2 Raman vibrational modes related to the MEA-CO₂-H₂O system
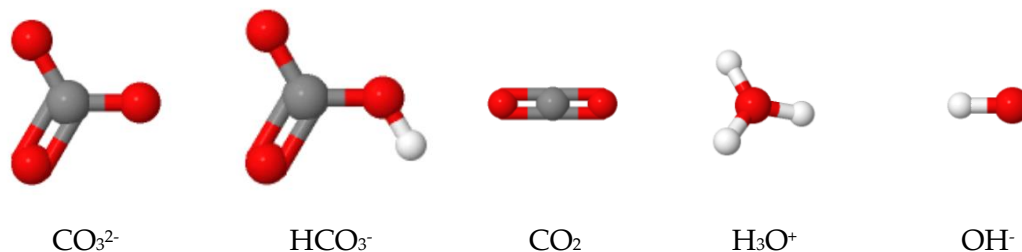
| CO_3^{2-} | HCO_3^- | CO_2 | H_3O^+ | OH^- |

Fig. 5:1. 3-D molecular structures of CO_3^{2-}, HCO_3^-, CO_2, H_3O^+ and OH^-

.

| $HOCH_2CH_2NH_2$ | $HOCH_2CH_2NH_2COO^-$ | $HOCH_2CH_2NH_3^+$ |
| (MEA) | (MEACOO⁻) | (MEAH⁺) |
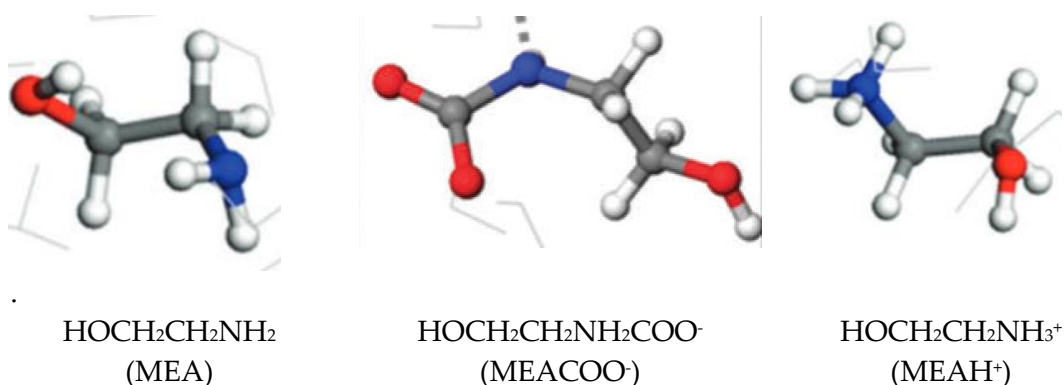
Fig. 5:2.   3-D molecular structures of MEA, MEACOO⁻ and MEAH⁺

Fig. 5:1 and Fig. 5:2 show 3-D structures for the chemical species that are found in a CO_2 loaded aqueous monoethanolamine solution in equilibrium or non-equilibrium conditions. A linear molecule (one where all the atoms are in a straight line in space, eg: carbon dioxide) consisting of N atoms, has 3N - 5 fundamental vibrations. A nonlinear molecule with N atoms has 3N - 6 fundamental vibrations (Socrates, 2000). Vibrations can be Raman active or infrared active. The characteristic absorptions of functional groups over the entire infrared region can be found in literature which assist to identify the Raman active bands for the above molecular structures (Larkin, 2011; Socrates, 2000). Fig. 5:3, Fig. 5:4 and Fig. 5:5 provide a summary of Raman active vibrational modes that can be typically observed for the species in an MEA-CO₂-H₂O. This summary was used as guideline to select wavelength ranges for calibration models in the following sections.
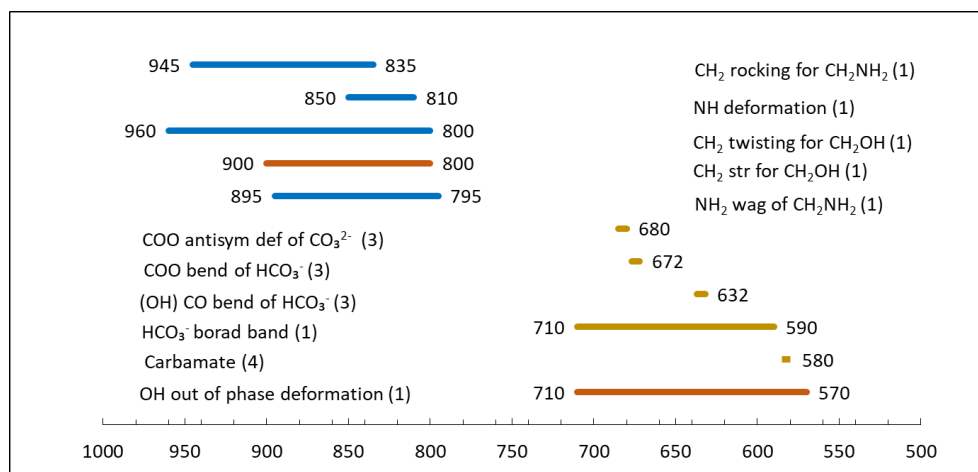
Literature references are mentioned within brackets are,
(1) (Socrates, 2000), (2) (Larkin, 2011), (3) (Davis *et al.*,
1972a), (4)(Samarakoon *et al.*, 2013)

Fig. 5:3. Vibrational assignments of the chemical species present in an MEA-CO2-H2O system between Raman shift from 500 to 1000 cm-1
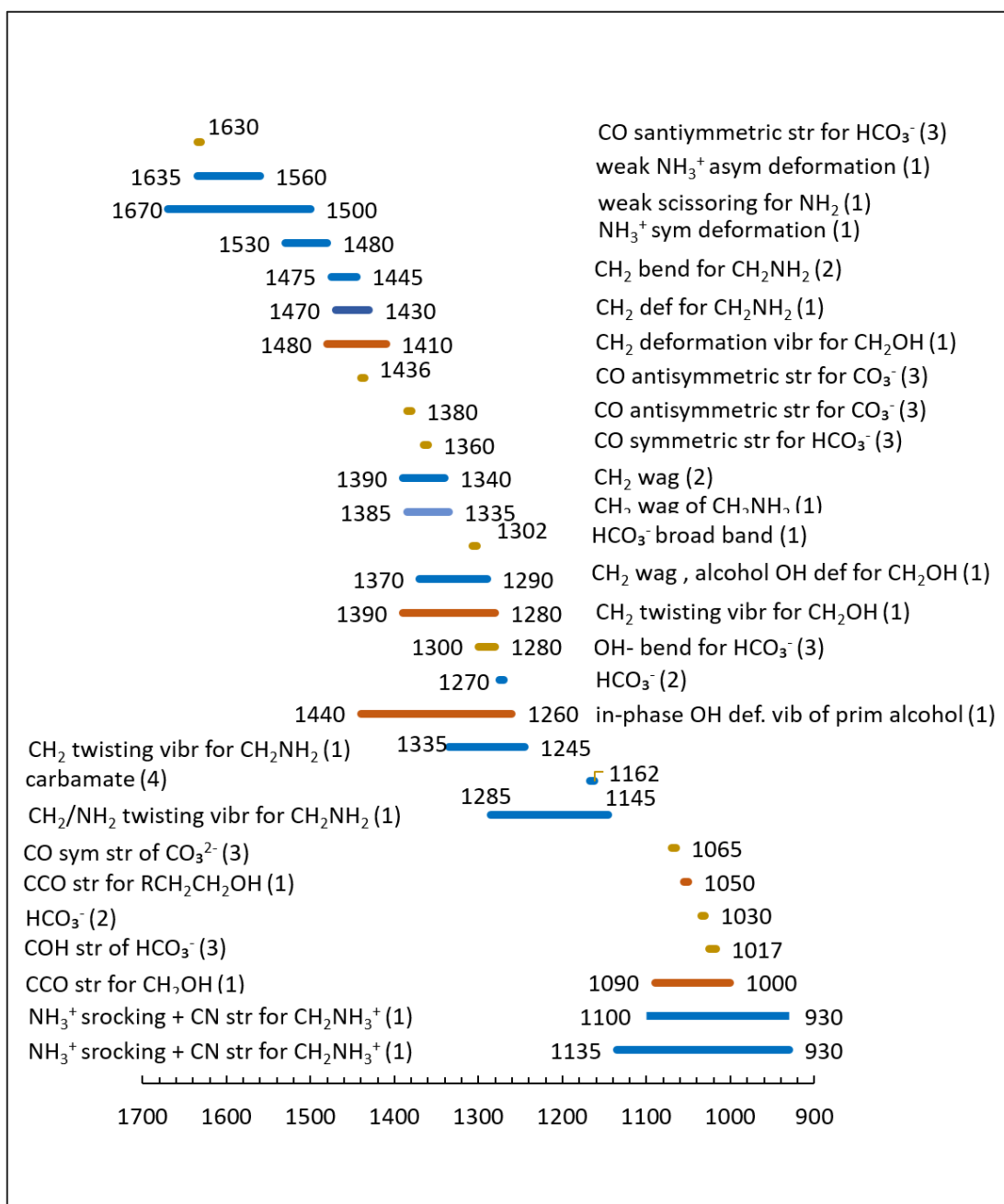
Literature references are mentioned within brackets where (1) (Socrates, 2000), (2) (Larkin, 2011), (3) (Davis *et al.*, 1972a), (4)(Samarakoon *et al.*, 2013)

Fig. 5:4. Vibrational assignments of the chemical species present in an MEA-CO$_2$-H$_2$O system between Raman shift from 900 to 1700 cm^{-1}
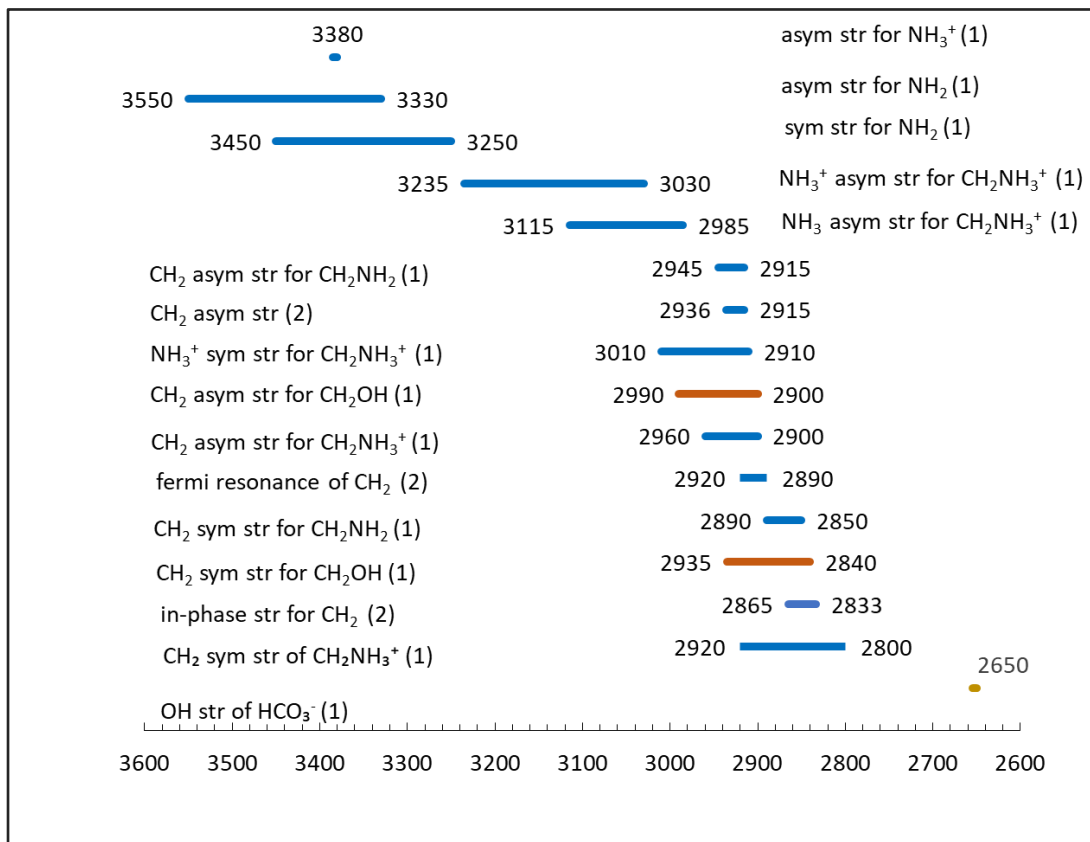
Literature references are mentioned within brackets where (1) (Socrates, 2000), (2) (Larkin, 2011), (3) (Davis *et al.*, 1972a), (4)(Samarakoon *et al.*, 2013)

Fig. 5:5. Vibrational assignments of the chemical species present in an MEA-CO₂-H₂O system between Raman shift from 2600 to 3600 cm⁻¹

A typical multivariate calibration model is developed in three stages as shown in Fig. 5:7. In the first stage, the X calibration data is used to build a relationship with the Y calibration data. This relationship (model) is then used to predict new Y data based on X validation data. This predicted Y validation data is compared with the measured Y validation data. The model is optimized to achieve a minimum deviation between the predicted and measured Y validation data. The process flow of the chemometric model development used in this study is explained in Fig. 5:10 when X data were Raman spectroscopic measurements and Y data were chemical concentration of a component or a group of components.

Fig. 5:6 shows the experimental set up which includes the Raman spectrometer (Kaiser RXN2 analyzer), fibre optic cables (5m in length) and Raman MR immersion probe (1/4 inch diameter probe head).
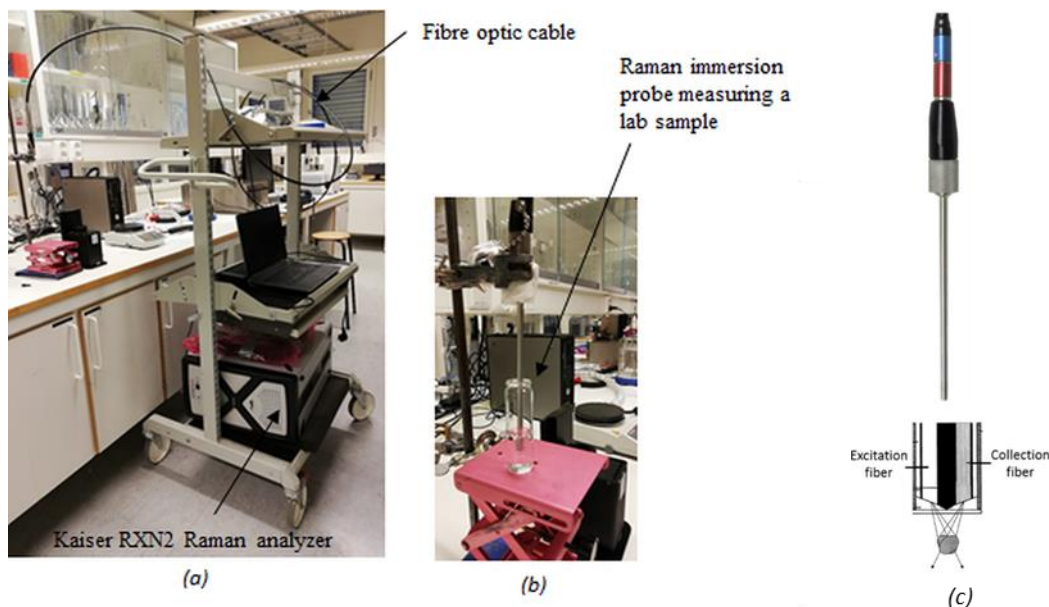
Fig. 5:6. (a) RXN2 analyzer and the fiber optic cables; (b). lab experimental set up using Raman immersion probe to measure a lab samples(c) Fiber configuration of the immersion probe providing focus at the tip of the optics (diagram from (Lyndgaard, 2013))
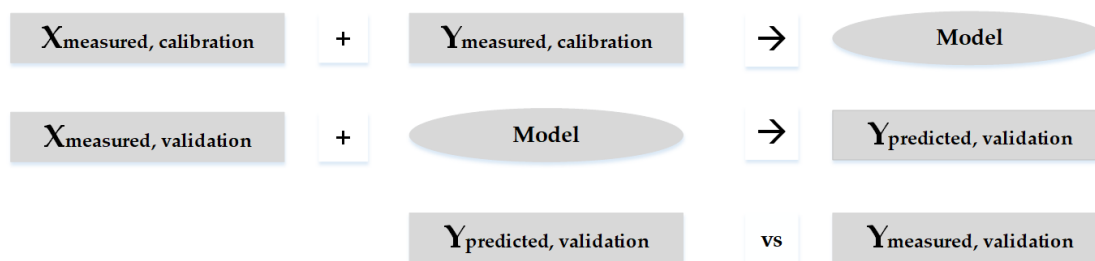
Fig. 5:7. Multivariate model calibration and validation

As shown in Fig. 5:7, the calibration and validation objects are CO_2 loaded aqueous amine samples while calibration and validation measurements (X_{cal} and X_{val}) are Raman spectra of them. X_{cal} and X_{val} were preprocessed and mean-centered while Y_{cal} and Y_{val} were mean-cantered and then models were calibrated and validated with preprocessed data. Raman measurements of these samples spanned in the wavenumber region from 100 to 3426 cm^{-1} as shown in Fig. 5:8 which show different Raman intensities based on their compositions.

The initial run of the calibration models was performed for raw Raman data using the entire wavelength but the model predictability was poor due to the inclusion of noisy (unwanted) wavenumbers. Therefore the optimum wavelength range was selected

which also included vibrational modes of the specie to which the model was built. The optimum preprocessing combination for the X data set of MEA-CO$_2$-H$_2$O solution was found as baseline correction using the Whittaker filter (Eilers, 2003) with lamba = 100 and P = 0.001, scaling by standard normal variate (SNV) and finally mean centering for X data. Fig. 5:9 shows baseline corrected Raman measurements for some of the X$_{cal}$ data where arrow marks point to some Raman active vibrational modes related to CO$_3^{2-}$, HCO$_3^-$, MEACOO$^-$, MEA and MEAH$^+$. In addition, Table 5.3 shows vibrational modes identified in this study. The information provided by the PLS loading plot was used in combination of the vibrational modes to select the variable range in this study. PLS toolbox 7.3 in Matlab 2016a was used for preprocessing and data analysis.

Table 5.3. Vibrational assignments of species in MEA-CO$_2$-H$_2$O system

(modified table from (Jinadasa *et al.*, 2017))

Specie	Frequency (cm^{-1}) observed in		Vibrational mode [reference]	Bands identified in		
	our studies	literature		1	2	3
MEA	417	417	CC deformation (Socrates, 2000)	√	√	√
	481	481	CC deformation (Socrates, 2000)	√	√	√
	843	845	CH$_2$ rocking + CN stretching (Batista De Carvalho *et al.*, 1995)	√	√	√
	871	873	CH$_2$ rocking + CN stretching (Batista De Carvalho *et al.*, 1995)	√	√	√
	1029	1030	CN stretching (Larkin, 2011)	√	√	√
	1464	1460	CH bend (Larkin, 2011)	√	√	√
	2885	2870	CH$_2$ symmetric stretch (Larkin, 2011)	√	√	√
	2934	2930	CH$_2$ asymmetric stretch (Larkin, 2011)	√	√	√
MEACOO$^-$	1160	1155	C N stretching (Coates, 2006)		√	√
MEAH$^+$	1277	1274	N-CH stretch (Tseng *et al.*, 2010)		√	√
	1320	1320	CC stretch (Tseng *et al.*, 2010)		√	√
	2894	2700-3000	NH$_2^+$ stretching (Socrates, 2000)		√	√
	2975	2700-3000	NH$_2^+$ stretching (Socrates, 2000)		√	√
CO$_3^{2-}$	1070	1065	Symmetric CO stretching (Davis *et al.*, 1972b)		√	√
	1385	1380	Antisymmetric CO stretching (Davis *et al.*, 1972b)		√	√
HCO$_3^-$	1024	1017	C-OH stretching (Davis *et al.*, 1972b)		√	√
CO$_2$	1278	1274	CO$_2$ symmetric stretch + CO$_2$ bend overtone (Larkin, 2011)		√	√
	1389	1383	CO$_2$ Symmetric stretch + CO$_2$ bend overtone (Larkin, 2011)		√	√

1 = in CO$_2$ unloaded 30% MEA samples; 2 = in calibration and validation samples – PLSR; 3 = lean and rich amine streams in USN rig
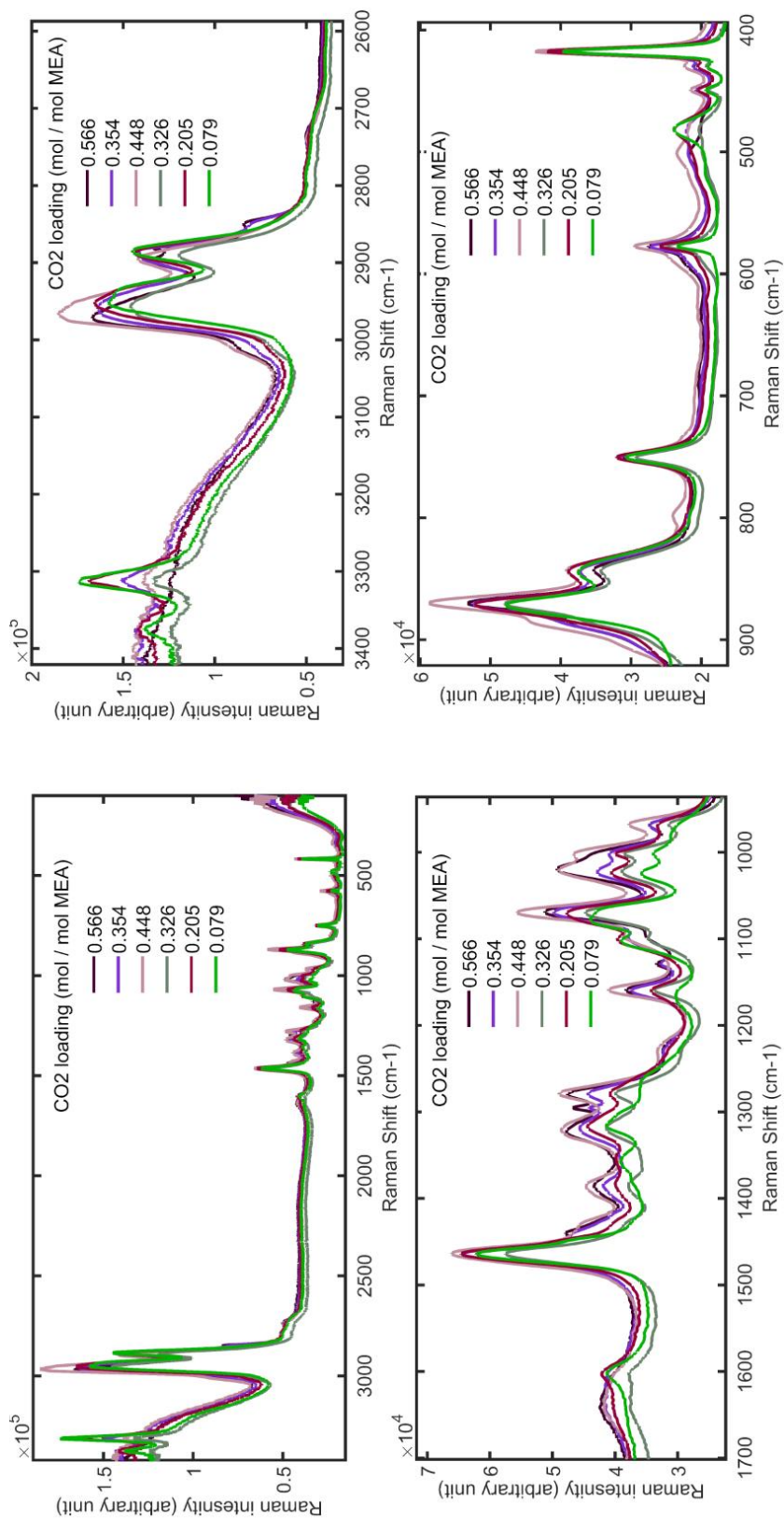
Fig. 5:8. Raman spectra for CO₂ loaded MEA samples ; wavelength region (a) [3426-100]cm⁻¹, (b) [3426-2600]cm⁻¹(a) , [1700-1000]cm⁻¹(a) [1000-400]cm⁻¹
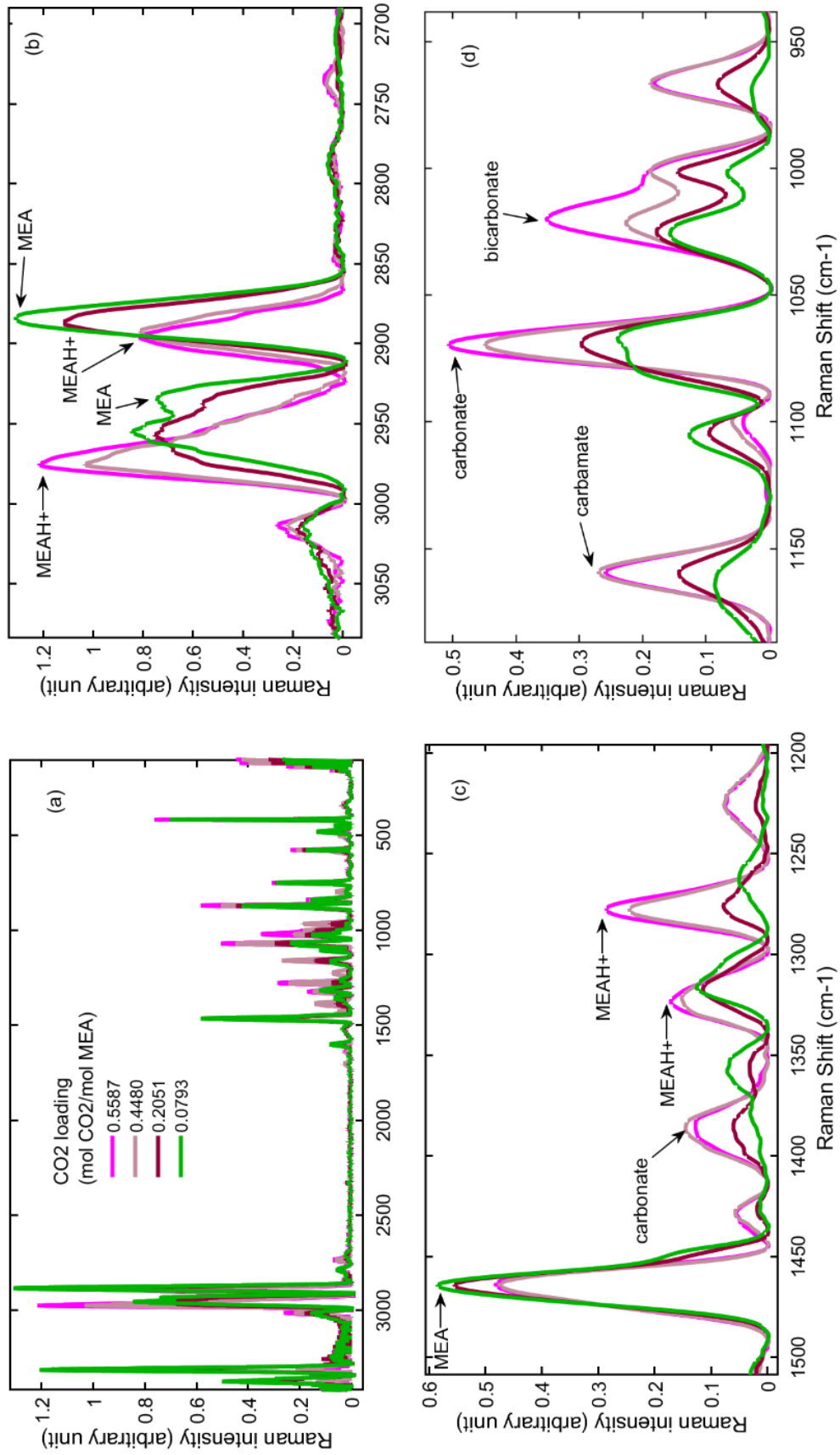
Fig. 5.9. Baseline corrected Raman spectra for CO$_2$ loaded MEA samples ; wavelength region (a) [3426-100]cm^{-1}, (b) [3050-2700]cm^{-1}, (c) [1500-1200]cm^{-1}, (d) [1150-950]cm^{-1}
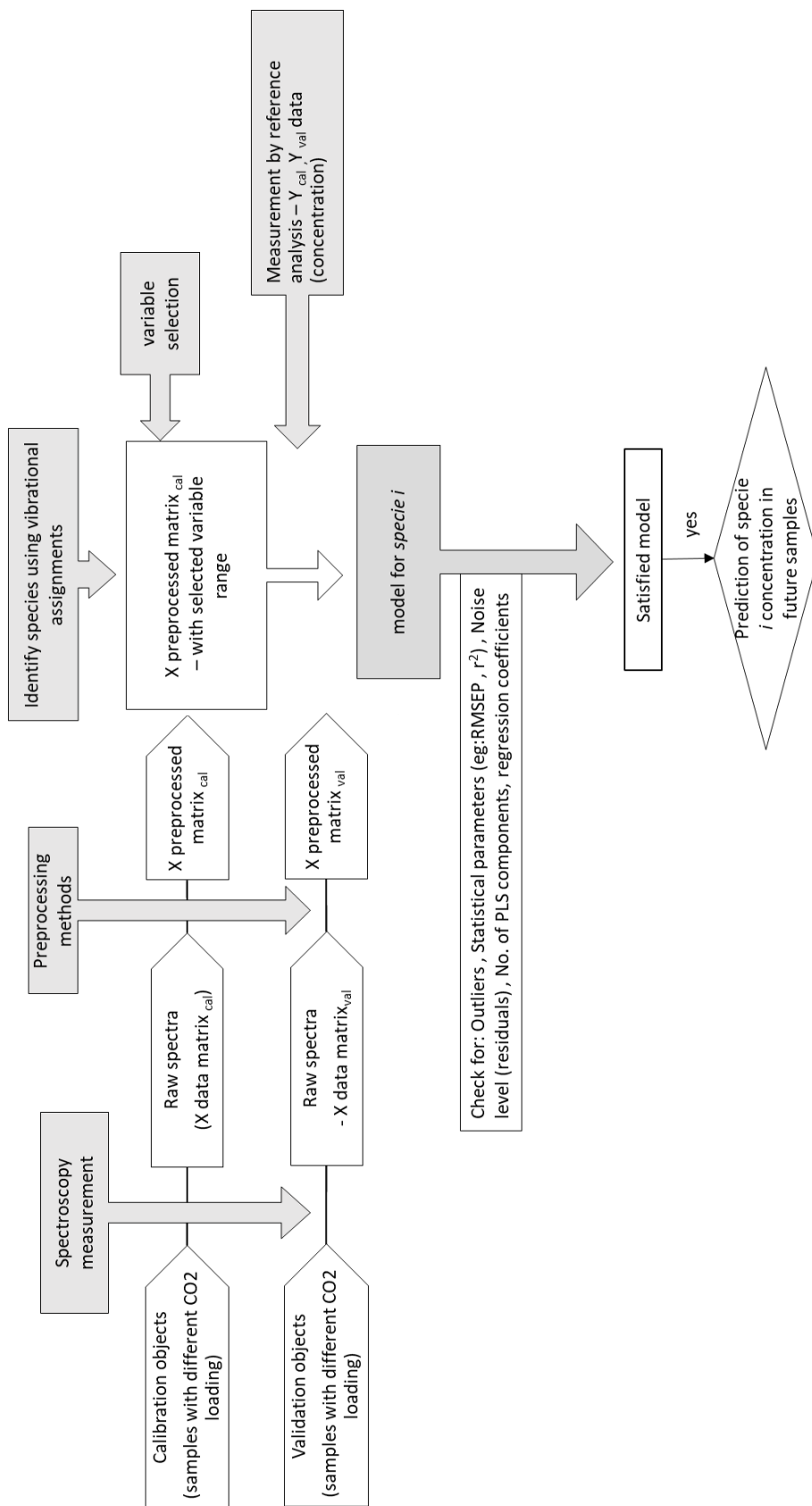
Fig. 5:10. Process flow of the chemometric model development for specie i (refer Fig. 6:4 for the extended version of the process flow)

Results of the seven chemometric models are presented in Fig. 5:11 and Fig. 5:12 where the predicted vs measured concentrations of the calibration and validation samples are shown for all the seven models and an additional model prepared for total CO_2 loading with the units of mol CO_2 per kg H_2O. These results are also presented in Paper A.
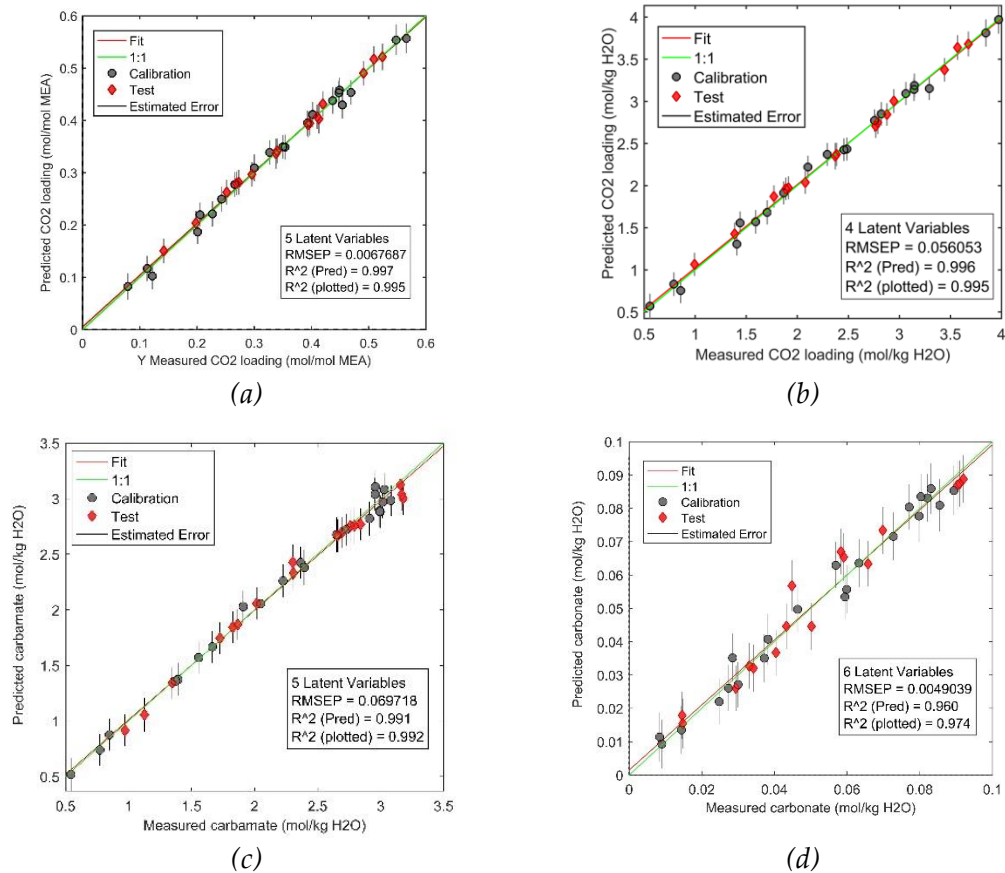
Fig. 5:11. Comparison of measured vs predicted concentrations for validation dataset using the developed models; (a). CO_2 loading model (mol/mol MEA); (b). CO_2 loading model (mol/kg H_2O); (c). carbamate (mol/kg H_2O); (d). carbonate (mol/kg H_2O); plots also include calibration data

For each model, the number of PLS components selected (latent variable), RMSEP values, r^2 of the test set and calibration data, target line (as 1:1), regression line (fit) and estimated error from the model are presented. The definition of RMSEP is given in equation (9) where $y_{predicted}$ is the predicted value from the PLSR model, $y_{measured}$ is the measured value from NMR spectroscopy and I is the number of samples in the validation data set.

$$RMSEP = \sqrt{\frac{\sum_{i=1}^{I}(y_{predicted} - y_{measured})^2}{I}} \qquad (9)$$

(e)

(f)

(g)

(h)
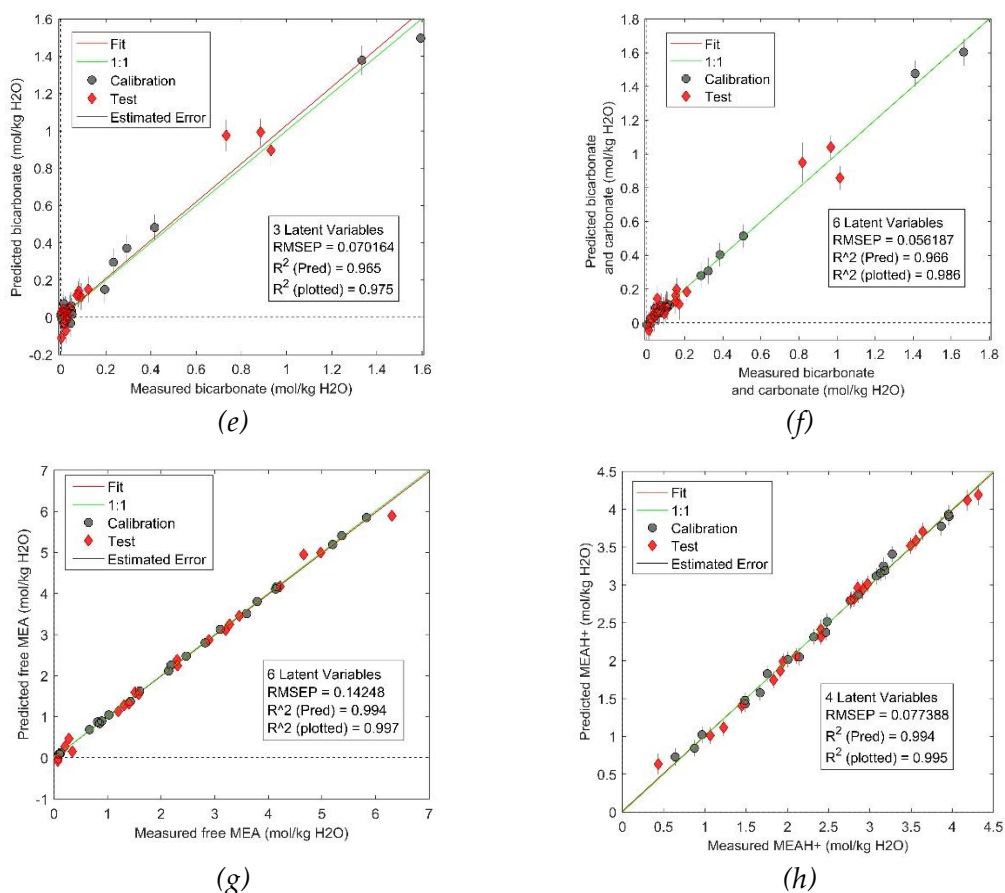
Fig. 5:12. Comparison of measured vs predicted concentrations for validation dataset using the developed models; (e). bicarbonate (mol/kg H$_2$O); (f). bicarbonate+carbonate (mol/kg H$_2$O); (g). free MEA (mol/kg H$_2$O); (h). protonated MEA (mol/kg H$_2$O); plots also include calibration data

The range of the initial calibration set was 0 to 0.612 CO$_2$ loading. After reducing outliers this range was contracted but remains in the industrial lean and rich CO$_2$ loading range. r^2 is more than 0.979 for calibration sets in all the models while that for prediction was gained more than 0.96. All the models are expressed in units of mol/kg H$_2$O. Molal concentration (amount of substance per mass of solvent) was used instead of molar concentration (amount of substance per unit of volume) to remove the effect of volume expansion when the temperature increases.
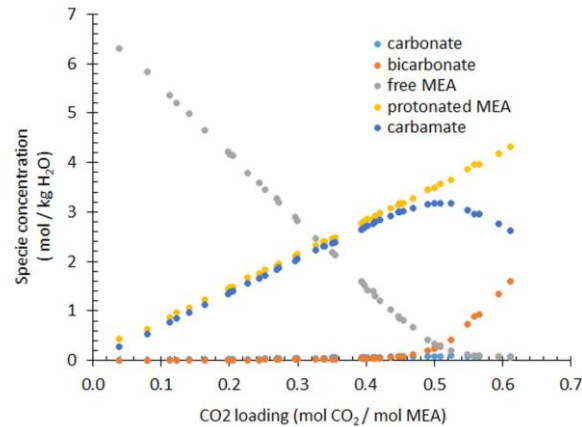
Fig. 5:13. ¹³C NMR analysis - concentration of different species vs CO₂ loading
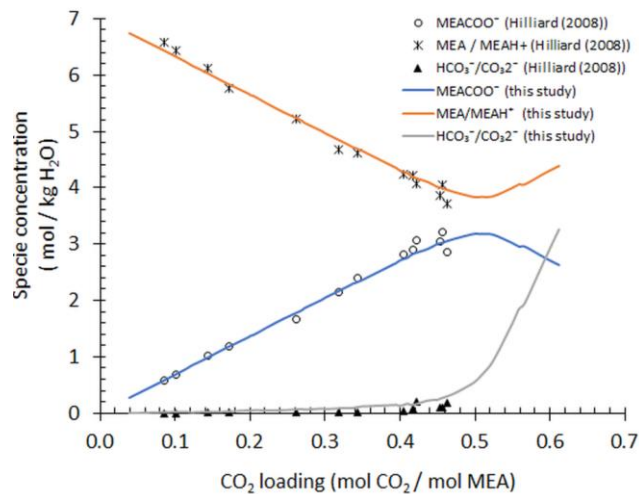
Fig. 5:14. Speciation for MEA-CO₂-H₂O system by NMR; Comparison of this study (after removing outliers) with work by Hilliard (2008)

Results in Fig. 5:11 and Fig. 5:12 reveal that the calibration and validation samples span unbiasedly in the concentration ranges for all the species except for plot (e) and (f). The reason can be explained by Fig. 5:13 which gives an overview of the NMR analaysed concentrations of all the species in the calibration and validation data. A sudden exponential increase of bicarbonate concentration after some CO₂ loading due to the increase of pH value in the system can be seen in this figure which is the reason for unbiased data in Fig. 5:12 (e) and (f).

The number of calibration and validation samples used for each model and the selected wavelength range which yielded the optimum RMSEP value are shown in Table 5.4.

Table 5.4. Summary of PLSR models for speciation

Model no:	Model name	Wavelength range [cm^{-1}]	Number of samples (after removing outliers)	
			Calibration	Validation
1	CO_2 loading (mol/mol MEA)	[770-901] ,[991-1202] ,[1398-1498]	22	16
	CO_2 loading (mol/mol kg H_2O)	[770-901] ,[991-1202] ,[1398-1498]	20	15
2	Carbamate	[1100-1200]	22	17
3	Carbonate	[1493-1404] , [1091-1047] , [853-895]	22	21
4	Bicarbonate	[1047-773]	21	21
5	Carbonate + bicarbonate	[1513-1410] , [1138-779]	21	22
6	Free MEA	[2996-2867] , [1508-803]	22	20
7	MEAH$^+$	[3010-2887] , [1336-1251]	22	20

5.3 From a 'bad' model to a' good' model

The chances of developing a calibration model to a satisfactory level in a single attempt are occasional. Several iterative cycles are performed to get a better prediction from a regression model. The results presented in Fig. 5:12 are those obtained after several such attempts. The aim of this section is to describe the possibilities to achieve a 'good' model (more robust, less prediction error) from an initial 'bad' model (unstable, high prediction error) using same calibration/validation X/Y data. Fig. 5:15, is an extended version of Fig. 5:10 where the dotted lines mark the options (A-I) that were followed in this chemometric study during the model development stage until a satisfied model is achieved. A detailed description of improvement strategies for a chemometric model is provided from 5.3.1 to 5.3.8, based on the experiences gained from this study.
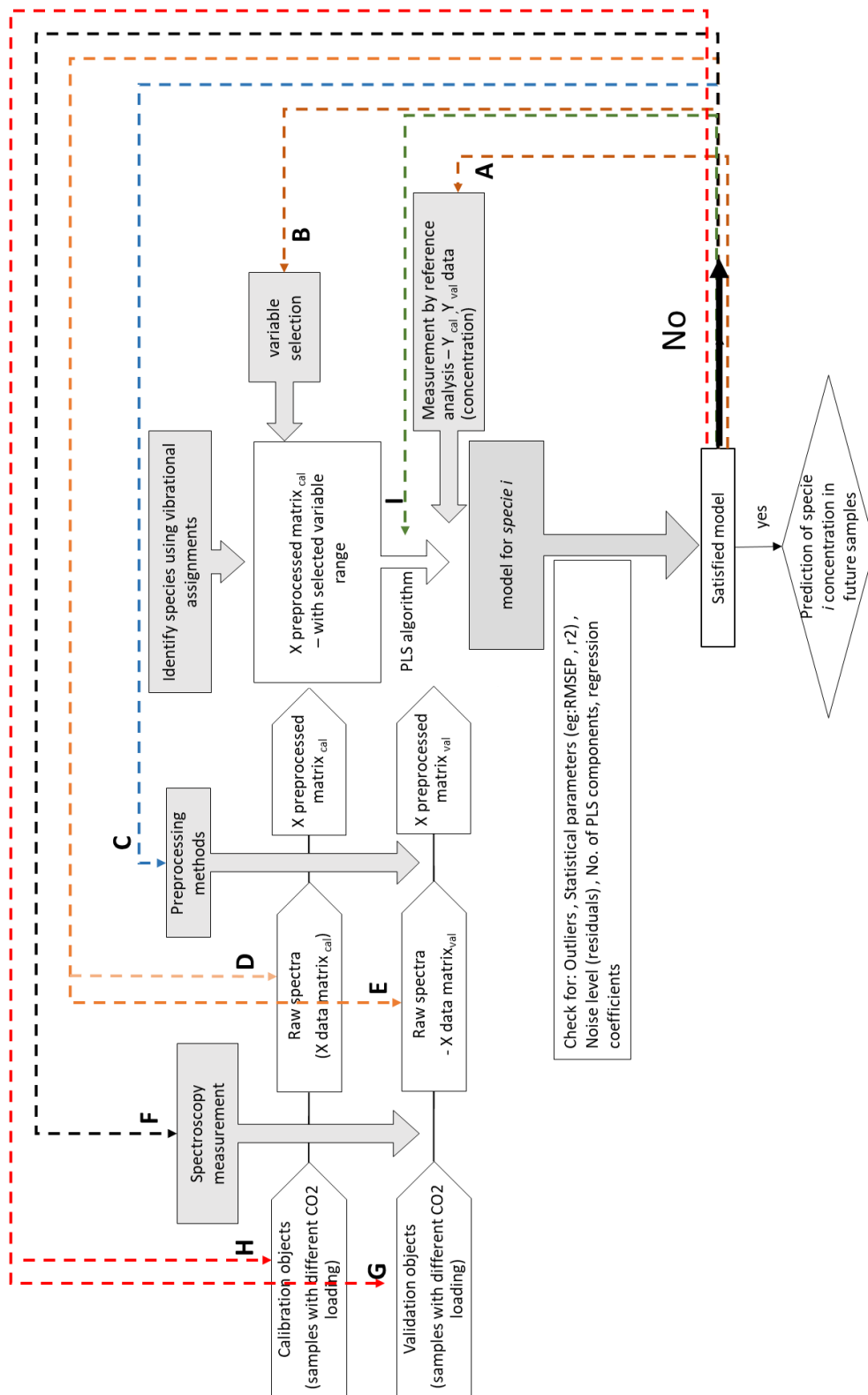
Fig. 5:15. Process flow of the chemometric model improvement strategies

5.3.1 Removing outliers

Outliers represent irrelevant (erroneous or abnormal) data with respect to the data structure of the majority samples. Presence of outliers in a model is responsible of making the model unstable, poor predictable or sometime mislead the entire model development process. Outliers represent some sort of 'bad' errors and should be eliminated, corrected or unaltered only after a thorough investigation because they sometimes reveal important information about the sample composition or process (Næs *et al.*, 1984). In PLS since both X and Y data are used, outliers can be in objects, variables or reference values which are associated with operator mistakes, instrument noise and drift, out-of-spec samples, incorrect sample preparations, sample deterioration due to environmental discrepancies, and sampling errors. In spectroscopic measurements cosmic spikes can be one of the reasons for X outliers which appear as very narrow peaks caused by high energy cosmic rays typically due to an issue in CCD detectors. These detectors have photon noise, dark noise and read noise which make such spikes. In chemometrics, outlier detection is scoped in entire cradle to grave process. But in conventional analytical chemistry or data analysis, outliers are just considered as errors in the analytical methods, results mis-manipulation and operator mistakes. Some people are over confident of the results from analytical instruments just because they are sophisticated and give digital results.
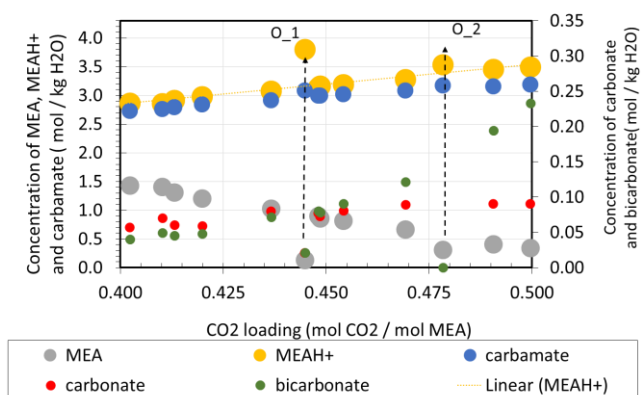
Fig. 5:16. Two outliers with abnormal specie concentrations spotted from Y data – calibration/validation samples in the CO_2 loading range 0.4 to 0.5

There are several ways to detect outliers. In this study, two outliers were early spotted by checking the *y* reference values. As shown in *Fig. 5:16* sample marked as O_1 and O_2 show an over estimated protonated MEA values and under-estimated carbonate, bicarbonate and free MEA values which could be easily identified as they are located outside of the trend after plotting the standard speciation graph for amine speciation data which is CO_2 loading vs. specie concentrations. It is always less time consuming and easy to detect such abnormalities using bi-plots other than reading tabulated values. Checking outliers in y reference values including checking whether standard procedures are followed and reference analysis instrument behaved normally for all the Y measurements. Such an investigation revealed that the reason for two outliers was a

measurement error from NMR instrument. Sample O_1 and O_2 did not show a peak for free amine and bicarbonate in the NMR spectra respectively. A, H, G, D and E in Fig. 5:15 marks the places where outliers in X and Y measurements should be spotted. Out of these D and E are referred for checking irrelevant data structures from X measurements. In spectroscopic data, the number of peaks, their position and intensity reveal information required for modelling and hence it is required to assure the accuracy and precision of the instrument for spectral resolution, wavenumber and intensity response. These factors are dependent on various components of the instrument such as optics, grating, detector, slit, laser excitation wavelength, temperature and time stability. Normally the vendor specifies the required time for wavelength and intensity calibration. They also provide guidelines of the maintenance frequency. If such calibration requirements are only for once (during the life time of the instrument) or annual basis, the user can set up an own schedule and procedure for a simple calibration. Throughout this study, an acetone Raman spectrum was taken before starting each new measurement series and was compared with a library spectrum for peak position and intensity as a confirmation that the instrument, fibre optic cables and immersion probes were performing as intended.

An abnormal spectrum is easy to identify in preprocessed data because they are de-noised. When such an observation is made it is mandatory to check whether it is spectroscopy related or sample related. Some of the operator related mistakes that can result in abnormal spectra are probes not cleaned well, lose connections between probe and fibre optic cables, contact of probe tip with foregin matters such as the walls of the sample container, inadequate probe immersion depth, air bubbles on the probe tip and fluoresence. In this study, the fluorescent effect from external lights was avoided by covering the sample containers with a black box (Jinadasa *et al.*, 2018b).
 Several mistakes can happen during the sample preparation stage such as not using properly cleaned glassware, sample inhomogeneity within same container, phase separation inside the sample container, evaporation of chemical components in the sample (solvents, water or carbon dioxide), change in environmental conditions that alter the chemical equilibrium, long time duration between X and Y measurements, sample deterioration due to inappropriate storage and interfrences from gaseous/solid or liquid impurities and they contribute for poor predictability in the model. t-u plots in PLS analysis provide opportunities to detect outliers easily while the residual Q vs. Hotteling T^2 diagrams (influence plots) also do the same job. In the paper (Rodionova *et al.*, 2004) samples in the calibration set are classified as insiders, outsider and absolute outsiders and the authors provide a method called SIC model connected to PLS modelling to identify outliers in calibration data.

5.3.2 Optimising signal to noise ratio

Maintaining a good signal to noise ratio (SNR) is required to view all the peaks related to a chemical mixture. SNR should be optimum to the eintre concentration in calibration data. Methods to obtain good SNR are ensuring that the instrument is cooled down sufficiently before measurements, have longer exposure times and increase number of

scans per measurement. The model development stage is normally performed in the laboratory where the total exposure time for sample measurements are not a time constraint but when the same model is used in process monitoring, this total exposure time determines the frequency of real time measurements where small time intervals between each measurement are preferred. Therefore SNR is a bottleneck between quality of the spectrum and how fast the the sample should be analyzed. In this study the optimized SNR was gained as 60 second total exposure time which included 6 scans each having 10 second individual exposure times.

5.3.3 Suitable preprocessing and variable selection

An unsatisfed model can be due to the worng chemometric approach used for model development (marked as B and C in Fig. 5:15).

The two main chemometric methodologies followed in this analysis were preprocessing and variable selection. While there are chemical, physical and instrumental ways to obtain a less noisy Raman data, a mathematcal preprocessing method can become the only feasible option to address some inherent or unavoidable properties in a Raman spectra. Such common properties are baseline drift, peak overlapping and wavenumber shifts. Basic preprocessing approaches applied to Raman data can be found in (Liland *et al.*, 2016). Fig. 5:17 shows how the fingerprint area of MEA-CO_2-H_2O Raman spectra behave for different preprocessing methods compared to raw spectra. Some of the preprocessing methods such as detrend, Savitzky Golay and SNV appear to make same conditioning but the subtle differences they have made on the spectra can only be concluded by making a proper quantitative analysis. Suitable preporcessing method/s is specific to the sample type and the measurement instrument. A preprocessing method which filters noise for a one chemical solution can amplify noise for another different solution. Quantitatively how these preprocessing methods affect to the model can be monitored by comparing the RMSEP for different combinations of preprocessing methods.

In this study, variable selection for each PLS model was chosen based on the knowledge of vibrational modes and the information gained from loading plots and regression coefficient plots. However, there are chemometric based mathematical solutions to determine the optimum variable ranges and these are very useful when analysing chemicals which do not have suffcent literature on their vibrational modes. Genetic algorithms and iPLS have proven their capcities for succesful variable selection from spectral measurements (Andersen *et al.*, 2010).
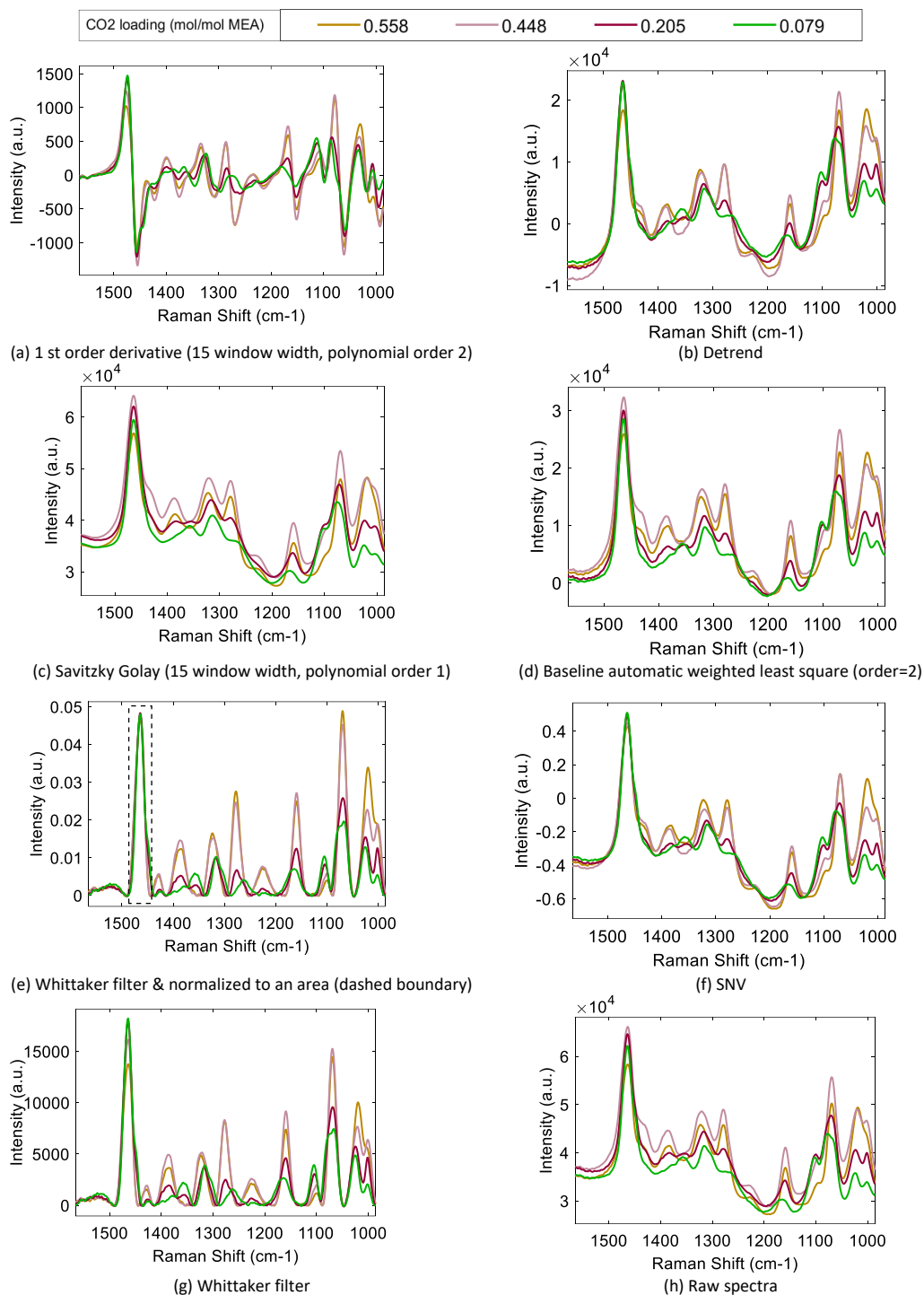
Fig. 5:17. Different preprocessing methods applied to Raman spectra of CO_2 loaded MEA

5.3.4 Cross validation or test set validation?

Another important aspect of yielding an overfitting or underfitting model is the type of validtion method. Namely there are three main validation approaches used in

chemometrics, leverage correction, cross validtion and test set validation. Although there are several published chemometrics models based on cross validation, the risk of getting an overfitting model is high as illustred in Fig. 5:18. In the reference literature from (Esbensen *et al.*, 2010a), a comprehensive description on how each type of validation methods affect to the model predictivity is presented. Their explanation is that the test set validation is the only valid paradigm and in contrary, cross-validation is a monolithic application and just a sub-optimal simulation of test set validation. They claim that the future prediction situation will have to be characterized by at least one new data set (test set) and eventhough the model RMSE for prediction is higher, test set validation makes a more robust model by inclusion of the sampling errors incurred in all 'future' situations in which the validated model must performed. This is the reason for using test set validation only for all the chemometric models developed in this research.
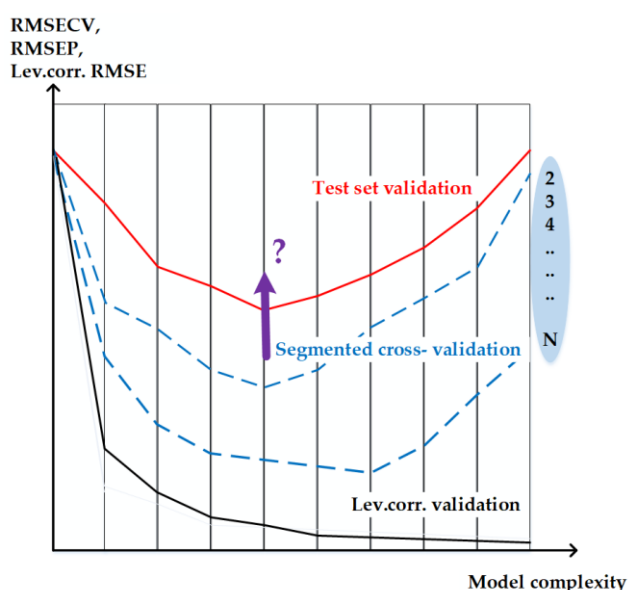
Fig. 5:18. Relationships between root mean square error RMSE of cross-validation (CV) / prediction (P) / leverage correction ((lev.corr.) as a function of model complexity (number of PLS components) Source : Modified diagram based on orginal work by (Esbensen *et al.*, 2010a)

5.3.5 Number of samples for calibration and validtion

Another important factor which should be considered even before the model development is started is the minimum number of samples in the calibration/validation set. Higher the number of samples, more robust the model is. Depending on the complexity and the diversity of the sampless, some model model might require hundreds or even thousands of samples for calibration. (Workman, 2001) suggests that 10 or more samples should be used in the calibration set for every principal component in the model. In early studies of chemometrics (Naes *et al.*, 1986) have shown that using

a fewer number of calibration samples and reduced number of wavelengths of the spectra, acceptable results can be obtained where the same number of calibration samples failed to achieve the same results with univariate approach (by MLR). Fig. 5:19 shows how the estimation error curve move depending on the amount of data. When the number of data and their preceision are higher a model can be developed with a less number of latent variables and lower prediction error than when using few or noisy data. Cost of sample preparation and analysis (specially the reference analysis), time and resoruces become constraints for having a large number of data set. In this study, cost of NMR analysis became the limiting factor for maximum number of calibration samples used in the initial model development.
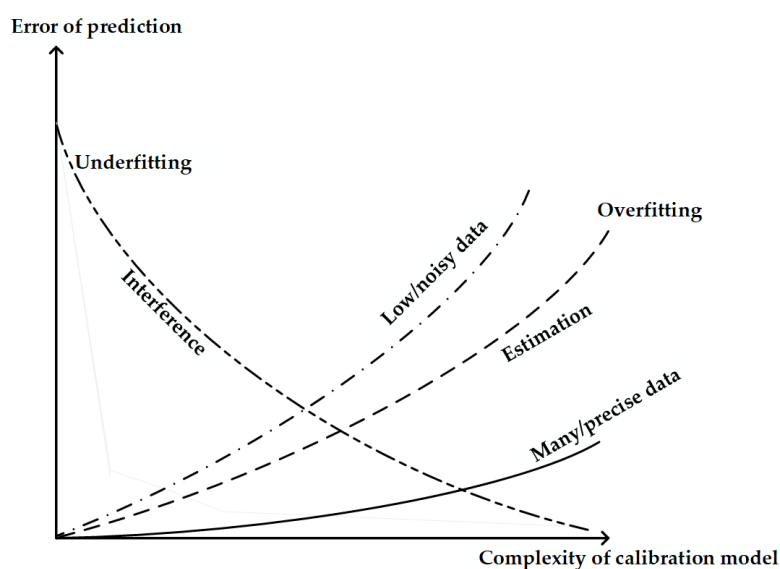
Fig. 5:19. The effect of increased amount of data and better data to the complexity and prediction error ; Modified diagram based on original work by (Næs *et al.*, 1984)

5.3.6 Type of regression model

In many analytical situations by spectroscopy, the instrument response is assumed to follow Beer's model where the instrument response is a linear function of chemical concentration and error. Alternative to Beer's model, MLR, PCR and PLSR develop relationship between chemical concentration and instrument response plus instrument noise in a different logic as shown in Fig. 5:20. This logic is a central part to the success of the prediction model development. Therefore, it is suggested to check which regression algorithm is the proper approach for the given task.

In practice, it is common to use PCA and linear PLS (commonly written as PLS) as the first chemometric method because of their ability in dimensionality reduction and the separation of chemical model from the noise part. But the new generation of chemometrics have more rigorous algorithms than the traditional regression algorithms

Multiple linear regression (MLR)	----->	Chemical concentration $c =$ $= f(instrument\ response\ x_1, x_2, \dots) + error$
Beer's model methods	----->	Instrument responses $x_1, x_2, \dots \dots, x_p =$ $f(chemical\ constructions\ c_1, c_2, \dots \dots, c_p) +$ $errors$
PLSR and PCR	----->	Chemical concentration $c =$ $f(regression\ factors\ a_1, a_2, \dots..) + errors$
		Instrument responses $x_1, x_2, \dots \dots, x_p =$ $g(regression\ factors\ c_1, c_2, \dots \dots, c_p) + errors$

Fig. 5:20. Comparison of different groups of indirect multivariate calibration methods Source : (Næs *et al.*, 1984)

PLS projection of data into latent variables was developed by Herman Wold and the team during 1975-1982 (Wold, 1975) and is built on maximising the covariance between X and Y data (Wold *et al.*, 2001). PLS is normally abbreviated to introduce linear partial least square regression. There are other approaches such as multiple linear regression (MLR), principle component regression (PCR), polynomial partial least square regression (poly-PLS) , spline partial least square regression (spline-PLS) and artificial neural network (ANN). Among these the most applied linear and non-linear calibrations methods are PLS and ANN respectively. The best fit out of these methods rely on the nature of the data and their non-linearity. In MLR, a linear signal to property relationship is assumed (a single variable – eg:peak height is regressed with a single property – eg: concentration). In PCR, the linear signal to property relationship is built after reducing the number of variables to principal components. A comparison of these methods (interms of their prediction error, computation time and ease of use) applied to NIR data for prediction gasoline properties can be found in (ref. comparison of linear and non linear models)

Some researchers have used combination of PLS algorithm with selection of the wavelength selection strategies such as genetic algorithm, interval PLS (Nørgaard *et al.*, 2000), uninformative varialbe eliminations (Centner *et al.*, 1996), competitive adaptive reweighing sampling (Li *et al.*, 2009) and successive projection algorithm (Araújo *et al.*, 2001). Numerous studies report modified versions of the original PLS algorithms and their applicability is again highly dependent on the nature of the data. Such examples are modification of PLS algorithm for fault diagnosis (Lee *et al.*, 2004) and for control community (Ergon *et al.*, 2001).

5.3.7   Choosing the right reference analysis method

The fundamental assumption behind developing a calibration model is believing the reference data and its analytical method, which in this study is the NMR spectroscopic measurements. If this analysis does not yield accurate results, then the entire process of model calibration is a failure. The most powerful method for studying chemical equilibria in aqueous alkanolamine solutions is NMR spectroscopy. The NMR analysis for speciation was used in this study based on the available literature results for speciation of amine systems. (Perinu *et al.*, 2014) reports that by NMR spectroscopy, quantification is in most cases easier for NMR spectra than for optical spectroscopy or chromatography as no calibration is necessary. (Böttinger *et al.*, 2008; Jakobsen *et al.*, 2005; Yang *et al.*, 2009) are some examples on recent NMR investigations on CO_2 absorption by aqueous amines. In paper A, a comparison of three different reference analysis method is given which determines the CO_2 loading of the calibration and validation samples used in this study which shows that although scientifically these three methods should give accurate measurements there can be chances of getting erroneous results which if used for calibration modelling can lead to problems.

5.3.8   Number of PLS components

After optimising all kinds of possibilities mentioned above, the model may still not be accepted due to higher prediction error. The aim of using multivariate calibration over traditional univariate analysis is to reduce the prediction error by modelling the interfearences (chemical or physical) from external environment. If the impact of these interferences are not correctly addressed during the model calibration, it will destroy the true value of the property to be predicted. These interferences are stored in one or more of the PLS components in the model together with the variations related to the main chemical/physical attributes in the system and a certain level of noise. Fig. 5:21 that the prediction error is composed with two components - the undelying error and the estimation error.
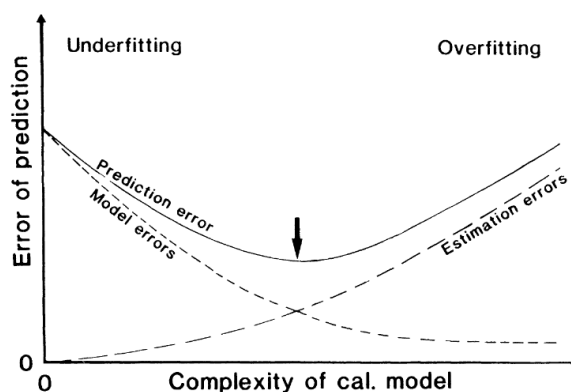
Fig. 5:21 . How underfitting and overfitting affect the prediction ability (Næs *et al.*, 1984)

As marked by the arrow the optimum number of components for the model must be used. Beyond this point the interference errors are reduced because of increasing amount of interfrences in the model with increasing number of compoents but the statistical errors are increased when including more independent model parameters from the data (Næs *et al.*, 1984).

5.4 In-situ Monitoring and Speciation - Introduction

The chemometric models developed which were validated in the lab (batch wise) are needed to be validated in the plant environment (continuous process) to check their predictable capacity and the robustness for speciation in steady and dynamic conditions. It was performed in two phases in this research. In the first phase, the Raman spectrometer was integrated at-line to an R&D prototype CO_2 capture plant which is located at USN, Porsgrunn, Norway. This USN CO_2 rig (Fig. 5:22) is specifically built for teaching and research purposes. In the second phase, the instrument was connected at-line to the Pilot-scale Advanced CO_2 Capture Technology (PACT) facilities, Sheffield, UK (Fig. 5:23). In each phase, CO_2 absorption and desorption process was continuously monitored through the spectrometer where two Raman immersion probes were connected to lean and rich amine lines. Spectra were acquired and chemical concentrations were determined from the calibration models developed. Manual samples were withdrawn from lean and rich amine lines during sometime intervals and they were compared with respective model predicted values. The initial calibration models were updated based on this comparison and models were finalised to perform in-situ speciation in future experiments for the two plants.

Fig. 5:22. CO_2 capture rig at USN, Norway

Fig. 5:23. Picture of PACT Core Facilities at Sheffield, UK

The two plants have main differences between equipment sizes, performance wise (CO_2 capture rate and solvent regeneration rate) and variability in process parameters such as liquid and gas flow rates. These differences allowed for a smooth transition of validation

approach from 'lab to process' because the learnings and experiences from phase 1 were useful for the success of phase 2 V&V (validation and verification). USN CO_2 rig has an absorber of diameter 0.1 m and 2.5 m height, steam heated desorber. It is operated with synthetic gas (air mixed with CO_2) upto 40 Nm3/h and a maximum liquid circulation rate of 250 kg/h. PACT solvent based capture plant has an absorber and desorber both having diameter 0.3 m and 8 m overall height. Typical flue gas flow rate and solvent flow rate are 200 m³/h and 1200 kg/h. Carbon dioxide removable rate is up to 50 kg/h with MEA and can remove 1 tonne of CO_2 per day using MEA (>85% capture). It has an integrated flue gas desulphurization and can use flue gas from coal or biomass co-firing in air or O_2/CO_2.

(Bingue *et al.*, 2014) say that there are three interconnected domains in process verification and validation process as user domain, problem domain and tool domain which is illustrated in Fig. 5:24. The validation and verification process is ended if and only these three domains are satisfied adequately. This domain concept was transformed into the validation of chemometric calibration model in this study such that the 'CO_2 capture process' became the user domain, 'in-situ speciation' became the problem domain and 'Raman spectroscopy' became the tool domain.
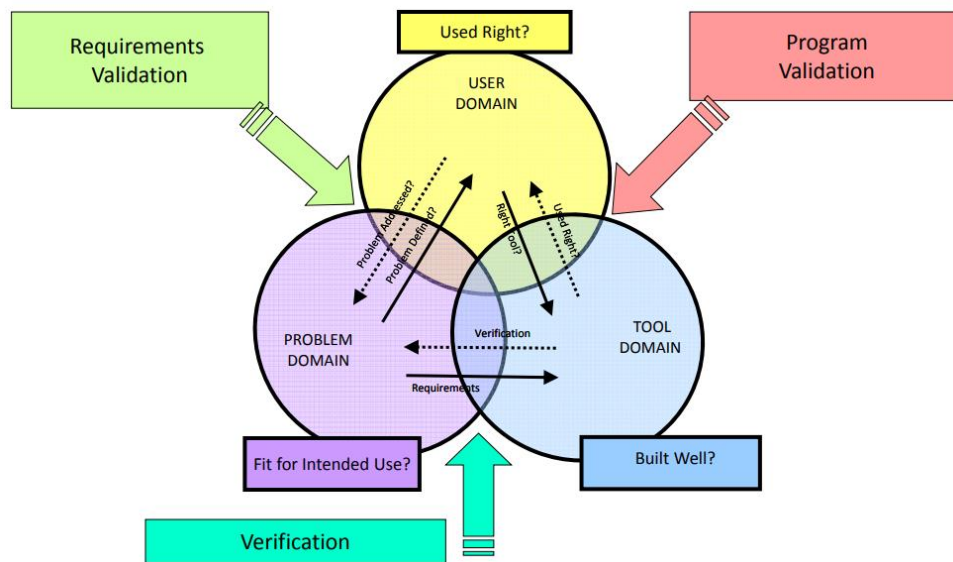
Fig. 5:24. Three domains in validation process; Source : (Bingue *et al.*, 2014)

The validation and verification process was ended up when the goal was achieved, which is 'Raman spectroscopy can be used for in-situ speciation in amine based CO_2 capture plant'. During this process, the Raman spectroscopy together with the chemometric models are implemented in the plant and tested for how and how far accurately [spectroscopy + models] can represent the 'real-process' by giving results for its intended use. Fig. 5:25 graphically represent this domain concept. After the validation process is successful, the Raman process analyser and the chemometric models are ready for real-time prediction of speciation in the CO_2 capture process
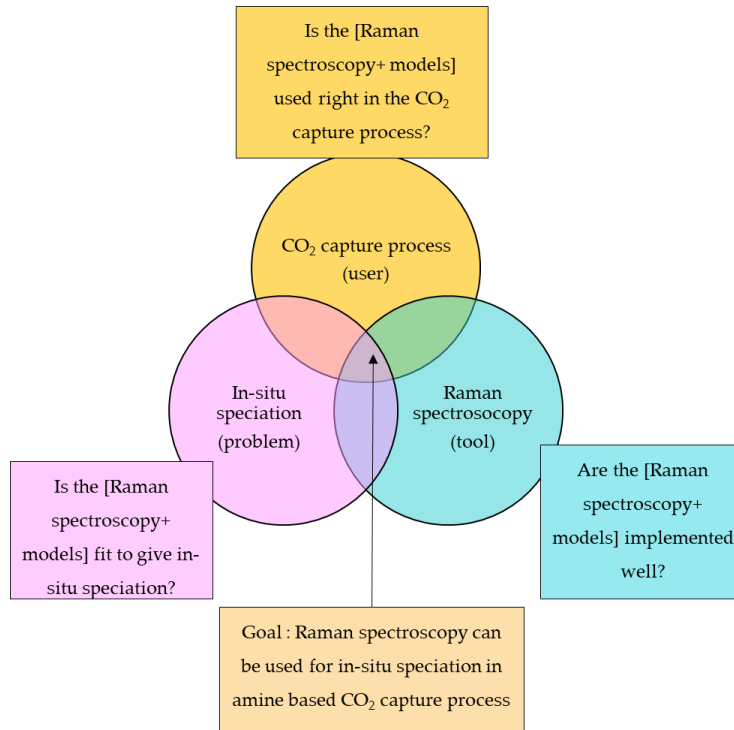
Fig. 5:25. Three domains in validation process for in-situ speciation of CO₂ capture process by Raman spectroscopy and chemometrics models

6 In-situ Monitoring and Speciation – Phase I

Graphical Abstract
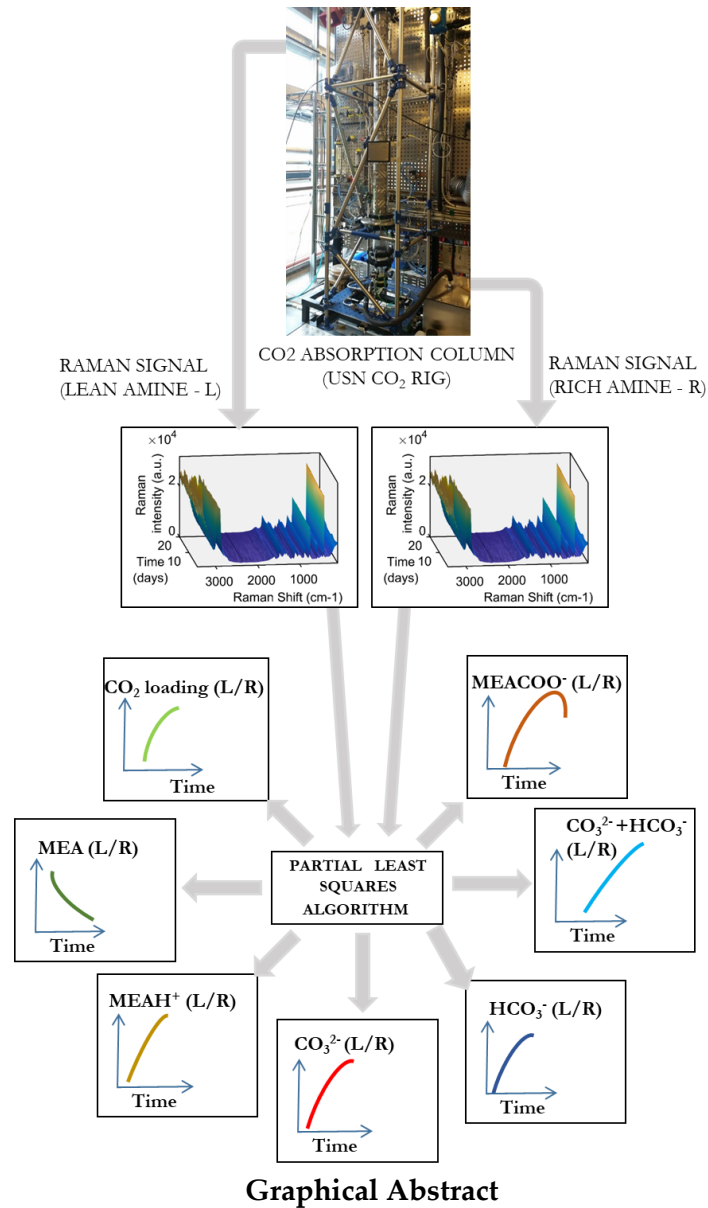
6.1 Understanding the process variations

As the first PAT implementation approach to a continuous operation, understanding the process and its variations reduce the number of experiments needed for validation and verification. This indirectly accelerates the success rate of validation while reducing the time and resources spent on unnecessary trials and mistakes. All the possible major and minor variations that can happen in the plant should be listed and discussed with plant engineers and plant operators. For instance, plant start up, shut down, interruptions from utility supply, pump & compressor failures, electric power cuts and changes from

upstream processes are typical variations. Some of these variations affect the property that is tested by the process analyser (eg: chemical concentration) while some affect the performance of the analyser. There can also be planned/unplanned process changes that have either high or low or no impact on the analyser outputs.

After a discussion with personnel who have experience with the operation of the CO_2 capture facility at USN, five process variations were listed as those which would influence to the speciation results of CO_2 absorption and the analyser performance. They are the amine flow rate, flue gas flow rate, temperature of the liquid inlet to the absorber, CO_2 % in the flue gas, and desorber regeneration state.

The capacity of the CO_2 rig is such that the possible changes in the process conditions mentioned can be spanned as liquid flow rate from 30-250 kg/hr, gas flow rate from 5-40 Nm^3/h, absorber liquid temperature inlet upto 55°C and CO_2 volumetric percentage in the flue gas upto 12 v/v%. (Øi *et al.*, 2017; Øi *et al.*, 2014). The responses of the chemometrics models must be reliable for all kinds of possible combinations of these process variations, steady state and dynamic plant conditions. Within a 4-day trial period, these conditions were changed for validation of the speciation models. The inlet CO_2 v/v% and the temperature of the absorber liquid inlet were maintained at 10 v/v% and 40°C respectively for all the cases. Since these two values were optimised parameters for the plant they were kept constant because changing them would not create an impact on the model predictions but only extend the time duration to achieve the loading saturation points in each trial. It would be a waste of time and resources. Day 1 tests included step changes in gas flow rate by 5 Nm^3/h in the range of 5-30 Nm^3/h, Day 2 tests for step changes in liquid flow rate by 10-15 kg/h in the range of 60-115 kg/h when the gas flow rate was constant at 30 Nm^3/h. Day 3 and Day 4 tests included step changes in liquid flow rate by 10 kg/h in the range of 300-115 kg/h when the gas flow rate was constant at 20 Nm^3/h. This experimental plan was somewhat close to a traditional approach where one or couple of parameters did vary while keeping other parameters constant. But it is not a recommended chemometric approach when there are several factors affecting to a model. But this trial was conducted with these conditions to maintain a balance between the practical limitations, time and requirement. During these 4 days, manual samples were withdrawn from the plant for laboratory analysis. Since the plan in the Table 6.1 does not possess abrupt changes in process parameters, additional 4 demonstration test cases were carried out as shown in Table 6.2 which also included the regeneration on/off condition and changes in flue gas CO_2 concentration. The gas flow rate, liquid flow rate, CO_2 % in the flue gas inlet were spanned between 4-30 Nm^3/h, 30-200 kg/h and 0-11 v/v% respectively which resulted in the lean and rich loading variations from 0.03-0.43 and 0.03-0.44 mol CO_2/mol MEA respectively. For all the test cases 7 chemometric models were used for prediction of total CO_2, carbonate, bicarbonate, carbamate, free MEA, protonated MEA in lean and rich amine streams. These model responses and validation results with offline measurements are presented in Paper B.

Table 6.1. Description of process conditions maintained during the 4-day trial period at CO_2 rig

Description of process conditions								
Run No:	Day	Time	CO_2 in (vol%)	CO_2 out (vol %)	Gas flow (Nm³/h)	Liquid flow (kg/h)	T2 (⁰C)	Reboiler Temp. (⁰C)
1	Day 1	11.41	9.9	0.7	5	39	39	120
2		11.52	10	2.8	10	39	39	120
3		12.02	10.1	4.8	15	33	37	120
4		12.18	9.9	6.1	20	40	38	119
5		12.31	10	6.9	25	40	39	119
6		12.43	10	7.3	30	40	37	120
7	Day 2	11.03	9.9	5.2	30	114	38	119
8		11.37	9.8	5.8	30	100	38	118
9		11.46	9.9	5.8	30	88	39	118
10		12.06	10.2	6.5	30	100	38	117
11		12.22	10.1	6.6	30	70	39	117
12		12.37	-	-	30	60	38	117
13	Day 3	11.41	10	5.2	20	112	33	117
14		11.55	10.2	5.36	20	100	38	117
15		12.10	9.8	5.4	20	90	39	117
16		12.27	10.1	5.23	20	80	39	118
17		12.44	10	5.55	20	70	39	118
18		12.57	9.9	5.7	20	60	34	118
19		13.09	9.9	5.9	20	50	36	118
20		13.26	9.8	6.1	20	40	37	118
21		13.37	9.8	6.8	20	30	37	119
22	Day 4	11.22	10.2	4.4	20	110	39	119
23		11.38	10.1	4.4	20	100	40	119
24		11.58	10.2	5	20	90	40.	119
25		12.23	10	5	20	80	40	118
26		12.46	10.1	5.7	20	70	39	118
27		13.04	10.2	5.7	20	60	39	119
28		13.27	9.9	6.3	20	50	39	119
T2 = Liquid temperature inlet to the absorber								

67

Table 6.2 Process conditions in the demonstration test cases and their impact to lean and rich loading - CO₂ rig

Description of process conditions in screening experiments – demonstration (*reg = regeneration in the desorber)					
Experiment	Gas flow rate (Nm³/h)	Liquid flow rate (kg/h)	CO_2 v/v% in flue gas	Desorber condition	lean loading	rich loading
Case 1	4	200	4	without reg*	0.03-0.06	0 .03-0.06
Case 4	4	200	0	with reg.	0.25-0.28	0.25-0.28
Case 1	4	150	0	without reg.	0.03-0.06	0 .03-0.06
Case 1	4	80	4	without reg.	0.03-0.06	0 .03-0.07
Case 3	4	30	10	with reg.	0.22-0.43	0.37-0.44
Case 1	14	200	4	without reg.	0.03-0.1	0.04-0.1
Case 2	14	150	10	without reg.	0.2-0.33	0.2-0.36
Case 3	14	150	11	with reg.	0.36-0.42	0.36-0.42
Case 2	14	150	0	without reg.	0.3-0.32	0.3-0.32
Case 3	14	150	0	with reg.	0.36-0.38	0.36-0.38
Case 4	14	150	0	with reg.	0.17-0.28	0.17-0.28
Case 1	14	80	4	without reg.	0.03-0.06	0.15-0.18
Case 4	14	80	4	with reg.	0.24-0.25	0.3-0.38
Case 4	14	80	10	with reg.	0.24-0.28	0.26-0.38
Case 1	14	30	4	without reg.	0.03-0.06	0.03-0.1
Case 4	14	30	10	with reg.	0.18-0.19	0.4-0.44
Case 3	14	30	10	with reg.	0.22-0.24	0.41-0.44
Case 1	30	200	4	without reg.	0.08-0.12	0.08-0.12
Case 1	30	200	10	without reg.	0.21-0.26	0.24-0.29
Case 1	30	150	4	without reg.	0.12-0.14	0.13-0.16
Case 1	30	150	10	without reg.	0.17-0.23	0.24-0.26
Case 3	30	150	11	with reg.	0.35-0.38	0.32-0.35
Case 1	30	80	4	without reg.	0.13-0.16	0.18-0.29
Case 1	30	80	10	without reg.	0.14-0.19	0.25-0.42
Case 1	30	30	4	without reg.	0.12-0.14	0.26-0.29
Case 1	30	30	10	without reg.	0.13-0.15	0.40-0.43
Range (for all the cases)	4-30	30-200	0-11		0.03-0.43	0.03-0.44

6.2 Correct installation of process analyser
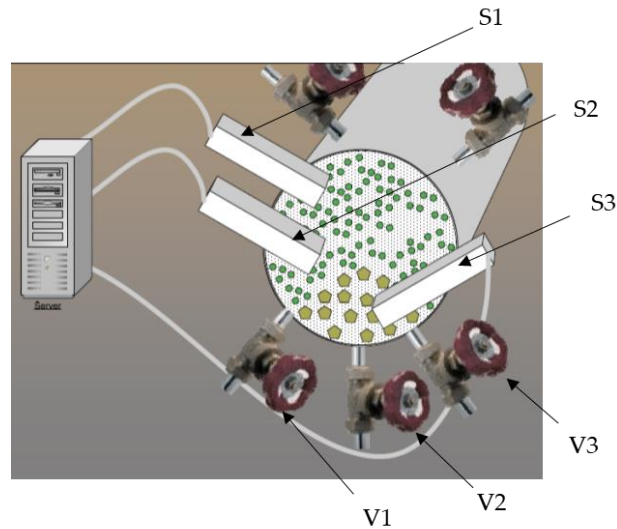
Fig. 6:1. Issue of representative sampling through a process valve and sensor (modified diagram from (Esbensen, 2009))

Process understanding allows designing a plant test trial conserving time, resources and money. The correct installation of the analyser allows getting reliable data from plant trial. The objective of the validation and verification process is to check the predictability and limitations of the models. Therefore the process analyser should be installed correctly to the plant such that its connection method, location of installation and mechanical set up at the installation do not hinder for giving "representative sampling". An integral part of validation of process analyzers is the comparison of analyser results with the offline methods. In CO_2 capture plants, both in industry and lab, the traditional method of analysing the liquid concentration is limited for determination of CO_2 loading and amine concentration which is commonly performed by titration. Experience in titration, availability of the chemicals and apparatus for titration measurements have made it the preferred option while other instruments which can determine complete chemical analysis are scarce. When a process analyser such as Raman spectrometer is intended to replace the traditional analysis method, the validation is performed by matching the process analyzer result at time *t* with the standard offline measurement which represents the same sample. Obtaining this kind of a representative process sampling is not straight forward from a liquid flowing stream. A simple explanation about this issue is schematically represented in Fig. 6:1 where a fluid flows inside a pipe; heterogeneity of the fluid is shown by two different coloured segments (eg: ions, molecules, particulate matters); valves (V1,V2,V3) represent locations of the manual sampling points while the sensor (S1, S2, S3) tips represent the area that they measure (Esbensen, 2009). This issue is critical when the fluid flow is less homogeneous. A typical example is when there is a mixture of different solvents having different densities where a phase separation can occur in a fluid stream. The chances of extracting a different sample from valve than that measured by the sensors is obvious from this figure.

If representative sampling cannot be obtained from both sensor and valve, then the entire validation becomes a failure (Esbensen, 2018; Esbensen, 2009; Petersen *et al.*, 2005).

In-line, on-line, at-line, or off-line sampling strategy can be used to connect a process sensor like Raman immersion probe to a process stream. Fig. 6:2 shows the differences between these strategies and how they influence the representability of the actual process by their measurement. Real-time measurements are only possible in in-line and on-line, however it is difficult to assure that the by-pass line always carries the same constituents to that of the main line in on-line installation. On the other hand if the process line has a large diameter, then there can be variations in concentration across the pipe cross-sectional area. In this case, the sensor measurement deviates far from the offline measurement (sample collected from the valve). The process flow should be fully closed in in-line case or the by-pass flow should be closed for sensor cleaning, sensor mounting/removing while the process is going on. However, they permit continuous process control.
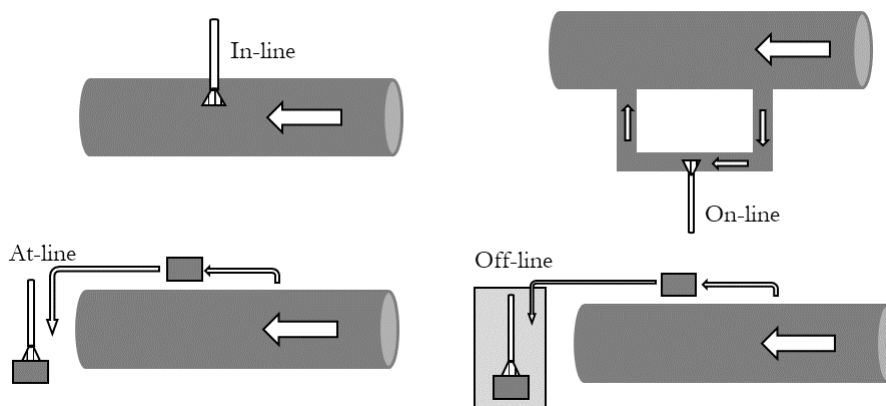
Fig. 6:2. Difference between in-line, on-line, at-line and off-line configurations

It was logical to select the in-line set up for connecting the Raman sensor and the process sampling valve to the CO_2 rig. Two in-line connections were built using standard Swagelok connections to the 1 cm outlet diameter process lines of rich and lean amine streams. Fig. 6:3 shows the orientation of the mechanical set up which was used to connect the two Raman probes to the process line. Fig. 6:3(a) represents the flow measurement which comes out from the absorber bottom while Fig. 6:3(b) shows the flow measurement which enters to the absorber top. These two locations are also shown in the process flow diagram *Fig. 6:4*.
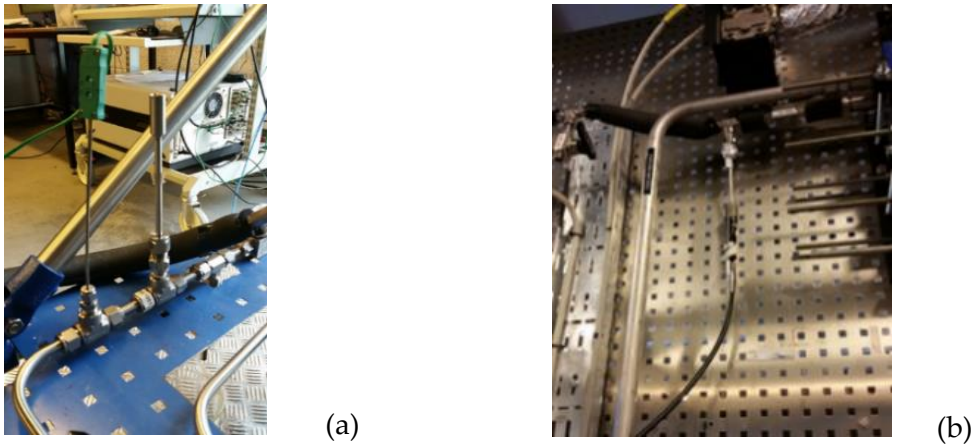
Fig. 6:3. Raman sensor in-line to the (a) rich amine stream, (b) lean amine stream
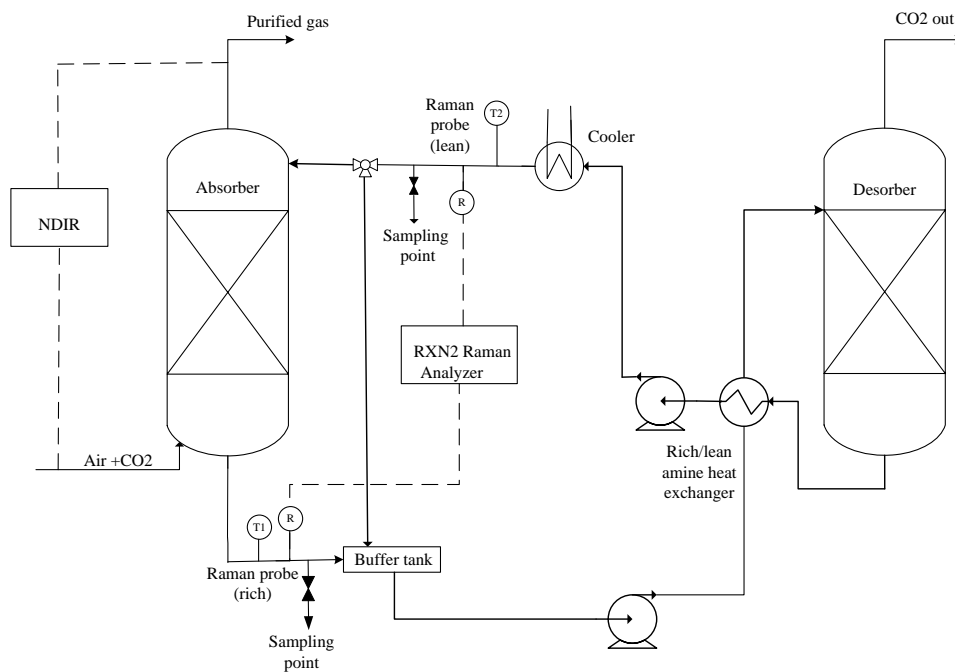
Fig. 6:4. Process flow diagram of the CO_2 rig; Raman probe locations to the lean & rich streams and sampling measuring points are shown

6.3   Updating the calibration model

The predicted results from the seven chemometric models (in Paper B) were finalised after a thorough investigation of model updating. Such a calibration update is required when a model calibrated and validated in laboratory behave less predictively in the process environment. This was performed in two steps as marked in the blue and green area in *Fig. 6:5*. In the figure an absorber is shown with gas and liquid flow directions. Connections of the offline sampling point and the Raman integration point for the rich amine line are also shown. This absorber represents the absorption column of the USN

CO_2 rig. Markers in blue belong to the initial steps where the existing model performance was analysed with respect to the plant operation. There were two Raman immersion probes connected to the lean and rich amine lines in the plant and the model deployment was same for both Raman measurements.
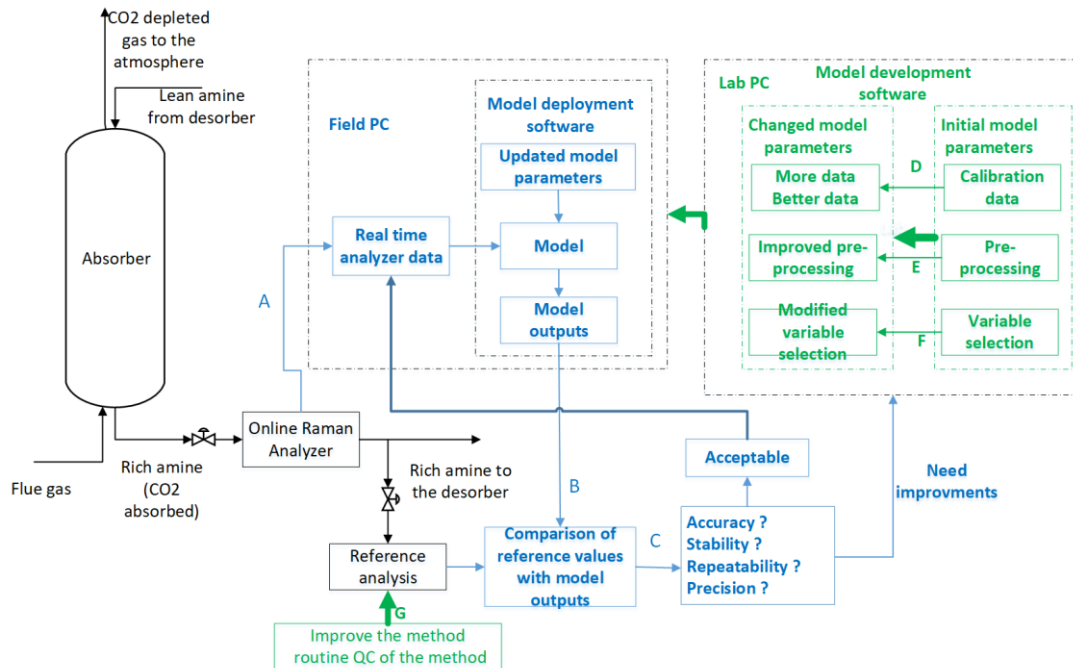
Fig. 6:5. Updating procedure of the lab-based calibration model to the CO_2 rig environment

According to Fig. 6:5, when the process is on-going the online Raman analyzer generates a pool of real-time data (step A) which is transferred simultaneously to the originally developed calibration model (lab-based). The original model parameters are first used to execute the real-time data and the model output (step B) values are compared with the values given by reference analysis. Through this comparison, an assessment is made on the accuracy, stability, repeatability and the precision of the predicted values. This assessment is made with the ideas, suggestions and complaints from the process engineers, operation management, process operators, maintenance technicians, project engineers and the chemometrician. This group of people can comment on the required precision of the analyzer, how often and to what extent the analyser outputs are useful to them, challenges with the sample extraction for reference analysis and associated errors and relationship of the model outputs to the plant trends. Based on this assessment, the existing chemometric model is improved. Such possible improvement strategies are listed in (Miller, 2010) and are mentioned briefly in Fig. 6:5 from step D to F. Step D implies using additional calibration data to the existing model to reduce the estimation error (refer Fig. 5:19). 'Better' extra calibration data can be used for the model such as those obtained from the process itself which inherit more process variations than the synthetic lab prepared samples. Several replicate sampling can be taken and time delays between X and Y measurements can be reduced. The next strategy is the

amendments made to the preprocessing and variable change in X data (step E and F). This strategy is required when the noise in the X data that is observed in the lab samples is not be the same as those generated in the process by a moving fluid. This can be due to many reasons. Diferent noise can be observed in spectra due to change in the configuration of the analyzer such as use of longer fibre optic cables for the plant trial, use of multiple immersion probes in the plant which are different than the ones used in the lab for model development, impurities or air bubbles in the process stream and impurities in the gas stream.

Similar to the improvements performed for the X calibration data, it is also important to assure the reliability of the reference analysis (Y data) method because it is the criteria that assesses the model predictions. A proper sampling protocol should be established when extracting samples from the plant, the method of transportation samples to the lab and preservation of the sample until lab analysis is performed (step G). This model updating is a continuous process to preserve the model predictive capacity.

Fig. 6:6 shows an example of the complete speciation interface for the rich amine stream when the CO_2 rig runs in a rather steady operation. Plot (a) and (b) show the increasing concentrations of protonated amine, carbamate, carbonate and bicarbonate and decreasing concentration of free amine as the CO_2 loading is increased in the process line. Fig. 6:6(c) shows determination of CO_2 loading with three different models/model combinations out of the total seven models. It provides an internal assurance of the model precision when reference validation analysis is not present for each specie.
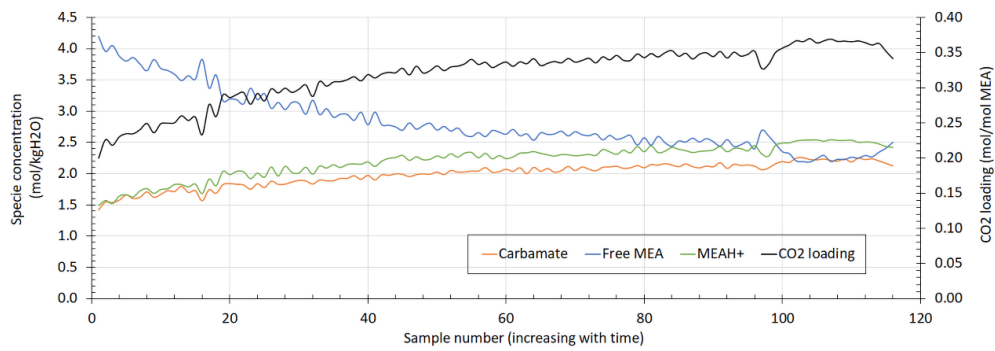
(a) Predicted concentrations for CO_2 loading, carbamate, free MEA and protonated MEA in lean amine line at USN mini pilot CO_2 capture plant
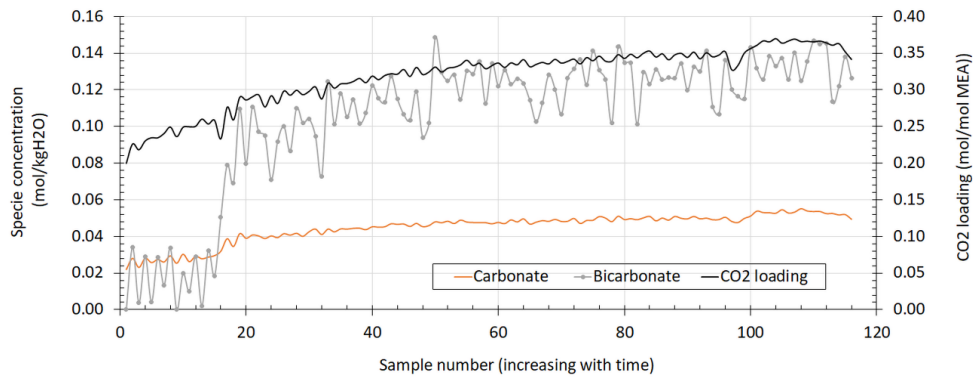
(b) Predicted concentrations for CO_2 loading, carbonate and bicarbonate in lean amine line at USN mini pilot CO_2 capture plant
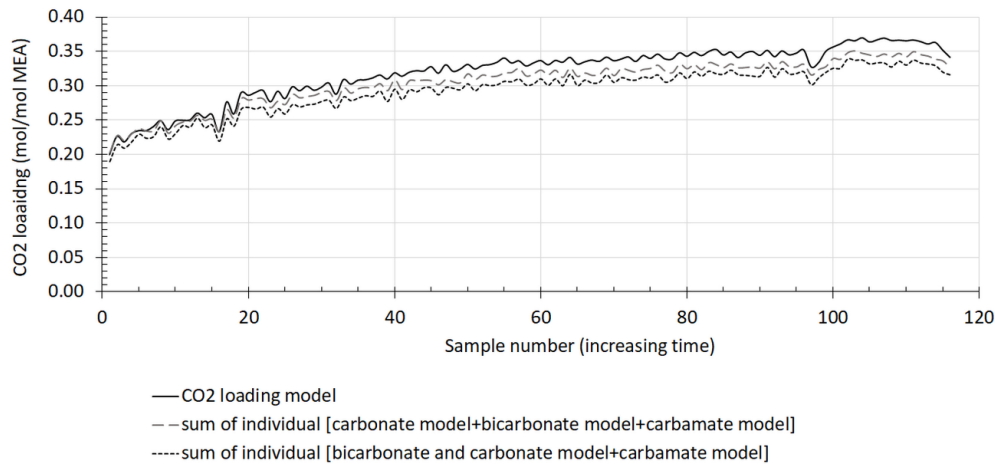
(c) Comparison of predicted total CO_2 loading in the system in three different combinations of developed models

Fig. 6:6. Demonstration of liquid phase complete speciation in rich amine for a test run in CO_2 rig

7 In-situ Monitoring and Speciation – Phase II
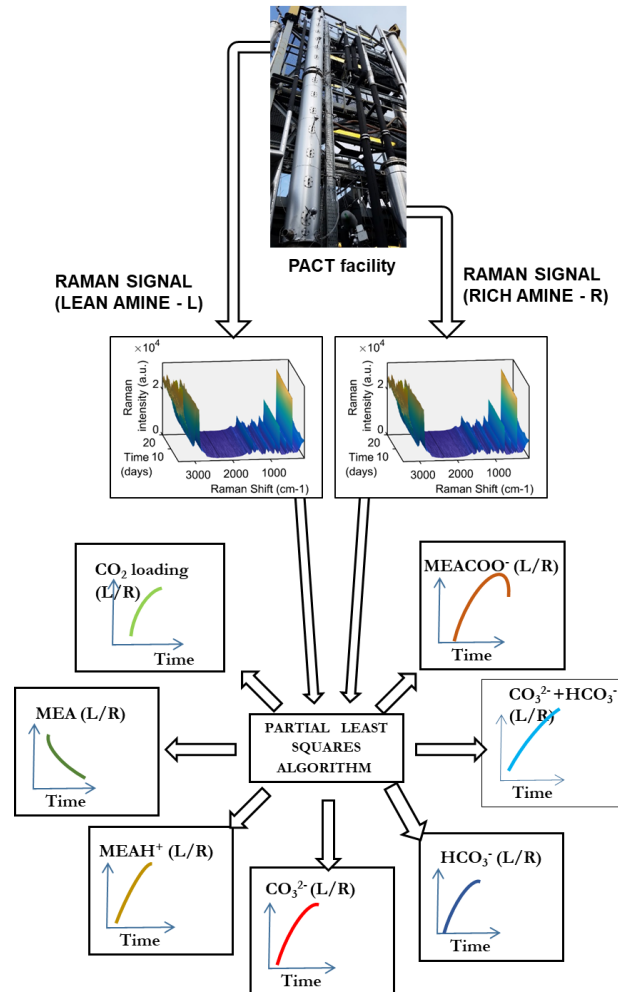
Graphical Abstract

Main products from a post combustion CO_2 capture process are the 'CO₂-depleted flue gas' from absorber top and 'product CO₂' from desorber top. The input materials are the flue gas from the power plant and makeup water for solvent preparation. The energy inputs are mainly hot water for the reboiler, cooling water for condensers and electricity for pumps, fans and compressors.

In a typical capture plant, flue gas flow rate, flue gas inlet temperature, steam flow rate, liquid flow rate, steam pressure, desorber pressure, solvent temperature at absorber inlet and solvent temperature at desorber inlet are controllable variables while CO_2 capture rate, reboiler duty, liquid/gas ratio, lean solvent loading and rich solvent loading are measured parameters.

In a typical manufacturing process, the process parameters are optimized to achieve required output quality. Supplementary the plant is adjusted to timely process variations from upstream and downstream. The situation is same for a CO_2 capture plant as well. The controllable process parameters are varied to achieve a higher CO_2 capture rate and less energy consumption. The capture plant is susceptible to changes generated within plant boundaries such as ramping up/down of process parameters due to imbalance/malfunctioning in process equipment, controllers and utilities. Further, the capture plant is constrained by the operation of its integrated emission source partner. This means that a post-combustion CO_2 capture should have flexible operations to the variations of the power stations such as varying electricity generation. Flø *et al.* (2015) mention three operating modes during peak electricity price periods which are, 1). power station exhaust gas is vented; 2).steam rate utilized for solvent regeneration is decreased and 3). rich solvent is stored in a tank and regenerated. Tait *et al.* (2016) considers five dynamic scenarios for a CO_2 capture plant which is integrated to a natural gas combined cycle (NGCC) plant when electricity price is high. They show the effect of gas turbine shut down/ start up, rapid stop of the flow of steam to the reboiler and the flue gas entering to the absorber (by-pass of capture plant), reboiler steam decoupling and rapid increase of reboiler steam flow to the CO_2 capture rate, lean loading, rich loading and absorber temperature profile. This concludes that the capture plant undergoes various types of dynamic situations. Understanding the variations of these parameters and the degree of their impact to the liquid concentrations is vital to launch an effective model validation for a process analyser implemented in a CO_2 capture plant to determining specie concentration.

7.1   Implementation of Raman spectrometer at PACT facility

7.1.1   Design of experimental plan

It is often difficult to understand all the possible permutations and effects on the absorption and desorption process of the capture plant and even if all such process variations are known, the economic factor, time and limited human resources prevent for testing all the combinations of such relationships. But DoE provides methods to understand the effects of possible multidimensional combinations and interactions of various parameters on product quality. As mentioned in Fig. 5:25, the goal of the validation process is to confirm that the Raman spectroscopy can be used for in-situ speciation in CO_2 capture plants. To reduce the complexity of experimental plan it is easy to set a single component as the 'output parameter' and the most suitable candidate is 'CO_2 loading' because almost all the species concentration vary relative to the CO_2 loading. So fundamentally, the validation process should record CO_2 loading values spanned unbiasedly in the operating range, including extreme values such as highest possible to the lowest possible. It should include sudden ramp up/down of CO_2 loading values due to fluctuations of controllable process parameters. To achieve these loading

variations which are due to both steady and dynamic operations, six process parameters were changes. They are solvent flow rate, flue gas inlet temperature, flue gas flow rate, solvent temperature at absorber inlet, CO_2 concentration in the flue gas and reboiler duty. The test was scheduled for 3 days as shown in Fig. 7:1. The process conditions for each day was decided to find answers for questions from Q1 to Q7 as shown in the figure. Objective of Day 3 tests were to see how the Raman based models were affected by presence of SO_2 in the flue gas. This would give an initial glimpse for the future model improvement strategy which is the development of Raman speciation models when solid/liquid/gaseous impurities presence in the MEA-CO_2-H_2O system.

.
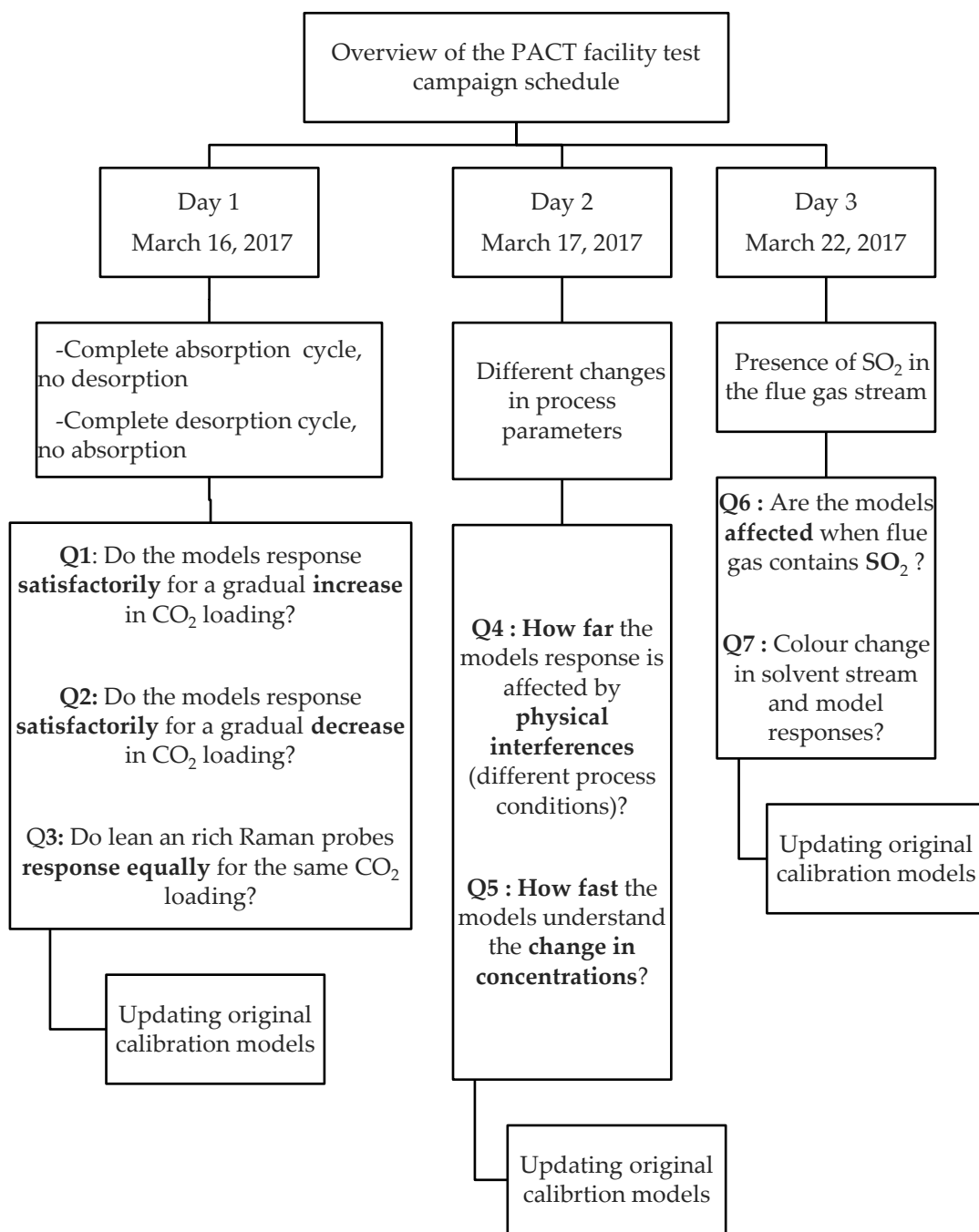
Fig. 7:1. Design of the plant schedule

7.1.2 Choosing installation location

The Raman RXN2 analyser is equipped with 4 channels where it has facilities to connect four Raman sensors to a single analyser each acquiring and saving signals at the same time. But the RXN2 analyser available at USN was equipped only with two Raman probes and extension cables during the plant trial at PACT. Therefore the two PAT sensors should be located in the plant such that to get the maximum data relationships.
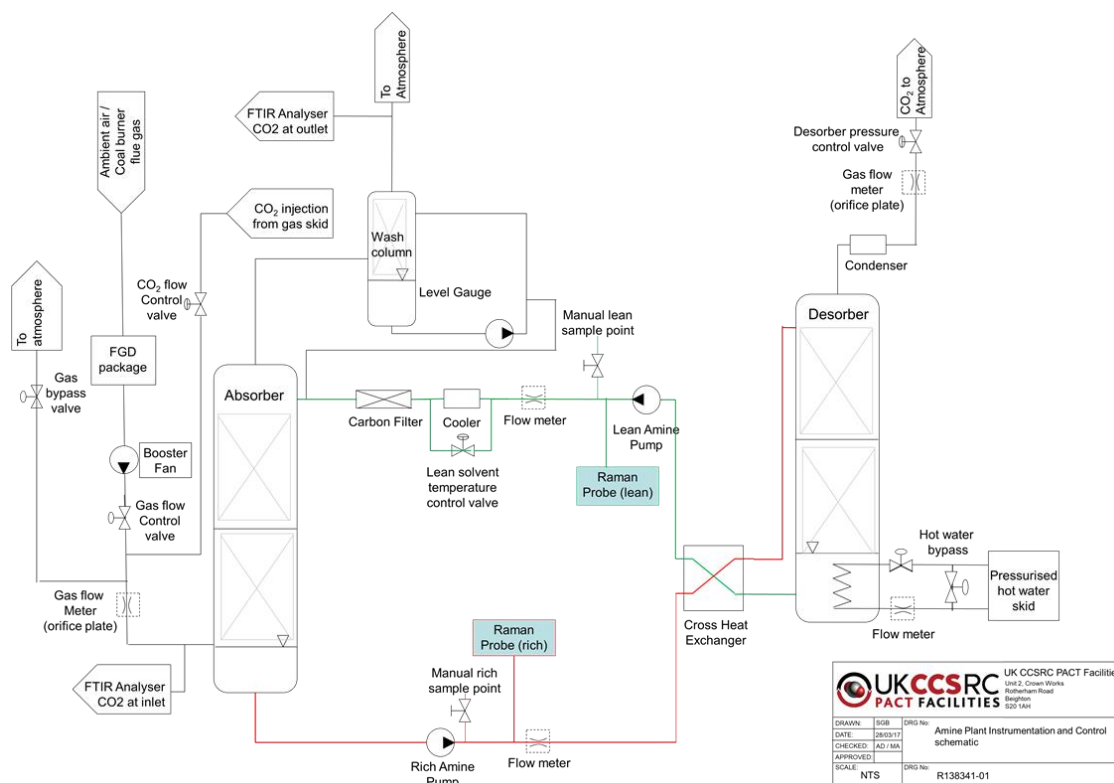
Fig. 7:2. Process flow diagram of PACT facility; (Locations of Raman probe in rich and lean streams are shown)

Having two PAT sensors in the liquid input and output streams to the absorber is useful for developing the mass balance to the absorber, to determine absorption capacity and to determine impact of process variations to the absorption. Locating two PAT sensors in the liquid input and output streams is useful the same performance evaluation of the desorber. There should be also manual sampling extraction points close to the sensor locations which provide opportunities for representative sampling to validate the analyser data. This will result to have a considerably a small time interval for a liquid volume (10 ml) to travel between the manual sampling point and the sensor location at typical liquid flow rate ranges for the plant. The liquid extraction from the sampling point should not create any impact to the sensor output such as by creating turbulence in the liquid stream. Similarly the probe tip should not immersed in areas where there is high turbulence and gas bubbles. Since the equilibrium reaction between CO_2 and amine is temperature sensitive, there should also be no temperature deviations between manual sampling point and Raman immersion probe. Considering all these facts and the

space availability of the process lines, one of two Raman sensors was located between the rich amine pump and cross flow heat exchanger (Raman probe- rich) and the remaining one was located between the lean amine pump and the cooler (Raman probe-lean) providing opportunities on commenting both absorber and desorber performance simultaneously (refer Fig. 7:2). Fig. 7:3 shows the connection points of the Raman sensors at the PACT facility.
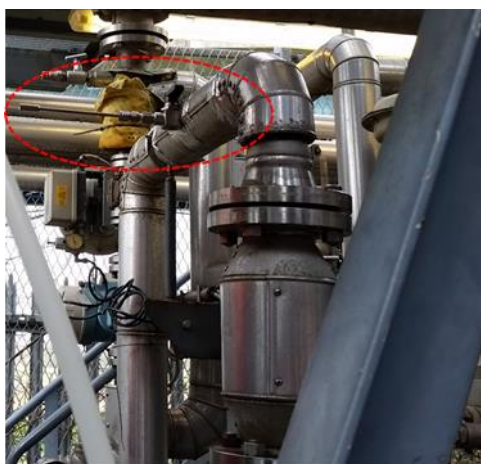
Raman probe 1 - rich amine line   Raman probe 2 - lean amine line

Fig. 7:3. Raman probe locations at the PACT capture plant (marked in circle)

7.2 Model validation results

Fig. 7:4 and Fig. 7:5 show raw and pre-processed Raman spectra recorded during the test campaign. Typical spectra challenges associated with the Raman measurements can be seen from raw data such as baseline drift.
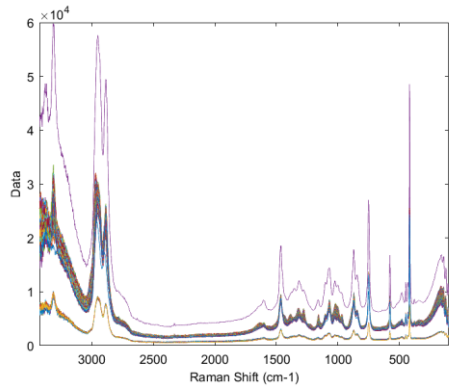
Day 1 – rich – raw spectra (365 spectra)
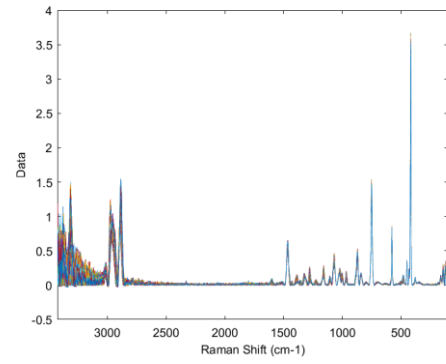
Day 1 – rich – preprocessed spectra (365 spectra)
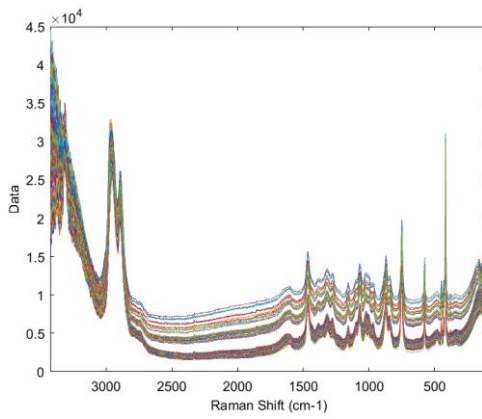
Day 2 – rich – raw spectra (383 spectra)
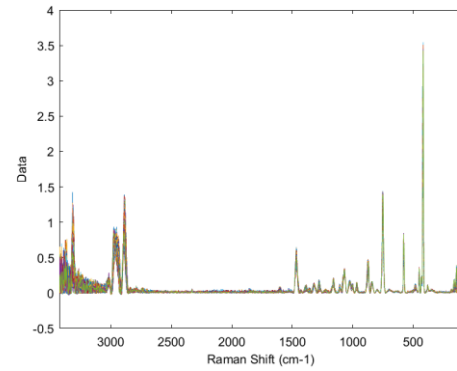
Day 2 – rich – preprocessed spectra (383 spectra)
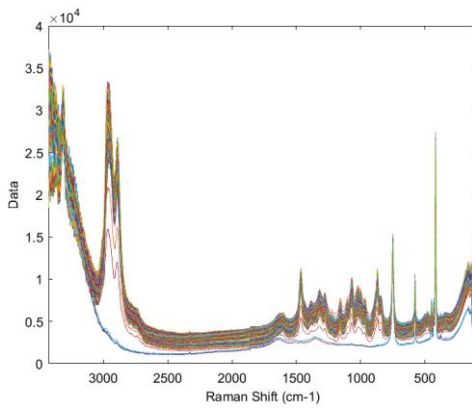
Day 3 – rich – raw spectra (362 spectra)
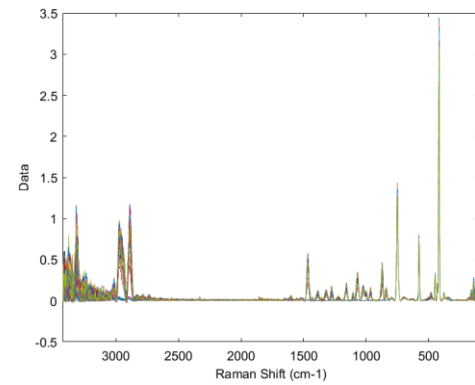
Day 3 – rich – preprocessed spectra (362 spectra)

Fig. 7:4. Raman measurements (probe 1) in the rich amine line (raw and preprocessed)
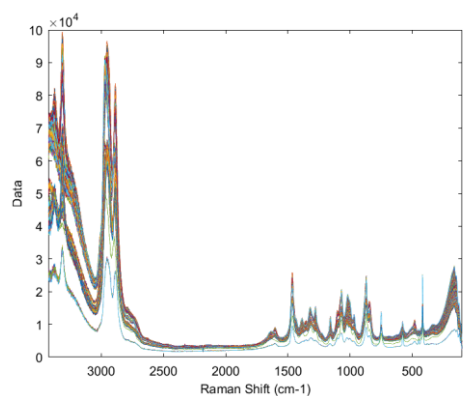
Day 1 – lean – raw spectra (330 spectra)   Day 1 – lean – preprocessed spectra (330 spectra)
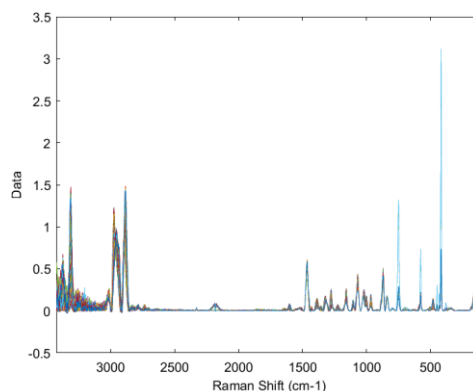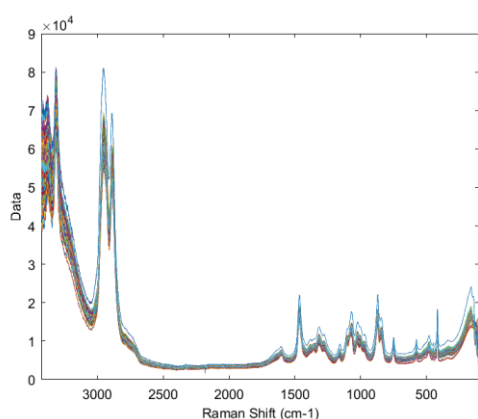
Day 2 – lean – raw spectra (351 spectra)   Day 2 – lean – preprocessed spectra (351 spectra)
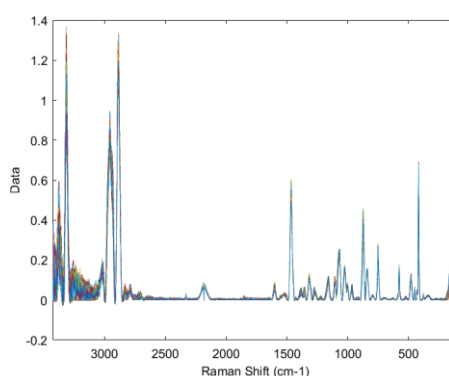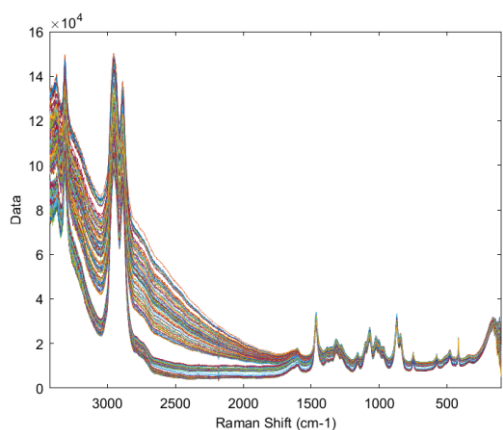
Day 3 – lean – raw spectra (346 spectra)   Day 3 – lean – preprocessed spectra (346 spectra)
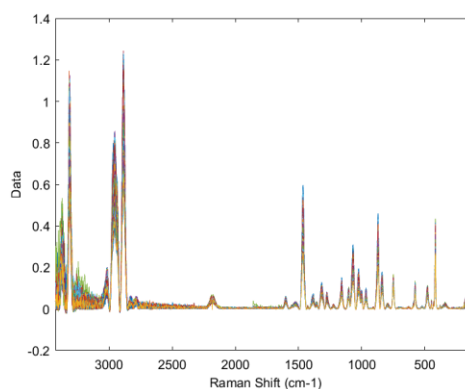
Fig. 7:5. Raman measurements (probe 2) in the lean amine line (raw and preprocessed)

Fig. 7:6 presents the region between wavenumber $700 - 1500$ cm^{-1} with some of selected Raman spectra from rich and lean streams showing their intensity variations around Raman active vibrational band. After preprocessing the spectra for baseline correction and noise reduction, the chemical information are easy to reveal based on their spectral changes. Fig. 7:6 is an indication that both Raman measurements show variations in the chemically important vibrational modes.
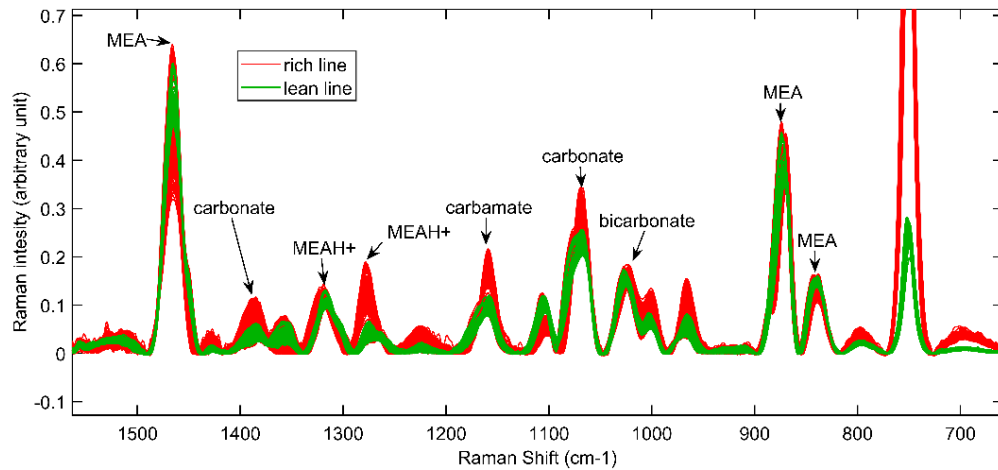
Fig. 7:6. Baseline corrected spectra (selected from lean and rich amine) showing their Raman intensity variations for carbon and amine species

7.3 Updating calibration models

In this section, the PLS prediction results are shown for all the chemometric models for the three tests. The only offline titration experiments performed related to this test campaign were CO_2 loading analysis (mol/mol MEA) and MEA concentration (w/w%). Results from these two analysis were used in different ways to understand the process trends, to update calibration models and to comment on the model predictions given by each calibration model.

Table A-1 and A-2 in appendix show the titration values for CO_2 loading (mol/mol MEA) with the Raman predictions for CO_2 loading(mol/mol MEA). The calibration models (Fig. 5:1and Table 5.1) were developed for 30 w/w % MEA but during the PACT campaign the solvent concentration was between 30-40 w/w%. Since the model 1 is expressed per amine moles, the effect of change in solvent concentration was negligible in model 1. This was also previously confirmed with the CO_2 rig results. However, we observed a large deviation (but almost a constant offset) between the predicted and measured CO_2 loading (mol/mol) for the lean amine Raman measurements. This measurement used a completely new hardware set up (immersion probe, fibre optic cable) which was not used during the initial calibration of the models and therefore this offset was assumed to be due to this new instrument accessories. The initial models were therefore calibrated following the routes shown in Fig. 5:15. The optimum model update for this campaign was a change in variable selection and the slope/bias correction (refer section 8.2.2).

Table 7.1. Description of available prediction models, units and conditions based on the results from PACT campaign

Output property (unit)	Models developed in lab *	Models developed/updated after PACT campaign**
CO_2 loading (mol/mol MEA)	1	PACT_1_1
CO_2 loading (mol/kg H_2O)		PACT_1_2
Carbamate (mol/kg H_2O)	2	PACT_2
Carbonate(mol/kg H_2O)	3	-
Bicarbonate (mol/kg H_2O)	4	-
Carbonate + bicarbonate (mol/kg H_2O)	5	PACT_5
Free MEA (mol/kg H_2O)	6	-
MEAH+ (mol/kg H_2O)	7	-
Free MEA + MEAH+ (mol/kg H_2O)	-	PACT_8
Total MEA (wt%)	-	PACT_9
***Total MEA (wt%)	-	PACT_10
Total MEA (mol/kg H_2O)	-	PACT_11

> * models developed with NMR speciation reference values; valid for 30 wt% MEA at room temperature (T) and pressure (P);
>
> ** Valid for T, P conditions and other process conditions maintained during PACT campaign;
>
> PACT_9 model was newly developed based on titration values obtained during PACT campaign;
>
> ***PACT_11 model was calculated based on the predictions from PACT_9 model; Other PACT models were results from initial lab based 7 models. Several calibration transfer procedures were used for model update.

A new notation was used to differentiate between the original speciation models with the updated or newly calibrated models after the PACT campaign as shown in Table 7.1. Fig. 7:7 to Fig. 7:12 present the comparison of CO_2 loading results from the Raman models (PACT_1_1 in Table 7.1) and the titration results.
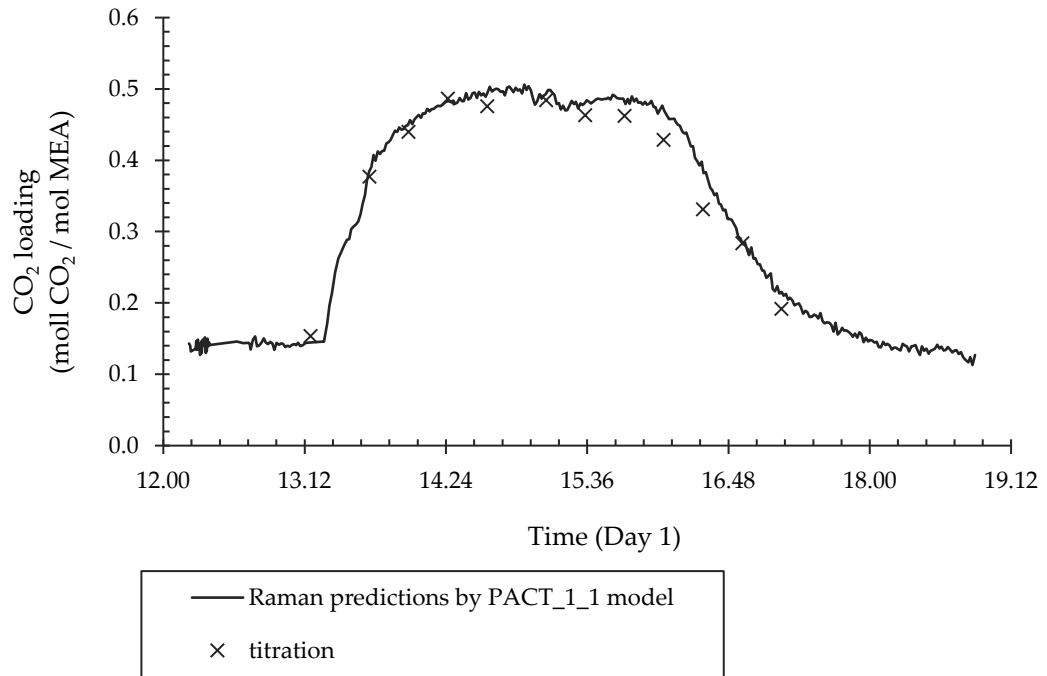
Fig. 7:7. CO₂ loading predictions by Raman spectroscopy and titration measurements with time - Day 1 rich line
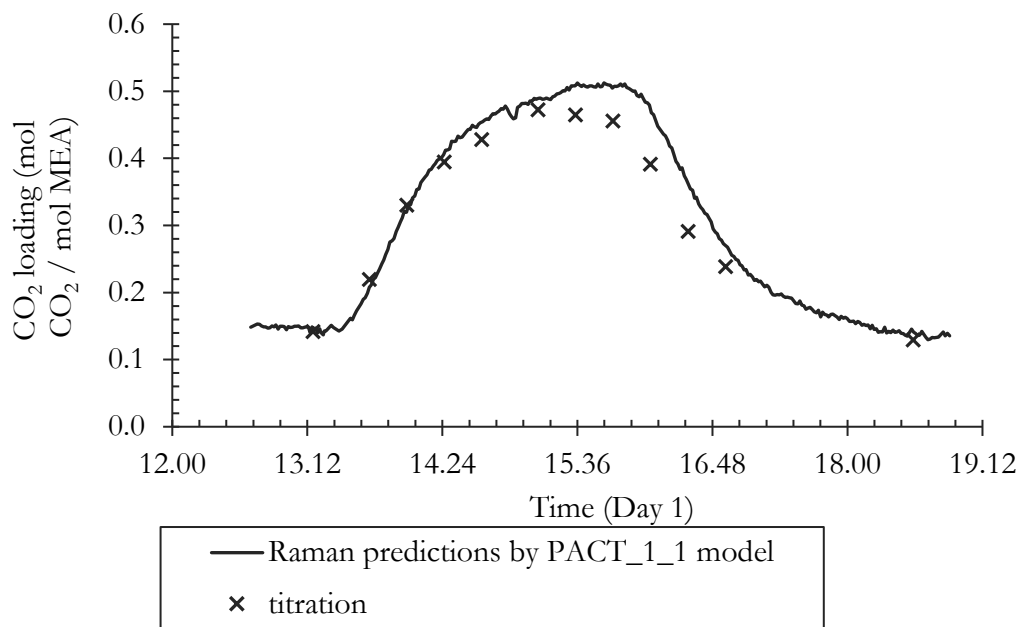
Fig. 7:8. CO₂ loading predictions by Raman spectroscopy and titration measurements with time - Day 1 lean line
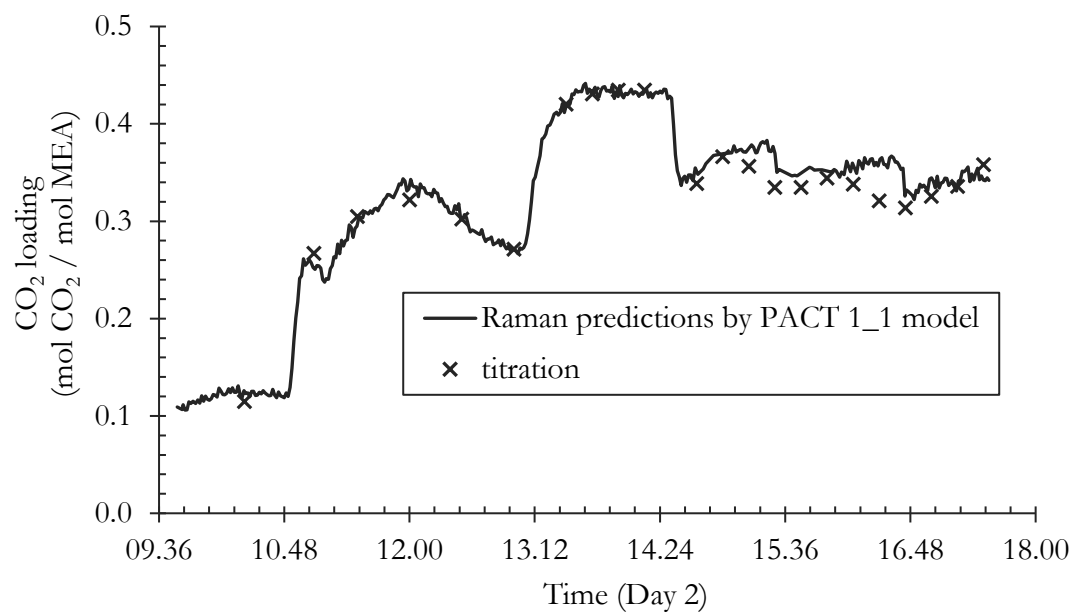
Fig. 7:9. CO₂ loading predictions by Raman spectroscopy and titration measurements with time - Day 2 rich line
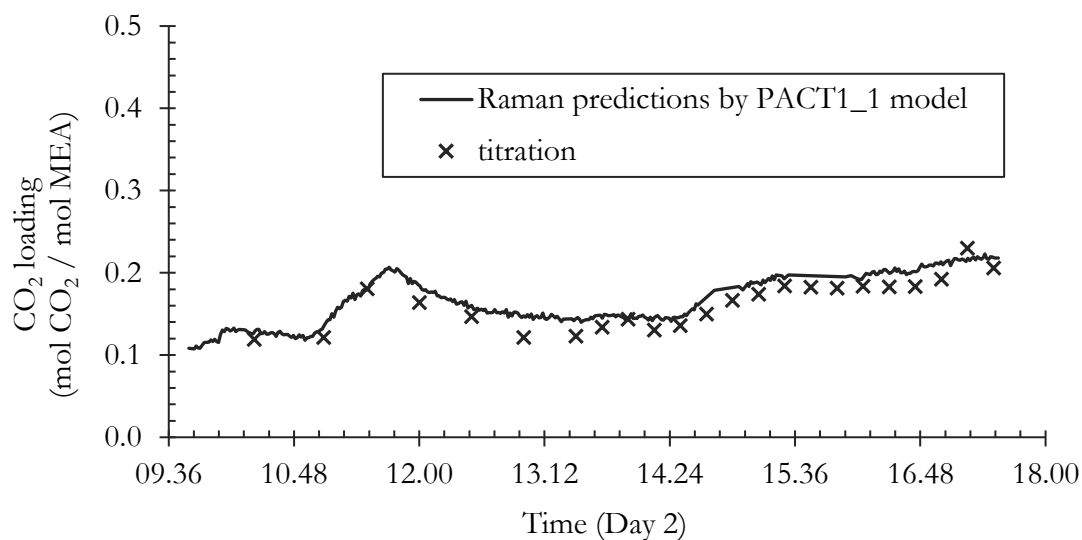
Fig. 7:10. CO₂ loading predictions by Raman spectroscopy and titration measurements with time - Day 2 lean line
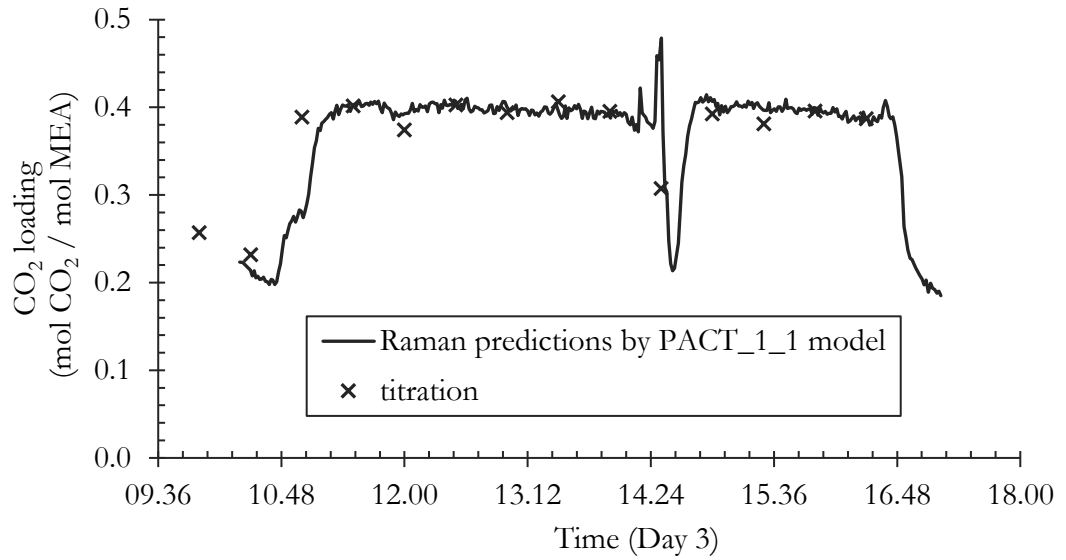
Fig. 7:11. CO₂ loading predictions by Raman spectroscopy and titration measurements with time - Day 3 rich line
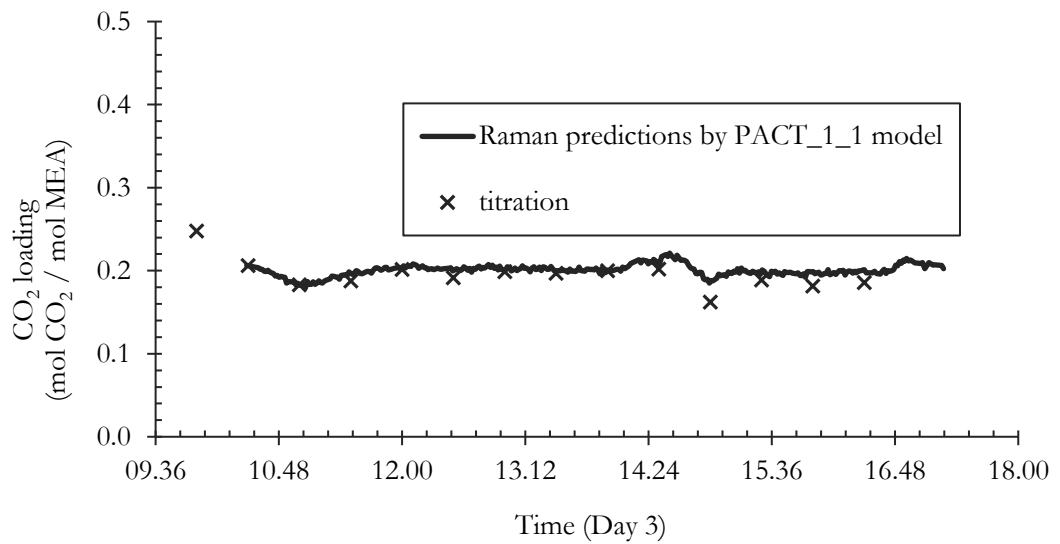
Fig. 7:12. CO₂ loading predictions by Raman spectroscopy and titration measurements with time - Day 3 lean line

7.4 Calibration of a new chemometric model to determine MEA w/w%

MEA weight percentage plays an important role in a continuous process because this value can be changed as the process is going on due to the water loss in the plant due to temperature effect. In the initial model developments, there was no separate MEA wt% model as all the models were developed for 30 w/w % MEA. Therefore with the results obtained in this plant trial, two models were developed for MEA concentration. One model was developed directly from the offline MEA weight measurements (Y_{cal}, Y_{val}) and taking the corresponding Raman spectra at the time of Y_{cal} and Y_{val} (X_{cal}, X_{val}). This model is mentioned as "PACT_9 model" was a completely new calibrated and validated chemometric model based on the first principals.

The second model is mentioned as "PACT_10 model" which was calculated by the values obtained from model predictions for MEA concentration in mol/kg H_2O. Fig. 7:13 presents the comparison between the titration results, PACT_9 model results and PACT_10 model results for MEA wt% for rich amine line. Fluctuations of the MEA wt% between adjacent measurements are rather large for Raman predictions. Predictability from "PACT_9 model" is better than the "PACT_10 model".
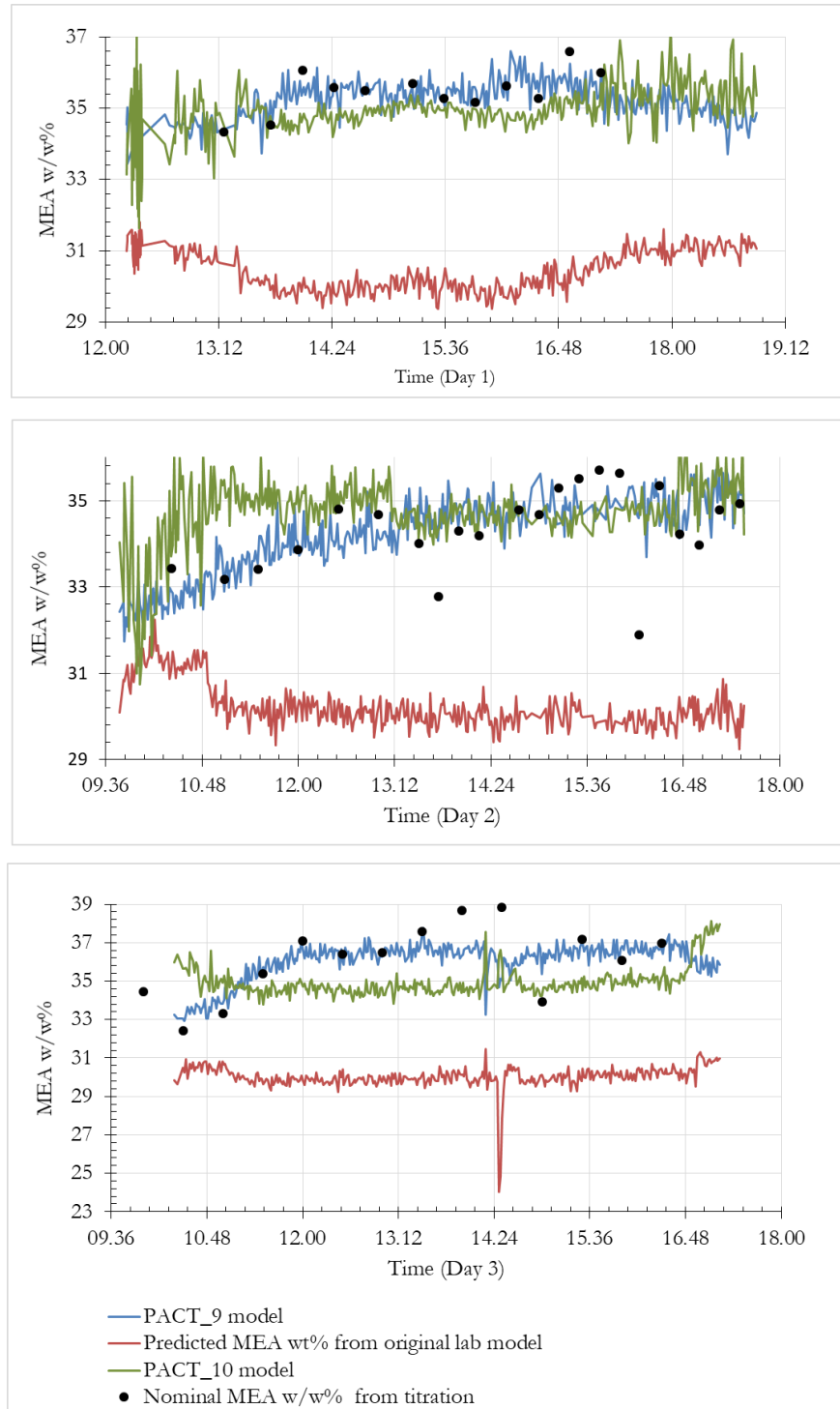
Fig. 7:13. Comparison of different predictions from models for MEA wt% with the titration values for rich amine line

7.5 Complete speciation
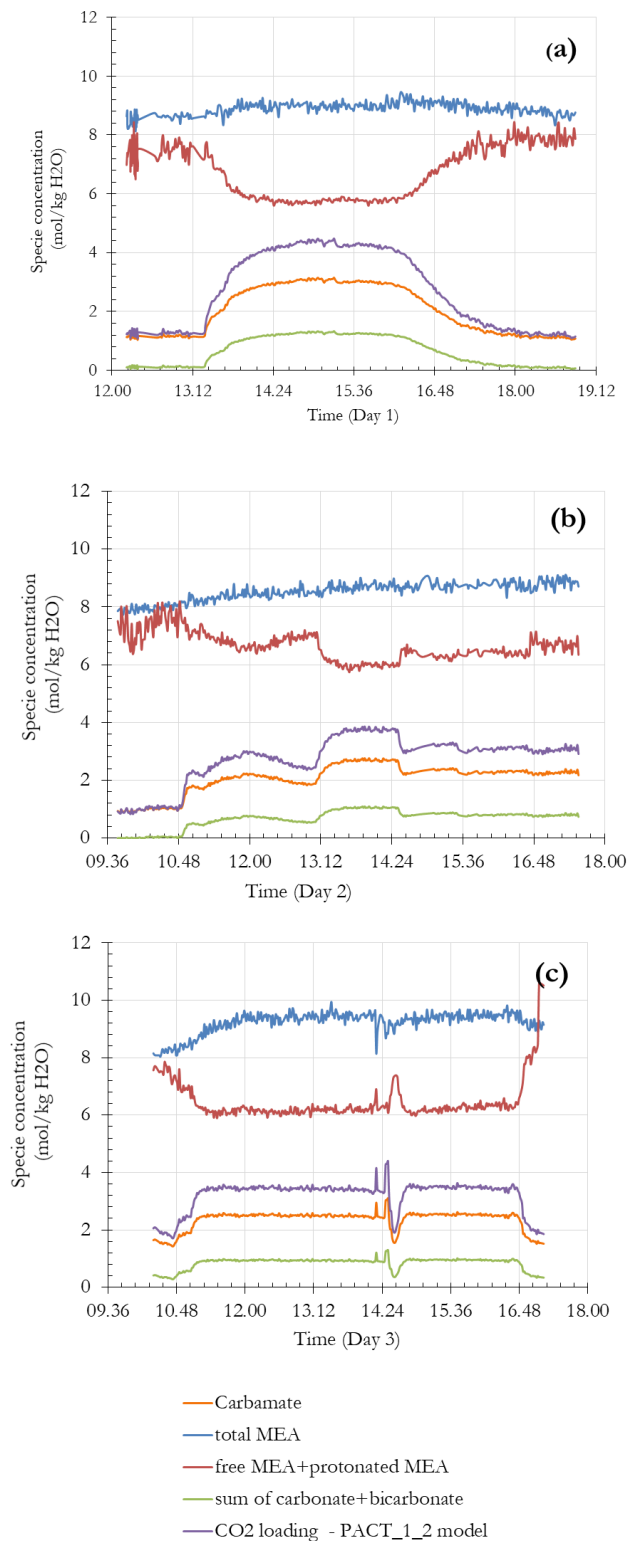
Fig. 7:14. Species concentration with time for rich amine stream

The main objective of this study was to observe complete speciation with time and Fig. 7:14 presents rich amine speciation with time observed during Day 1 (a), Day "(2) and Day (3) based on the updated speciation models for PACT plant. From these plots, it can be clearly distinguish how the relationship between chemical compositions in the equilibrium in the system. For example, when the CO_2 loading in the system is increased (upto 0.5), carbonate/ bicarbonate and carbamate concentrations are increased in the system.

7.6 Process understanding through PAT

As mentioned in section 1, one of the greatest advantages of using a PAT tool instead of a traditional offline analysis is the ability to use the results obtained from the PAT analyser to control, understand and gain knowledge about the process during an after a process cycle. In the carbon dioxide absorption desorption process by amine, the required local performance is to capture more CO_2 from the flue gas (absorption rate/ CO_2 removal efficiency) and strip out more CO_2 from the CO_2 absorbed amine (desorption rate/amine regeneration efficiency). But it is not always possible to maintain the capture plant at optimum process parameters to achieve higher absorption and desorption rates especially due to the dependency of the upstream combustion process (power plant / industrial unit). As a result the capture process need to be controlled in odd process conditions. For instance , (Tait *et al.*, 2016) mentions a strategy to capitalise on high electricity selling price by decoupling of steam flow from the reboiler such as flow of solvent to the absorber is reduced to 50% in addition to the reduction of hot water flow to zero. When the plant is switched to such a change, the data from a real-time process analyser can be used to comment on process trends and their impact to the absorption/desorption capacities. The process changes occurred during the 3 days were mapped with the Raman predictions and checked whether they generate sensible information.
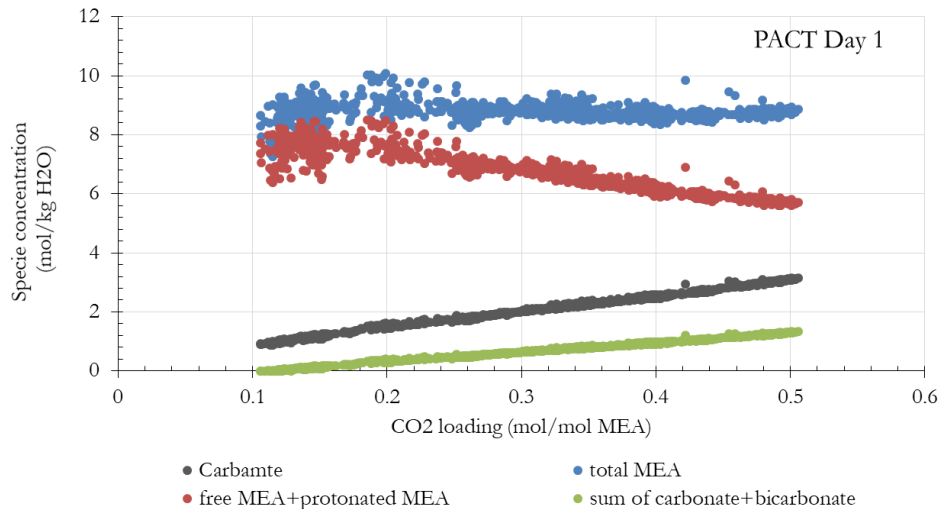
Fig. 7:15. Speciation results in Day 1 as function of total CO_2 loading (mol/mol MEA)
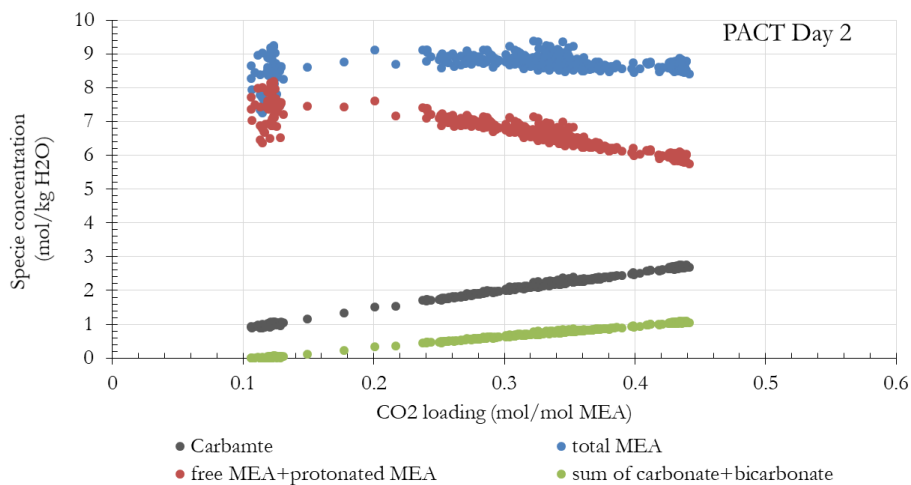
Fig. 7:16. Speciation results in Day 2 as function of total CO_2 loading (mol/mol MEA)
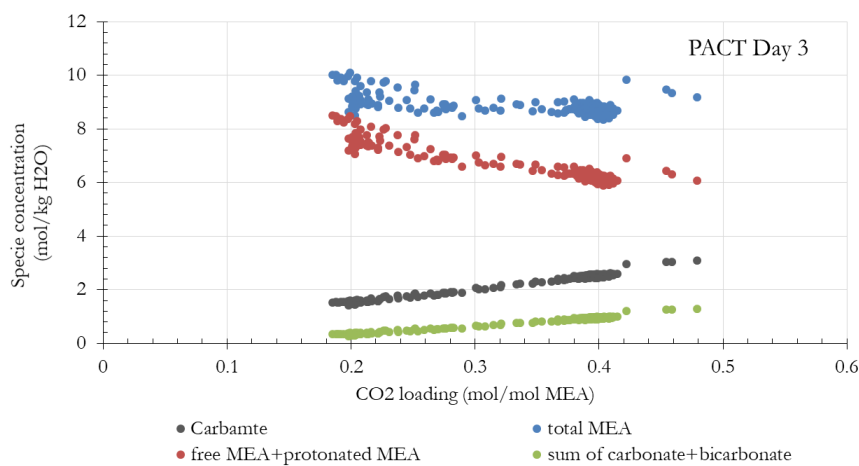
Fig. 7:17. Speciation results in Day 3 as a function of total CO_2 loading (mol/mol MEA)

8 Continuous Improvement

8.1 Impurities in the solvent stream vs model predictivity

The calibration models which predict liquid speciation in real-time plant operation become invalid when the solvent stream contains impurities. In a CO_2 capture plant, these impurities are introduced either from the flue gas stream entering to the absorber, or from the degradation products and heat stable salts or from make-up water. Although most of the research, simulation and modelling work are carried out on synthetic flue gas compositions where CO_2, O_2 and N_2 are the main components, CO_2 emission sources such as power plants and manufacturing facilities include several other chemical components. According to (Zhang *et al.*, 2017) flue gas from a 555 MWe natural gas combined cycle (NGCC) power plant includes 4.1% CO_2, 7.9% moisture, 12.1 % oxygen and 75.9% nitrogen from the exit of heat recovery steam generator while 550 MWe pulverized coal (PC) has 13.8% CO_2, 7.5% moisture, 3.6 % oxygen and 75.1% nitrogen from the exit of flue gas desulpharization unit. The flue gas from the NGCC power plant has a much higher O_2 concentration at 12.1% comparing with 3.6% for the PC case which may cause greater oxidative degradation problems for the amine based capture plant. Lee *et al.* (2008) found that flue gas from 500 MW pulverized coal combustion power plants could result in impurities of 500 and 3000 parts per million by volume (ppmv) of SO_2, 5-60 ppmv of SO_3, 10-40 ppmv of NO_2 and 5-100 ppmv of HCl. Apart from CO_2, NO_x, SO_2, CO, and small quantities of VOC, ammonia (NH_3), chlorine, and HCl may be emitted in the manufacture of Portland cement (Last *et al.*, 2011). emissions from natural gas-fired boilers and furnaces include CO, NO_x, CO, CO_2, CH_4, N_2O, VOCs, trace amounts of SO_2, and particulate matter (Last *et al.*, 2011). Chloride, nitrate and nitrite are sources for heat stable salts coming from make up water.

Technologies have resulted significant emission reductions such as selective catalytic reduction, flue gas desulphurization and activated carbon filtering. Therefore, the concentration of impurities in flue gas is considerably very low when entering the capture plant. However if they contaminate the solvent stream, the chemistry between CO_2 and amine is affected making adverse impact on absorption and desorption performance. For instance, SO_2, SO_3 and NO_2 (in the range of 10 – 40 ppmv) react with MEA and form heat-stable salts such as isothiocynatoethane and tetrahydrothiophene (Lee *et al.*, 2009). Heat stable salts are connected to the amine degradation. Amine degradation can be oxidative or thermal. It is an irreversible transformation of an absorbent solution into other compounds. Ammonia, aldehydes and carboxylic acids are primary oxidative degradation compounds and HEIA (N-(2-hydroxyethyl) imidazolidinone), HEEDA (N-(2-hydroxyethyl) ethylenediamine) and OZD (2-Oxazolidinone) are three main thermal degradation products. Anions of strong carboxylic acids (eg: formic acid and oxalic acid,) form heat stable salts (HSS) (Fytianos *et al.*, 2016). Common HSS species present in amine based gas units are nitrate, nitrite, formate, oxalate, acetate, sulfate, sulfite, phosphate, thiosulphate, thiocyanate and

glycolate (Stewart *et al.*, 1994). Source of flue gas and plant operational conditions mainly determine the amount of above unwanted chemical components in the capture plant.

The in-situ speciation predicted by the models presented in Table 7.1, may not be reliable when these chemical components present in the system. The solution is two-fold. 1). New models can be developed (calibration →validation→ demonstration) using samples containing degraded compounds and heat stable salts. 2). Existing models can be recalibrated with the same samples used in this study but with a different variable range. This range should exclude the Raman active bands related to those impurities. In the PAT perspective, solution 1 is more reliable than solution 2. An experiment was performed to determine the impact of these impurities to the multivariate models developed in this study. Eleven aqueous solutions containing potassium acetate, sodium oxalate, sodium formate, potassium sulphate, sodium hydrogen sulphite, sodium chloride, glycine, sulphanilic acid, nitric acid, sulphuric acid and formaldehyde solution were prepared and their Raman spectra were examined. Fig. 8:1 shows these spectra together with Raman spectra for loaded and unloaded MEA solutions. Spectra shown are baseline corrected and offset for clarity. The dashed boundary show the Raman variable range used for the multivariate models in this study. Almost all solutions exhibit one or more Raman active band in the areas within dashed lines. These areas contain Raman bands which are rich with chemical information for amine species (MEA, $MEAH^+$, $MEACOO^-$) and carbon species (CO_3^{2-}, HCO_3^-, $MEACOO^-$) and these bands were used for developing speciation models (refer Table 5.4).

Fig. 8:2 compares the Raman signal between a loaded 30% MEA, an unloaded 30% MEA, aqueous potassium acetate, potassium acetate in loaded MEA and potassium acetate in unloaded MEA. The Raman signals are shown from 780 cm^{-1} to 3420 cm^{-1}. The purpose of this comparison was to understand the presence of acetate in the amine solvent system to multivariate models. Three Raman active bands ([935, 1350 and 1417]cm^{-1}) were observed for all the acetate containing mixtures in the fingerprint region. Fig. 8:3 shows a similar spectral investigation when oxalate is introduced the amine system. Presence of oxalate introduces several Raman active bands in the fingerprint and low frequency region of the $MEA-CO_2-H_2O$ system. Similarly Fig. 8:4 to Fig. 8:9 show the effect of sulphate, sulphite, glycine, nitrate, nitrite and aldehyde. This investigation covers only a few number of compounds. However, there are hundreds of such degraded compounds and HSSs in a commercial scale amine based capture plant.
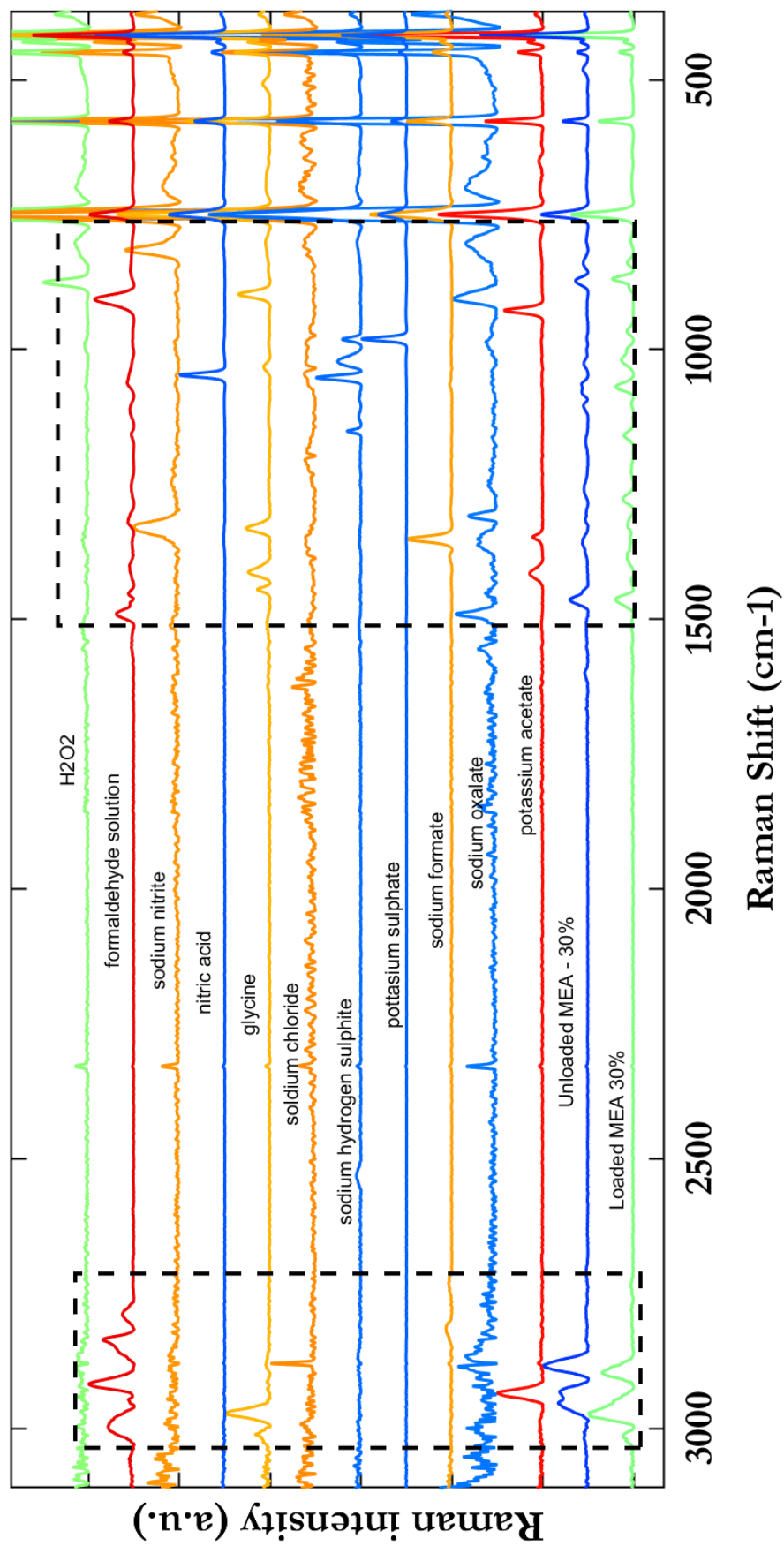
Fig. 8:1. Intersection of Raman active bands in an MEA-CO₂-H₂O system by HSSs

95
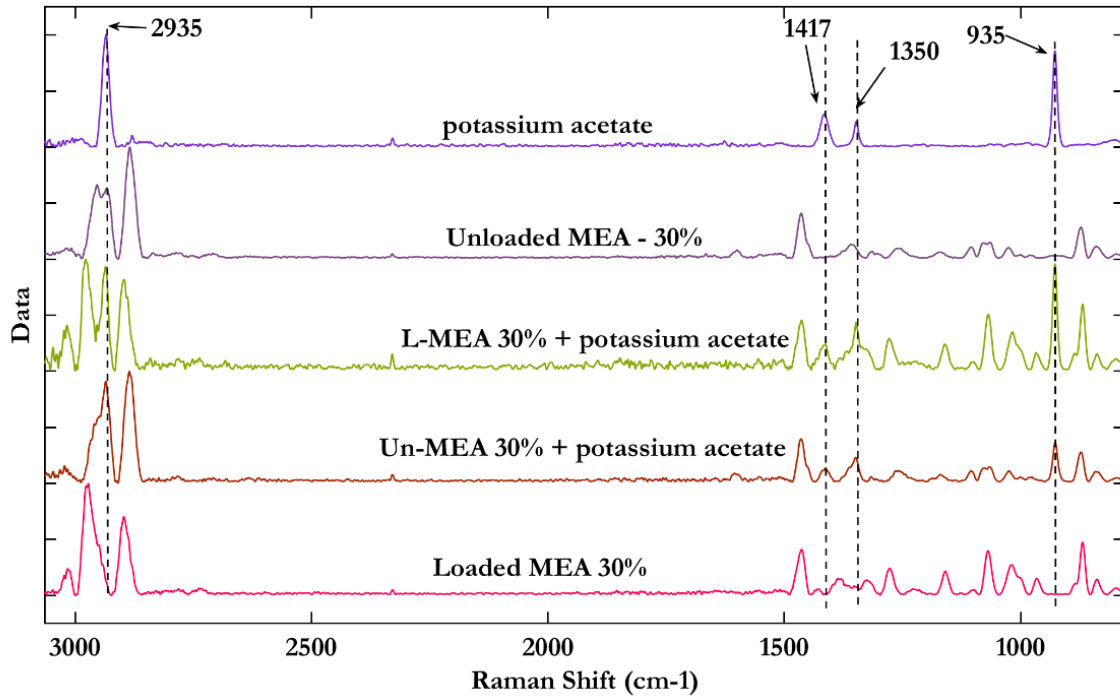
Fig. 8:2. Effect of acetate on CO₂ loaded aqueous MEA system
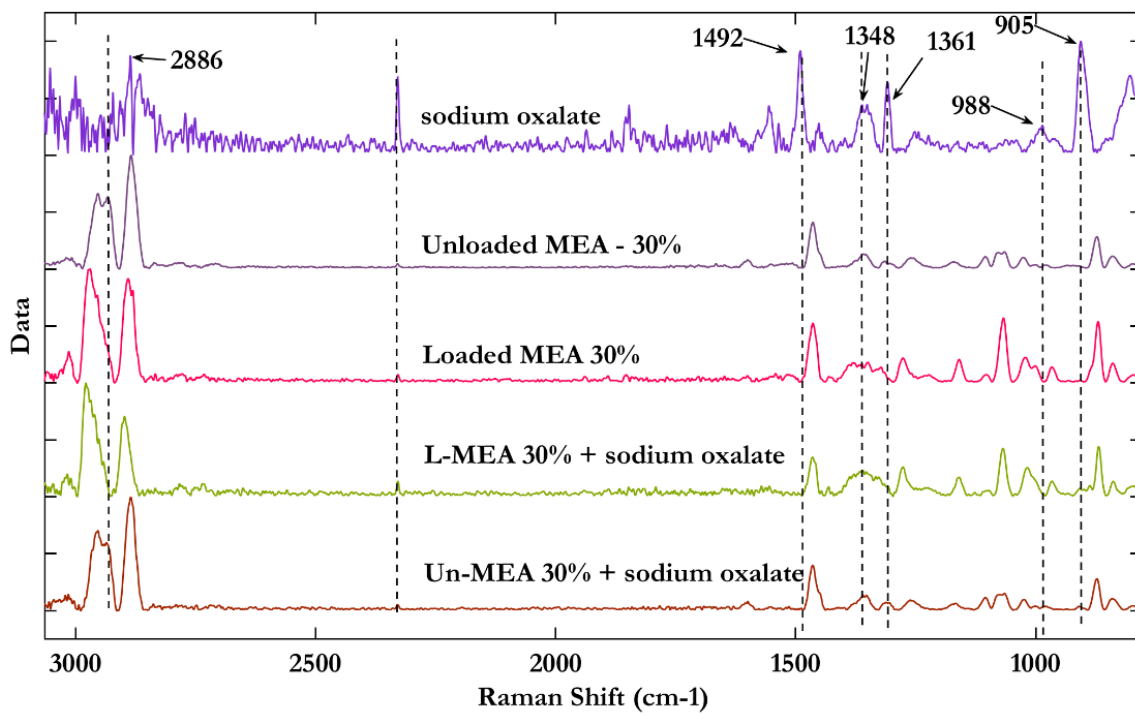
Fig. 8:3. Effect of oxalate on CO₂ loaded aqueous MEA system
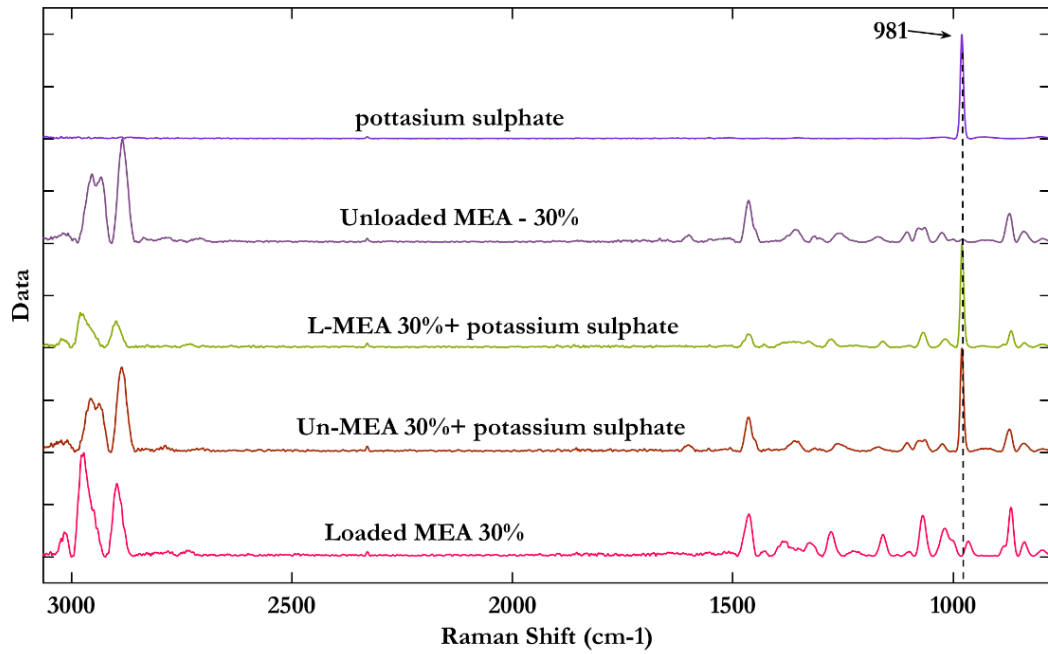
Fig. 8:4. Effect of sulphate on CO_2 loaded aqueous MEA system
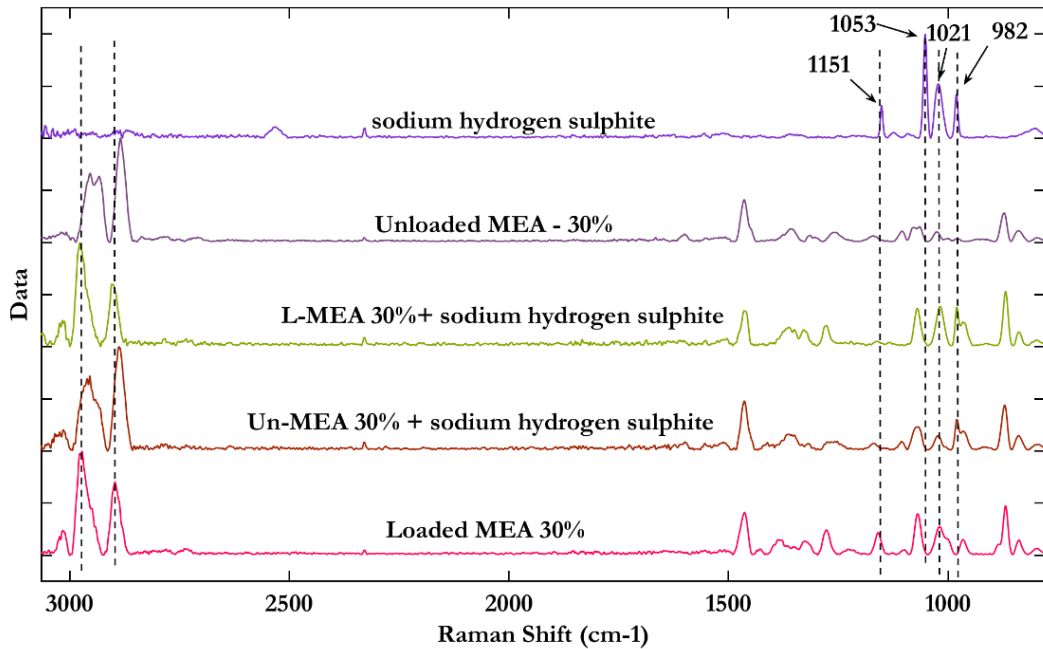
Fig. 8:5. Effect of hydrogen sulphite on CO_2 loaded aqueous MEA system
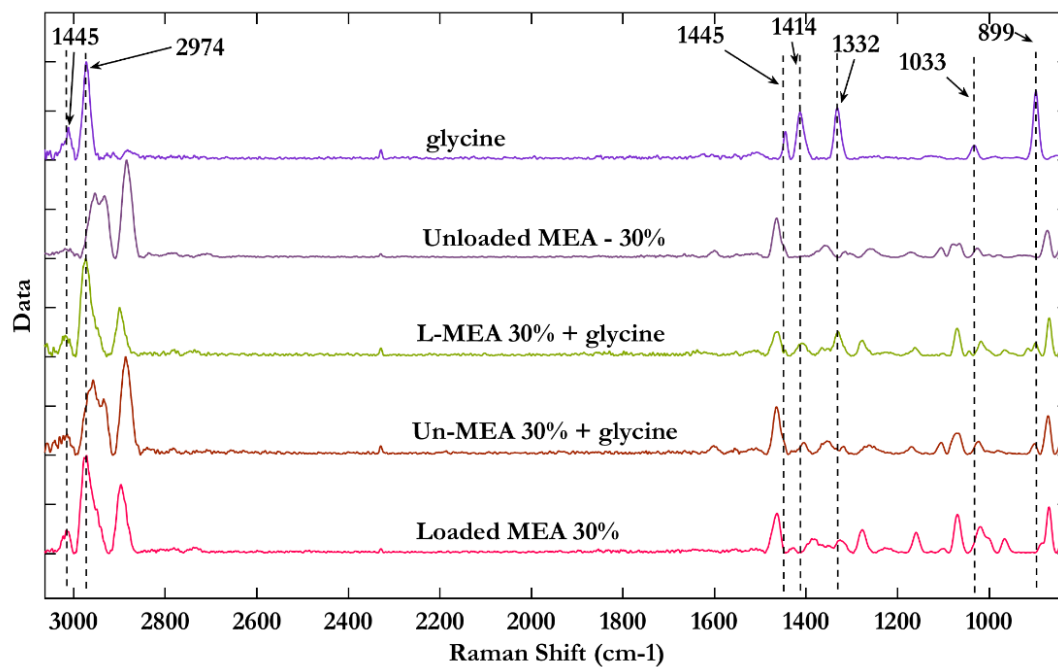
Fig. 8:6. Effect of glycine on CO_2 loaded aqueous MEA system
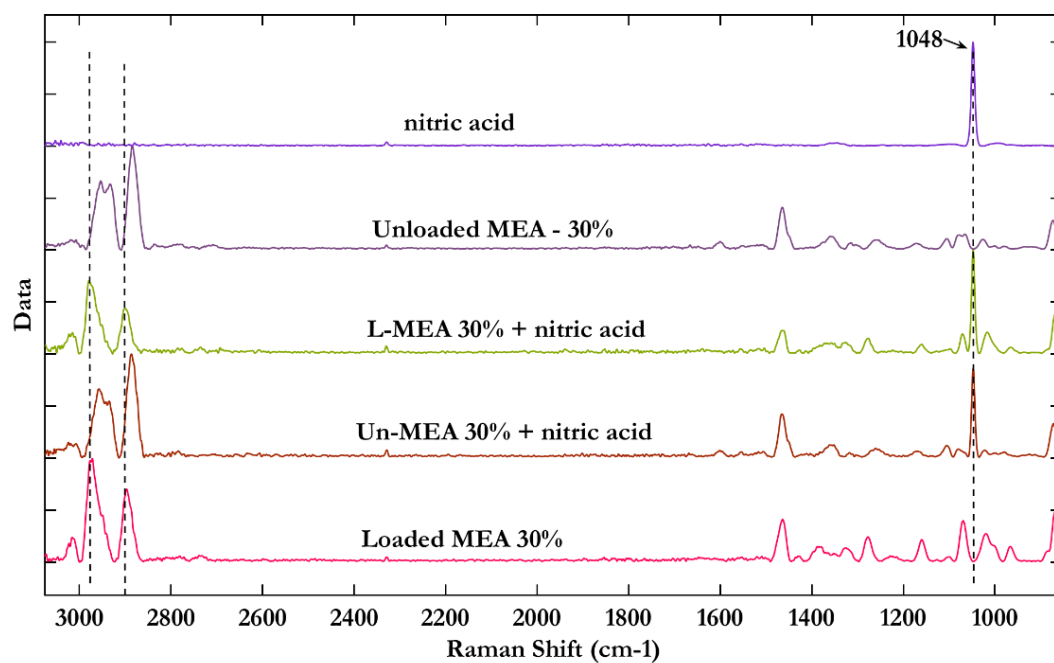
Fig. 8:7. Effect of nitrate on CO_2 loaded aqueous MEA system
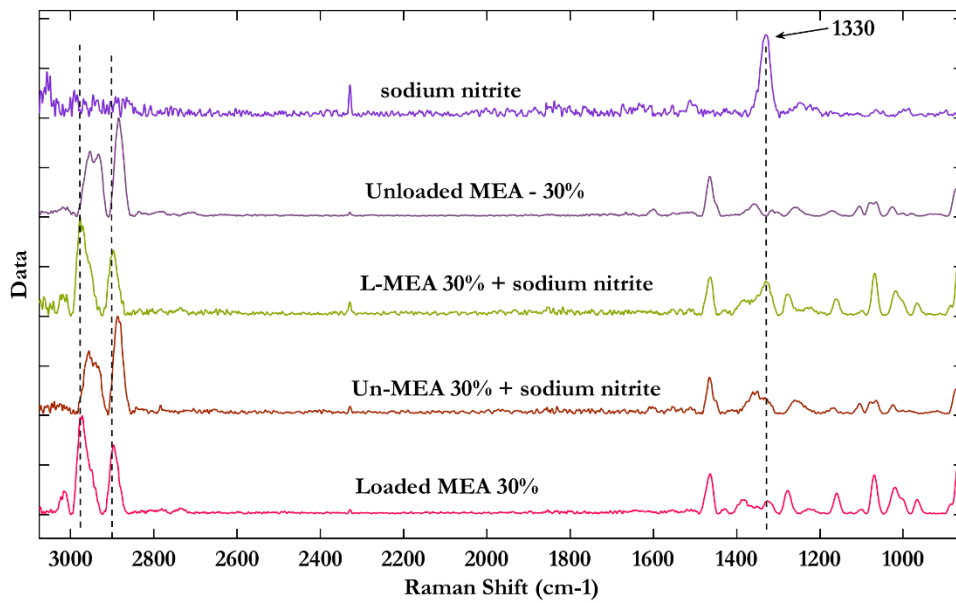
Fig. 8:8. Effect of nitrite on CO_2 loaded aqueous MEA system
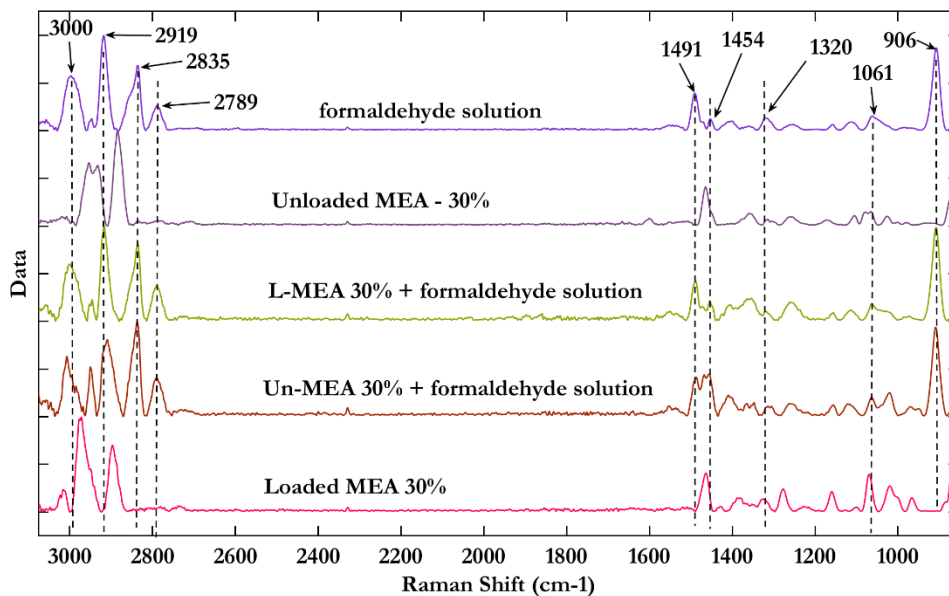
Fig. 8:9. Effect of aldehyde on CO_2 loaded aqueous MEA system

The conclusion from this investigation is that the presence of impurities in the solvent stream reduces the robustness of the multivariate models developed in this study. The speciation will be over predicted or under predicted. It is recommended to perform a similar experiment with thermal and oxidative degradation products which were not included in this experiment. In addition samples from pilot plant facilities which contain degraded solvents can be used for the analysis. New multivariate models should be developed addressing these scenarios.

8.2 Lifecycle management of PAT procedure

8.2.1 Risk assessment

The predictability of the chemometric models developed/updated so far during this PhD research are valid only to the calibrated & validated conditions in the respective cases. The original models developed in lab (section 5) went through a number of changes in mini-pilot scale experiments (CO_2 rig) and pilot scale (PACT) experiments. The effect of different impurities in flue gas, make up water and solvent degradation products to the model predictivity was understood with the investigation in section 8.1. When the environmental conditions lie beyod the boundary limits (valid region) of multivariate models, the process analyser may still provide a result which is not reliable. Several chemical and physical factors contribute to such abnormalities and therefore it is important to set up a risk assessment plan to respond when the calibration model performance show abnormalities.

Table 8.1. Example of a risk assessment based on FMEA

6 **M** category	Failure mode	Failure cause	Failure effect
MAN	Incorrect handing of analyser infrastructure; chemometrics software	Operator not trained	Incorrect results
MACHINE	Probe; Fibre optic cables	Probe tip not cleaned; Permanent damage to the fibre optic cables due to bending	Incorrect results
MATERIALS	Contamination in flue gas; Contamination in solvent stream	NOx, SOx, HSS, degradation products	Over/under predicted results
METHOD	Manual sampling; Offline analysis method	Sampling errors during sample extraction, transportation to the lab, and sample preparation for chemical analysis, Errors in chemical analysis	Predictions and offline measurements are not matched
MOTHER NATURE	Loose connections between analyzer accessories	Hollow accessories are contaminated with solvent vapour, water vapour, rain water, particulate matters	Damage to the analyzer
MEASUREMENT	Improper signal/noise ratio	Higher laser temperature; Saturation of spectral output	Analyser malfunctioning; No spectral change with time

This plan is useful specially for people such as plant operators who use the process analyser in the plant but have little or no knowledge about chemometrics or PAT. Table 8.1 shows an example of a risk assessment plan based on failure mode and effects analysis (FMEA) (Abou El Hassan *et al.*, 2017). It introduces some of the potential failures which make the Raman spectrometer unsuccessful for intended purpose (complete speciation) when it is used in the same capture plants or different plants. These failures are divided into 6 categories as **m**an, **m**achine, **m**aterials, **m**ethod, **m**other nature and **m**easurement and are known as '6M category'. This FMEA should be extended further to include risk priority numbers to identify risk level, an action plan and control mechanism for each failure.

8.2.2 Calibration model maintenance

These types of risk assessments encourage to find preventive actions for failures. Physical failures can be prevented with careful practices such as careful handling of process accessories and proper training of operator. The chemical failures can be addressed with a proper calibration model maintenance plan. Fig. 8:10 provides a roadmap to sustain or improve models over time and changing conditions with the least amount of cost and effort (Wise *et al.*, 2015). Based on the experiences with CO_2 rig and PACT trials, this roadmap describes adequately the challenges with the PAT tool in this study and hence is recommended to follow. It contains model updating methods which are slope/bias correction, adding samples to calibration set and instrument standardization and calibration transfer procedures (GLS = Generalized Least Squares; OSC = Orthogonal Signal Correction; DS = Direct Standardization ; PDS = Piece-wise Direct Standardization; SST = Spectral Space Transformation).
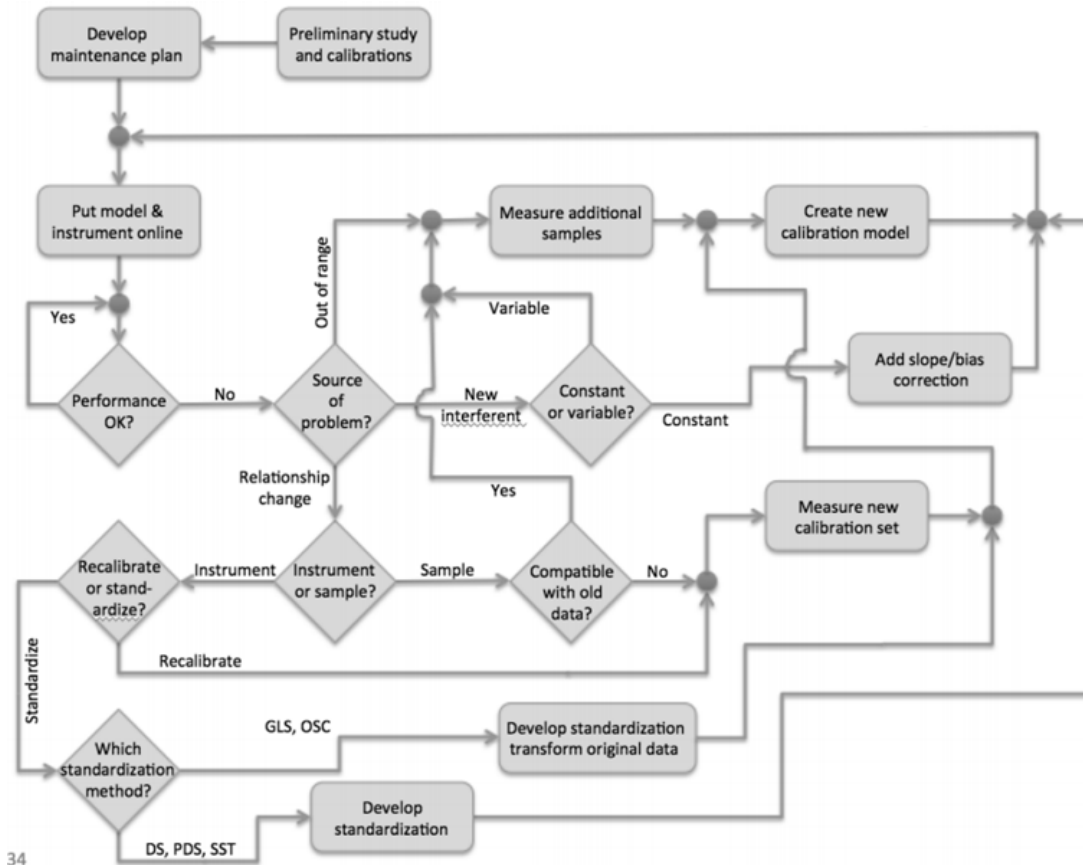
Fig. 8:10. Model maintenance flow chart (Source : (Wise *et al.*, 2015))

Information given in Fig. 8:10 is comparable to the 'laboratory to in-situ speciation model update' approach that was followed in this study.

9 Conclusion and Recommendations

Carbon capture and sequestration is obligatory to reach climate change mitigation targets and keep the global atmospheric temperature increase well below 2 °C. Commercial deployment of several large scale CO_2 capture facilities should be established within the next few years to agree with 2DS scenario. The ability of process analytical technology to increase efficiency, reduce time-consuming activities and facilitate intelligent decisions through timely measurements is useful to improve R & D activities, pilot plant campaigns and chemical management in the CO_2 capture process.

Liquid phase speciation by Raman spectroscopy together with multivariate modelling is such a process analytical technology which was the focus of this research study. Conventional aqueous monoethanolamine system was selected for this study because it is the preferred CO_2 capture technology for commercial deployment. The procedure of converting a spectroscopic signal into a concentration value is not straight forward and includes several steps which are, the preparation of samples for calibration and validation, sample measurements from the spectrometer and reference analysis from a standard reliable method, data pretreatment, variable selection, multivariate calibration and validation. Each of these steps must be addressed carefully to obtain a reliable and robust calibration model for the process analyser. Seven multivariate calibration models were developed under this study to predict the species concentrations of carbonate, bicarbonate, carbamate, sum of carbonate and bicarbonate, protonated amine, free amine and CO_2 loading in an MEA-CO_2-H_2O system. The models were demonstrated in continuous operation at CO_2 rig, USN and PACT Facility, Sheffield and calibration models were further updated to yield better predictability for each situation. In addition, Raman spectroscopic measurements acquired during PACT campaign and the corresponding offline titration measurements were used to develop a new calibration model to predict amine weight percentage. Reliability of the Raman spectroscopic measurements together with multivariate calibration models were assessed during PACT campaign. In-situ speciation opens opportunities of using this spectrometer for other areas such as to understand chemical kinetics, reaction mechanisms, process optimization, fault detection and process control.

Fig. 9:1 illustrates a complete process analytical technology overview that can be applied to a CO_2 capture plant when a single process analyser such as Raman spectroscopy is used for speciation. It shows the application of chemometrics in different aspects where PLSR is used to characterise chemical concentrations and MSPC is used to detect process abnormalities and fault detection. Long term results of the routine laboratory measurements, spectroscopic measurements and process data (eg: pressure, temperature, flow rate and flue gas properties) are used to build relationships between different attributes which can be used to enhance process understanding. For example, the time required for saturation of the rich amine line can be monitored by Raman CO_2 loading predictions while process conditions which make this saturation faster or slower can be found by mapping process data. Start of formation of heat stable salts and

degradation products can be detected from the spectrometer while the process conditions that trigger the degradation can be mapped from process data. Concepts of Theory of Sampling should be adhered during both lab sampling and process sampling. There is also an opportunity to make a plant-wide chemometric evaluation as shown in Fig. 9:1 to build relationships between gas measurements from flue gas input, gas output from absorber top, gas output from desorber top, specifications of process equipment, process parameters, hot and cold water utilities and levelized cost of electricity (for CCS integration in power plants). As mentioned in section 8, the developed method should undergo continuous improvement to preserve its reliability to various physical and chemical interferences that were not included in the initial model development stage. Specially the model predictivity, limitations and fluorescent which can arise from discoloration of solvent due to degradation should be assessed with future plant trails.

Raman spectroscopy reveals chemical information in MEA-CO_2-H_2O system. It is easy to integrate into the capture facility for real-time speciation monitoring. However, solvent degradation and colour change are the main challenges to resolve when continuing this instrument for a long period in the plant. The solvent is transformed from colourless to yellow, orange, brown, dark brown and finally black with time. Fluorescence from coloured compounds hinder the chemical information in Raman spectra. Therefore it is recommended to investigate the spectral behaviour and model predictivity when solvent degradation is started in a real capture plant. Other disadvantage of the method is that a chemometric model development is time-consuming. Reference analysis (^{13}C NMR analysis in this study) are normally expensive. The prediction results are valid only to the conditions maintained for calibration data and therefore the models are required to update for specific applications. The Kaiser RXN2 analyzer used in this study was compatible for outdoor use, could be remotely operated and was easy to integrate to capture plants inline. But the instrument is expensive and improper handling can cause the instrument and its accessories to be permanently damaged. For instance, amine leaks or amine vapours can damage the analyser if they are not properly sealed. The instrument uses 785 nm NIR diode laser with 400 mW maximum power. Direct contact of laser cause permanent eye damage and the operator should always follow the laser safety rules.
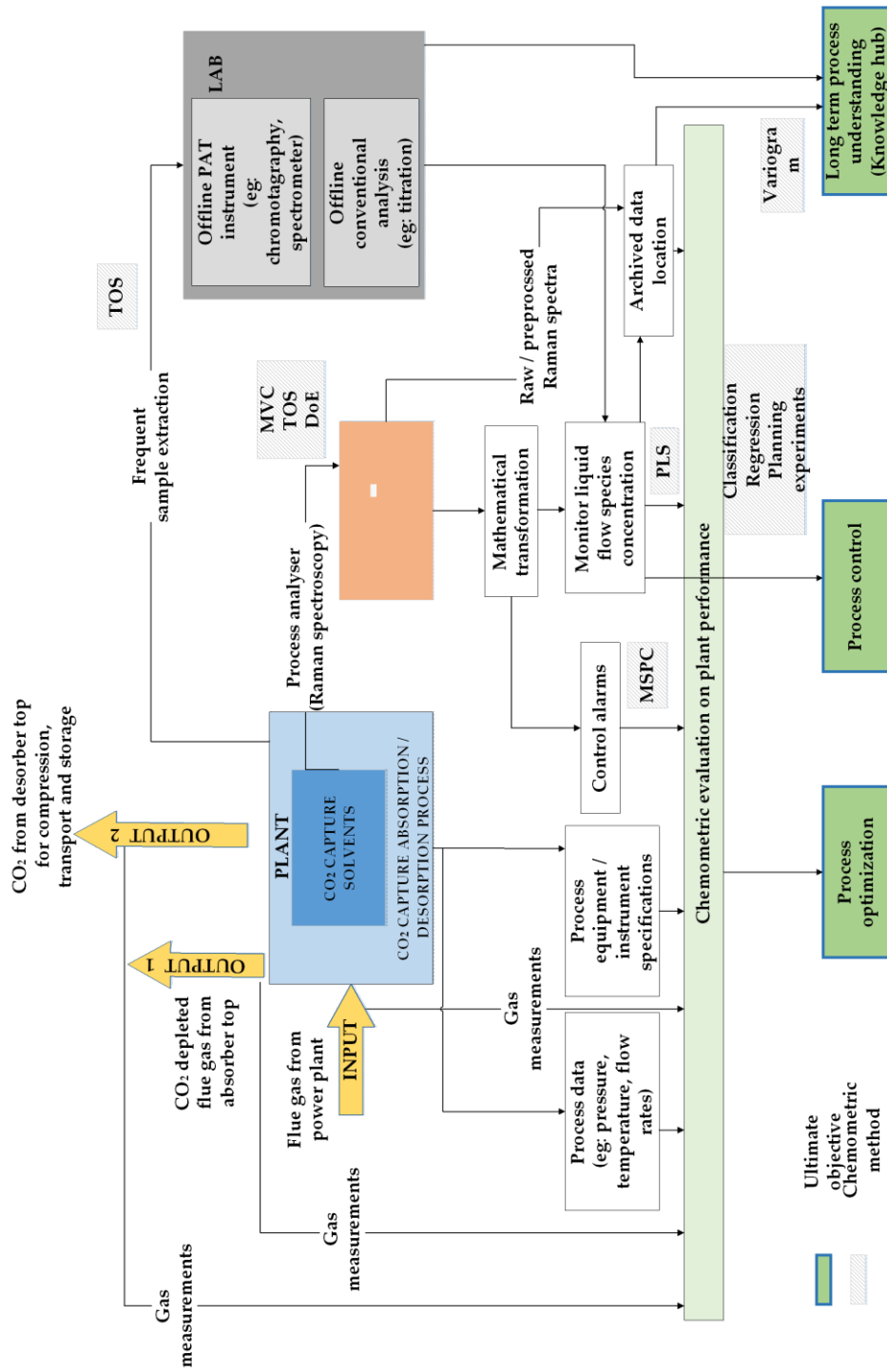
Fig. 9:1. Complete PAT overview for the CO₂ capture process after integrating the Raman spectroscopy

References

Abou El Hassan, D. S., Elsherpieny, E. A., Kholif, A. M., & Khorshid, M. A. (2017). The role of failure mode and effects analysis in improving the quality performance of dairy laboratories. *Journal of Food Safety, 37*(4). doi:10.1111/jfs.12364

Andersen, C. M., & Bro, R. (2010). Variable selection in regression - a tutorial. *Journal of Chemometrics, 24*(11 - 12), 728-737. doi:10.1002/cem.1360

Araújo, M. C. U., Saldanha, T. C. B., Galvão, R. K. H., Yoneyama, T., Chame, H. C., & Visani, V. (2001). The successive projections algorithm for variable selection in spectroscopic multicomponent analysis. *Chemometrics and Intelligent Laboratory Systems, 57*(2), 65-73. https://doi.org/10.1016/S0169-7439(01)00119-8

Archane, A., Fürst, W., & Provost, E. (2011). Influence of poly(ethylene oxide) 400 (PEG400) on the absorption of CO_2 in diethanolamine (DEA)/H_2O systems. *Journal of Chemical & Engineering Data, 56*(5), 1852-1856. 10.1021/je100854j

Archane, A., Gicquel, L., Provost, E., & Fürst, W. (2008). Effect of methanol addition on water–CO_2–diethanolamine system: Influence on CO_2 solubility and on liquid phase speciation. *Chemical Engineering Research and Design, 86*(6), 592-599. 10.1016/j.cherd.2008.03.005

ASTM. (2010). ASTM UOP 826 : Carbon dioxide in amine solution In: American Society for Testing and Materials.

Austgen, D. M., Rochelle, G. T., Peng, X., & Chen, C. C. (1989). Model of vapor-liquid equilibria for aqueous acid gas-alkanolamine systems using the electrolyte-NRTL equation. *Industrial Engineerign Chemistry, 28*(7), 1060-1073. 10.1021/ie00091a028

Batista De Carvalho, L. A. E., & Teixeira-Dias, J. J. C. (1995). Raman spectra, conformational stability and normal coordinate analysis of ethylmethylamine. *Journal of Raman Spectroscopy, 26*, 653–661.

Beumers, P., Brands, T., Koss, H.-J., & Bardow, A. (2016). Model-free calibration of Raman measurements of reactive systems: Application to monoethanolamine/water/CO_2. *Fluid Phase Equilibria, 424*, 52-57. https://doi.org/10.1016/j.fluid.2015.10.004

Bingue, E. W. P., & Cook, D. A. (2014). A Practical Approach to Verification and Validation. http://conferences.computer.org/stc/2014/papers/5034a024.pdf

Bohning, J. J., Misra, T. N., & Choudhury, M. (1998). *An International Historic Chemical Landmark. The Raman Effect* (Vol. 2019). Calcutta: the Office of Communications, American Chemical Society

BP. (2018a). BP Energy Outlook 2018 edition. https://www.bp.com/content/dam/bp/en/corporate/pdf/energy-economics/energy-outlook/bp-energy-outlook-2018.pdf

BP. (2018b). *BP Statistical Review of World Energy* London

BP. (2019). *BP Energy Outlook : 2019 edition*.

Böttinger, W., Maiwald, M., & Hasse, H. (2008). Online NMR spectroscopic study of species distribution in MEA–H_2O–CO_2 and DEA–H_2O–CO_2. *Fluid Phase Equilibria, 263*(2), 131-143. https://doi.org/10.1016/j.fluid.2007.09.017

Caplow, M. (1968). Kinetics of carbamate formation and breakdown. *Journal of the American Chemical Society, 90*(24), 6795-6803. 10.1021/ja01026a041

Centner, V., Massart, D.-L., de Noord, O. E., de Jong, S., Vandeginste, B. M., & Sterna, C. (1996). Elimination of uninformative variables for multivariate calibration. *Analytical Chemistry, 68*(21), 3851-3858. 10.1021/ac960321m

Chen, C.-C., & Evans, L. B. (1986). A local composition model for the excess Gibbs energy of aqueous electrolyte systems. *AIChE Journal, 32*(3), 444-454. doi:10.1002/aic.690320311

Coates, J. (2006). Interpretation of Infrared Spectra, A Practical Approach. In *Analytical Chemistry*: John Wiley & Sons, Ltd.

Crooks, J. E., & Donnellan, J. P. (1989). Kinetics and mechanism of the reaction between carbon dioxide and amines in aqueous solution. *Journal of the Chemical Society, Perkin Transactions 2*(4), 331-333. 10.1039/P29890000331

Danckwerts, P. V. (1979). The reaction of CO_2 with ethanolamines. *Chemical Engineering Science, 34*(4), 443-446. https://doi.org/10.1016/0009-2509(79)85087-3

Davidson, R. M. (2007). *Post-combustion carbon capture from coal fired plants - solvent scrubbing*. United Kingdom http://www.iea-coal.org.uk/content/default.asp?PageId=802

Davis, A. R., & Oliver, B. G. (1972a). A vibrational-spectroscopic study of the species present in the CO_2–H_2O system. *Journal of Solution Chemistry, 1*(4), 329-339. 10.1007/bf00715991

Davis, A. R., & Oliver, B. G. (1972b). A vibrational-spectroscopic study of the speciespresent in the CO2-H2O system. *Journal of Solution Chemistry, 1*, 329–339.

Deming, S. N., Palasota, J. A., & Palasota, J. M. (1991). Experimental design in chemometrics. *Journal of Chemometrics, 5*(3), 181-192. doi:10.1002/cem.1180050306

Derks, P. W. J., Huttenhuis, P. J. G., van Aken, C., Marsman, J.-H., & Versteeg, G. F. (2011). Determination of the liquid-phase speciation in the MDEA-H$_2$O-CO$_2$ system. *Energy Procedia, 4*, 599-605. https://doi.org/10.1016/j.egypro.2011.01.094

Deshmukh, R. D., & Mather, A. E. (1981). A mathematical model for equilibrium solubility of hydrogen sulfate and carbon dioxide in aqueous alkanolamine solutions. *Chemical Engineering Science, 36*(2), 355-362.

Diab, F., Provost, E., Laloué, N., Alix, P., Souchon, V., Delpoux, O., & Fürst, W. (2012). Quantitative analysis of the liquid phase by FT-IR spectroscopy in the system CO2/diethanolamine (DEA)/H2O. *Fluid Phase Equilibria, 325*, 90-99. https://doi.org/10.1016/j.fluid.2012.04.016

Duddu, P. (2015). The 10 worst blackouts of the last 50 years. Retrieved from https://www.power-technology.com/features/featurethe-10-worst-blackouts-in-the-last-50-years-4486990/

Eilers, P. H. C. (2003). A Perfect smoother. *Analytical Chemistry, 75*(14), 3631-3636.

Einbu, A., Ciftja, A. F., Grimstvedt, A., Zakeri, A., & Svendsen, H. F. (2012). Online analysis of amine concentration and CO$_2$ loading in MEA solutions by ATR-FTIR spectroscopy. *Energy Procedia, 23*, 55-63. https://doi.org/10.1016/j.egypro.2012.06.040

Ergon, R., & Esbensen, K. (2001). A didactically motivated PLS prediction algorithm. *Modeling, Identification and Control, 22*(3), 131-139. 10.4173/mic.2001.3.1

Esbensen, K. (2018). Pierre Gy (1924-2015): The key concept of sampling errors. *Spectroscopy Europe, 30*(4), 25-28.

Esbensen, K. H. (2009). Process sampling – the missing link in Process Analytical Technology (PAT). https://www.camo.com/downloads/ESS-2009/process-sampling-missing-link-pat.pdf

Esbensen, K. H., & Geladi, P. (2010a). Principles of Proper Validation: use and abuse of re-sampling for validation. *Journal of Chemometrics, 24*(3 - 4), 168-187. doi:10.1002/cem.1310

Esbensen, K. H., Guyot, D., Westad, F., & Houmoller, L. P. (2010b). *Multivariate data analysis: in practice*: CAMO Software

Faramarzi, L., Kontogeorgis, G. M., Thomsen, K., & Stenby, E. H. (2009). Extended UNIQUAC model for thermodynamic modeling of CO$_2$ absorption in aqueous alkanolamine solutions. *Fluid Phase Equilibria, 282*(2), 121-132. https://doi.org/10.1016/j.fluid.2009.05.002

FDA. (2004). FDA Guidance for Industry: PAT - A Framework for Innovative Pharmaceutical Development, Manufacturing and Quality Assurance Retrieved from http://www.gmp-compliance.org/guidemgr/files/PAT-FDA-6419FNL.PDF

Flø, N. E., Knuutila, H., Kvamsdal, H. M., & Hillestad, M. (2015). Dynamic model validation of the post-combustion CO_2 absorption process. *International Journal of Greenhouse Gas Control, 41*, 127-141. https://doi.org/10.1016/j.ijggc.2015.07.003

Fytianos, G., Ucar, S., Grimstvedt, A., Hyldbakk, A., Svendsen, H. F., & Knuutila, H. K. (2016). Corrosion and degradation in MEA based post-combustion CO_2 capture. *International Journal of Greenhouse Gas Control, 46*, 48-56. https://doi.org/10.1016/j.ijggc.2015.12.028

GCCSI. (2014). *The global CCS status 2014*. Australia

GCCSI. (2018). *The Global Status of CCS: 2018*. Australia

Geers, L. F. G., van de Runstraat, A., Joh, R., Schneider, R., & Goetheer, E. L. V. (2011). Development of an online monitoring method of a CO_2 capture process. *Industrial & Engineering Chemistry Research, 50*(15), 9175-9180. 10.1021/ie102418m

Guenard, R., & Thurau, G. (2010). Implementation of Process Analytical Technologies. In Bakeev, K. A. (Ed.), *Process Analytical Technology: Spectroscopic Tools and Implementation Strategies for the Chemical and Pharmaceutical Industries* (pp. 17-36). Chichester: John Wiley & Sons, Ltd.10.1002/9780470689592.ch2

Halstensen, M., Jilvero, H., Jinadasa, W. N., & Jens, K.-J. (2017). Equilibrium measurements of the NH_3-CO_2-H_2O system: Speciation based on Raman spectroscopy and multivariate modeling. *Journal of Chemistry, 2017*, 13. 10.1155/2017/7590506

Henrik, J., Jens, K.-J., Normann, F., Andersson, K., Halstensen, M., Eimer, D., & Johnsson, F. (2015). Equilibrium measurements of the NH_3–CO_2–H_2O system – measurement and evaluation of vapor–liquid equilibrium data at low temperatures. *Fluid Phase Equilibria, 385*, 237-247.

Herzog, H., Drake, E., & Adams, E. (1997). *CO2 Capture, Reuse, and Storage Technologies for Mitigating Global Climate Change : A White Paper*. US

Hessen, E. T., Haug-Warberg, T., & Svendsen, H. F. (2009). Thermodynamic models for CO_2-H_2O-alkanolamine systems, a discussion. *Energy Procedia, 1*(1), 971-978. https://doi.org/10.1016/j.egypro.2009.01.129

Hilliard, M. D. (2008). *A predictive thermodynamic model for an aqueous blend of potassium carbonate, piperazine, and monoethanolamine for carbon dioxide capture from flue gas.* (PhD), The University of Texas at Austin, Austin, Texas.

Hosking, J., Mudu, P., & Dora, C. (2011). *Health co-benefits of climate change mitigation - Transport sector Health in the green economy*. Switzerland

Howell, N. K., Arteaga, G., Nakai, S., & Li-Chan, E. C. Y. (1999). Raman Spectral Analysis in the C–H Stretching Region of Proteins and Amino Acids for Investigation of Hydrophobic Interactions. *Journal of Agricultural and Food Chemistry, 47*(3), 924-933. 10.1021/jf981074l

Idris, Z., Jens, K. J., & Eimer, D. A. (2014). Speciation of MEA-CO_2 adducts at equilibrium using Raman spectroscopy. *Energy Procedia, 63*, 1424-1431. https://doi.org/10.1016/j.egypro.2014.11.152

IEA. (2013a). *Redrawing the Energy - Climate Map. World Energy Outlook Special Report*. Paris

IEA. (2013b). *Technology roadmap carbon capture and storage* Paris

IEA. (2015). *Energy Technology Perspectives 2015. Mobilising Innovation to Accelerate Climate Action*. Paris

IEA. (2016). *Ready for CCS retrofit. The potential for equipping China's existing coal fleet with carbon capture and storage*. Paris

IEA. (2017a). *Energy Technology Perspectives 2017. Catalysing Energy Technology Transformations*. Paris

IEA. (2017b). *Global Energy & CO_2 Status Report 2017*. Paris

IEA. (2017c). *Tracking Clean Energy Progress 2017. Energy Technology Perspectives 2017 Excerpt Informing Energy Sector Transformations*. Paris

IEAGHG. (2014). *Assessment of Emerging CO_2 Capture Technologies and Their Potential to Reduce Costs, Report 2014/TR4*. UK

IPCC. (2007). *Climate Change 2007: The Physical Science Basis. Contribution of Working Group I to the Fourth Assessment Report of the Intergovernmental Panel on Climate Change* Cambridge University Press, Cambridge, United Kingdom and New York, NY, USA

IPCC. (2014). *Climate Change 2014: Mitigation of Climate Change. Contribution of Working Group III to the Fifth Assessment Report of the Intergovernmental Panel on Climate Change*.

Jackson, P., Robinson, K., Puxty, G., & Attalla, M. (2009). In situ Fourier Transform-Infrared (FT-IR) analysis of carbon dioxide absorption and desorption in amine solutions. *Energy Procedia, 1*(1), 985-994. https://doi.org/10.1016/j.egypro.2009.01.131

Jakobsen, J. P., Krane, J., & Svendsen, H. F. (2005). Liquid-phase composition determination in CO_2−H_2O−alkanolamine systems: An NMR study. *Industrial & Engineering Chemistry Research, 44*(26), 9894-9903. 10.1021/ie048813+

Jinadasa, M. H. W. N., Chandra, K. A., & Halstensen, M. (2018a, 26-28 September 2018). *System development for on-line monitoring using Raman spectroscopy for CO_2 absorption by MEA*. Paper presented at the 59th Conference on Simulation and Modelling (SIMS 59), Oslo Metropolitan University, Norway.10.3384/ecp18153328

Jinadasa, M. H. W. N., Jens, K.-J., & Halstensen, M. (2018b). Process Analytical Technology for CO_2 Capture. In Karamé, I., Shaya, J., & Srour, H. (Eds.), *Carbon Dioxide Chemistry, Capture and Oil Recovery*: IntechOpen.10.5772/intechopen.76176

Jinadasa, M. H. W. N., Jens, K.-J., Øi, L. E., & Halstensen, M. (2017). Raman spectroscopy as an online monitoring tool for CO_2 capture process: Demonstration using a laboratory rig. *Energy Procedia, 114*, 1179-1194. https://doi.org/10.1016/j.egypro.2017.03.1282

Jinadasa, W. N., Jens, K.-J., Pfeifer, C., Ronasi, S., Solar, C. B., & Halstensen, M. (2016). *Principal Component Analysis applied to CO_2 absorption by propylene oxide and amines*. Paper presented at the 9th EUROSIM Congress on Modelling and Simulation, Oulu, Finland.10.3384/ecp17142207

Kachko, A., van der Ham, L. V., Bakker, D. E., van de Runstraat, A., Nienoord, M., Vlugt, T. J. H., & Goetheer, E. L. V. (2016a). In-Line Monitoring of the CO2, MDEA, and PZ Concentrations in the Liquid Phase during High Pressure CO2 Absorption. *Industrial & Engineering Chemistry Research, 55*(13), 3804-3812. 10.1021/acs.iecr.6b00141

Kachko, A., van der Ham, L. V., Bardow, A., Vlugt, T. J. H., & Goetheer, E. L. V. (2016b). Comparison of Raman, NIR, and ATR FTIR spectroscopy as analytical tools for in-line monitoring of CO_2 concentration in an amine gas treating process. *International Journal of Greenhouse Gas Control, 47*, 17-24. https://doi.org/10.1016/j.ijggc.2016.01.020

Kent, R. L., & Elsenberg, B. (1976). Better Data for Amine Treating. *Hydrocarbon Process, 55*(2), 87-90.

Knudsen, J., Bade, O., Askestad, I., Gorset, O., & Mejdell, T. (2014). *Pilot plant demonstration of CO_2 capture from cement plant with advanced amine technology* (Vol. 63).10.1016/j.egypro.2014.11.682

Larkin, P. (2011). *Infrared and Raman Spectroscopy; Principles and Spectral Interpretation* (1 ed.). USA: Elsevier

Last, G. V., ,, & Schmick, M. T. (2011). *Identification and Selection of Major Carbon Dioxide Stream Compositions*. Richland, Washington

Lean, J. L., & Rind, D. H. (2008). How natural and anthropogenic influences alter global and regional surface temperatures: 1889 to 2006. *35*(18). doi:10.1029/2008GL034864

Lee, G., Han, C., & Yoon, E. S. (2004). Multiple-Fault Diagnosis of the Tennessee Eastman Process Based on System Decomposition and Dynamic PLS. *Industrial & Engineering Chemistry Research, 43*(25), 8037-8048. 10.1021/ie049624u

Lee, J.-Y., Keener, T., & Yang, Y. J. (2008). *Impacts of flue gas impurities in sequestered CO2 on groundwater sources: A process analysis and implications for risk management*. Paper presented at the US EPA/DOE/EPRI Combined Power Plant Air Pollutant Control Symposium: "Mega Symposium", Baltimore. 10.3155/2008CP175.19

Lee, J.-Y., Keener, T. C., & Yang, Y. J. (2009). Potential flue gas impurities in carbon dioxide streams separated from coal-fired power plants. *Journal of the Air & Waste Management Association, 59*(6), 725-732. 10.3155/1047-3289.59.6.725

Leung, D. Y. C., Caramanna, G., & Maroto-Valer, M. M. (2014). An overview of current status of carbon dioxide capture and storage technologies. *Renewable and Sustainable Energy Reviews, 39*, 426-443. https://doi.org/10.1016/j.rser.2014.07.093

Li, H., Liang, Y., Xu, Q., & Cao, D. (2009). Key wavelengths screening using competitive adaptive reweighted sampling method for multivariate calibration. *Analytica Chimica Acta, 648*(1), 77-84. https://doi.org/10.1016/j.aca.2009.06.046

Li, J., Zhang, H., Gao, Z., Fu, J., Ao, W., & Dai, J. (2017). CO2 capture with chemical looping combustion of gaseous fuels: An overview. *Energy & Fuels, 31*(4), 3475-3524. 10.1021/acs.energyfuels.6b03204

Li, Y.-S., & Church, J. S. (2014). Raman spectroscopy in the analysis of food and pharmaceutical nanomaterials. *Journal of Food and Drug Analysis, 22*(1), 29-48. https://doi.org/10.1016/j.jfda.2014.01.003

Liguori, S., & Wilcox, J. (2017). Chapter 11 - Silica Membranes Application for Carbon Dioxide Separation. In Basile, A. & Ghasemzadeh, K. (Eds.), *Current Trends and Future Developments on (Bio-) Membranes* (pp. 265-294): Elsevier.https://doi.org/10.1016/B978-0-444-63866-3.00011-X

Liland, K. H., Kohler, A., & Afseth, N. K. (2016). Model-based pre-processing in Raman spectroscopy of biological samples. *47*(6), 643-650. doi:10.1002/jrs.4886

Long, D. A. (2002). Classical Theory of Rayleigh and Raman Scattering. In *The Raman Effect: A Unified Treatment of the Theory of Raman Scattering by Molecules*: John Wiley & Sons Ltd

Luis, P. (2016). Use of monoethanolamine (MEA) for CO_2 capture in a global scenario: Consequences and alternatives. *Desalination, 380*, 93-99. https://doi.org/10.1016/j.desal.2015.08.004

Lyndgaard, L. B. (2013). *Apppplications of Raman Spectroscopy and Multivariate Data Analysis in Food and Pharmaceutical Sciences.* (PhD), University of Copenhagen, Copenhagen.

Masohan, A., Ahmed, M., Nirmal, S. K., Kumar, A., & Garg, M. O. (2009). A simple pH-based method for estimation of CO_2 absorbed in alkanolamines. *Indian Journal of Science and Technology 2*(4), 59-64. 10.17485/ijst/2009/v2i4/29433

Miller, C. E. (2010). Chemometrics in Process Analytical Technology (PAT). In Bakeev, K. A. (Ed.), *Process Analytical Technology*.doi:10.1002/9780470689592.ch12

Montañés, R. M., Flø, N. E., Dutta, R., Nord, L. O., & Bolland, O. (2017). Dynamic process model development and validation with transient plant data collected from an MEA test campaign at the CO_2 Technology Center Mongstad. *Energy Procedia, 114*, 1538-1550. https://doi.org/10.1016/j.egypro.2017.03.1284

Morton, F., Laird, R., & Northington, J. (2013). The National Carbon Capture Center: Cost-effective test bed for carbon capture R&D. *Energy Procedia, 37*, 525-539. https://doi.org/10.1016/j.egypro.2013.05.139

Naes, T., Irgens, C., & Martens, H. (1986). *Comparison of Linear Statistical Methods for Calibration of NIR Instruments* (Vol. 35).10.2307/2347270

NASA/GISS. (2018, 08/02/2018). Global Temperature. Retrieved from https://climate.nasa.gov/vital-signs/global-temperature/

Ni, F., & Scheraga, H. A. (1985). Resolution enhancement in spectroscopy by maximum entropy fourier self-deconvolution, with applications to Raman spectra of peptides and proteins. *16*(5), 337-349. 10.1002/jrs.1250160512

Nichola McCann, D. P., Xiaoguang Wang, William Conway, Robert Burns, Moetaz Attalla, Graeme Puxty, Marcel Maeder. (2009). Kinetics and Mechanism of Carbamate Formation from CO2(aq), Carbonate Species, and Monoethanolamine in Aqueous Solution. *The Journal of Physical Chemistry A, 113*(17), 5022-5029. 10.1021/jp810564z

NOAA/ESRL. (2019). Trends in Atmospheric Carbon Dioxide. Retrieved from https://www.esrl.noaa.gov/gmd/ccgg/trends/

Norişor, M., Badea, A., & Dincă, C. (2012). Economical and technical analysis of CO_2 transport ways. *UPB Scientific Bulletin, Series C: Electrical Engineering, 74*(1), 127-138.

Næs, T., & Martens, H. (1984). Multivariate calibration. II. Chemometric methods. *TrAC Trends in Analytical Chemistry, 3*(10), 266-271. https://doi.org/10.1016/0165-9936(84)80044-8

Nørgaard, L., Saudland, A., Wagner, J., Nielsen, J. P., Munck, L., & Engelsen, S. B. (2000). Interval Partial Least-Squares Regression (iPLS): A Comparative Chemometric Study with an Example from Near-Infrared Spectroscopy. *Applied Spectroscopy, 54*(3), 413-419. 10.1366/0003702001949500

Ohno, K., Inoue, Y., Yoshida, H., & Matsuura, H. (1999). Reaction of Aqueous 2-(N-Methylamino)ethanol Solutions with Carbon Dioxide. Chemical Species and Their Conformations Studied by Vibrational Spectroscopy and ab Initio Theories. *The Journal of Physical Chemistry A, 103*(21), 4283-4292. 10.1021/jp984821q

Olivier, J. G. J., Schure, K. M., & Peters, J. A. H. W. (2018). *Trends in global CO_2 and total greenhouse gas emissions: 2018 report*. The Hague

OpenDataSoft. Large Scale Carbon Capture Projects Database. Retrieved 31/01/2019 https://data.opendatasoft.com/explore/embed/dataset/large-scale-carbon-capture-projects-database@kapsarc/table/?disjunctive.capture_type&disjunctive.country&disjunctive.industry&disjunctive.primary_storage_type&disjunctive.project_lifecycle_stage&disjunctive.project_name&sort=time_period

Pelletier, M. J. (1999). *Analytical applications of Raman spectroscopy*. Oxford: Blackwell Science

Perinu, C., Arstad, B., & Jens, K.-J. (2014). NMR spectroscopy applied to amine–CO_2–H_2O systems relevant for post-combustion CO_2 capture: A review. *International Journal of Greenhouse Gas Control, 20*, 230-243. https://doi.org/10.1016/j.ijggc.2013.10.029

Petersen, L., & Esbensen, K. H. (2005). Representative process sampling for reliable data analysis−a tutorial. *19*(11 - 12), 625-647. doi:10.1002/cem.968

Posey, M. L., & Rochelle, G. T. (1997). A thermodynamic model of Methyldiethanolamine−CO_2−H_2S−water. *Industrial & Engineering Chemistry Research, 36*(9), 3944-3953. 10.1021/ie970140q

Puxty, G., Bennett, R., Conway, W., & Maher, D. (2016). A comparison of Raman and IR spectroscopies for the monitoring and evaluation of absorbent composition during CO2 absorption processes. *International Journal of Greenhouse Gas Control, 49*, 281-289. https://doi.org/10.1016/j.ijggc.2016.03.012

Raksajati, A., Ho, M. T., & Wiley, D. E. (2018). Comparison of solvent development options for capture of CO_2 from flue gases. *Industrial & Engineering Chemistry Research, 57*(19), 6746-6758. 10.1021/acs.iecr.8b00283

Richner, G., & Puxty, G. (2012). Assessing the chemical speciation during CO_2 absorption by aqueous amines using in situ FTIR. *Industrial & Engineering Chemistry Research, 51*(44), 14317-14324. 10.1021/ie302056f

Robert Guenard, G. T. (2010). Implementation of Process Analytical Technologies. In Bakeev, K. A. (Ed.), *Process Analytical Technology Spectroscopic Tools and Implementation Strategies for the Chemical and Pharmaceutical Industries* (2 ed.). UK: John Wiley & Sons Ltd

Robinson, K., McCluskey, A., & Attalla, M. I. (2011). An FTIR spectroscopic study on the effect of molecular structural variations on the CO_2 absorption characteristics of heterocyclic amines. *ChemPhysChem, 12*(6), 1088-1099. doi:10.1002/cphc.201001056

Rodionova, O. Y., Esbensen, K., & Pomerantsev, A. (2004). Application of SIC (simple interval calculation) for object status classification and outlier detection - comparison with regression approach. *Journal of Chemometrics, 18*(9), 402-413. doi:10.1002/cem.885

Rogers, W. J., Bullin, J. A., Davison, R. R., Frazier, R. E., & Marsh, K. N. (1997). FTIR method for VLE measurements of acid-gas–alkanolamine systems. *AIChE Journal, 43*(12), 3223-3231. doi:10.1002/aic.690431210

Roussel, S., Preys, S., Chauchard, F., & Lallemand, J. (2014). Multivariate data analysis (Chemometrics). In al., C. P. O. D. e. (Ed.), *Process Analytical Technology for the Food Industry, Food Engineering Series*. New York Springer Science Business Media. DOI 10.1007/978-1-4939-0311-5_2

Samarakoon, P. A. G. L., Andersen, N. H., Perinu, C., & Jens, K.-J. (2013). Equilibria of MEA, DEA and AMP with bicarbonate and carbamate: A Raman study. *Energy Procedia, 37*, 2002-2010. https://doi.org/10.1016/j.egypro.2013.06.080

Sato, M., & Hansen, J. (2019). Updating the Climate Science. What Path is the Real World Following? Retrieved from http://www.columbia.edu/~mhs119/EnergyConsump/

Socrates, G. (2000). *Alkane Group Residuals: C–H Group Infrared and Raman Characteristic Group Frequencies: Tables and Charts* (3 ed.). West Sussex: John Wiley & Sons Ltd

Souchon, V., Aleixo, M. d. O., Delpoux, O., Sagnard, C., Mougin, P., Wender, A., & Raynal, L. (2011). In situ determination of species distribution in alkanolamine-H_2O-CO_2 systems by Raman spectroscopy. *Energy Procedia, 4*, 554-561. https://doi.org/10.1016/j.egypro.2011.01.088

Stewart, E. J., & Lanning, R. A. (1994). *Reduce amine plant solvent losses; Part 1* (Vol. 74:6)

Stott, P. (2016). How climate change affects extreme weather events. *352*(6293), 1517-1518. 10.1126/science.aaf7271 %J Science

Svensson, R., Odenberger, M., Johnsson, F., & Strömberg, L. (2004). Transportation systems for CO_2 - application to carbon capture and storage. *Energy Conversion and Management, 45*(15), 2343-2353. https://doi.org/10.1016/j.enconman.2003.11.022

Tait, P., Buschle, B., Ausner, I., Valluri, P., Wehrli, M., & Lucquiaud, M. (2016). A pilot-scale study of dynamic response scenarios for the flexible operation of post-combustion CO_2 capture. *International Journal of Greenhouse Gas Control, 48*, 216-233. https://doi.org/10.1016/j.ijggc.2015.12.009

Templeton, Douglas M. , Ariese, F., Cornelis, R., Danielsson, L.-G., Muntau, H., Leeuwen, H. P. V., & Łobiński, R. (2000). Guidelines for terms related to chemical speciation and fractionation of elements. Definitions, structural aspects, and methodological approaches. *Pure Applied Chemistry, 72*(8), 1453–1470.

Thomsen, K., & Rasmussen, P. (1999). Modeling of vapor–liquid–solid equilibrium in gas–aqueous electrolyte systems. *Chemical Engineering Science, 54*(12), 1787-1802. https://doi.org/10.1016/S0009-2509(99)00019-6

Tseng, C.-L., Chen, Y.-K., Wang, S.-H., Peng, Z.-W., & Lin, J.-L. (2010). 2-Ethanolamine on TiO2 Investigated by in Situ Infrared Spectroscopy. Adsorption, Photochemistry, and Its Interaction with CO2. *The Journal of Physical Chemistry A, 114*(27), 11835-11843.

van der Ham, L. V., Bakker, D. E., Geers, L. F. G., & Goetheer, E. L. V. (2014). Inline monitoring of CO_2 absorption processes using simple analytical techniques and multivariate modeling. *Chemical Engineering and Technology, 37*(2), 221-228. doi:10.1002/ceat.201300249

van Eckeveld, A. C., van der Ham, L. V., Geers, L. F. G., van den Broeke, L. J. P., Boersma, B. J., & Goetheer, E. L. V. (2014). Online monitoring of the solvent and absorbed acid gas concentration in a CO_2 capture process using monoethanolamine. *Industrial & Engineering Chemistry Research, 53*(13), 5515-5523. 10.1021/ie402310n

Versteeg, G. F., & van Swaaij, W. P. M. (1988). On the kinetics between CO_2 and alkanolamines both in aqueous and non-aqueous solutions—I. Primary and secondary amines. *Chemical Engineering Science, 43*(3), 573-585. https://doi.org/10.1016/0009-2509(88)87017-9

Vogt, M., Pasel, C., & Bathen, D. (2011). Characterisation of CO_2 absorption in various solvents for PCC applications by Raman spectroscopy. *Energy Procedia, 4*, 1520-1525. https://doi.org/10.1016/j.egypro.2011.02.020

Wang, M., Joel, A. S., Ramshaw, C., Eimer, D., & Musa, N. M. (2015). Process intensification for post-combustion CO_2 capture with chemical absorption: A critical review. *Applied Energy, 158*, 275-291. https://doi.org/10.1016/j.apenergy.2015.08.083

Wang, Y., Zhao, L., Otto, A., Robinius, M., & Stolten, D. (2017). A review of post-combustion CO_2 capture technologies from coal-fired power plants. *Energy Procedia, 114*, 650-665. https://doi.org/10.1016/j.egypro.2017.03.1209

Weiland, R. H., & Trass, O. (1969). Titrimetric determination of acid gases in alkali hydroxides and amines. *Analytical Chemistry, 41*(12), 1709-1710. 10.1021/ac60281a024

Wise, B. M., & Roginski, R. T. (2015). A Calibration Model Maintenance Roadmap. *IFAC-PapersOnLine, 48*(8), 260-265. https://doi.org/10.1016/j.ifacol.2015.08.191

Wold, H. (1975). Soft modeling by latent variables: the nonlinear iterative partial least squares approach. *Journal of Applied Probability, 12*(S1), 117-142. 10.1017/S0021900200047604

Wold, S. (2015). Chemometrics and Bruce: Some Fond Memories. In *40 Years of Chemometrics – From Bruce Kowalski to the Future* (Vol. 1199, pp. 1-13): American Chemical Society.doi:10.1021/bk-2015-1199.ch001

Wold, S., & Josefson, M. (2006). Multivariate Calibration of Analytical Data. In Meyers, R. A. & Brown, S. D. (Eds.), *Encyclopedia of Analytical Chemistry*: John Wiley & Sons.doi:10.1002/9780470027318.a5205

Wold, S., Sjostrom, M., & Eriksson, L. (2001). PLS-regression: A Basic Tool of Chemometrics. *Chemometrics and Intelligent Laboratory Systems, 58*(2), 109-130. 10.1016/S0169-7439(01)00155-1

Wong, M. K., Bustam, M. A., & Shariff, A. M. (2015). Chemical speciation of CO2 absorption in aqueous monoethanolamine investigated by in situ Raman spectroscopy. *International Journal of Greenhouse Gas Control, 39*, 139-147. https://doi.org/10.1016/j.ijggc.2015.05.016

Wong, M. K., Shariff, A. M., & Bustam, M. A. (2016). Raman spectroscopic study on the equilibrium of carbon dioxide in aqueous monoethanolamine. *RSC Advances, 6*(13), 10816-10823. 10.1039/C5RA22926J

Workman, J. (2001). NIR spectroscopy calibration basics. In Burns, D. A. & Ciurczak, E. W. (Eds.), *Handbook of Near-Infrared Analysis* (pp. 123-149). Boca Raton: CRC Press

Yang, Q., Bown, M., Ali, A., Winkler, D., Puxty, G., & Attalla, M. (2009). A carbon-13 NMR study of carbon dioxide absorption and desorption with aqueous amine

solutions. *Energy Procedia, 1*(1), 955-962. https://doi.org/10.1016/j.egypro.2009.01.127

Zhang, W., Sun, C., Snape, C. E., Irons, R., Stebbing, S., Alderson, T., . . . Liu, H. (2017). Process simulations of post-combustion CO_2 capture for coal and natural gas-fired power plants using a polyethyleneimine/silica adsorbent. *International Journal of Greenhouse Gas Control, 58*, 276-289. https://doi.org/10.1016/j.ijggc.2016.12.003

Øi, L. E., Hansen, P. M., & Henriksen, M. (2017). CO_2 absorption efficiency and heat consumption measured at high gas to liquid ratios in laboratory rig. *Energy Procedia, 114*, 1273-1281. https://doi.org/10.1016/j.egypro.2017.03.1381

Øi, L. E., Lundberg, J., Pedersen, M., Hansen, P. M., & Melaaen, M. C. (2014). Measurements of CO_2 absorption and heat consumption in laboratory rig. *Energy Procedia, 63*, 1569-1577. https://doi.org/10.1016/j.egypro.2014.11.166

PART 3

Published and submitted papers

Paper A

In-situ monitoring method for CO$_2$ capture process - complete liquid speciation

In-situ Monitoring Method for CO_2 Capture Process – Complete Liquid Speciation

M. H. Wathsala N. Jinadasa*, Klaus-Joachim Jens, Maths Halstensen

Applied Chemometrics and Research Group (ACRG), Faculty of Natural Sciences and Maritime Sciences – University of South-eastern Norway, Post box 235, N-3603 Kongsberg, Norway

ABSTRACT

A reliable in-situ liquid analysis method is crucial in the deployment of CO_2 capture plants in industrial scale. A method for determining chemical concentration profiles in an amine based CO_2 capture process by continuous measurements from Raman spectroscopy is presented. Total CO_2 loading, concentration of protonated amine, free amine, carbonate, bicarbonate, carbamate and sum of carbonate and bicarbonate in a lab scale or industrial scale capture process can be quantified directly and fast such as in every minute using the developed method and hence Raman spectroscopy becomes a versatile tool for process monitoring, thermodynamic modeling and plant optimization scenarios. In the model development stage, Raman spectroscopy measurements from 30 w/w% MEA solution at 25°C and atmospheric pressure were calibrated and validated with complete speciation results from NMR reference analysis. A chemometric based approach was used to develop prediction models using partial

least square regression because of its superiority than univariate analysis to handle spectroscopic data. Validation results show an acceptable prediction accuracy for all seven models. The paper presents a complete guide for the model development that can be imitated to similar solvent systems. Raman spectroscopy can be easily integrated in-line to any location in the CO_2 capture plant and it has a non- invasive, zero sampling handling approach and hence is a promising candidate for in-situ monitoring.

1. INTRODUCTION

Amine scrubbing has been in practice to separate CO_2 from natural gas since 1930 and is considered as a robust technology for CO_2 capture from coal-fired power plants [1]. Due to the availability of related engineering and technical knowledge, the amine technology is closest to retrofit of existing power plants as a post-combustion capture solution. Speciation values (concentration of species) of amine-CO_2-H_2O system plays a substantial role to characterize vapour liquid equilibrium, thermodynamic modelling, reaction mechanisms and reaction kinetics and further helps to improve process configuration, process parameters and scale up scenarios. In real-time applications, they can be used as manipulators for process control.

In this study, we present the development of speciation models, which can be used for complete speciation of an MEA-CO_2-H_2O system. The models are based on Raman spectroscopic measurements which were regressed by the PLSR multivariate regression technique (partial least square regression)[2,3] with reference values obtained from NMR spectroscopy. The models can be used in both offline and in-situ operation and provide a simple, fast and robust approach for real-time observation of speciation data in both dynamic and steady state conditions. This paper explains the methodology of how the models were developed and how they are used in application. The base case for CO_2 removal by an aqueous monoethanolamine solution is reported as absorption taking place by 30 w/w % MEA solution

at 40°C at atmospheric pressure. Typical lean loading can vary between 0.1 to 0.3 mol CO_2/mol MEA[4] and rich loading can go as high as 0.5 mol CO_2/mol MEA. The experiments in this study was carried out at atmospheric pressure and room temperature with 30 wt% MEA and the CO_2 loading was spanned from upto 0.6120 mol / mol MEA. The upper limit of the loading was the highest achievable CO_2 concentration using our CO_2 loading set up. Raman spectroscopy as a process analytical technology has shown a significant progress for speciation in amine based chemical systems during past ten years. Enabling Raman spectroscopy for speciation minimizes the number of experiments required during plant design and operation while increasing the amount of information extracted in experiments and trials. It also supports pilot plant tests and commercial CO_2 capture test facilities providing required concentration variations during the absorption and desorption process representing a role as a controller for many process parameters.

1.1 Chemistry of CO_2 with aqueous MEA

The chemical reaction between primary amines such as MEA with CO_2 has been reviewed several times in recent and past literature[5]. MEA contains one amine functional group and one alcohol functional group. Tthe reaction between amine and CO_2 by two steps as shown in equation 1 and 2[6] which was first introduced by [7] and reintroduced by [8].

$$CO_{2(aq)} + R_1R_2NH \leftrightarrow R_1R_2N^+HCOO^- \qquad (1)$$

$$R_1R_2N^+HCOO^- + B \leftrightarrow R_1R_2NCOO^- + BH^+ \qquad (2)$$
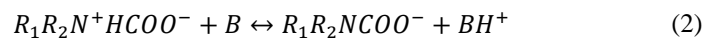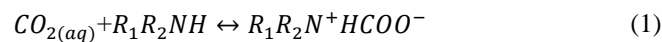
Here CO_2 reacts with the amine to form an intermediate and this intermediate immediately reacts with another molecule (B) to form a carbamate and a protonated amine. This reaction describes the carbamate formation where B is a base, usually a second amine molecule. The mechanism is usually referred as the zwitterion mechanism. However, the bicarbonate formation cannot be described by zwitterion reaction. Bicarbonate/carbonate formation,

protonation/deprotonation of amine, carbamate formation further can be described using equation (3) to (12).

$$H_2O \leftrightarrow OH^- + H^+ \tag{3}$$
$$CO_{2(aq)} + OH^- \leftrightarrow HCO_3^- \tag{4}$$
$$CO_{2(aq)} + H_2O \leftrightarrow H_2CO_3 \tag{5}$$
$$H_2CO_3 \leftrightarrow HCO_3^- + H^+ \tag{6}$$
$$HCO_3^- \leftrightarrow CO_3^{2-} + H^+ \tag{7}$$
$$RNH_2 + H^+ \leftrightarrow RNH_3^+ \tag{8}$$
$$RNH_2 + HCO_3^- \leftrightarrow RNHCO_2^- + H_2O \tag{9}$$
$$RNH_2 + CO_2 \leftrightarrow RNHCOOH \tag{10}$$
$$RNHCO_2^- + H^+ \leftrightarrow RNHCOOH \tag{11}$$
$$RNHCO_2^- + H_2O \leftrightarrow HCO_3^- + RNH_2 \tag{12}$$
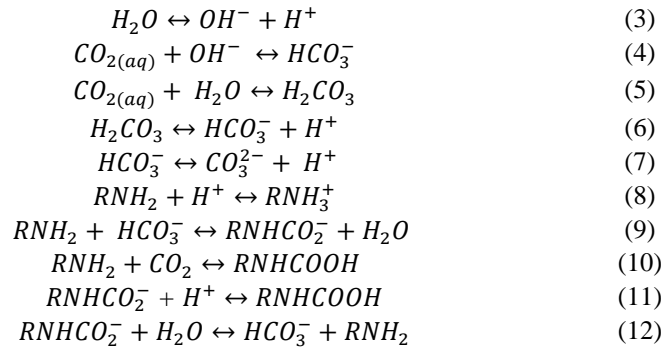
The equations show water dissociation, carbon dioxide hydrolysis, carbonate/bicarbonate formation, amine protonation, carbamation and decarbamation. These reactions generate a pool of cations and anions which include $OH^-, H^+, HCO_3^-, CO_3^{2-}, RNHCO_2^-$ and RNH_3^+ which are in equilibrium. The graphical representation of these reactions[9] which is presented in Fig. 1 shows that there are three parallel, reversible reactions of the free amine with CO2, carbonic acid, and the bicarbonate ion; the relative importance of the three paths is strongly pH dependent.
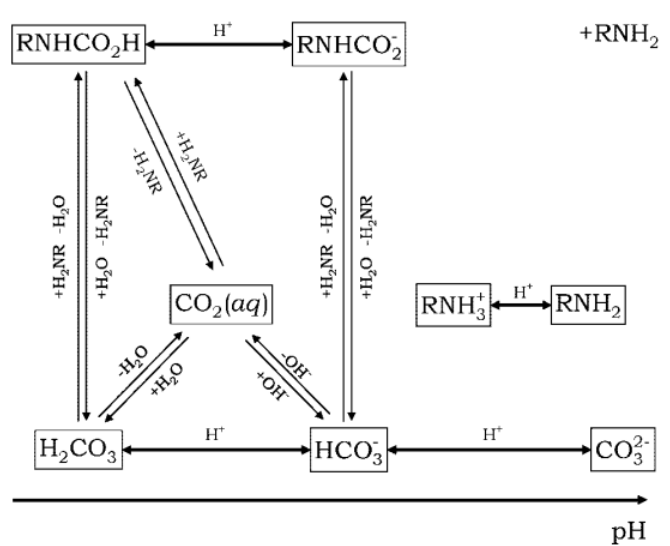
Fig. 1.General reaction scheme including all reactions between amine, the CO2/carbonate group and protons. Single line/double arrow represent instantaneous protonation equilibria, double lines represent kinetically observable reactions for which rate constants are known in literature (Adapted with permission[9]. Copyright (2009) American Chemical Society

4

1.2   Motivation

The most popular method for determining CO_2 removal efficiency in CO_2 capture plants is gas phase analysis using gas analyzers such as FTIR[10]. Liquid phase analysis in practice are mostly offline and laboratory-based but is one of routine tasks in any CO_2 capture related R&D work and pilot plant trials. Depending on the requirement, the frequency of this offline analysis varies but more conclusions that are useful can be derived if in-situ analysis is possible where plant trends can be observed with respect to different parameters such as time, process conditions and system configuration. Analysis of CO_2 loading by $BaCl_2$ titration-precipitation method is commonly used but it is time consuming and tedious and the analysis takes around 2 hours per sample for an experienced chemist. Time-consuming methods are not suitable candidates for plant operations. During offline measurements, samples are collected from the system and the method of sample extraction, sample preservation, transportation to the lab, and mass/volume reduction of sample for chemical analysis increase the sampling error percentage and becomes less representative to the required measurement.

The ideal situation for in-situ analysis is direct measurement of the composition. Although several methods have been proposed they are still in the probationary period and are tested in pilot plant trials for validation in different process conditions. No reliable methods have yet been recommended/accepted for standard use in CO_2 capture plants among the research community. The most popular three composition readings from a CO_2 capture plant are the CO_2 loading, solvent capacity and degradation products. From lab to industry, the standard methods of analysis composition are acid-base titrations, total inorganic carbon analysis, ion chromatography and gas chromatography. The National Carbon Capture Centre, USA uses automatic titration for determining CO_2 loading in some of their R&D work [11]. Another solution is calculating the CO_2 loading based on correlation from direct measurements such as pH, density, viscosity, conductivity and temperature of the solvent streams. In one of the

dynamic test campaign at TCM Mongdad Plant, CO_2 loading was determined in lean and rich lines based on a correlation from direct measurement readings for total alkalinity, density and temperature of the solvent [12]. The relationship between such physical properties and chemical properties are complex and requires a detailed knowledge on solvent concentration, CO_2 loading and temperature[13]. ^1H, ^{13}C, ^{15}N NMR data are growing interest in the speciation of amine-CO_2-H_2O. It is a non-invasive analytical technique, which allows the study of atoms that have nuclei with a magnetic moment. NMR can also characterize unknown compounds without the use of any standard reference. NMR studies were carried out to investigate the liquid-phase composition in samples where various amounts of CO_2 were dissolved in different alkanolamines at various temperatures[14]. A literature review on NMR spectroscopy applied to amine–CO_2–H_2O is presented [15] based on approximately 50 articles. The main drawback of ^{13}C NMR spectroscopy is its long measurement times such as hours. However, there are instances where NMR has been used for online monitoring[16,17] for speciation and reaction monitoring but the time scale between each measurements were 1-2 hours.

Liquid analysis using vibrational or absorption spectroscopic methods such as IR, NIR, Raman have growing interest due to their low acquisition times and applicability for in-situ monitoring. A screening experiment was performed[18] to investigate the relations between UV-vis spectroscopy, density, refractive index, conductivity, and pH and a multivariate chemometric method was developed[19] combining density, conductivity, refractive index, and sonic speed measurements for monitoring of acid gas and MEA concentrations in CO_2 absorption processes in the presence of some degradation products. this multivariate model predictivity in the presence of degradation products was also compared[20]. A predictive statistical model was built using chemometrics method and measurements of density, pH, conductivity, sound velocity, refractive index, and Near InfraRed (NIR) spectroscopy and concentrations of MDEA, PZ, and CO_2 were predicted real-time[21]. Measurements of carbon

dioxide and hydrogen sulfide in aqueous solutions of DEA using FTIR is presented in earlier studies[22]. Since then the use of FTIR for speciation in CO_2 loaded aqueous amine have been performed by several researchers such as FT-IR for DEA system[23], PLS +ATR-method for MEA system[24] and FTIR- ATR for monitoring CO_2, SO_x, and solution of β-alanine and potassium hydroxide [25]. FTIR was used for MDEA system[26], ATR-FTIR was used[27] for MEA, DEA, and AMP systems while ATR-FTIR was used [28] for four industrial capture solvents.

A completely different approach is presented [29] where they used indirect spectral hard modelling to calibrate Raman data. Recently, a comparison of vibrational spectroscopic methods for liquid speciation is reported[30] who made a comparison between the IR-ATR and Raman spectroscopy by developing PLS models to predict amine and CO_2 concentrations in a blend of MEA and 3-piperidinemethanol. They experienced that fluorescence disturbed the Raman measurement acquisition in pilot plant data while IR-ATR was successful. Raman, NIR and ATR FTIR methodsvwere compared[31] in CO_2 loaded MEA solutions where they claim that all three spectroscopies well suit for the application.

Speciation using molar scattering factor and ClO_4^- internal standard for Raman measurements were performed for MEA, DEA and AMP[32], for MEA systems[33,34] and for aqueous N-methylpiperidine, 2-methylpiperidine and 4-methylpiperidine[35]. Calibration plots for bicarbonate, carbonate and carbamate species based on peak areas of various concentration of individual species are presented[36] which can be used for speciation in amine systems. A qualitative analysis from Raman spectroscopy for MEA, diglycolamine and MDEA for reaction monitoring with CO_2 was studied[37] and they found that the temperature dependency of Raman spectroscopy can be neglected in this temperature range of 25°C to 60°C. Raman investigations were done for different concentrations of CO_2 loaded MEA, DEA and MDEA[38]. Reference spectra were recorded from CO_3^{2-}, HCO_3^- and protonated amine solutions which

were used to quantify species in MDEA and ^{13}C NMR spectroscopy was used to compare the Raman speciation.

In summary, for the prediction of individual species, calibration models developed based on pure components have been used in many studies mentioned above assuming that the system obeys Beer Lambert law. Absorption and vibrational spectra of the CO_2 loaded amine solutions contain overlapping peaks in the same area detected by individual spectrum and hence isolating this region is challenging and can result in losing information. Regression with data obtained by thermodynamic models lacks of reliability because even the thermodynamic models are based on assumptions and may not always true for transient conditions. Some studies present only the speciation for total CO_2 loading and solvent concentration. The analysis performed using internal standard are not suitable for in-situ monitoring.

In general, Raman spectroscopy can identify many organic and inorganic substances from their specific spectral patterns, gives weak scattering for water, can be used for remote sensing as the Raman light can be transmitted via fibre optic cables over long distances, no sample preparation needed, non-destructive and needs only a small volume for analysis. Several research have been done analyzing Raman spectra both univariately and multivariately to quantify concentration profiles in CO_2 capture plants. The Applied Chemometrics and Research Group (ACRG) at University of South-Eastern Norway (USN) has developed a method using Raman spectroscopy which is described in this paper, to determine chemical concentration profiles in an MEA-CO_2-H_2O system based on multivariate analysis. The method was validated by results from mini-pilot CO_2 capture plant facility in Porsgrunn, Norway[39]. The developed method can be used for laboratory experiments, R&D tasks, pilot plant operations and commercial applications of the CO_2 absorption process.

1.3 Raman spectroscopy and PLSR

The Raman spectrometer available at USN is the Kaiser RXN2 analyzer with 785 nm laser wavelength, 400 mW maximum laser power and 100-3425 cm-1 spectral range. An immersion optic probe is connected to the RXN2 analyzer via a fibre optic cable, which conveys the laser light back and forth from instrument to sample. The Raman scattered light is displayed by the analyzer as a plot of Raman intensity (y-axis) which is the Raman scattered radiation and Raman wavenumber (x-axis) which is the frequency difference from the incident radiation[40]. Peaks, which appear in this plot and their intensity, carry information about the chemicals present in the system and their composition respectively. Based on the Fig. 1 almost all the reactions happen in the MEA-CO_2-H_2O system are related to each other. A change in concentration in one component affect to the overall equilibrium in the system. The system is also pH dependent. PLSR models have been proven a successful candidate in the analysis of CO_2 capture solvents. In our previous study of CO_2 absorption in chilled ammonia [41] and CO_2 capture in four different amine types including MEA[42], the use of PLSR method for chemical speciation are reported. In this study, we report how PLSR method was used to combine Raman and NMR spectroscopic data to achieve a reliable complete speciation in amine system.

2 Methodology

2.1 Experimental Procedure

'Loaded solution' refers to 30 w/w% MEA with CO_2 bubbled while 'unloaded solution' refers to 30 w/w% MEA without CO_2 bubbled in this text. Two CO_2 loaded sample sets were prepared separately in room temperature and pressure (25 ^{0}C and 1 bar) maintaining the same experimental conditions. One set included 23 calibration samples and the other set was 22 validation samples. CO_2 received from "AGA" with an initial mole fraction of 0.9999, and MEA, received from "Merck" with an initial mole fraction of 0.995, were used as received. For the preparation of 30 % MEA stock solutions, pure MEA and Milli-Q water (18.2 MΩ·cm)

was degassed using Rotavapor® R-300. Two amine stock solutions to obtain 30 w/w% were prepared by mixing degassed Milliq water and 99% MEA gravimetrically using analytical balance (Mettler Toledo AS120S within ± 0.0001 g) followed by stirring at 400 rpm for 30 minutes to ensure homogeneity in the mixture. One stock solution was loaded with CO_2 to react with the MEA molecules present in the solution by bubbling a CO_2 gas stream (0.15 L/min) through a fritted glass and bubbling was carried out for a sufficient time for the 30 % MEA solution to load with equilibrium CO_2 concentration at the experimental temperature and pressure. This CO_2 loaded solution was then allowed to cool down to the room temperature and stirred at 400 rpm in a closed vessel for another 30 minutes. The stock solution was then allowed to reach equilibrium for 24 hours in a closed container prior to further analysis. The loaded amine sample series in the calibration set were prepared by diluting the CO_2 loaded aqueous amine solution with unloaded solution in different mass ratios. This resulted in a series of CO_2 loading samples spanning from a higher to lower CO_2 loading level. Each sample was approximately 10 g weighed in total and was prepared in airtight glass bottles. The same procedure was followed when preparing the validation sample set.

In this study, three analysis methods were used namely $BaCl_2$-titration, Raman spectroscopy and NMR spectroscopy. The purpose of titration was to determine CO_2 loading and MEA concentration while NMR measurements determined the concentrations of free MEA, protonated MEA, carbonate, bicarbonate and carbamate in each calibration and validation samples. [43,44] showed that the uncertainty of $BaCl_2$ titration method is ±1.3% and ±2%. It is possible to get a reliable quantification of peak area fractions down to 0.05% by NMR [45]. The Raman measurements were regressed based on the NMR speciation data and PLSR models were developed.

2.1.1 Titration

Determining the CO_2 loading and amine concentration using $BaCO_3$ precipitation titration method is describe below. Approximately, 0.25 g of the loaded sample was mixed with 50 cm^3 of 0.3 M $BaCl_2$ and 50 cm^3 of 0.1 M NaOH. The mixture was boiled for 7 minutes, and cooled down to room temperature. The sample was then filtrated, and the $BaCO_3$ filter cake was transferred to 100 cm^3 of degassed, deionized water. Stirring was carried out to dissolve all $BaCO_3$ particles. The mixture was then titrated with 0.1 M HCl (from Merck) until the solution reached pH 2. The sample was then boiled at 270^0C for 7 minutes and titrated with 0.1 M NaOH (from Merck) to achieve pH 7, which was the end point for the acid-base titration. The mass of the sample and volumes of HCl and NaOH added during the titration were used for the calculation of CO_2 loading. Another 1 g of CO_2 loaded sample was mixed with 100g of deionized water and titrated with 1M HCl. The exact weight of CO_2 loaded sample and the volume of 1 M HCl were used to calculate the MEA concentration. All the samples in the calibration set, validation set and the stock solution were titrated using the above procedure.

2.1.2 Raman measurements

Before taking Raman measurements, the Raman immersion probe was cleaned with deionized water followed by acetone to remove any impurities on the probe tip. Raman measurements are light sensitive. Therefore, each sample to be measured were wrapped in an aluminum foil to get rid of disturbances from fluorescence from the background light. The sample to be measured was placed inside a plastic black box to further avoid fluorescent disturbances and the Raman immersion probe was dipped into the solution [42]. The distance between the tip of the Raman probe and the bottom of the sample container was maintained to be more than 2.5 mm and absence of air bubbles on the tip of the Raman probe was ensured. Fig. 2 shows the Raman set up used for this study which includes the laser excitation unit, fibre optic cable, immersion probe. The Raman instrument (RXN2 Kaiser Raman System) was then

configured. The signal to noise ratio was optimized by varying the acquisition time and number of scans. The best compromise between the acquisition time and spectral quality of a Raman measurement for an MEA-CO_2-H_2O solution was configured as 6 scans having 10-second exposure time per each scan and this configuration was maintained for all the measurements in this study. Data were acquired and saved using iC Raman 4.1 software.
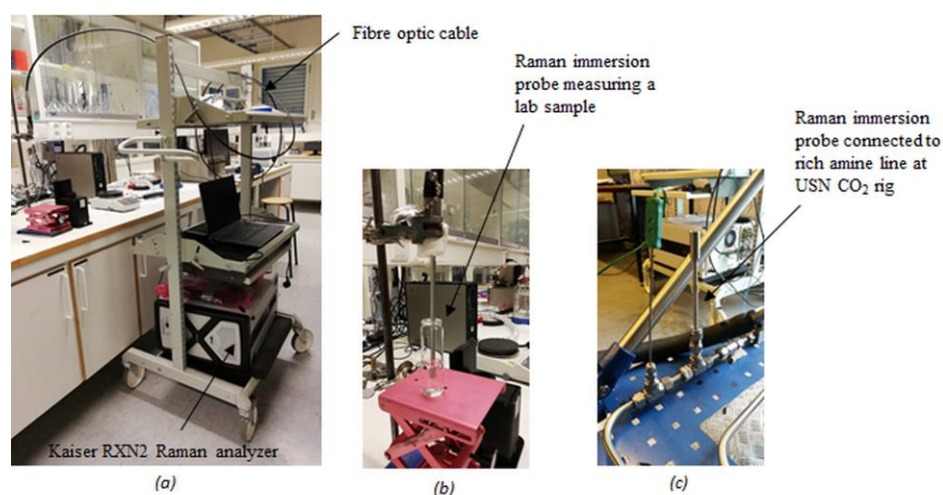
Fig. 2 .Raman set up used for the study

2.1.3 NMR measurements

Quantitative ^{13}C NMR experiments were carried out at 298 K for all the calibration and validation to quantify the species formed in solution. The experimental method was similar to the reported method in[46]. ^{13}C-NMR experiments were performed by 9.4 T on a Bruker Avance III 400 MHz spectrometer using a BBFO Plus double resonance probehead and the spectra were acquired using MestreNova software v 7.1.1. Acetonitrile (CH_3CN) and deuterated water (D_2O), inserted in a sealed capillary, were used as the standard reference and lock solvents, respectively.

2.1.4 Selection of calibration/validation set and other process conditions during experiment

As presented in [47], in typical CO_2 absorption and desorption process by MEA, 30 wt% is used where gas contacts the aqueous MEA at 1 atm. Typical values for lean loading is 0.1-

0.22mol/mol MEA, and the rich loading is 0.4-0.5 mol/mol MEA. Typically, the absorber inlet temperature of the liquid is maintained at 40°C and exothermic reaction between CO_2 and MEA creates a temperature increase in the system. The concentration of the chemical intermediates are dependent on the temperature. Since the final goal of this study was model development to use Raman spectroscopy as an in-situ application in CO_2 absorption plants, the conditions for the calibration and validation set was selected to represent a typical MEA based plant condition. Therefore MEA concentration for all the samples in this study were kept at 30wt% and CO_2 loading was selected to span between the lowest and highest loading level that could be obtained from our experimental loading set up which was from 0.039-0.6120 mol / mol MEA. All the experiments were performed at atmospheric pressure of 1 atm. Since the temperature of the MEA solution is not constant along the absorption/desorption tower or anywhere else in the absorption/desorption process cycle it is not possible to justify which temperature is reasonable for this experiment. As a strategy to cater for this temperature problem, the concentration in each model were expressed as mol/kg H_2O instead of mol/L of the solution. Preparing the samples and performing analysis at room temperature allowed the samples to maintain similar chemical equilibrium conditions throughout the experiment. The homogeneity within the sample container of each calibration and validation set was also important to get representative measurements in this experiment. From each 10 g weighed CO_2 loaded sample, first the Raman signal was taken and then a portion was taken to determine CO_2 loading and MEA concentration by titration. Another portion was transferred to a different container to measure NMR spectra. The sample portion used for three types of analysis should be representative to each other and therefore analysis of samples only after they have reached equilibrium was a mandatory step in this study.

2.1.5 Model development to predict concentrations

After having the measurements from both Raman and NMR spectroscopy for all the calibration and validation samples, a chemomtric approach was followed to develop seven models to predict the species concentration. Data analysis was done by PLS toolbox 7.3 in Matlab 2016a. Model development steps are shown Fig. 3 for a particular specie. The main challenges in developing chemometric based regression models are selecting the suitable preprocessing method/s, variable range, number of PLS components and optimum prediction error. There are different preprocessing techniques available in chemometrics such as mean centering, auto scaling, Savitzky Golay, baseline correction, multiplicative scatter correction. The main objective of the preprocessing is to correct abnormal features of the spectra, filter the noise and and achieve meaningful chemical information. Their applicability is strongly dependent on the type of the solution, interference with other chemical impurities in the system, type of instrument and auxiliaries, noise coming from the instrument and instrument parts as well as environmental conditions. Selecting the optimum preprocessing method was a trial and error technique. As shown in Fig. 3 first a preprocessing method or a combination of two or three such methods were proceeded with the rest of the steps according to Fig. 3. If the final PLSR model was not satisfied, preprocessing method/s was altered. The optimum preprocessing combination for the data set of MEA-CO_2-H_2O solution resulted as baseline correction by Whittaker filter [48] with lamba = 100 and $P = 0.001$, standard normal variate and mean centering. The preprocessed X data matrix was then used to identify most suitable variable range. This variable range should include the vibrational modes of the specie to which the model is built. Performing a PCA (principle component analysis) provides additional benefit to quick identification of samples showing abnormal Raman measurements using their score plot and important variables using the loading plot. The information provided by the loading plot was used in combination of the vibrational modes to select the variable range in

this study. PLSR calibration and validation using the test set method was finally performed using Matlab and the resulting model was evaluated with their statistical results. Use of test set validation method strengthened the model to consist real data and variance generating factors such as sampling errors than using cross validation method which over-estimates the model by giving a lower RMSE because of its monolithic behavior [49]. Until a satisfactory model was developed, an iteration was performed by varying the preprocessing methods and variable range. The final model was saved in the PLS toolbox which can be directly used to feed with data from Raman instrument for future CO_2 loaded samples and predict the specie concentrations.
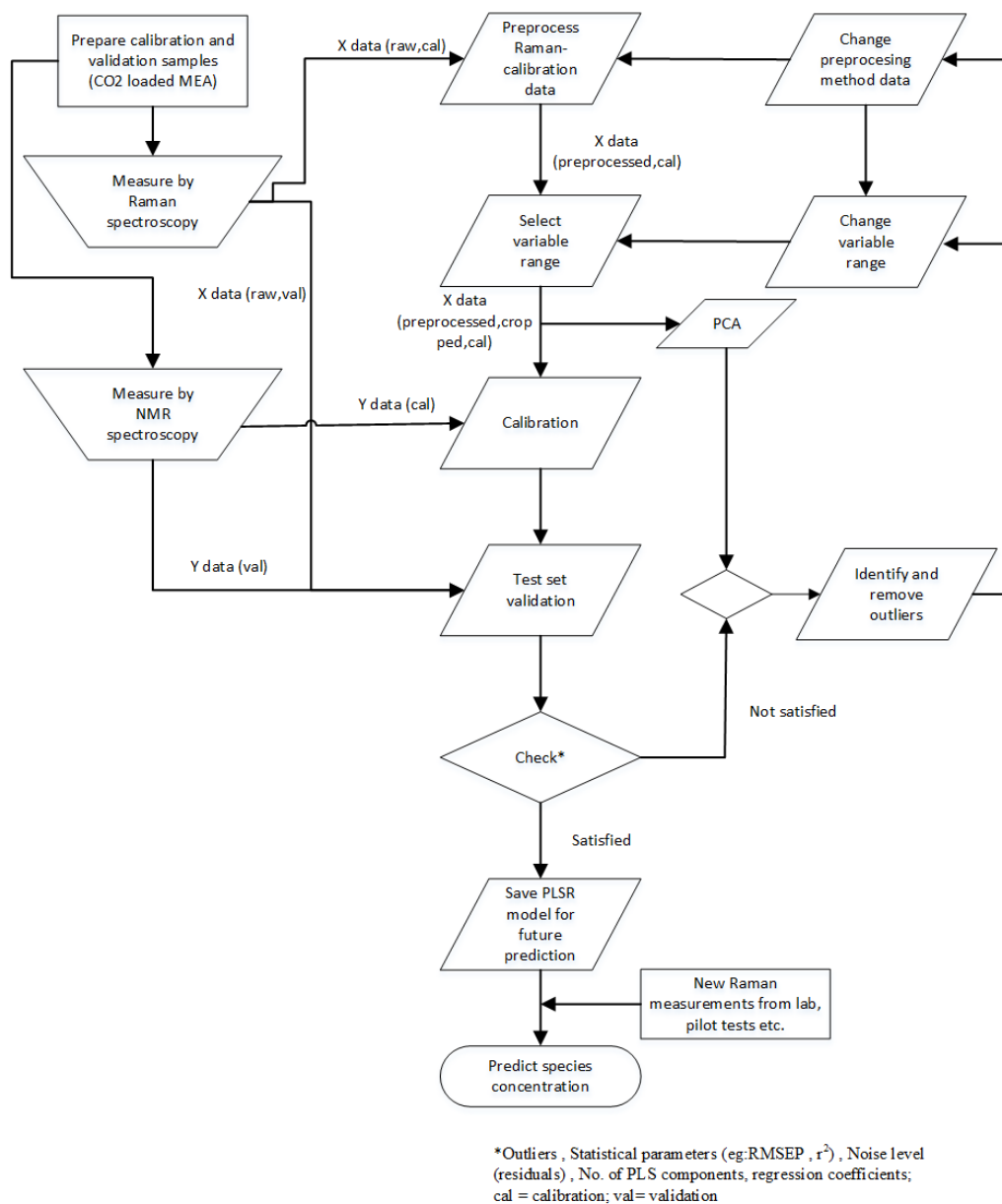
Fig. 3. Development of a PLS model for a specie using Raman spectroscopy and NMR spectroscopy

3   Results and Discussion

Speciation analysis by ^{13}C NMR spectroscopy, $BaCl_2$ precipitation-titration method for loading analysis and Raman spectroscopy followed by the model development combining the two spectroscopic methods are presented in this section.

3.1 ^{13}C NMR results

Based on the CO_2 loading of calibration and validation samples, the peak intensity and the width for each specie appeared differently in ^{13}C NMR measurements. To calculate the area integrals, the ^{13}C NMR spectra were fitted and the area of each peak was related to that of the C-2# of the CH_3CN standard [46] . Example for a ^{13}C NMR spectra and assignment of peaks is shown in Fig. 4. According to this figure, intensity at 166.16 ppm was assigned to C which appear in C of the carbonate and bicarbonate reversible reaction. Intensity at 60.25 ppm and 42.4 ppm were assigned to two Cs in the alkyl group (R) of MEA/MEAH+. C in the two alkyl groups of amine carbamate were assigned to 61.91 ppm and 43.9 ppm while the C in COO$^-$ group was assigned to 165.23 ppm. C related to the CH_3CN standard appears at 119.74 ppm and 1.47 ppm.
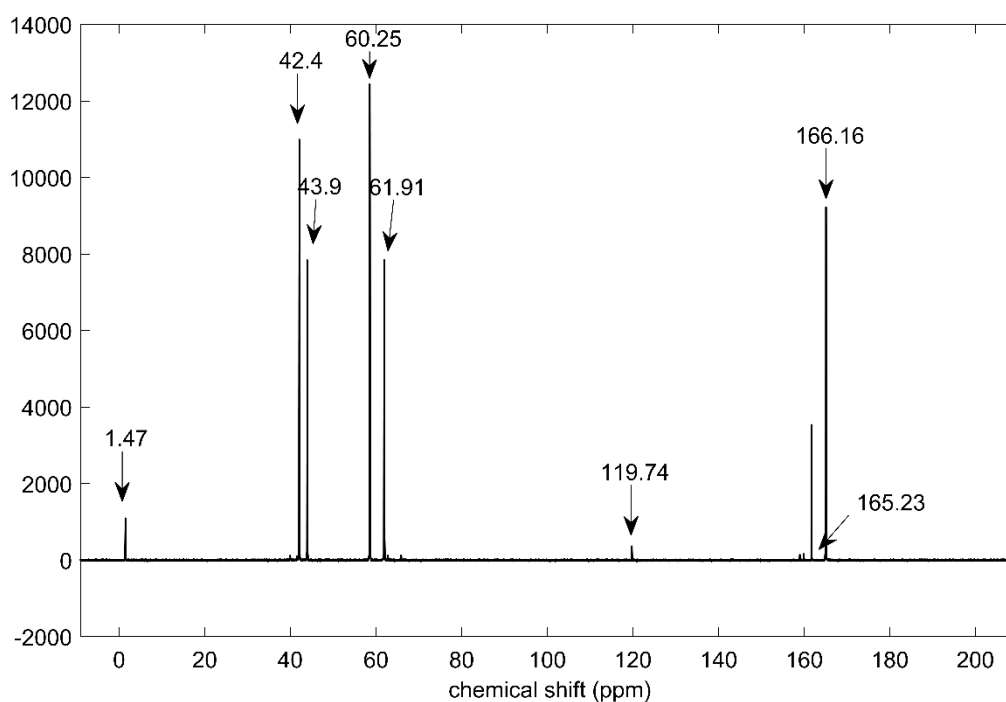
Fig. 4. Example for ^{13}C NMR spectra for a CO_2 loaded MEA sample

Fig. 5 shows the calculated species concentration using NMR measurements expressed in units of moles per kg water for each calibration and validation sample with respect to their total

CO_2 loading expressed in units of moles per moles of amine. The lowest and highest CO_2 loading reported were 0.039 and 0.612 mol / mol MEA respectively. When the CO_2 loading was increased, the amount of carbonate, bicarbonate, carbamate and protonated MEA were increased while free MEA concentration was decreased. Carbamate concentration was increased with increasing CO_2 loading until 0.5 loading and then decreased gradually. This is due to the stoichiometry of the reaction between CO_2 and MEA.
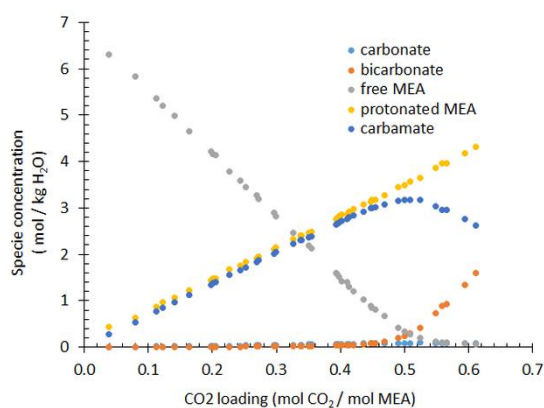
Fig. 5. ^{13}C NMR analysis - concentration of different species with respect to the CO_2 loading
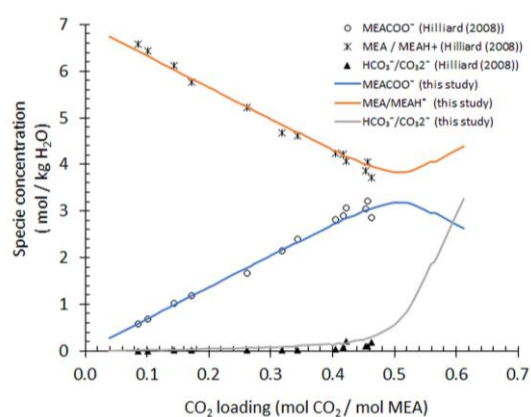
Fig. 6. Speciation for MEA-CO_2-H_2O system by NMR; Comparison of this study (after removing outliers) with work by Hilliard (2008)

The model results by Raman spectroscopy is dependent on the accuracy of the reference method which in this case is the ^{13}C NMR. The ^{13}C NMR speciation of this study was compared with the study[50] for 7 M MEA solution at 27^0C and is shown in Fig. 6. A comparison of $BaCl_2$ titration-precipitation results, loading estimated by dilution ratio and NMR based loading values are presented in Fig. 7. When the CO_2 loading of the stock solution and the weight ratio between the CO_2 loaded and unloaded sample is known, the CO_2 loading of each calibration and validation sample can be calculated based on dilution ratio. The titration was performed by the same operator once per sample and is the average of three replicates. Theoretically all these three methods should yield a same result.
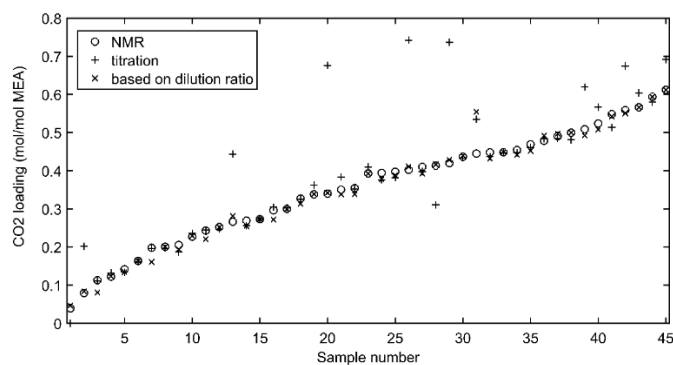
Fig. 7. Comparison of CO₂ loading based on mass ratio of loaded/unloaded and NMR results

There is a good match between NMR measurements with calculated CO_2 loading based on dilution ratio. There is also a considerable match between the $BaCl_2$ titration results and NMR measurements for about 75% of samples. Errors associated with dilution factor comes mainly from weighing errors. On the other hand, titration includes several sources of errors such as sampling errors, sample and chemical preparation errors, titration apparatus errors, human errors[43]. This is an evidence to show that when an analysis involves many operations to a sample (chemical preparation, sample transferring, boiling, volume reduction, such as those in titration procedure), the error percentage is increased and that error can be minimized when analysis is performed with respect to 'representative process sampling'[51]. Lower deviations could be observed between the results from dilution-based calculation and NMR measurements. Such an accuracy is an indication that all the samples were at homogenous condition, equilibrated and minimal error in both measurement techniques which resulted representative samples.

3.2 Raman experiments

When calibration and validation samples were measured using the Raman spectroscopy, a plot of Raman shift vs. intensity was obtained by the iC Raman software. For each sample (object), there is an arbitrary value (peak intensity) for each Raman shift between 100 cm^{-1} to

19

3426 cm^{-1} (variables) and this data is called raw data. Fig. 8 shows some of raw Raman spectra varied with different CO_2 loadings.
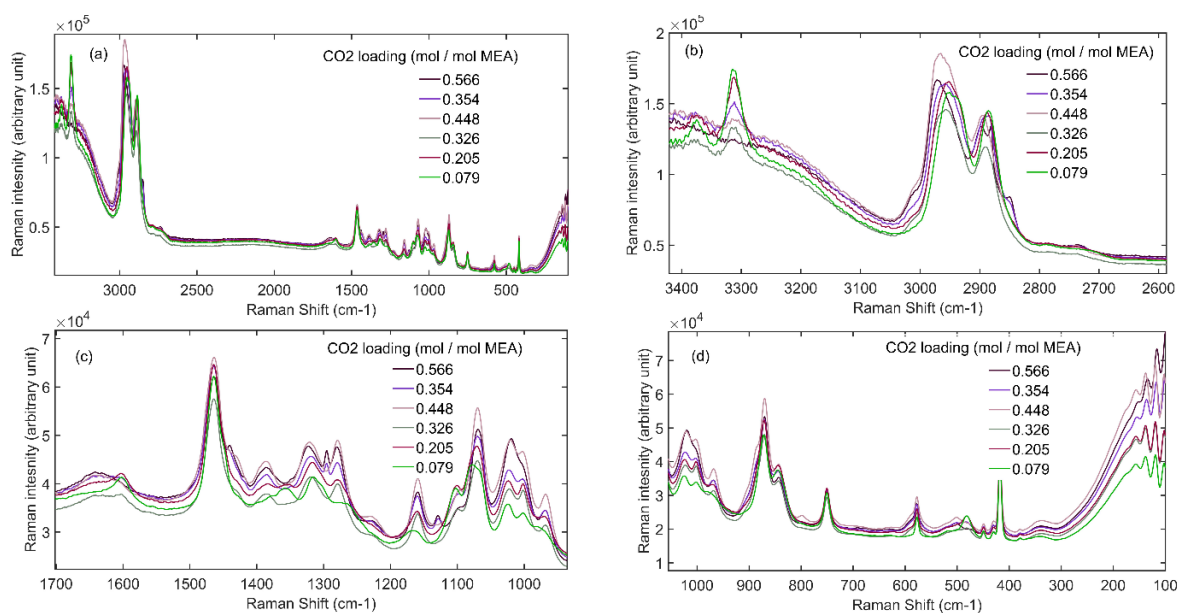
Fig. 8. Raman spectra for CO₂ loaded MEA samples ; wavelength region (a) [3426-100]cm⁻¹, (b) [3426-2600]cm⁻¹(a) , [1700-1000]cm⁻¹(a) [1000-100]cm⁻¹

Between the Raman shift from 100-3426 cm^{-1}, all features of Raman bands such as strong, weak, broad and sharp were observed. All the samples showed noisy measurements in low and high frequency levels (before 250 cm^{-1} and after 3250 cm^{-1}) which were assumed to be noise from the instrument and its accessories and a flat broad area in the middle range approximately from 1750 cm^{-1} to 2500 cm^{-1} showing hardly any significant chemically important details. Since there are many neighboring peaks in some wavelength areas, spectral features has been shown with respect to different variable sections in Fig. 8. The Raman phenomenon is based on vibrational changes of Raman scattered electromagnetic radiation. Vibrational modes relevant to different chemical species in MEA-CO_2-H_2O which are reported in Fig. 9, can be compared with Fig. 8. Most of the strong vibrational modes mentioned in literature for each chemical specie in the solution were observed in this study. These vibrational modes provide key information to identify and isolate important peaks. However, with reference to Fig. 8 and

20

Fig. 9 it is visible that the peak isolation is challenging due to the overlapping Raman features. For all the amine and carbon species in the system have more than one frequency which vary with respect to CO_2 loading. The variation of the peak intensities for increasing CO_2 loading is not systematic due to the baseline drift and the correlation between different Raman shifts. Overlapping features can be resolved through spectral deconvolution and band fitting [34]. The peak maximum frequency, peak height, width, and shape (Gaussian, Lorentzian, or mixed) are commonly used for regression. Raman intensity is affected by instrumental settings, such as laser power, as well as sample factors. The peak height, shape and area are affected by these factors and in univariate analysis these factors are minimized by normalizing species peak against another component which in most cases an internal standard. The models developed using such techniques have limitations such as inability for in-situ usage or over/under predicting due to noise.

3.3 PLSR models

According to studies[38,52-54] different vibrational modes for the wavenumber region from [500-1700] cm^{-1} and [2600-3600] cm^{-1} that can be identified in a CO_2 loaded aqueous amine solution is summarized Fig. 9. The information in Fig. 9 shows that Raman peaks changing with concentrations are located in this region but not as Gaussian shapes but as several correlated overlapping peaks. This is an evident for why the traditional univariate approach fails in this chemical system and the need of considering more than one variable to regress with a specie concentration. Therefore in the current study calibration was performed using variable groups instead of using a region related to an individual peak. In multivariate analysis, overlapping and baseline shifted spectra are addressed to overcome inclusion of noisy information to the model and prevent exclusion of important chemical information from the model. The exact lengths and margins of the variable group were decided by trial and error which gave the lowest RMSEP value for PLSR models. Several plots are derived during a PLS

calibration and validation procedure using a chemometrics software. These plots can be used to understand more about data structure, pattern, correlations between data, uncommon samples with respect to the majority of data(outliers) and correlation of data with the property to be measured.
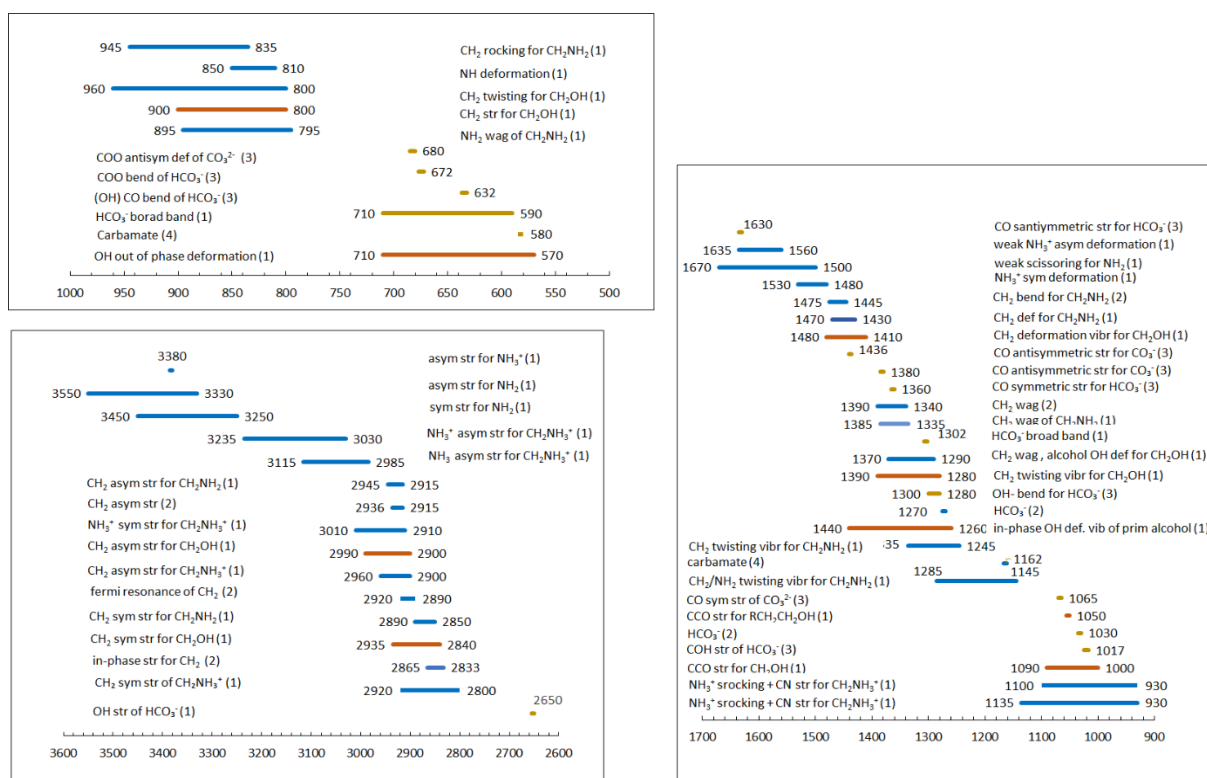
Fig. 9. Vibrational assignments of species in CO2 loaded MEA solution; Numbering refers to following literature,(1)[52] , (2)[53] , (3)[54] , (4)[32]

From Fig. 10 to Fig. 16 PLSR model results are presented. Our interest in this paper is to see the predictability of chemical concentration by the Raman spectroscopy in anMEA-CO$_2$-H$_2$O system than presenting an in-depth analysis of the chemometric evaluation of data. Therefore for each PLSR model, the spectral changes, regression coefficient vector and the measured vs predicted values for test set data are shown. RMSEP (root mean square error of prediction) compares the predictions of test set (validation samples) with reference values and is used to assess the predictability of multivariate models. Regression coefficient vector is software generated based on the data given (preprocessed calibration data, variable range and number

of PLS components in the model). Positive regression coefficients come from the positively correlated peaks to the predicted parameter. The plot of RMSEP variation determines the optimum number of PLS components to be selected for the final model. When a lower number of PLS components are used for a model such as one or two, less noise is included but may sometimes exclude important chemical information too. Finally each model is presented with a plot (Fig. 17) which matches the concentration of reference set (also called as test set/validation set) with respect to the predicted value. This graph is the evidence of how well the model predicts completely new CO_2 loaded MEA solutions. The statistical parameters presents the number of PLS components used for the model, RMSEP value and r^2 for calibration and test set.

3.3.1 CO_2 loading model

CO₂ reacts with MEA to produce different chemical species as shown in Fig. 1 where the C species are converted into carbonate, bicarbonate and carbamate. When developing the model for CO_2 loading (mol/mol MEA) in the system, the vibrational modes which exist in the system relevant to carbon species were accounted. Fig. 10(a) shows the spectral variation and Fig. 10(b) shows the regression coefficients for the 770-901 cm⁻¹, 991-1202 cm⁻¹ and 1398-1498 cm⁻¹ variable range for CO_2 loading model. Positive regression coefficients are related to the vibrational modes of carbamate, carbonate and bicarbonate. When the CO_2 loading in a sample is increased the concentrations of carbonate, bicarbonate and carbamate (upto 0.5 loading) is increased and the vibrational modes of these specie appear positively in the regression coefficient plot.
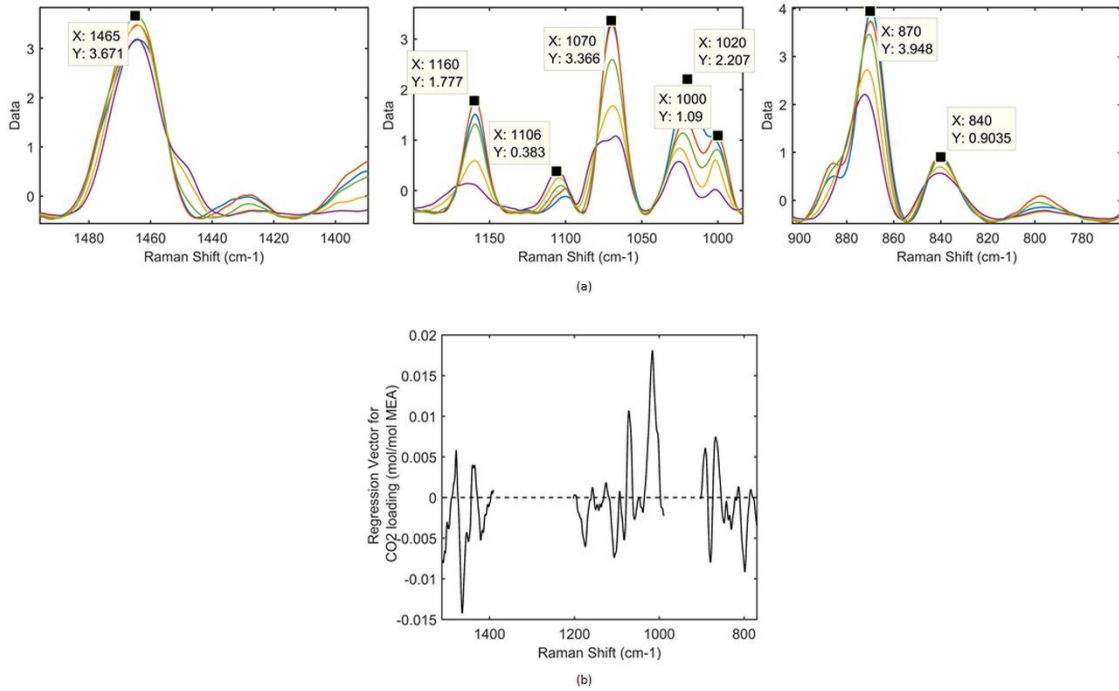
Fig. 10. PLSR model for CO2 loading ; (a) Preprocessed spectra and (b) Regression coefficients in the selected wavelength

3.3.2 Carbamate model

With reference to the Fig. 1 carbamate concentration is dependent on the concentration of amine and CO_2. Fig. 11 shows the wavenumber region and regression coefficient vector for carbamate. The variable range which yielded the lowest RMSEP for carbamate model was between 1100 to 1200 cm^{-1} which included C-N stretching vibration of carbamate at 1159cm^{-1} (this study) and it showed ±1 cm^{-1} peak shift for some measurements.
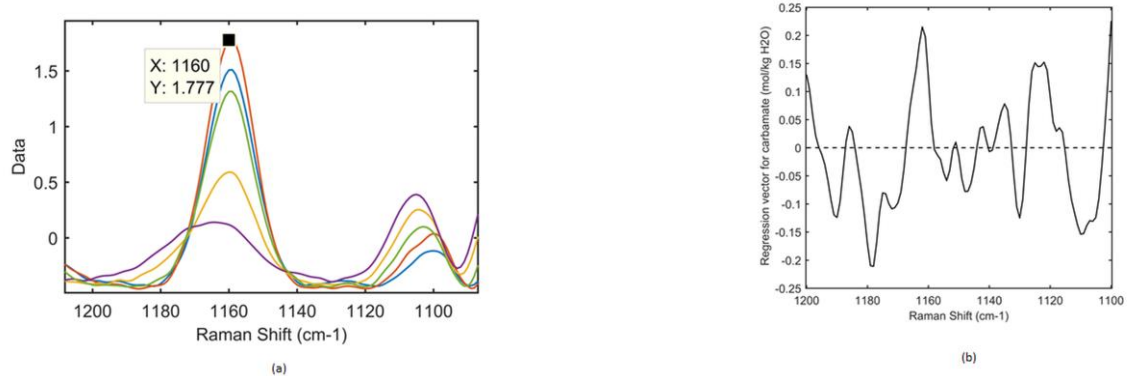
Fig. 11. PLSR model for carbamate ; (a) Preprocessed spectra and (b) Regression coefficients in the selected wavelength

24

3.3.3 Carbonate model

In the MEA-CO_2-H_2O system carbonate is produced in small quantities compared to other chemical concentrations and is not produced at low CO_2 loadings. It is produced when the pH is higher in the system (Fig. 1). In carbonate model (Fig. 12), three variable ranges were selected which are 853-895, 1047-1091 and 1404-1493 cm^{-1}. According to the regression coefficients Fig. 12(b), there are positively and negatively related variables to the model.
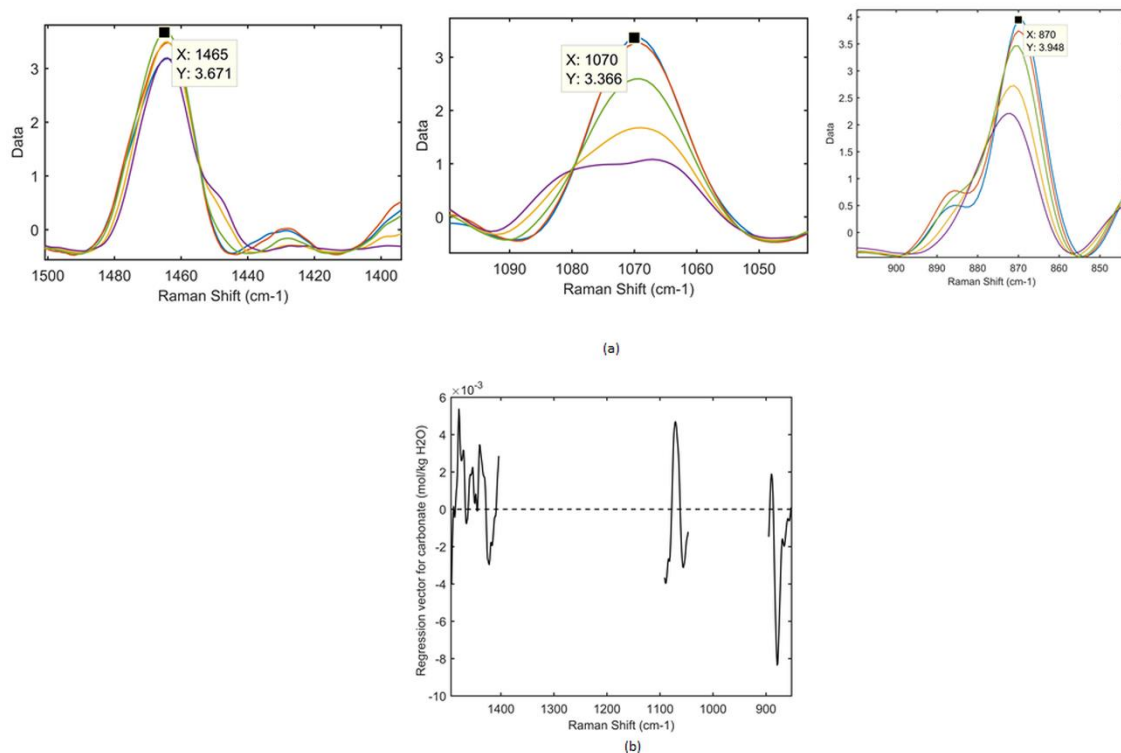
Fig. 12. PLSR model for carbonate ; (a) Preprocessed spectra and (b) Regression coefficients in the selected wavelength

3.3.4 Bicarbonate model

As shown in Fig. 1 when the pH of the solution changes both the ionic form and their concentration varies. Conversion of carbonate into bicarbonate is taken place when pH is decreased when the solution goes from strong base to weak base. When the CO_2 loading is increased carbonate, bicarbonate, carbamate and protonated amine are increased but at loadings

higher than 0.5, protonated amine continues to further rise by reacting with carbamate and the

CO_2 which is released to the system is converted to bicarbonate. Fig. 13(a) shows several peaks

varying with CO2 loading value in the variable range from 773-1047 cm-1. In Fig. 13(b) the

highest positive regression coefficient at the C-OH stretching vibration of HCO3- is recorded

at 1021cm-1.
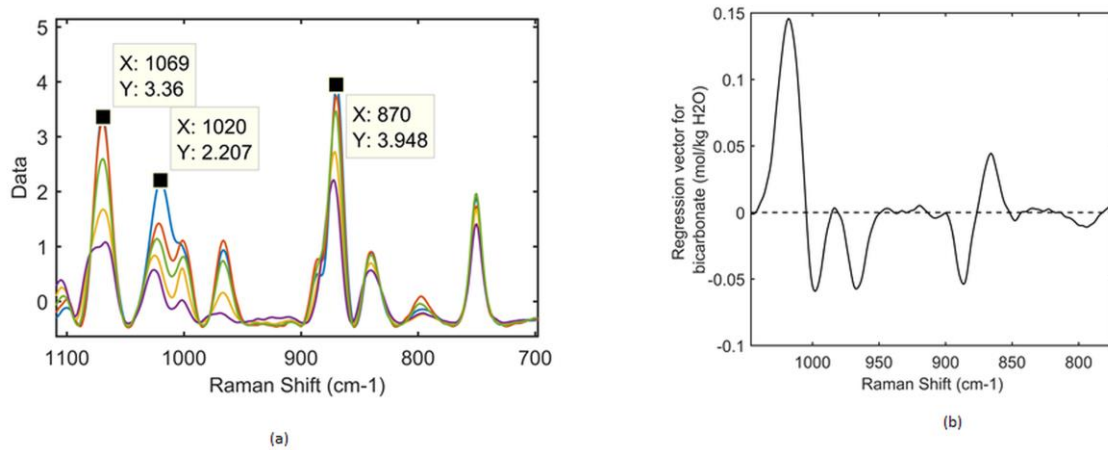
Fig. 13.PLSR model for bicarbonate ; (a) Preprocessed spectra and (b) Regression coefficients in the selected wavelength
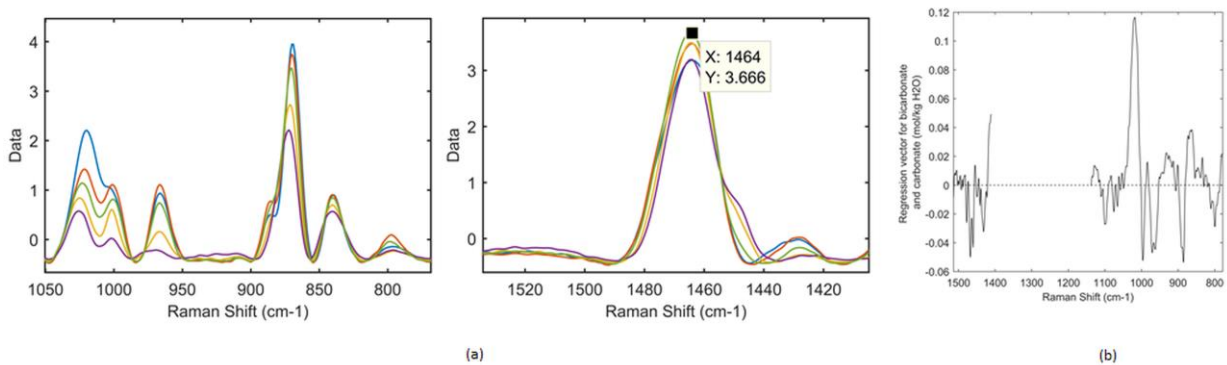
Fig. 14. PLSR model for sum of carbonate and bicarbonate ; (a) Preprocessed spectra and (b) Regression coefficients in the selected wavelength

3.3.5 Carbonate and bicarbonate model

The total of carbonate and bicarbonate concentrations can be obtained from individual

models of carbonate and bicarbonate developed in this study. The uncertainly is higher when

summing up the results from two models and therefore a separate model was developed to quantify the total of carbonate and bicarbonate concentration (Fig. 14). A larger variable range was selected to the model to include the variation of both carbonate and bicarbonate concentrations. The lowest RMSEP was given by the wavelength range from 779-1138 cm^{-1} and 1410-1513 cm^{-1}. In the regression coefficient plot, in Fig. 14(b) 1021 cm^{-1} shows the highest positive impact.

3.3.6 Free MEA model

The vibrational modes for monoethanolamine lie across the entire wavenumber region as shown in Fig. 9 Intitally the free MEA Model was calibrated and validated including wavenumber region above 2600 cm^{-1} but the resulting RMSEP was very high due to the dependency of amine species on carbon species in the system. By further adding the variable ranges related to carbonate, bicarbonate and carbamate a less prediction error was gained. The selected range was from 803-1508 cm^{-1} and 2867 to 2996 cm^{-1}. Highest positive and negative impact of regression coefficients lie in the region of 2867 to 2996 cm^{-1} (Fig. 15(b)).
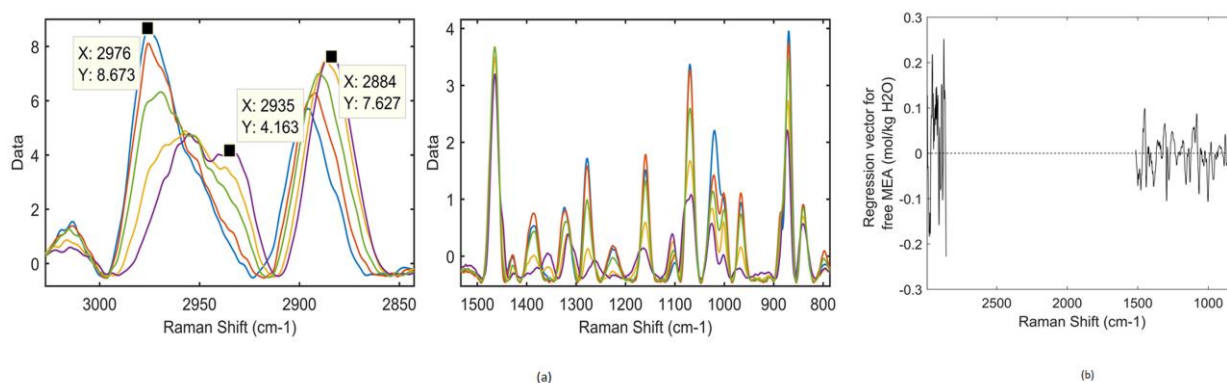
Fig. 15. PLSR model for free MEA ; (a) Preprocessed spectra and (b) Regression coefficients in the selected wavelength
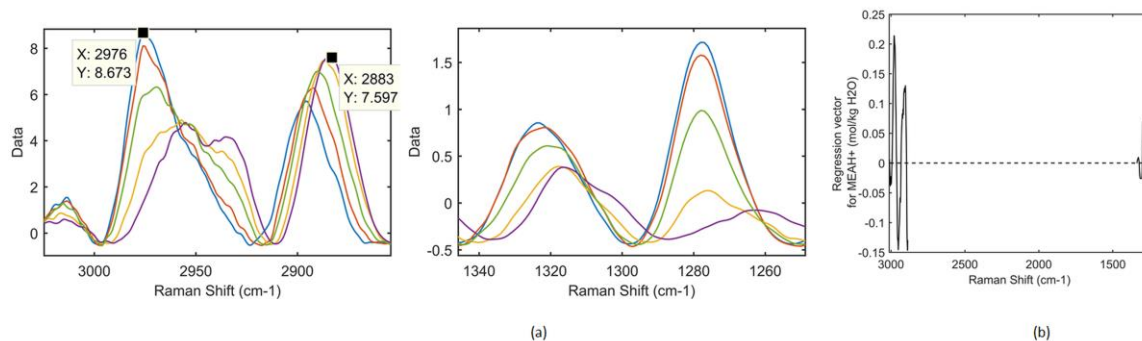
Fig. 16. PLSR model for protonated MEA ; (a) Preprocessed spectra and (b) Regression coefficients in the selected wavelength

3.3.7 MEAH⁺ model

The selected variable range is from 1251-1336 cm^{-1} and 2887 -3010 cm^{-1} and however significant impact comes from the higher wavenumber region for the model prediction as seen in Fig. 16(b).

3.4 Model predictivity

Fig. 17 displays the model results as a function of measured concentration vs predicted concentration for test set samples. It also shows the calibration samples in the same plot. The measured concentrations are those obtained from NMR spectroscopy while the predicted concentrations are those which were predicted by the model. Eight plots are presented representing model results for CO2 loading in unit of mol/ mol MEA, CO2 loading in unit of mol/ kg H2O and molal concentration of [carbonate, bicarbonate, carbamate, sum of bicarbonate and carbamate, free MEA, protonated MEA]. For all the models, number of PLS components selected, RMSEP values, r^2 of the test set (as (R^2(Pred)) and calibration data (as R^2(plotted)), target line (as 1:1), regression line (fit) and estimated error from the model are presented.

(a)

(b)

(c)

(d)

(e)

(f)

(g)   *(h)*
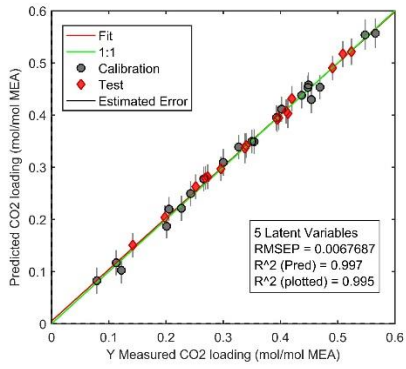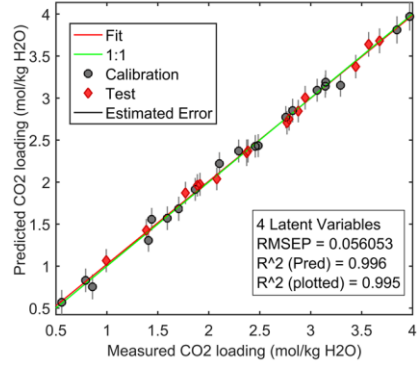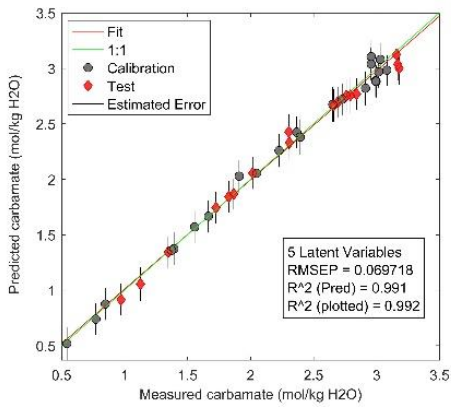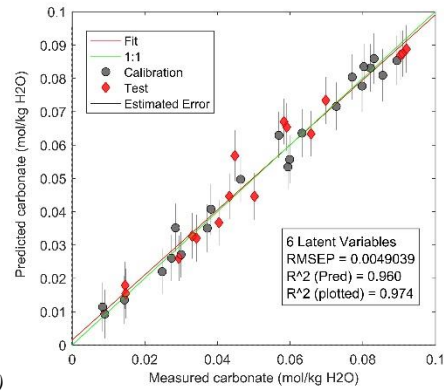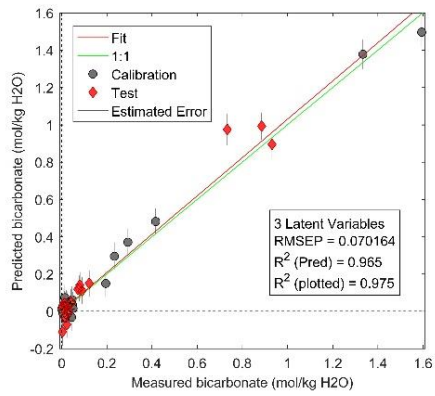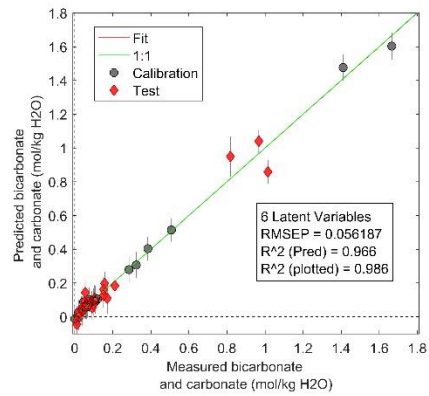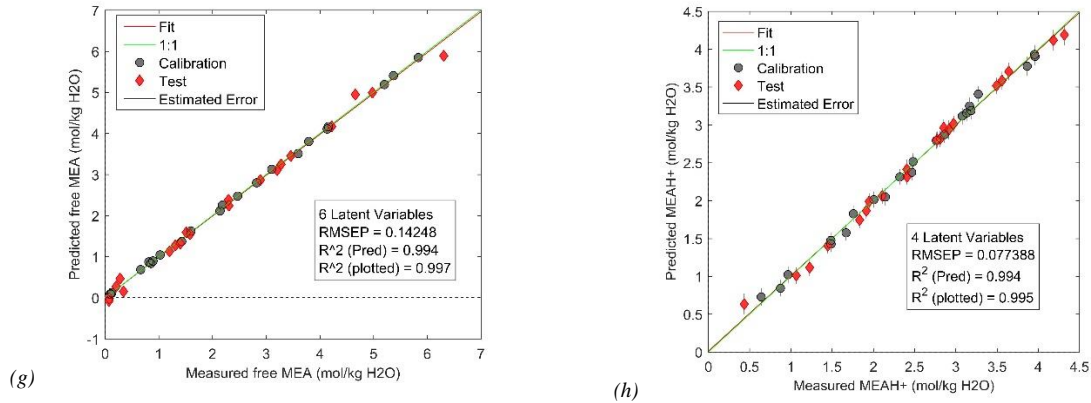
Fig. 17 :Comparison of measured vs predicted concentrations for validation dataset using the developed models; plots include calibration data ; R^2(plotted)=R^2(calibration)

The number of calibration and validation samples used for each model and the selected wavelength range which yielded the optimum RMSEP value and number of PLS components are shown in Table 1. The range of the initial calibration set was upto 0.612 loading, but after reducing outliers this range was lowered but sufficiently covers the industrial lean and rich loading levels. r^2 is more than 0.979 for calibration sets in all the models while that for prediction was gained more than 0.96. All the models are temperature independent as the concentrations are expressed in mol/kg H_2O. CO_2 loading model is presented here both in mol/kg H2O basis and in the units of traditional interpretation which is mol CO_2/ mol MEA to ease for better understanding.

3.5 Demonstration of model use

A chemometric model validation by a completely new data set provides a guarantee that they provide reasonable results for estimation of the interested property for future samples. This completely new data set which we call as validation set in this text, is a valid representation of the relevant 'heterogeneity information' pertaining to the future use [49]. In many chemometrics model development, cross validation and leverage-corrected validation have been used but these methods use the same calibration data set used for model development thus the model over-fits to the purpose. A detailed description of the importance of test set validation is given[49]. Since the Raman spectroscopic model development in this study is not limited to be used for batch samples, it is interesting to know how the models response when estimating the concentration profiles in continuous process in a real CO_2 capture plant. We have reported the use of these models in such a process [39] and the Raman measurements generated at the same test campaign have been used for demonstration of reaction monitoring here. The Raman instrument was intergrated to the rich amine line as shown in Fig. 2(c), few centimeters after the absorber amine outlet in the CO_2 rig available at University of South-eastern Norway. The measurements represent the absorber amine outlet composition. Industrial processes include many process variations and hence models should be updated for individual processes. This model re-validation to the plant can include less or extremely more work and that depends on the process, analytical instrument and measurement types. In the demonstration example, the plant trend based on the total CO_2 loading and different specie concentration is explained with time highlighting the importance of these models together with Raman instrument as a mandatory process measurement in a CO_2 capture plant.

Fig. 18 shows the Raman predictions when the absorption column reaches equilibrium CO_2 loading with time while Fig. 19 represents the same scenario but with different initial CO_2 loading and with some abrupt process variations which make changes to the liquid

composition. According to both figures, the carbamate, protonated MEA and carbonate predictions follow the same trend as CO_2 loading and free amine inversely obey the trend which is chemically acceptable for CO_2 loading less than 0.5. The carbon species in the system can exist as carbonate, bicarbonate and carbamate under equilibrium conditions and since the Raman probe was connected to the amine line very close to the CO_2 gas inlet to the absorber, there can also be small amounts of dissolved CO_2 in the system which with time will absorb to the solvent. Fig. 18(c) and Fig. 19(c) show a comparison of predictions from three model combinations; total CO_2 loading model, [carbonate model + bicarbonate model + carbamate model] and [sum of bicarbonate and carbonate model + carbamate model].
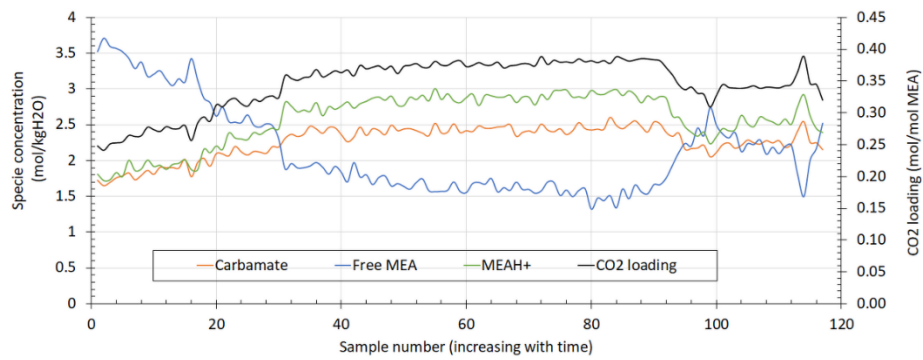
(a) Predicted concentrations for CO2 loading, carbamate, free MEA and protonated MEA in rich amine line at USN mini pilot CO2 capture plant
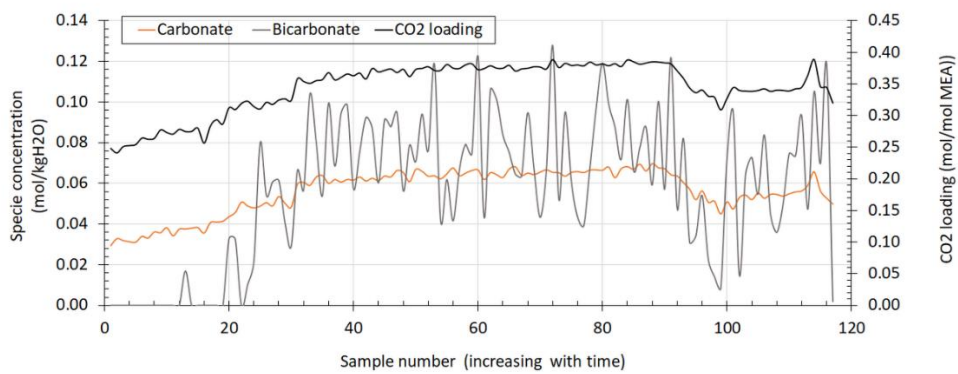
(b) Predicted concentrations for CO2 loading, carbonate and bicarbonate in rich amine line at USN mini pilot CO2 capture plant
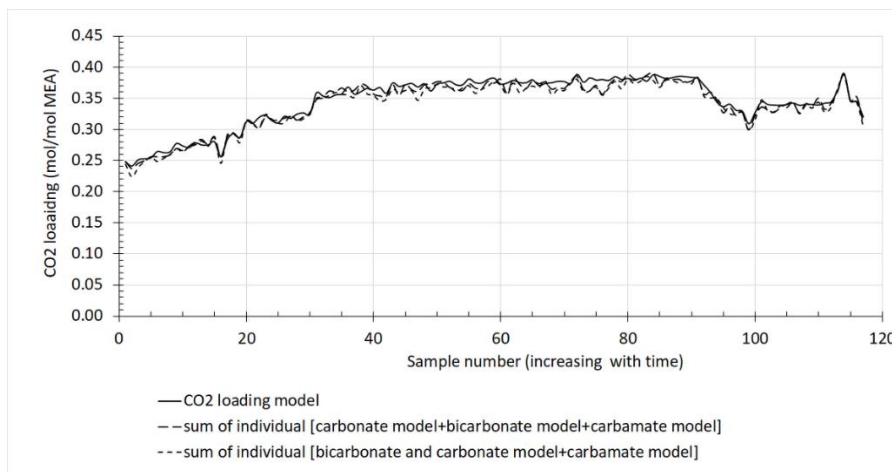
(c) Comparison of predicted total CO2 loading in the rich amine line using three different combinations of developed models

Fig. 18. Demonstration of the model performance - test 1
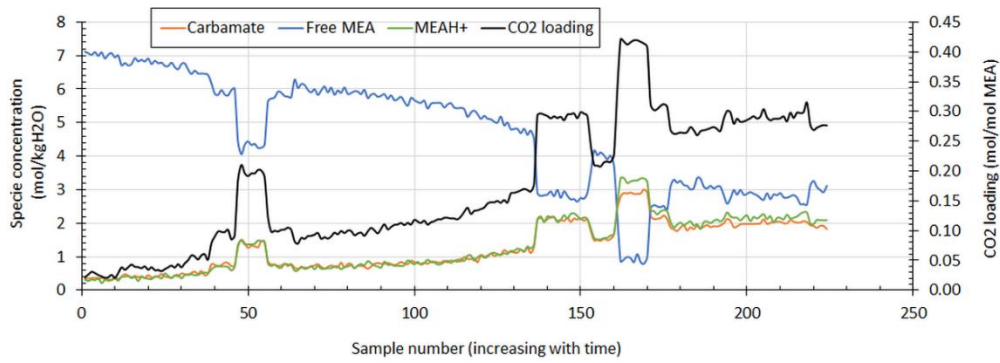
(a) Predicted concentrations for CO₂ loading, carbamate, free MEA and protonated MEA in rich amine line at USN mini pilot CO₂ capture plant
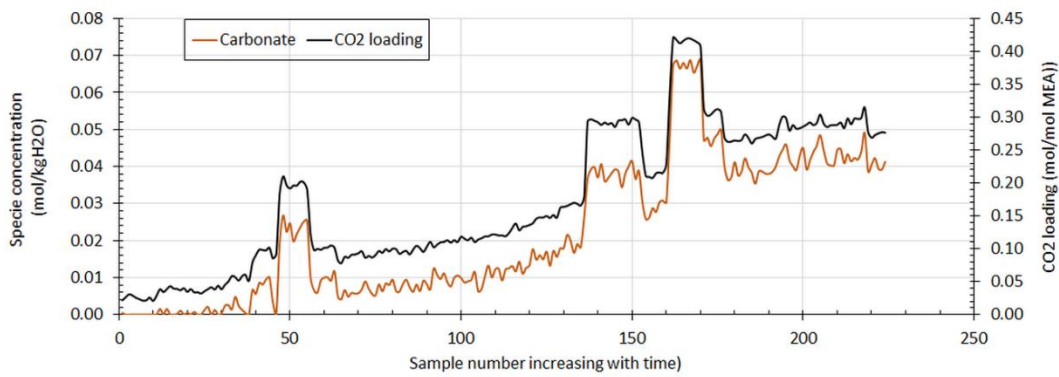
(b) Predicted concentrations for CO₂ loading, and carbonate in rich amine line at USN mini pilot CO₂ capture plant; bicarbonate predictions were almost zero and hence not shown in the plot
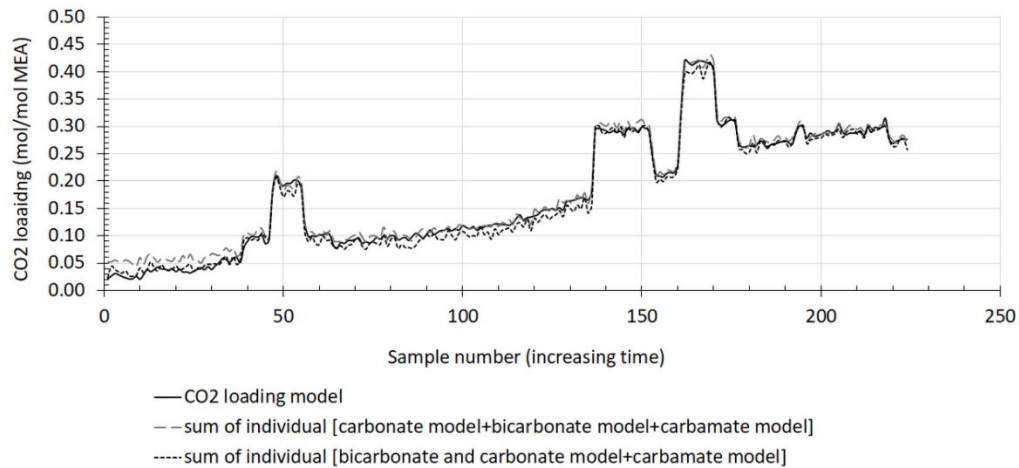
(c) Comparison of predicted total CO₂ loading in the system in three different combinations of developed models

Fig. 19. Demonstration of the model performance - test 2

4   Conclusion

Raman spectroscopy is a promising analytical method for obtaining quantitative and qualitative information on the species distribution in MEA-CO_2-H_2O systems due to its fast response, non-invasive approach and applicability for in-situ monitoring. But the raw Raman signals originally come as a combination of both chemical information and noise. Multivariate calibration methods can handle such noisy measurements to extract hidden chemical information. In this study, the model development approach using Raman spectroscopic measurements together with multivariate modeling using test set validation method is described for a complete speciation of CO_2 loaded aqueous amine solutions where differently CO_2 loaded 30 w/w% MEA solutions were used for demonstration. The seven models developed, were used to estimate in-situ speciation from in-line measurements acquiring from a mini-pilot scale MEA based CO_2 capture plant. Such an in-situ speciation facility is mandatory requirement for complete deployment of CO_2 capture plants in industrial scale. The study highlights the importance of using multivariate analysis methods over traditional univariate analysis to interpret chemically important information. Models developed from experimental results accounting real variations in a process system are far reliable than theoretical models based on assumptions. Raman spectroscopic measurements is a potential candidate for in-situ monitoring of speciation in CO_2 capture plants. The same modelling approach described in this paper can be applied for other amines and amine blends.

Notes

The authors declare no conflicts of interest.

AUTHOR INFORMATION

Corresponding Author

*Email : wathsala.jinadasa@usn.no

Author Contributions

The manuscript was written through contributions of all authors.

ACKNOWLEDGMENT

REFERENCES

[1]   G. T. Rochelle *Science* **2009**, *325*, 1652.
[2]   K. H. Esbensen, Guyot, D., Westad, F., Houmoller, L.P *Multivariate data analysis: in practice*; CAMO Software, 2010.
[3]   H. Martens, Tormod, N. *Multivariate calibration*; John Wiley & Sons: Canada, 1989
[4]   C. D. Jean-Marc Amann, Mohamed Kanniche, Chakib Bouallou *Scientific Study and Research* **2007** *VIII*.
[5]   J. E. Crooks, J. P. Donnellan *Journal of the Chemical Society, Perkin Transactions 2* **1989**, 331.
[6]   G. F. Versteeg, W. P. M. van Swaaij *Chem. Eng. Sci.* **1988**, *43*, 573.
[7]   M. Caplow *J. Am. Chem. Soc.* **1968**, *90*, 6795.
[8]   P. V. Danckwerts *Chem. Eng. Sci.* **1979**, *34*, 443.
[9]   N. McCann, D. Phan, X. Wang, W. Conway, R. Burns, M. Attalla, G. Puxty, M. Maeder *J. Phys. Chem. A* **2009**, *113*, 5022.
[10]   E. S. Hamborg, V. Smith, T. Cents, N. Brigman, O. F. Pedersen, T. De Cazenove, M. Chhaganlal, J. K. Feste, Ø. Ullestad, H. Ulvatn, O. Gorset, I. Askestad, L. K. Gram, B. F. Fostås, M. I. Shah, A. Maxson, D. Thimsen *Energy Procedia* **2014**, *63*, 5994.
[11]   F. Morton, R. Laird, J. Northington *Energy Procedia* **2013**, *37*, 525.
[12]   R. M. Montañés, N. E. Flø, R. Dutta, L. O. Nord, O. Bolland *Energy Procedia* **2017**, *114*, 1538.
[13]   C. A. Wardhaugh L.T. In *Energy Efficient Solvents for CO2 Capture by Gas-Liquid Absorption.* ; Budzianowski WM, Ed.; Green Energy and Technology. Springer, : Cham, 2017, p 27.
[14]   J. P. Jakobsen, J. Krane, H. F. Svendsen *Ind. Eng. Chem. Res.* **2005**, *44*, 9894.
[15]   C. Perinu, B. Arstad, K.-J. Jens *Int. J. Greenh. Gas Con.* **2014**, *20*, 230.
[16]   W. Böttinger, M. Maiwald, H. Hasse *Fluid Phase Equilib.* **2008**, *263*, 131.
[17]   Q. Yang, M. Bown, A. Ali, D. Winkler, G. Puxty, M. Attalla *Energy Procedia* **2009**, *1*, 955.
[18]   L. V. van der Ham, D. E. Bakker, L. F. G. Geers, E. L. V. Goetheer *Chem. Eng. Technol.* **2014**, *37*, 221.
[19]   A. C. van Eckeveld, L. V. van der Ham, L. F. G. Geers, L. J. P. van den Broeke, B. J. Boersma, E. L. V. Goetheer *Ind. Eng. Chem. Res.* **2014**, *53*, 5515.

[20]   L. V. van der Ham, A. C. van Eckeveld, E. L. V. Goetheer *Energy Procedia* **2014**, *63*, 1223.

[21]   A. Kachko, L. V. van der Ham, D. E. Bakker, A. van de Runstraat, M. Nienoord, T. J. H. Vlugt, E. L. V. Goetheer *Ind. Eng. Chem. Res.* **2016**, *55*, 3804.

[22]   W. J. Rogers, J. A. Bullin, R. R. Davison, R. E. Frazier, K. N. Marsh *AICHE J.* **1997**, *43*, 3223.

[23]   F. Diab, E. Provost, N. Laloué, P. Alix, V. Souchon, O. Delpoux, W. Fürst *Fluid Phase Equilib.* **2012**, *325*, 90.

[24]   A. Einbu, A. F. Ciftja, A. Grimstvedt, A. Zakeri, H. F. Svendsen *Energy Procedia* **2012**, *23*, 55.

[25]   L. F. G. Geers, A. van de Runstraat, R. Joh, R. Schneider, E. L. V. Goetheer *Ind. Eng. Chem. Res.* **2011**, *50*, 9175.

[26]   P. W. J. Derks, P. J. G. Huttenhuis, C. van Aken, J.-H. Marsman, G. F. Versteeg *Energy Procedia* **2011**, *4*, 599.

[27]   G. Richner, G. Puxty *Ind. Eng. Chem. Res.* **2012**, *51*, 14317.

[28]   P. Jackson, K. Robinson, G. Puxty, M. Attalla *Energy Procedia* **2009**, *1*, 985.

[29]   P. Beumers, T. Brands, H.-J. Koss, A. Bardow *Fluid Phase Equilib.* **2016**, *424*, 52.

[30]   G. Puxty, R. Bennett, W. Conway, D. Maher *Int. J. Greenh. Gas Con.* **2016**, *49*, 281.

[31]   A. Kachko, L. V. van der Ham, A. Bardow, T. J. H. Vlugt, E. L. V. Goetheer *Int. J. Greenh. Gas Con.* **2016**, *47*, 17.

[32]   P. A. G. L. Samarakoon, N. H. Andersen, C. Perinu, K.-J. Jens *Energy Procedia* **2013**, *37*, 2002.

[33]   M. K. Wong, A. M. Shariff, M. A. Bustam *RSC Advances* **2016**, *6*, 10816.

[34]   M. K. Wong, M. A. Bustam, A. M. Shariff *International Journal of Greenhouse Gas Control* **2015**, *39*, 139.

[35]   M. Y. O. Fandiño, J. S. Cox, and P. R. Tremaine In *Acid Gas Extraction for Disposal and Related Topics*; Ying Wu JJC, Weiyao Zhu, Ed.; Scrivener Publishing: Beverly, 2016, p 81.

[36]   Z. Idris, K. J. Jens, D. A. Eimer *Energy Procedia* **2014**, *63*, 1424.

[37]   M. Vogt, C. Pasel, D. Bathen *Energy Procedia* **2011**, *4*, 1520.

[38]   V. Souchon, M. d. O. Aleixo, O. Delpoux, C. Sagnard, P. Mougin, A. Wender, L. Raynal *Energy Procedia* **2011**, *4*, 554.

[39]   M. H. W. N. Jinadasa, K.-J. Jens, L. E. Øi, M. Halstensen *Energy Procedia* **2017**, *114*, 1179.

[40]   Kaiser 2018.

[41]   M. Halstensen, H. Jilvero, W. N. Jinadasa, K.-J. Jens *Journal of Chemistry* **2017**, *2017*, 13.

[42]   M. H. W. N. Jinadasa, K.-J. Jens, M. Halstensen In *Carbon Dioxide Chemistry, Capture and Oil Recovery*; Iyad Karamé JS, Hassan Srour, Ed.; IntechOpen: 2018.

[43]   C. K. Jayarathna, A. B. Elverhøy, Y. Jiru, D. Eimer *Energy Procedia* **2013**, *37*, 834.

[44]   S. Ma'mun, NTNU, 2005.

[45]   M. Maiwald, H. H. Fischer, Y.-K. Kim, H. Hasse *Anal. Bioanal. Chem.* **2003**, *375*, 1111.

[46]   C. Perinu, B. Arstad, A. M. Bouzga, J. A. Svendsen, K. J. Jens *Ind. Eng. Chem. Res.* **2014**, *53*, 14571.

[47]   G. T. R. S. Freguia **2003**, *49*, 1676.

[48]   P. H. C. Eilers *Anal. Chem.* **2003**, *75*, 3631.

[49]   K. H. Esbensen, P. Geladi *J. Chemometrics* **2010**, *24*, 168.

[50]   M. D. Hilliard, The University of Texas at Austin, 2008.

[51]   K. H. Esbensen, P. Paasch-Mortensen In *Process Analytical Technology: Spectroscopic Tools and Implementation Strategies for the Chemical and Pharmaceutical Industries*; 2 ed.; Bakeev KA, Ed.; John Wiley & Sons, Ltd: Chichester, UK, 2010.

[52]   G. Socrates *Alkane Group Residuals: C–H Group Infrared and RamanCharacteristic Group Frequencies: Tables and Charts*; 3 ed.; John Wiley & Sons Ltd, 2000.

[53]   P. Larkin *Infrared and Raman Spectroscopy; Principles and Spectral Interpretation*; 1 ed.; Elsevier, 2011, IR and Raman Spectra–Structure Correlations: CharacteristicGroup Frequencies.

[54]   A. R. Davis, B. G. Oliver *J. Solution Chem.* **1972**, *1*, 329.

Table 1. Summary of PLSR models for speciation

Model name	Wavelength range (cm^{-1})	Number of samples (after removing outliers)	
		Calibration	Validation
CO_2 loading (mol/mol MEA)	[770-901] ,[991-1202] ,[1398-1498]	22	16
CO_2 loading (mol/mol kg H_2O)	[770-901] ,[991-1202] ,[1398-1498]	20	15
Carbamate	[1100-1200]	22	17
Carbonate	[1493-1404] , [1091-1047] , [853- 895]	22	21
Bicarbonate	[1047-773]	21	21
Carbonate + bicarbonate	[1513-1410] , [1138-779]	21	22
Free MEA	[2996-2867] , [1508-803]	22	20
$MEAH^+$	[3010-2887] , [1336-1251]	22	20

Paper B

Raman Spectroscopy as an Online Monitoring Tool for CO$_2$ Capture Process: Demonstration Using a Laboratory Rig

Raman Spectroscopy as an Online Monitoring Tool for CO2 Capture Process: Demonstration Using a Laboratory Rig

M.H. Wathsala N. Jinadasa, Klaus-J. Jens, Lars Erik Øi, Maths Halstensen*

Faculty of Technology, University College of Southeast Norway, 3918, Porsgrunn, Norway

Abstract

A laboratory CO2 capture rig at USN was used as a demonstration plant to show the feasibility of Raman spectroscopy for online monitoring of speciation in CO2 capture process. The spectroscopy was integrated to lean and rich amine streams and experiments were carried out in dynamic and steady state conditions. Multivariate models were used to predict the speciation with time. Predicted CO2 and MEA concentrations were compared with offline analysis and the ion speciations were compared with a thermodynamic model. Results indicated that the Raman spectroscopy together with chemometrics based approach is an effective tool for online monitoring of speciation.

1. Introduction

According to IEA Technology Roadmap 2013[1], the next step for many CO2 capture technologies is to move to demonstration scale by 2020. Successful demonstration criteria should include online monitoring and real time analysis where the need of process analytical methods such as infrared, Raman and nuclear magnetic resonance spectroscopy will become an integral part in CO2 capture plants in near terms. There is an emerging research interest of using these analytical techniques from lab to industrial scale as online monitoring tools for speciation in

---

* Corresponding author. Tel.: +47 35575187; fax: +47 35575001.
  E-mail address: maths.halstensen@hit.no

MEA-CO2-H2O system ([2-4]). Raman spectroscopy is a powerful Process Analytical Technology (PAT) and its feasibility for fast response, remote sampling and water-independent spectral features, make it a possible candidate for online applications in CO2 capture process than IR spectroscopy or NMR spectroscopy. The Raman phenomenon is based on vibrational changes of Raman scattered electromagnetic radiation. Previous studies [5-7] show that the Raman signal is highly rich with chemical information on carbon and amine species. However, converting Raman spectra into chemical information requires data pre-processing prior to interpretation and quantification. Raman intensity is always a combination of noise and chemical signal due to changes of baseline and peak overlaps and may result in erroneous data interpretation. Chemometrics is a multivariate analysis approach which is often preferred to deal with these spectral challenges and is used to calibrate reliable prediction models [8]. In PAT applications, widely used chemometrics method for regression modelling is partial least square regression (PLSR). The output of a PAT instrument comes with hundreds of wavenumbers which are more or less important with the measured property. Using PLS method, x variables (wavenumbers) are correlated with y variable (measured property), such that covariance between x and y are maximized.

This study is the second step of ongoing research at University College of Southeast Norway (USN) to enable Raman spectroscopy for industrial scale CO2 capture process. In the first step, Raman and multivariate based PLS models were calibrated and validated for complete speciation analysis of CO2 absorption process based on lab scale experiments. Measurements were taken at equilibrium conditions. In the second step, which is described in this paper, the models were assessed in terms of predictability and robustness in insitu application.

1.1. Chemistry and speciation

Reaction of aqueous alkanolamines with carbon dioxide involves an acid–base buffer mechanism where it finally forms a large number of carbon species and amine species in the liquid phase. The equilibrium reactions can be written as shown in (1) to (6).

$$H_2O + H_2O \Leftrightarrow H_3O^+ + OH^- \tag{1}$$

$$CO_2 + H_2O \Leftrightarrow H_2CO_3 \tag{2}$$

$$H_2CO_3 + H_2O \Leftrightarrow HCO_3^- + H_3O^+ \tag{3}$$

$$HCO_3^- + H_2O \Leftrightarrow CO_3^{2-} + H_3O^+ \tag{4}$$

$$R_1R_2NH + H_3O^+ \Leftrightarrow R_1R_2NH_2^+ + H_2O \tag{5}$$

$$2R_1R_2NH + CO_2 \Leftrightarrow R_1R_2NCOO^- + R_1R_2NH_2^+ \tag{6}$$

Overall mass balance for amine species in the solution can be defined as the summation of protonated amine, carbamate and free amine (7) while that for carbon species is the sum of bicarbonate, carbonate and molecular CO2 (8).

$$C_{MEA\ total} = C_{MEA+} + C_{MEACOO^-} + C_{free\ MEA} \tag{7}$$

$$C_{total\ CO2} = C_{HCO_3^-} + C_{MEACOO^-} + C_{CO_3^{2-}} + C_{CO2} \tag{8}$$

Thermodynamic property models related to MEA-CO2-H2O systems represent vapor-liquid equilibrium (VLE) and they are extensively used in process design and optimization. Kent and Eisenberg model [9], Deshmukh and Mather Model [10] and electrolyte nonrandom-two-liquid (NRTL) model[11] are some of such models referred in CO2 capture research.

2. Experimental section

2.1. CO2 rig at USN

The rig consists of an absorption column with an inner diameter of 0.1 m and height of 2.5 m. Desorption column has an inner diameter of 0.26 m, a packing height of 1 m with a steam heated reboiler. The maximum liquid circulation and gas flow rates are 250 kg/h and 40 Nm3/h respectively. Fig. 1 shows the process flow diagram of the rig. A buffer tank is located between the absorber and the desorber. Liquid is loaded to the buffer tank before the circulation begins and synthetic CO_2 is fed to the system by mixing with an air supply to the required volumetric ratio. Locations of Raman sensors, T1/T2 temperature sensors and nondispersive infrared sensor (NDIR) for CO_2 gas measurement are shown in the figure. Two manual sampling valves are located soon after the Raman flow cells to extract samples for offline analysis.
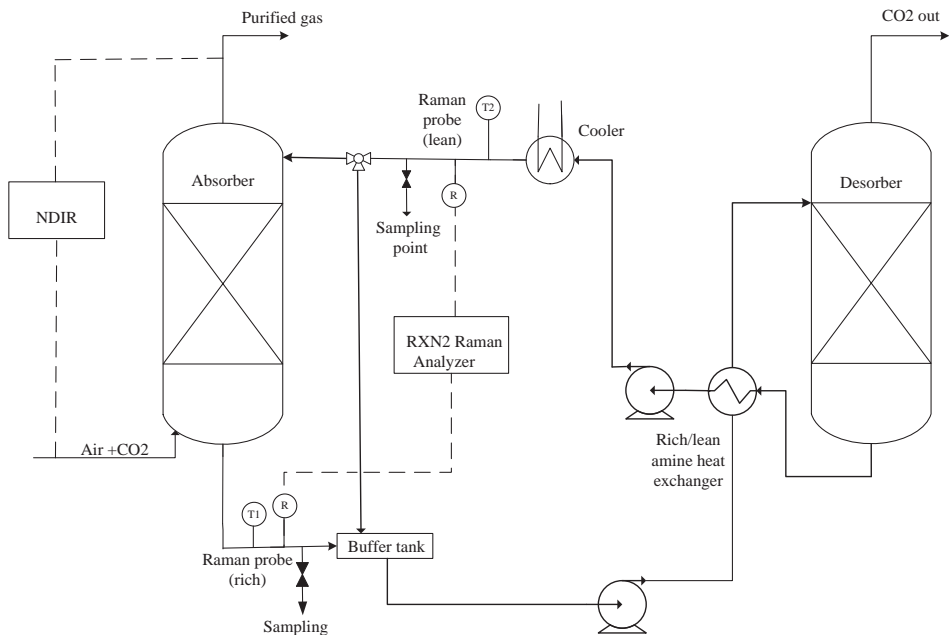
(a). Process flow diagram of CO2 rig
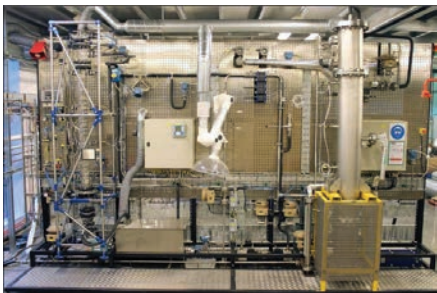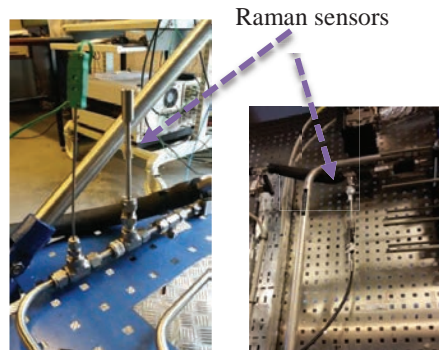
(b) Picture of CO2 rig   *(c) Raman sensor locations ; rich stream (left), lean stream (right)*

Fig. 1: Layout of USN CO2 rig (R=Raman sensor; T=Temperature sensor)

2.2. Instruments and chemicals

RXN2 portable multichannel Raman spectrometer (Kaiser Optical Systems Inc.) was the newly integrated system to the rig. The instrument is equipped with NIR dioder laser with wavelength of 785 nm spanning in the spectral range of 100–3425 cm-1. Four fiber optic probes can be connected and utilized through an automatic sequential scanning system that is integrated into the instrument. The Raman spectra were acquired using a short-focus (200 µm)-sapphire-window- Hastelloy probe optic which should be in direct contact with a solution. 99% MEA solvent purchased from VWR was used for the rig experiments. 0.1M Sodium hydroxide (NaOH), 0.1 M hydrochloric acid (HCl) and 1 M HCl purchased from Merck were used for the titration experiments. Titrator Mettler Toledo T50, were used for determining pH, CO_2 loading and MEA concentration.

2.3. PLSR models and predictions

There are six PLSR models developed using different CO_2 loaded 30% MEA equilibrium samples at room temperature and pressure. The aim of these models were to enable Raman spectroscopy to use as an analytical method for speciation of MEA-CO_2-H_2O system. Five out of these models can predict the species of carbonate, bicarbonate, carbamate, protonated amine and free amine and the remaining one can predict the total CO_2 loading. 23 calibration and 22 validation samples were used for the model development. Quantitative analysis of species distribution for each sample was performed by ^{13}C NMR experiments. Raman spectra were collected, smoothed and important wavenumbers were cropped based on the prior knowledge on their characteristic Raman bands. They were then regressed with respect to the species concentrations (y variable) in Matlab PLS toolbox to develop PLS models. Table 1 summarises the results of these models for 6 constituents including the range and root mean square error of prediction (RMSEP). The definition of RMSEP is given in (9) where $y_{predicted}$ is the predicted value from the PLSR model, $y_{reference}$ is the measured value and I is the number of samples in the validation data set.

Table 1 : Summary of 6 PLSR models

Species	Range $\pm$ RMSEP
CO2 loading (mol CO2 / mol MEA)	$(0.0 – 0.49) \pm 0.0109$
Carbonate (mol / kg H2O)	$(0.0 – 0.09) \pm 0.0033$
Bicarbonate (mol / kg H2O)	$(0.0 – 1.33) \pm 0.0519$
Carbamate (mol / kg H2O)	$(0.0 – 3.08) \pm 0.0565$
MEAH+ (mol / kg H2O)	$(0.0 – 3.9) \pm 0.054$
Free amine (mol / kg H2O)	$(0.0 -5.8) \pm 0.236$

$$RMSEP = \sqrt{\frac{\sum_{i=1}^{I}\left(y_{predicted} - y_{reference}\right)^2}{I}} \tag{9}$$

These PLSR models can be used to predict the species concentrations in future MEA-CO_2-H_2O samples based on their Raman spectra.

2.4. Screening experiments – model validation

Tasks carried out in this research are twofold. First set of experiments were meant to assess the validity of the PLSR models against offline measurements while the second set was aimed at demonstrating the model capacity in dynamic process situations.

Table 2 : Description of process conditions in screening experiments – model validation

Run No:	Day	Time	CO2 in (vol%)	CO2 out (vol %)	Gas flow (Nm3/h)	Liquid flow (kg/h)	T1 (^{0}C)	T2 (^{0}C)	Boiler temperature (^{0}C)	CO2 removal efficiency
1	Day 1	11.41	9.9	0.7	5	39	46	39	120	0.93
2		11.52	10	2.8	10	39	40	39	120	0.72
3		12.02	10.1	4.8	15	33	32	37	120	0.52
4		12.18	9.9	6.1	20	40	27	38	119	0.38
5		12.31	10	6.9	25	40	24	39	119	0.31
6		12.43	10	7.3	30	40	22	37	120	0.27
7	Day 2	11.03	9.9	5.2	30	114	38	38	119	0.47
8		11.37	9.8	5.8	30	100	35	38	118	0.41
9		11.46	9.9	5.8	30	88	33	39	118	0.41
10		12.06	10.2	6.5	30	100	31	38	117	0.36
11		12.22	10.1	6.6	30	70	29	39	117	0.35
12		12.37	-	-	30	60	24	38	117	-
13	Day 3	11.41	10	5.2	20	112	37	33	117	0.48
14		11.55	10.2	5.36	20	100	38	38	117	0.47
15		12.10	9.8	5.4	20	90	38	39	117	0.45
16		12.27	10.1	5.23	20	80	37	39	118	0.48
17		12.44	10	5.55	20	70	35	39	118	0.44
18		12.57	9.9	5.7	20	60	41	34	118	0.42
19		13.09	9.9	5.9	20	50	31	36	118	0.40
20		13.26	9.8	6.1	20	40	27	37	118	0.37
21		13.37	9.8	6.8	20	30	23	37	119	0.30
22	Day 4	11.22	10.2	4.4	20	110	42	39	119	0.59
23		11.38	10.1	4.4	20	100	41	40	119	0.57
24		11.58	10.2	5	20	90	40	40.	119	0.54
25		12.23	10	5	20	80	37	40	118	0.5
26		12.46	10.1	5.7	20	70	35	39	118	0.45
27		13.04	10.2	5.7	20	60	33	39	119	0.44
28		13.27	9.9	6.3	20	50	31	39	119	0.41

In the *'model validation'* experiments, the rig was operated for 4 days changing liquid flow rates (30 - 115 kg/h) and gas flow rates (5-20 Nm^3/h). The absorber liquid inlet temperatures was set to 40^0C and the CO2 content to the absorber was maintained at 10 vol-% to allow sufficient CO2 to react with MEA. Raman spectra were acquired in 1 minute intervals by the Raman analyser and automatically imported to Matlab/Labview interface where further signal processing was done and selected Raman wavenumbers were exported to perform PLSR model predictions. Only one Raman probe was used during these experiments except for run 1-6. At certain times, 28 liquid samples were collected manually from the sampling points located adjacent to each Raman probe locations for offline measurements.

Key process conditions of the test rig during 4-day trials are given in Table 2. Run 1-6 was related to increasing the gas flow from 5 to 30 Nm^3/h while maintaining the liquid flow at 40 kg/h. In Run 7-12, liquid flow was decreased from 115 to 60 kg/h while keeping gas flow constant at 30 Nm^3/h. Run 13-21 and 22-28 are similar trials where liquid flow was decreased from 115 to 30 kg/h while keeping gas flow constant at 20 Nm^3/h. CO2 removal efficiency calculated based on gas flow measurements by NDIR is also included in Table 2.

2.5. Screening experiments – demonstration

The purpose of screening experiments-demonstration was to see the effect of dynamic process conditions to the model predictions. The easily controllable process conditions of the rig were gas flow rate, liquid flow rate, CO2 % in flue gas and absorber inlet temperature. CO2 concentration in the rich and lean streams was expected to vary in the range of 0-0.45 when the above conditions were varied. Variations of MEA concentrations were also expected due to the water loss at high temperatures of the desorber operation. Four demonstration cases were defined with

varying process conditions as shown in Table 3. Only one case was run per day and each case was around 2.5 hour duration.

Table 3: Description of process conditions in screening experiments – demonstration ((*reg = regeneration in the desorber))

Experiment	Gas flow rate (Nm^3/h)	Liquid flow rate (kg/h)	CO2 v/v% in flue gas	Desorber condition	lean loading	rich loading
Case 1	4	200	4	without reg*.	0.03-0.06	0 .03-0.06
Case 4	4	200	0	with reg.	0.25-0.28	0.25-0.28
Case 1	4	150	0	without reg.	0.03-0.06	0 .03-0.06
Case 1	4	80	4	without reg.	0.03-0.06	0 .03-0.07
Case 3	4	30	10	with reg.	0.22-0.43	0.37-0.44
Case 1	14	200	4	without reg.	0.03-0.1	0.04-0.1
Case 2	14	150	10	without reg.	0.2-0.33	0.2-0.36
Case 3	14	150	11	with reg.	0.36-0.42	0.36-0.42
Case 2	14	150	0	without reg.	0.3-0.32	0.3-0.32
Case 3	14	150	0	with reg.	0.36-0.38	0.36-0.38
Case 4	14	150	0	with reg.	0.17-0.28	0.17-0.28
Case 1	14	80	4	without reg.	0.03-0.06	0.15-0.18
Case 4	14	80	4	with reg.	0.24-0.25	0.3-0.38
Case 4	14	80	10	with reg.	0.24-0.28	0.26-0.38
Case 1	14	30	4	without reg.	0.03-0.06	0.03-0.1
Case 4	14	30	10	with reg.	0.18-0.19	0.4-0.44
Case 3	14	30	10	with reg.	0.22-0.24	0.41-0.44
Case 1	30	200	4	without reg.	0.08-0.12	0.08-0.12
Case 1	30	200	10	without reg.	0.21-0.26	0.24-0.29
Case 1	30	150	4	without reg.	0.12-0.14	0.13-0.16
Case 1	30	150	10	without reg.	0.17-0.23	0.24-0.26
Case 3	30	150	11	with reg.	0.35-0.38	0.32-0.35
Case 1	30	80	4	without reg.	0.13-0.16	0.18-0.29
Case 1	30	80	10	without reg.	0.14-0.19	0.25-0.42
Case 1	30	30	4	without reg.	0.12-0.14	0.26-0.29
Case 1	30	30	10	without reg.	0.13-0.15	0.40-0.43
Range (for all the cases)	4-30	30-200	0-10		0.03-0.43	0.03-0.44

3. Results and discussion

A CO2 loaded MEA sample produces a Raman spectrum with several bands from 300 to 1700 cm-1, a broad area from 1700 to 2700 cm-1 and a couple of sharp overlapped bands from 2850 to 3050 cm-1 as illustrated in Fig. 2. Characteristic Raman bands and vibrational assignments of the species that were found in liquid phase of unloaded MEA and CO2 loaded aqueous MEA during this study are given in Table 4. All the Raman bands identified in CO2 loaded 30% MEA samples at equilibrium conditions in the calibration and validation set used for PLSR models could be identified in the Raman signals acquired during this online study.
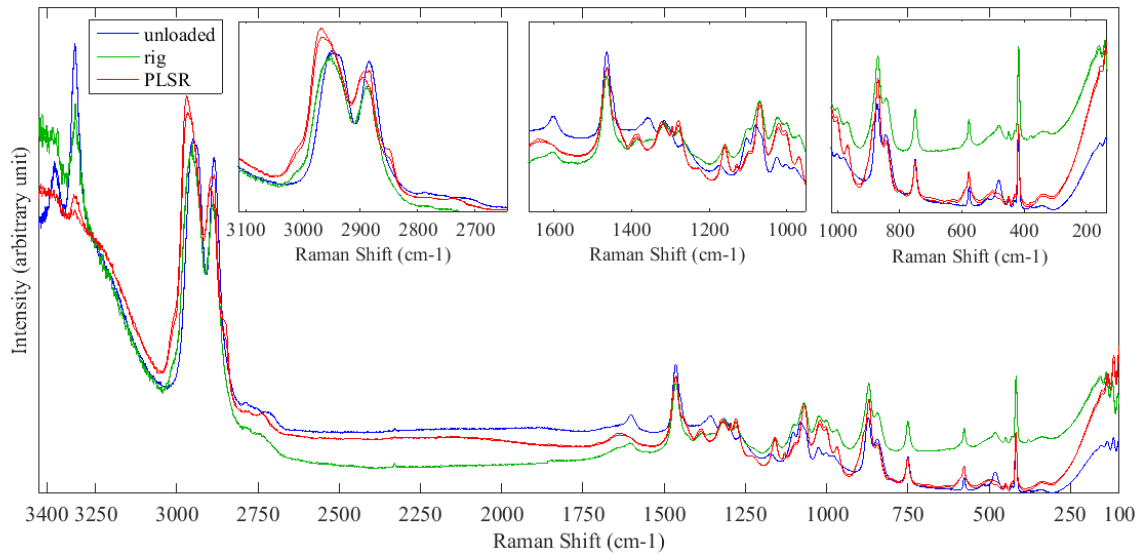
Fig. 2 : Comparison of Raman signals for CO2 loaded and unloaded MEA

Table 4: Vibrational assignments of species in MEA-CO2-H2O system

Specie	Frequency (cm-1)	Frequency (cm-1) (Literature)	Vibrational mode [reference]	Bands identified in		
				CO2 unloaded 30% MEA samples	calibration and validation samples - PLSR	lean and rich amine streams in USN rig
MEA	417	417	CC deformation [12]	√	√	√
	481	481	CC deformation [12]	√	√	√
	843	845	CH2 rocking + CN stretching [13]	√	√	√
	871	873	CH2 rocking + CN stretching [13]	√	√	√
	1029	1030	CN stretching [14]	√	√	√
	1464	1460	CH bend [14]	√	√	√
	2885	2870	CH2 symmetric stretch [14]	√	√	√
	2934	2930	CH2 asymmetric stretch [14]	√	√	√
MEACOO$^-$	1160	1155	C N stretching [15]		√	√
MEAH+	1277	1274	N-CH stretch [16]		√	√
	1320	1320	CC stretch [16]		√	√
	2894	2700-3000	NH$_2$+ stretching [12]		√	√
	2975	2700-3000	NH$_2$+ stretching [12]		√	√
CO32-	1070	1065	Symmetric CO stretching [17]		√	√
	1385	1380	Antisymmetric CO stretching [17]		√	√
HCO3 -	1024	1017	C-OH stretching [17]		√	√
CO2	1278	1274	CO2 symmetric stretch + CO2 bend overtone [14]		√	√
	1389	1383	CO2 Symmetric stretch + CO2 bend overtone [14]		√	√

The comparison of Raman bands between CO2 loaded samples and unloaded amine samples give an indication about the newly appeared Raman bands due to the CO2 absorption by amine.

3.1. Screening experiments – model validation

Based on the equilibrium or non-equilibrium conditions, variations of different CO2 loadings and amine concentration with time was expected in the CO2 rig operation. According to the experimental conditions stated for run 1-28 in Table 2, the behavior of model predictions in such dynamic environment was assessed. By applying six PLSR models, species concentrations of each run were predicted using Matlab PLS toolbox and results are shown in Table 5. 28 runs given in Table 5-1 corresponds to the same run number in Table 2. From the results presented in Table 5-1 and 5-2, total CO2 loading determined from offline titration measurement can be compared with the CO2 loading – PLS model predictions as well as the summation of carbonate-bicarbonate-carbamate – PLS models. In run number 8-L and 20-R, predictions highly deviate from the rest of runs and this was assumed due to an instrument noise. The difference between the CO2 loading – PLS model and the summation of PLS predictions by three carbon species (carbonate + bicarbonate + carbamate) was assumed to be equal to the molecular CO2 which had not reacted with amine. This difference was higher in rich stream than the lean stream as rich stream Raman measurement point was located very close to the CO2 inlet to the absorber and hence more CO2 could exist in aqueous level. Less quantitative difference between column 1 and 9, is an indication of the validity of CO2 loading – PLS predictions.

Table 5-1 : Speciation results from 28 runs;
(Uc = uncertainties calculated by Matlab Toolbox(Uc = uncertainties calculated by Matlab Toolbox)

			Predictions from PLSR models					
			Column 1	Column 2	Column 3	Column 4	Column 5	Column 6
Run no:	Day	Time (L=lean; R= rich)	CO2 loading ± Uc* (mol / mol MEA)	Carbonate ± Uc (mol / kg H2O)	Bicarbonate ± Uc (mol / kg H2O)	Carbamate ± Uc (mol / kg H2O)	MEAH+ ± Uc (mol / kg H2O)	Free MEA ± Uc (mol / kg H2O)
1	Day 1	11:41 - R	0.3319 ± 0.0173	0.049± 0.006	0.041± 0.021	2.352± 0.143	2.50± 0.24	2.28± 0.36
3		12:02 - R	0.4118 ± 0.0176	0.065± 0.007	0.055± 0.021	2.706± 0.144	2.81± 0.22	1.63± 0.38
6		12:43 - R	0.4290 ± 0.0178	0.069± 0.007	0.057± 0.022	2.793± 0.144	2.86± 0.22	1.47± 0.39
1		11:41 - L	0.2244± 0.0174	0.030± 0.007	0.011± 0.021	1.437± 0.146	1.39± 0.23	4.19± 0.41
3		12:02 - L	0.2361± 0.0174	0.028± 0.007	0.021± 0.021	1.297± 0.148	1.40± 0.21	4.35± 0.42
6		12:43 - L	0.2591± 0.0173	0.038± 0.007	0.023± 0.021	1.465± 0.146	1.97± 0.28	3.97± 0.40
8	Day 2	11:37 - R	0.2345± 0.0175	0.034± 0.006	0.029± 0.020	1.519± 0.150	2.38± 0.32	2.94± 0.37
10		12:06 - R	0.4066± 0.0179	0.066± 0.007	0.056± 0.021	2.291± 0.151	2.82± 0.22	2.00± 0.38
12		12:37 - R	0.4436± 0.0173	0.079± 0.008	0.072± 0.021	2.432± 0.147	3.72± 0.36	1.84± 0.37

8		11:37 - L	0.2774± 0.0174	0.106± 0.015	0.108± 0.034	0± 0.406	3.20± 0.71	6.38± 0.54
10		12:06 - L	0.2850± 0.0173	0.041± 0.006	0.031± 0.020	2.119 0.143	2.12± 0.23	2.81± 0.39
12		12:37 - L	0.3075± 0.0173	0.049± 0.006	0.039± 0.020	2.093± 0.143	2.38± 0.23	2.84± 0.39
14	Day 3	11:55 - R	0.3985± 0.0176	0.065± 0.006	0.064± 0.021	2.628± 0.144	2.51± 0.26	1.79± 0.41
16		12:27 - R	0.3111± 0.0175	0.047± 0.007	0.045± 0.020	1.893± 0.145	2.23± 0.26	2.99± 0.36
18		12:57 - R	0.2849± 0.0176	0.045± 0.006	0.045± 0.020	1.911± 0.143	2.10± 0.24	3.09± 0.37
20		13:26 - R	0.3832± 0.0178	0.089± 0.010	0.122± 0.030	0± 0.442	3.19± 0.78	7.07± 0.59
14		11:55 - L	0.4221± 0.0173	0.068± 0.007	0.070± 0.021	2.761± 0.144	2.59± 0.25	1.71± 0.39
16		12:27 - L	0.2805± 0.0173	0.044± 0.006	0.051± 0.021	0.515± 0.267	3.21± 0.66	4.62± 0.41
18		12:57 - L	0.2604± 0.0173	0.040± 0.006	0.036± 0.020	1.742± 0.144	1.86± 0.25	3.54± 0.38
20		13:26 - L	0.4360± 0.0173	0.072± 0.007	0.068± 0.021	2.869± 0.145	2.83± 0.25	1.40± 0.42
23	Day 4	11:38 - R	0.3424± 0.0174	0.055± 0.006	0.055± 0.021	2.321± 0.143	2.46± 0.22	2.18± 0.39
25		12:23 - R	0.2232± 0.0175	0.028± 0.006	0.032± 0.020	1.566± 0.144	1.83± 0.25	3.76± 0.37
27		13:04 - R	0.2600± 0.0177	0.036± 0.006	0.031± 0.020	1.775± 0.143	1.87± 0.24	3.37± 0.36
29		13:56 - R	0.3859± 0.0175	0.066± 0.006	0.058± 0.021	2.541± 0.143	2.59± 0.22	2.00± 0.39
23		11:38 - L	0.4195± 0.0174	0.068± 0.007	0.068± 0.021	2.618± 0.143	2.82± 0.22	1.67± 0.39
25		12:23 - L	0.2734± 0.0173	0.040± 0.007	0.030± 0.020	1.697± 0.144	1.90± 0.25	3.53± 0.37
27		13:04 - L	0.2672± 0.0173	0.037± 0.006	0.031± 0.020	1.763± 0.143	1.94± 0.27	3.43± 0.37
29		13:56 - L	0.3837± 0.0173	0.070± 0.006	0.056± 0.021	2.274± 0.143	2.42± 0.32	2.31± 0.46

Table 5-2 : Offline measurements and calculated species concentrations based on PLS models

Run no:	Day	Time (L=lean; R= rich)	Column 7 pH	Column 8 Total MEA (w/w%)	Column 9 CO2 (mol / mol MEA)	Column 10 = (column 1-11) Molecular CO2 (mol / mol MEA)	Column 11 = (column 2+3+4) Sum of carbon species (mol / mol MEA)
				Offline measurements		Calculated concentrations based on Raman PLS predictions	
1	Day 1	11:41 - R	10.1	38.6	0.3286	-0.001	0.333
3		12:02 - R	9.8	40.2	0.3593	0.029	0.383
6		12:43 - R	9.7	27.5	0.5754	0.033	0.396
1		11:41 - L	10.5	38.8	0.2258	0.016	0.209
3		12:02 - L	10.5	38.6	0.2232	0.048	0.188
6		12:43 - L	10.5	39.7	0.2682	0.057	0.202
8	Day 2	11:37 - R	10.3	32.3	0.2303	0.008	0.226
10		12:06 - R	10.0	33.7	0.4451	0.080	0.326
12		12:37 - R	9.8	33.4	0.3952	0.136	0.308
8		11:37 - L	10.4	32.7	0.2618	0.272	0.005
10		12:06 - L	10.3	33.0	0.2730	-0.019	0.304
12		12:37 - L	10.2	33.6	0.3063	0.018	0.290
14	Day 3	11:55 - R	9.9	34.0	0.3972	0.015	0.383
16		12:27 - R	10.3	33.7	0.3010	0.041	0.270
18		12:57 - R	10.3	34.1	0.2756	0.012	0.273
20		13:26 - R	9.8	35.2	0.3974	0.379	0.004
14		11:55 - L	9.8	37.2	0.3958	0.027	0.395
16		12:27 - L	10.3	33.9	0.2684	0.216	0.065
18		12:57 - L	10.4	34.6	0.2514	0.013	0.248
20		13:26 - L	9.7	36.1	0.4392	0.028	0.408
23	Day 4	11:38 - R	10.1	35.8	0.3534	0.005	0.338
25		12:23 - R	10.4	35.0	0.2510	0.001	0.222
27		13:04 - R	10.4	35.8	0.2610	0.003	0.257
29		13:56 - R	9.9	37.6	0.4020	0.026	0.360
23		11:38 - L	9.8	36.7	0.4122	0.047	0.372
25		12:23 - L	10.4	36.4	0.2742	0.032	0.242
27		13:04 - L	10.4	36.9	0.2640	0.016	0.251
29		13:56 - L	9.7	39.2	0.5048	0.055	0.328

3.2. CO2 absorption profiles with time

Observation of CO2 absorption with time is an important aspect to understand the CO2 removal efficiency, absorption rate and the impact of process conditions to the absorber performance. Raman analyser was configured to collect data with total exposure time of 1 minute during this study. Therefore fast responses as well as numerous predictions were obtained during a total run time of couple of hours. Fig. 3-6 show how predicted CO2 loading evolve with time for four different days run time (given in Table 2). Offline titration results at some certain times are also presented in each graph for comparison.

Fig. 3 is related to run 1-6 where the gas flow rate in the rig was changed from 5 to 30 Nm^3/h while keeping the liquid flow rate at 40 kg/h. Two channels of the Raman analyser were operated at the same time and hence lean and rich amine stream profiles could be observed simultaneously. Eventhough the gas flow rate was increased from time 11.41 to 12.43, a considerable change in CO2 concentration in both streams cannot be observed. Raman predictions for lean amine stream shows better fit with the titration results than the rich amine stream. This was assumed to be due to the more dynamic conditions at the rich stream measurement location. For all the other runs, only one channel of the Raman analyser was used and both rich and lean stream could not be monitored simultaneously (Fig. 4-6). Switching of the operating channel between two Raman probes (lean and rich amine streams) during the run time was performed instead.
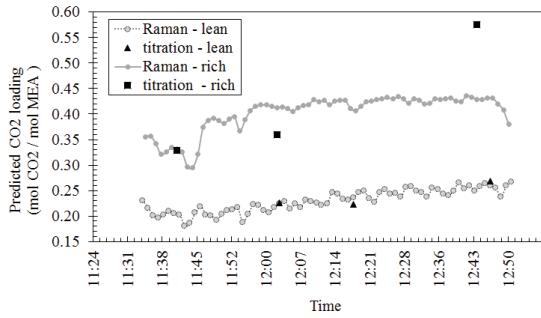
Fig. 3 : Comparison of titration and Raman predictions for CO2 loading (run 1-6)
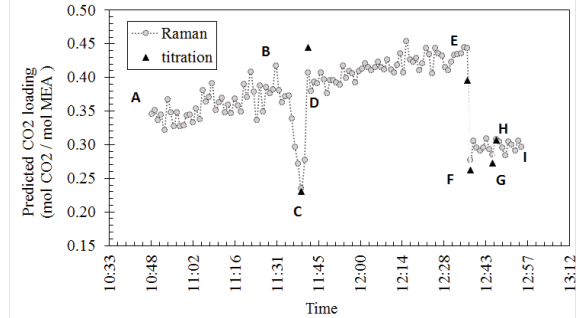
Fig. 4 : Comparison of titration and Raman predictions for CO2 loading (run 7-12)

Run 7-12 was monitored using one channel in the Raman analyser switching the channel between two streams time to time. According to Fig. 4, Point A-B , D-E and H-I are measurements from the rich stream. C and F-G are those for lean stream. During the time from B-C and E- F, Raman probe was transferred from rich to the lean amine stream and from C -D, it was transferred from rich to lean amine stream, so the predictions during these time intervals do not represent actual process stream variations. From time 11.03 to 12.37, the liquid circulation was decreased from 114 to 60 kg/h maintaining a gas flow rate at 30 Nm3/h. Titration measurements follow the trend of Raman predictions. Heavily fluctuating CO2 concentration in adjacent time intervals is an indication of the instability of the process.

Run 13-21 and 22-30 represent two sets of replicate experiments with similar process conditions of gas and liquid flow rates. According to Fig. 5 and 6, they have different initial CO2 concentrations in lean and rich amine streams.
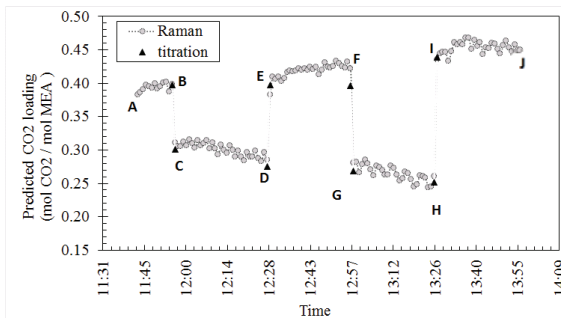
Fig. 5: Comparison of titration and Raman predictions for CO2 loading (run 13-21)
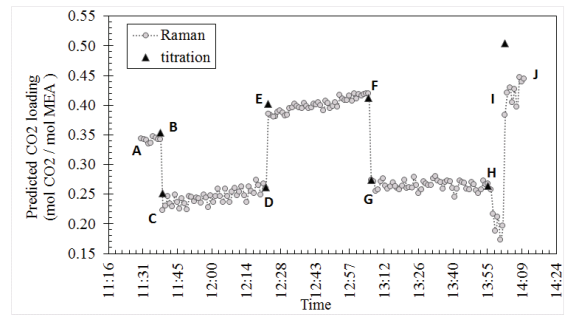
Fig. 6: Comparison of titration and Raman predictions for CO2 loading (run 22-30)

A-B, E-F and I-J are rich streams and C-D and G-H are lean streams. Good fit between predictions and titration measurements imply that the change in liquid flow rate from 112 to 30 kg/hr with time hasnot affected adversely to the predictability of the models. Rich stream shows increasing CO2 loading with time while the lean stream for run 13-21 has a decreasing CO2 content in lean stream as its initial value is higher than the minimum obtainable value for lean stream under this process conditions for the rig. For run 22-30, it shows that the lean stream has almost acquired this minimum level of concentration from the beginning and fluctuates around a same mean value with time. Time interval between each run on a certain day, was around 10-15 minutes and no investigation was done to check whether this allowance was enough to acquire maximum possible absorption/desorption by the unit. Therefore, no conclusions were made on the effect of different process variations to CO2 absorption / desorption rate

3.3. Demonstration of liquid concentration profiles

Results from the four demonstration cases are given in Table 3, are presented in this section to show how the models simultaneously predict CO2 loadings in lean and rich amine streams. Trials were performed after plugging two Raman channels to both streams and performing random variations in absorber inlet temperature, gas flow rate, liquid flow rate, regeneration conditions and CO2 percentage in flue gas. All cases started with the same CO2 content in lean and rich streams. Results are outlined in Fig. 7.

(a) Case 1

(b) Case 2

(c) Case 3

(d) Case 4
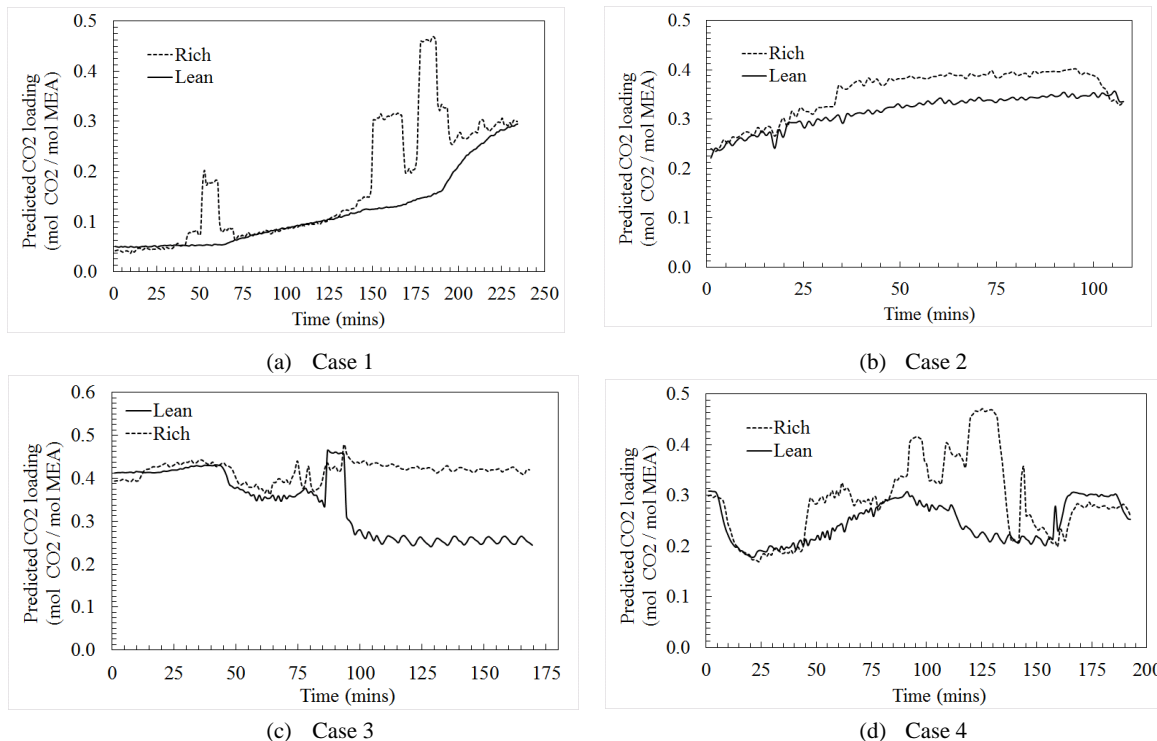
Fig. 7: Prediction of CO2 concentration in lean and rich amine streams amidst of different process conditions
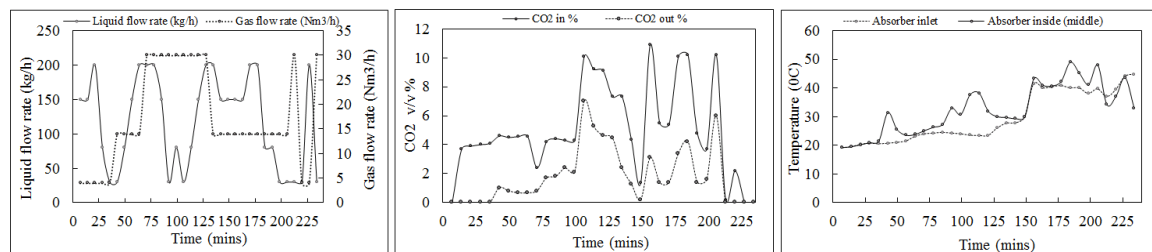
Fig. 8 : Changes of liquid and gas flow rates, CO2 percentage in flue gas stream and temperature in the absorber with time – Case 1

In Fig. 7 - Case 1 demonstrates the CO2 loading – PLS predictions when the rig was running without regeneration of the rich stream. Process conditions related to case 1 are presented in Fig. 8. In this trial, the absorber inlet temperature was increased gradually from 20^0C to 30^0C until 160 minutes. After that it was maintained with an average temperature of 40^0C until the end of the run. The fluctuations of CO2 concentration at some points can be correlated to changes in liquid flow rate, gas flow rate, absorber inlet/inside temperature and CO2 percentage in the flue gas stream with reference to information in Fig. 8. As an example, in rich stream, the increase in CO2 loading from 50 to 75 minutes was due to the changes of liquid to gas ratio (L/G) and between 150-175 minutes and 175-200 minutes was due to increase in CO2 % in inlet flue as stream.

Case 2 was aimed to monitor the steady state achievement with time when the flue gas flow rate and liquid flow rate were kept constant and absorber inlet was set to a fixed value. In this trial, gas flow rate was 14 Nm^3/h, liquid flow rate was 150 kg/h while absorber inlet temperature was 40^0C and CO2 content in the flue gas stream was 10-11%. Both lean and rich amine streams started with same CO2 level. Continuous CO2 supply to the absorber and favourable reaction temperature (40^0C) made the rich stream to have a higher absorption rate than the lean amine stream. After 97 minutes CO2 mixing to the flue gas was stopped which ended both rich and lean streams to reach an equalised in CO2 loading of 0.33 at the end of the run.

The effect of regeneration and liquid to gas ratio on the CO2 absorbed amine stream, can be visualized in Fig. 7-case 3. In this trial, CO2 percentage in the flue gas was maintained at 10-11%. There was no steam supply to the desorber upto 46 minutes. Since the initial CO2 level in both stream was higher than 0.39 mol CO2/mol MEA, upto 46 minutes the increase of CO2 level was very small. At 45 minutes, boiler in the desorber was started and it reached 120^0C by 75 minutes. As a result, the CO2 content in lean stream started to decrease. Simultaneously, rich stream CO2 content was also decreased as the L/G ratio was decreased from 150/14(kg/Nm^3) to 150/30(kg/Nm^3). At 85 minutes, change in L/G as 30/4(kg/Nm^3) resulted in a sudden peak in CO2 level in lean amine stream, however it ended up of final CO2 content of 0.227 mol CO2/mol MEA with time. Simultaneously, rich stream achieved a steady concentration level. In summary, Fig. 7 – case 3 is an example for the ability of the Raman online monitoring tool to observe the effect of regeneration and steady state operation conditions.

Case 4 describes the effect of CO2 volume fraction in the flue gas stream on the responses of lean and rich amine stream concentrations. Initially, both streams showed a loading of 0.29 mol CO2/ mol MEA. L/G ratio was 150/14(kg/Nm^3) but there was no CO2 in the gas flow and the desorber was operated with 120^0C boiler temperature. As a result of regeneration, CO2 was removed in the circulation liquid and reached a content of 0.178 mol CO2/mol MEA by 22 minutes. At 46 minutes, CO2 supply was started with 10% and again at 170 minutes, CO2 supply was stopped while L/G ratio was increased to 200/4(kg/Nm3). Both changes resulted to reach a CO2 content around 0.3 in lean and rich streams loading. Changes of other process conditions during 46 to 170 minutes, are not reported here. Based on the observations made during these demonstration cases, Raman signals gave ample opportunities to understand and monitor online concentration variations with respect to process dynamics in the system.

3.4. Prediction of species profiles

Based on the four test cases described in section 3.3, a complete speciation analysis was performed using 6 PLSR models. These species distribution curves with time can be used to understand which equilibrium chemical reactions

were affected most or least by different process conditions. Fig. 9 and 10 gives the plots for case 1 and 2, where it shows species distribution curves with respect to the CO2 loading for lean and rich streams. There is also a comparison of results with a theromodynamic equilibrium model data for 30% MEA at 40^0C calculated based on the Kent Eisenberg(KE) model [18]. To convert species concentrations in mol/L in KE model into mol/kg H2O at different CO2 loadings, densities available in [19] were used.
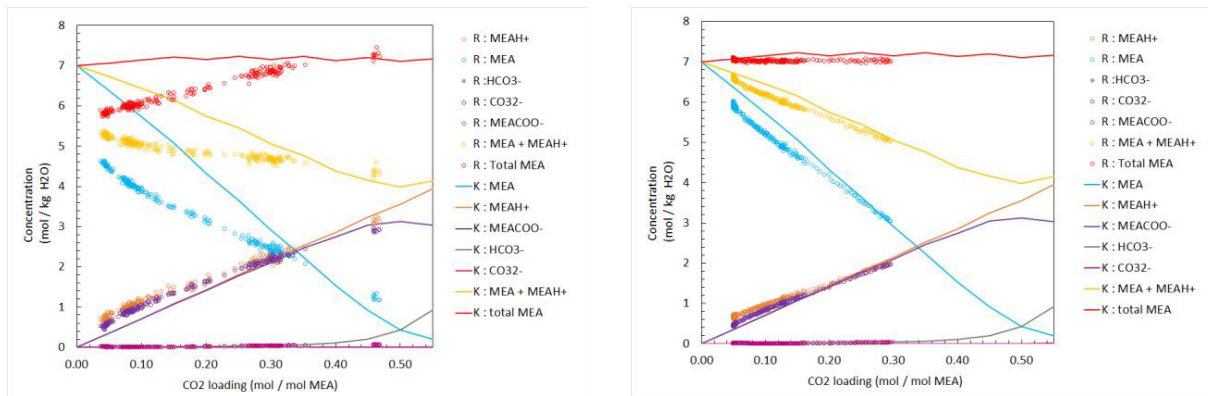
(a)   rich stream   (b)   lean stream

Fig. 9 : Species concentration against CO2-MEA molar loading – Case 1

According to Fig. 9-a, case 1 trial shows that Raman signals acquired from rich amine stream was sensitive to most of the process changes than the lean amine stream(Fig. 9-b). In case 1, there was no steam supply to the desorber. Eventhough the absorber inlet liquid temperature was maintained at a constant value, changes in process conditions resulted in different temperatures inside the absorber (refer table 2) which affected to the equilibrium species concentrations. Kent Eisenberg thermodynamic model represents the species distribution at a constant temperature and for a constant total amine concentration. Therefore a good match between the thermodynamic model (at 40^0C) and Raman predictions cannot be expected, specially for rich amine stream which only obtained 40^0C after 165 minutes of operation. Further, differences of total amine concentration between lean and rich amine streams at any specific time are indications of chemically unsteady state condition of the system.
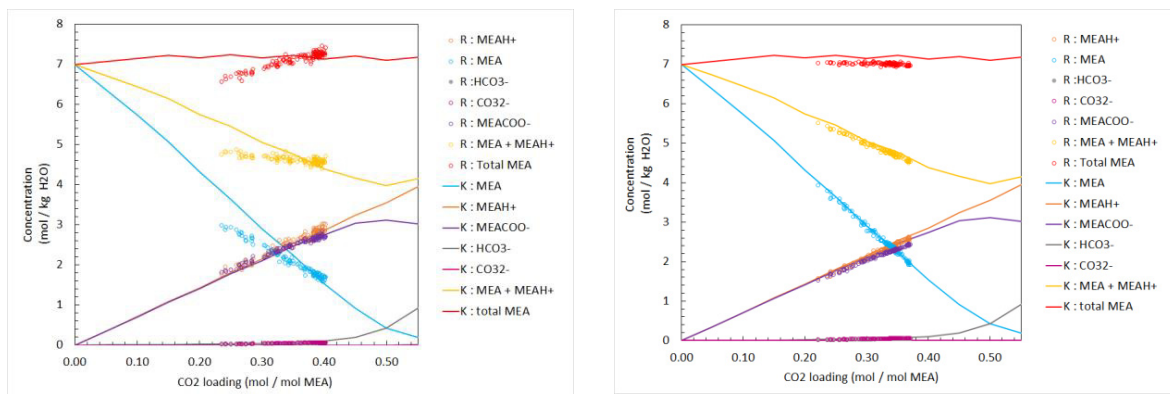
(a) rich stream   (b) lean stream

Fig. 10: Species concentration against CO2-MEA molar loading – Case 2

Fig. 10 is related to similar speciation analysis for case 2. According to the description given in section 3.3 for case 2, the aim of the trial was to monitor the speciation when process conditions were maintained at constant levels. Fig. 10-a implies that at lower CO2 loading values, the rich amine stream was not at steady conditions which was previously observed in Fig. 7-b. Fig. 7-b also claims that rich stream reached a reasonably steady state loading of 0.37 after 35 minutes. Raman predictions after 0.37 loading in Fig. 10-a also shows good fit with the Kent Eisenberg thermodynamic equilibrium model. Therefore there is an integrated match between information given by Fig. 7-b and 10-a. Lean amine stream (absorber liquid inlet) temperature and other process conditions were maintained at fixed values and therefore equilibrium conditions can be expected from the beginning of the trial in case 2-lean stream. This is proved based on the results in Fig. 10-b which reasonably match with the thermodynamic data.

4. Conclusion

In this study, the suitability of Raman spectroscopy combined with multivariate analysis methods was assessed to monitor online speciation of CO2 absorption process. Speciation predictions were based on six PLSR models developed for Raman spectroscopy. Total CO2 content predicted by the Raman PLS model was compared with offline titration analysis of the samples withdrawn during the measurement campaign. Titration measurements claimed a good alignment with predicted values. The ability of the models to cope with changing process conditions and the degree of predictability in equilibrium and non-equilibrium conditions were assessed using four demonstration cases. Speciation were compared with Kent Eisenberg thermodynamic model data and could logically explained. Based on this study, it was proved that Raman analyser is an efficient online process analytical tool to monitor liquid phase speciation in CO2 absorption process by MEA and gives fast and robust responses. However, it is recommended to perform offline ^{13}C NMR measurements to check the validity of predicted species concentration. The benefit of an online measurement tool for CO2 capture process is huge as they can be used to optimize process conditions, understand the chemistry in absorption process and abnormal functionalities in the plant as illustrated in this feasibility study. Integrating the Raman spectroscopy to the CO2 rig at USN, has now allowed more chance to explore the system operation with detailed understanding on absorption process.

Acknowledgement

References

[1] IEA, Technology roadmap carbon capture and storage in, International Energy Agency Paris, France, 2013.
[2] Alexander Kachko V M, Pauls Christoph, Stephan Hochgeschurz, Bathen Dieter ,Pasel Christoph, Bardow Andr, Speciation of MEA-H2O-CO2 by Raman spectroscopy :The impact of spectral analysis, in: 7th Trondheim CCS Conference, Trondheim, 2013.
[3] Geers L, Van De Runstraat A, Joh R, Schneider R, Goetheer E, Development of an Online Monitoring Method of a CO2 Capture Process, Industrial & Engineering Chemistry Research, 50 (2011) 9175-9180.
[4] Einbu A, Ciftja A F, Grimstvedt A, Zakeri A, Svendsen H F, Online analysis of amine concentration and CO2 loading in MEA solutions by ATR-FTIR spectroscopy at process conditions, Energy Procedia, (2012) 55-63.
[5] Souchon V, Aleixo M d O, Delpoux O, Sagnard C, Mougin P, Wender A, Raynal L, In situ determination of species distribution in alkanolamine- H2O - CO2 systems by Raman spectroscopy, Energy Procedia, 4 (2011) 554-561.
[6] Vogt M, Pasel C, Bathen D, Characterisation of CO2 absorption in various solvents for PCC applications by Raman spectroscopy, Energy Procedia, 4 (2011) 1520-1525.
[7] Wong M, Bustam M, Shariff A, Chemical speciation of CO2 absorption in aqueous monoethanolamine investigated by in situ Raman spectroscopy, International Journal of Greenhouse Gas Control, 39 (2015) 139-147.

[8] Alexandr Kachko L V v d H, André Bardow, Thijs J.H. Vlugt, Earl L.V. Goetheer, Comparison of Raman, NIR, and ATR FTIR spectroscopy as analytical tools for in-line monitoring of CO2 concentration in an amine gas treating process, International Journal of Greenhouse Gas Control, 47 (2016) 17-24.

[9] Kent R L, Eisenberg B, Better Data for Amine Treating, Hydrocarbon Process, 55 (1976) 87-90.

[10] Deshmukh R, Mather A, A Mathematical Model for Equilibrium Solubility of Hydrogen Sulfate and Carbon Dioxide in Aqueous Alkanolamine Solutions, Chemical Engineering Science, 36 (1981) 355-362.

[11] Austgen D, Rochelle G, Peng X, Chen C, Model of Vapor-Liquid Equilibria for Aqueous Acid Gas-Alkanolamine Systems Using the Electrolyte-NRTL Equation, Industrial Engineerign Chemistry, 28 (1989) 1060-1073.

[12] Socrates G, Alkane Group Residuals: C–H Group Infrared and RamanCharacteristic Group Frequencies: Tables and Charts, 3 ed., John Wiley & Sons Ltd, 2000.

[13] Batista De Carvalho L, Teixeira-Dias J, Raman spectra,conformational stability and normal coordinate analysis of ethylmethylamine, Journal of Raman Spectroscopy, 26 (1995) 653–661.

[14] Larkin P, in: Infrared and Raman Spectroscopy; Principles and Spectral Interpretation, Elsevier, 2011, pp. 73-115.

[15] Coates J, Interpretation of Infrared Spectra, A Practical Approach, in: Analytical Chemistry, John Wiley & Sons, Ltd., 2006.

[16] Tseng C-L, Chen Y-K, Wang S-H, Peng Z-W, Lin J-L, 2-Ethanolamine on TiO2 Investigated by in Situ Infrared Spectroscopy. Adsorption, Photochemistry, and Its Interaction with CO2, The Journal of Physical Chemistry A, 114 (2010) 11835-11843.

[17] Davis A R, Oliver B G, A vibrational-spectroscopic study of the speciespresent in the CO2-H2O system, Journal of Solution Chemistry, 1 (1972) 329–339.

[18] Øi L E, Removal of CO2 from exhaust gas, in, Telemark University College, Porsgrunn, 2012.

[19] Amundsen T G, Øi L E, Eimer D A, Density and Viscosity of Monoethanolamine + Water + Carbon Dioxide from (25 to 80) °C, Journal of Chemical & Engineering Data, 54 (2009) 3096-3100.

Paper C

(Book Chapter)

Process Analytical Technology for CO₂ Capture

Process Analytical Technology for CO$_2$ Capture

M.H. Wathsala N. Jinadasa, Klaus-J. Jens and
Maths Halstensen

Additional information is available at the end of the chapter

http://dx.doi.org/10.5772/intechopen.76176

Abstract

Carbon capture and storage, which is also known as CCS, is an obligatory climate change
mitigation technology to reduce the carbon dioxide gas emissions to the atmosphere thus
limiting the average global temperature increase to 2°C. Process analytical technology is a
scientific tool to improve process qualities and performance through timely measurements.
This chapter describes how process analytical technology can be imbedded to a carbon
capture technology by giving a detailed example of implementation of a process analyzer
to CO$_2$ capture by alkanolamine absorption process. Such an implementation requires success in five elements, which are described in this chapter. They are as follows: selecting an
appropriate process analyzer, integration between the analyzer and the process, model
development to enable the analyzer to predict a process-related chemical or physical attribute, use of the developed model in real-time application and use of the data obtained from
the analyzer as an input to a process control unit. Partial least square regression model is
a useful chemometric-based method to extract hidden chemical information in measurements from a process analyzer. In this chapter, four partial least square regression models
are presented, which are developed to predict CO$_2$ concentration for four different alkanolamine solutions when these amines are used to absorb CO$_2$ from a combustion process.

Keywords: climate change, carbon dioxide capture, process analytical technology,
process analyzers, chemometrics, partial least square regression, Raman spectroscopy

1. Introduction

1.1. Carbon dioxide and climate change

The Earth's atmosphere contains greenhouse gases such as water vapor, methane, ozone, carbon dioxide and nitrous oxide in trace levels, which have the ability to trap heat. By trapping

heat, temperature of the atmosphere increases which is referred to *greenhouse gas effect*. The greenhouse gas effect is a naturally occurring function in the atmosphere, but when the greenhouse gas level exceeds a certain amount, it couples with the climate and changes the natural equilibrium in the environment. Climate change mitigation actions are a top priority across the world today to fight the greatest environmental threat mankind has ever faced. Carbon dioxide (CO_2) is not the strongest greenhouse gas but among all greenhouse gases, it is the most unwanted as it has made the highest influence to the climate change during the past 270 years [1]. While promoting green technologies such as renewable energy sources to reduce and avoid CO_2 emissions to the atmosphere, capturing CO_2 from the current emission sources is required to reach the climate change mitigation targets such as the 2°C target. Major CO_2 emission point sources are fossil fuel and biomass energy facilities, cement, iron & steel and petrochemical industry.

CO_2 capture and storage (CCS) is a three-step process consisting of CO_2 capture from emission sources; CO_2 transportation to storage sites and store in underground geological formations. In combustion processes, CO_2 can be captured either in pre-combustion or in post-combustion mode.

1.2. Carbon dioxide capture technologies

CO_2 can be separated from flue gas or fuel gas stream by processes such as absorption, adsorption, membrane separation, chemical looping, hydrate based separation, biochemical methods and cryogenic distillation. Among these separation technologies, the absorption process is the most mature because the basic technology is well known. Typical sorbents are alkanolamines and potassium bicarbonate. The most preferred option for retrofitting existing plants is post combustion capture technology (PCC), where CO_2 is scrubbed from the flue gas after combustion has taken place.

1.2.1. CO_2 capture by aqueous alkanolamine solvents

The basic reaction mechanism between CO_2 and pure amines/alkanolamines is the same; hence, both compound classes can be used for CO_2 capture. Although theoretically pure amine can enhance the performance of CO_2 capture than aqueous amines, pure amines and even high-concentrated aqueous amine solutions show implications in plant operations. Several experiments, pilot plant tests and theoretical simulations have been carried out to investigate the optimum amine concentration for CO_2 capture systems [2, 3]. Amine volatility for pure amine is, in general, higher than aqueous alkanolamine volatility. When the amine concentration is increased, amine degradation rate becomes higher [4] and the cost required for amine oxidation inhibitors is increased. CO_2 capture plants using higher amine concentrations require higher reboiler duty [5] and larger water washing sections. Therefore, aqueous alkanolamine solutions are preferred than pure amines. Furthermore, aqueous alkanolamines and in particular aqueous MEA are the commercial workhorse solvents for the CO_2 capture related gas sweetening industry [6].

The IEA CCS road map requires to achieve 100 or more projects by 2020 to reduce the CO$_2$ capture energy penalty by 7% points by proving CO$_2$ capture technologies ready for large scale and demonstrating retrofit for 85% CO$_2$ capture [7]. The most common and cost-effective technology is absorbing CO$_2$ chemically into aqueous alkanolamine solutions such as mono-ethanolamine, monoethanolamine-glycol mixtures, diethanolamine, diglycolamine, diisopropanolamine, methyldiethanolamine, and mixed amines (including sterically hindered amines) [8–11]. Establishing CO$_2$ capture technology by MEA still have challenges, which have to be solved within a short period of time, such as equipment corrosion, solvent degradation, high solvent regeneration energy requirement and possible solvent emissions to the environment.

1.2.2. Chemical reactions of the CO$_2$-alkanolamine-H$_2$O system

A series of parallel equilibrium and kinetic reactions occur during CO$_2$ absorption into aqueous amine solution. This results in an electrolyte solution including ions such as OH$^-$, HCO$_3^-$, CO$_3^{2-}$, RNHCO$_2^-$ and RNH$_3^+$ as shown in reactions from Eqs. (1)–(10). Here R represents an alkyl group such as CH$_3$ or C$_2$H$_5$. Reaction of CO$_2$ with this solution is a Brønsted acid-base neutralization reaction leading to a drop in solution pH as CO$_2$ is absorbed. The chemical composition of this solution varies according to overall solution pH.

Carbon dioxide gas physically dissolves in water to give a solvated form of carbon dioxide which is, CO$_{2(aq)}$ (Eq. (2)). Thereafter, CO$_{2(aq)}$ reacts chemically with water to give carbonic acid (Eq. (4)) which forms equilibria with bicarbonate (Eq. (5)) and carbonate (Eq. (6)) ions according to the respective pKa values. Amines are categorized as primary (RNH$_2$), secondary (R$_2$NH), tertiary (R$_3$N) and sterically hindered amines (e.g., t-RNH$_2$) based on their chemical structure. Amine reactivity of the CO$_2$-alkanolamine-water system is determined by the N atom lone electron pair in a Zwitterion reaction mechanism [7]. Accepting a proton at the N lone electron pair, amines react as Brønsted bases according to a Brønsted acid–base reaction type. The N lone electron pair can also react with, for example, the carbon atom of the CO$_2$ molecule according to a Lewis acid-base reaction type. Carbonic acid reacts in aqueous solution with all amines in a 1:1 manner by a Brønsted acid-base reaction type to form protonated amine bicarbonate. Primary and secondary alkanolamines may also react rapidly with CO$_2$ through a Lewis acid-base reaction type to form amine carbamate. During carbamate formation, two amine molecules react with one CO$_2$ molecule; therefore, aqueous amine solutions forming protonated amine bicarbonate only achieve a higher CO$_2$ loading than aqueous primary or secondary amine solutions forming amine carbamates only.

$$H_2O \leftrightarrow OH^- + H^+ \tag{1}$$

$$CO_{2(g)} + H_2O \leftrightarrow CO_{2(aq)} \tag{2}$$

$$CO_{2(aq)} + OH^- \leftrightarrow HCO_3^- \tag{3}$$

$$CO_{2(aq)} + H_2O \leftrightarrow H_2CO_3 \tag{4}$$

$$H_2CO_3 \leftrightarrow HCO_3^- + H^+ \tag{5}$$

$$HCO_3^- \leftrightarrow CO_3^{2-} + H^+ \tag{6}$$

$$RNH_2 + H^+ \leftrightarrow RNH_3^+ \tag{7}$$

$$RNH_2 + CO_2 \leftrightarrow RN + H_2CO_2 \tag{8}$$

$$RN + H_2CO_2 \leftrightarrow RNHCO_2^- + H^+ \tag{9}$$

$$RNHCO_2^- + H_2O + RNH_3^+ \leftrightarrow RNH_2 + RNH_3^+ + HCO_3^- \tag{10}$$
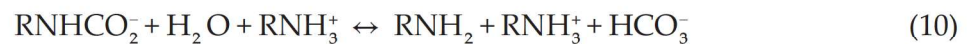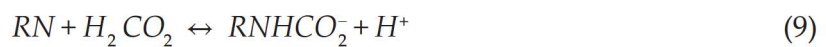
These equilibrium equations (Eqs. (1)–(10)) can be manipulated for amine and absorbed CO_2 considering the carbon and amine balance. The total number of moles of the CO_2 is the sum of moles of carbonate, bicarbonate, carbamate ions and molecular $CO_{2(aq)}$. The total number of amine moles is the sum of moles of protonated amine, free amine and carbamate ions. The mole ratio of CO_2:amine is known as CO_2 loading. This value represents the CO_2 absorption capacity by the amine and is considered as a crucial technology-related value. The reaction pathway for primary, secondary and tertiary amines is described in [12]. Primary and secondary amines react with CO_2 to form carbamates which limits their theoretical CO_2 absorption capacity to 0.5 mol CO_2/mol amine. Tertiary amines do not possess free proton in the nitrogen atom and hence do not directly react with CO_2. Their reaction pathway first involves increasing the hydroxyl ion concentration which contributes to react with CO_2 to produce bicarbonate. Therefore, they have a higher theoretical CO_2 absorption capacity which can go upto 1 mol CO_2/mol amine.

2. Process analytical technology and CO_2 capture

With reference to [13], *process analysis* is the chemical or physical analysis of materials in a process stream through in-line or on-line analyzer. *Process analyzers* can measure directly physical or chemical attributes in a system and supply data. Some key features of process analysis with respect to the laboratory analysis are: the speed of the analysis, zero manual sample handling and ability to integrate real-time data with process control. Process analytical technology (PAT) was originally defined by Food and Drug Administration (FDA) for pharmaceutical industry, as *a system for designing, analyzing, and controlling manufacturing through timely measurements (i.e., during processing) of critical quality and performance attributes*

of raw and in-process materials and processes, with the goal of ensuring final product quality [14]. However, PAT is a tool which can be applied to any process industry to increase its productivity by supplying product/process-related information real-time. Today, from laboratory to industrial scale, process analytical technology has replaced most of traditional methods to determine process-related attributes providing opportunities to understand chemical mechanisms, plant performance and optimization. CO$_2$ capturing is a continuous chemical process or a mass transfer operation where raw materials (e.g., flue gas from a power plant) are converted into a product (e.g., CO$_2$-free-flue gas) in a process plant (e.g., absorption and desorption units). Unlike other industrial applications, CO$_2$ capturing is not an economically profitable process; instead it creates and additional burden to the economy such as increasing the cost of electricity production which creates a drawback for implementation. PAT has a considerable potential to support the strategies and methodologies to reach CCS targets. The concept of PAT within the CCS framework is not yet a well-discussed topic. However, the use of process analyzers in the CCS scientific research area has been gradually increasing during the last decade. This includes research on using different process analyzers to replace traditional laboratory methods, to understand reactions in the molecular level, and solvent selection based on spectroscopic data.

2.1. Implementation of a PAT tool for a CO$_2$ capture process

A successful and robust implementation of PAT is required to gain its widespread benefit to a process. It also saves money, time and resources. Since PAT applies to an entire product cycle, the implementation process should be modeled with simultaneous approach to sub-models such as business, production process, management, engineering, health-safety & environment and customer perspective. Although process analytical technologies improve the speed of the analysis, the stage of introducing such a technology requires knowledge, time and tremendous scientific work. Five elements are identified regarded to this stage and described in this section. **Figure 1** shows these five elements of a PAT implementation approach.
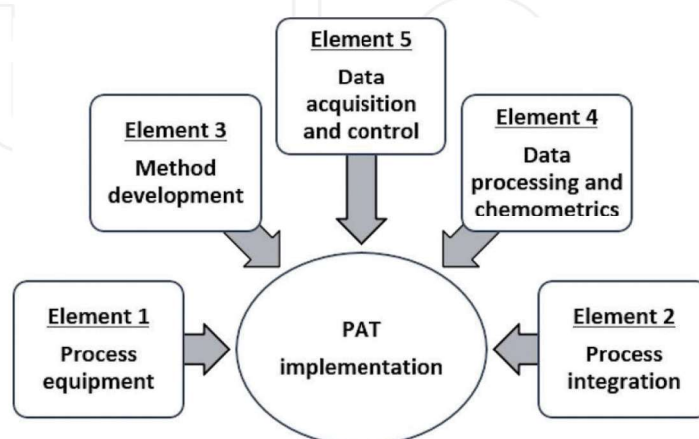
Figure 1. Elements of PAT implementation.

Element 1: Selecting a suitable process instrument for an application is challenging due to the variability of the availability. To determine a particular attribute of the process such as an analyte concentration, several simple to sophisticated measurement technologies are available. The vendors claim the general features of the instruments they sell but how deeply, accurately and precisely they response to our own application and the limitation of usage are unknown until we purchase the instrument and experience its measurements. Since PAT tools are expensive compared to traditional chemical analysis systems, the user may wish to use it for different applications. For instance, an R&D institution wants to use an analyzer to measure transparent liquid samples but later they also wish to analyze high turbid samples. An example is analysis of alkanolamine samples from an industrial CO_2 capture plant where samples are normally transparent when the fresh amines are used but will gradually become opaque due to thermal and oxidative degradation when the plant is operated continuously. If the user purchases an analyzer which only responses to transparent samples and is disturbed due to the fluorescence effect of turbidity in a sample, then this analyzer will stop its function when the solvent degradation starts. Therefore, if the investment requirement is to use this instrument throughout several days of plant operation, then the instrument selection becomes invalid and the whole implementation becomes unsuccessful. To avoid such disappointments in later stages of a PAT implementation, one should always thoroughly assess the selection criteria of the PAT tool. To ease this operation, the process can be started with categorizing available analyzers based on their selectivity, performance, limit of detection, complexity of usage, how it fits to the indoor and outdoor industrial environment as well as the budget. Analyzers can measure physical properties such as refractive index, thermal conductivity and viscosity. There are electrochemical analyzers measuring conductivity, pH and spectroscopic analyzers measuring concentration or any other attribute which is related to electromagnetic interaction. A detailed description about different types of process analyzers can be found in [15].

When selecting a suitable process analyzer, it becomes crucial whether the instrument can be easily integrated to the process system. Some instruments require advance mechanical modifications to the existing system or process stream in the installation process, which make them abatement only to that function. For example, if the requirement is plugging a sensor to a high-flow process stream, the engineer should assure that the plugging mechanism can withstand the maximum pressure of the system. Meanwhile, the process flow should not damage to the sensor. This kind of plugging modifications is normally fixed or permanent, and if the sensor is required to remove from the system, the process flow should be stopped and demand time. These practical problems restrict the analyzer only to this application. If we consider an insertion probe in a liquid stream, there are some critical factors affecting to the quality of the signal. They are angle of insertion, penetration depth, and turbulence of the process flow (as at some flow rates there can be bubble formation). If a probe, which has a higher penetration depth than the sample height of the measurement in an experimental set up, is selected to use, the set up should be modified to increase the sample height than the required penetration depth. If the probe is going to be inserted to a small diameter pipe, where the penetration depth is higher than the diameter, and the probe cannot be inserted to the pipeline directly. In such a case, a flow cell with higher diameter should be included to the

existing line. The volume of the new flow cell should not be larger to create stagnant places, dead zones, and inhomogeneous mixture. This can be challenging because the plant needs to be shut down before the modification. The required mechanical interface may not be easy or straightforward at some instances. Therefore, the engineer experiences the dilemma whether he should select an analyzer, which fits to the system, or he should change the system to fit to the analyzer. Normally, process analytical instruments are superior in giving fast responses. If the interest is online monitoring of concentration changes or reaction kinetics, the analyzer should give fast responses such as measurements in every minute. Frequency of calibration/ maintenance of the analyzer, cleaning requirement between successive scans, required training or expertise to operate the instrument, whether the instrument can be operated continuously throughout an entire process or an experiment cycle are also limiting factors.

Element 2: Process integration implies the method of measurement taken from the application. After selecting the required process analyzer, the sample measurement is carried out inline, at line or online. Examples for inline are: an immersion probe which directly contact with the sample inside the process equipment, process line or flow cell. In such an instance, sample dilution or probe cleaning prior to each measurement is impossible. On the other hand, the user has the ability to do so if there is an autonomous sampling system, which is called on-line. There are some process analyzers, which cannot be physically integrated to the process such as liquid chromatography. Samples that are withdrawn from the process (grab samples) either manually or automatically are measured offline and called at-line measurements. Grab samples associate with the highest percentage of sampling errors.

Element 3: Process analytical instruments give both qualitative and quantitative analysis. Qualitative analysis gives the first impression to understand whether it is meaningful and worth to develop a method for quantitative analysis by a particular instrument. Process analytical instruments are calibrated and validated before they are used to demonstrate that it is suitable for intended purpose. Normally, calibration means to ensure that the instrument readings are accurate with reference to established standards. Calibration can be used before using an instrument such as a weighing balance or a pH meter. Vendor specifies when and how frequently the equipment is needed to calibrate. Normally, the validation refers that the equipment installed correctly and performing without an error comparably to the one used before. These vendors' specified calibration and validation are straightforward.

However, in the PAT terminology, *calibration and validation* imply converting the instrument signals/measurements to be suitable to perform a specific analysis. Based on measurements taken as a set of samples (*calibration set*), a multivariate regression model is developed to predict an attribute. The model prediction performance is validated based on another set of samples (*validation set*) prepared under similar environmental conditions as the *calibration set*. The model is tuned until the prediction error becomes lower than an acceptable value. For example, a model can be developed based on measurements from a spectrometer performed for a calibration set and validation set to predict pH of some chemicals. The same instrument can be used to develop models for other applications such as determining a concentration of a sample, to determine individual concentrations in a mixture of chemicals or analyzing an impurity of a sample. These kinds of model developments to analyze indirect property

are the main expectation from a PAT tool. The method of model development is described under Section 3 for an application in a CO_2 capture process. The calibration and validation procedure should follow the guidelines specified in *Theory of Sampling (ToS)* [16] and *Design of Experiment (DoE)*.

Element 4: Data processing and chemometrics are a subcategory of model development stage. When it comes to the implementation stage of a process analyzer to the plant, the researcher has experience from laboratory experiments or batchwise experiments on what kind of data treatment is needed. Usually raw data coming out from a process analyzer such as a spectrometer contain noise. The information in the data is hidden within this noise. Preprocessing makes data easier to read, understand and interpret. There are also some instances where univariate methods are implemented and/or data processing is not essential. After preprocessing, the data can be used as input to a chemometric model such as a principle component analysis (PCA) model or partial least square regression (PLSR) model. Different chemometric tools have different advantages. For example, PCA can be used to identify trends of variation in the data with respect to time or process conditions, and PLSR can be used to predict process features based on indirect measurements. PLSR is widely used in process applications for quantitative purposes. One such example can be found in [17] where it shows the use of PLSR to quantify all chemical ions present in a CO_2 capture laboratory rig operated by aqueous amine. Another example of PLSR model development and ion speciation is shown in [18] for CO_2 capture by ammonia process. A detailed description for PLSR theory, calibration and validation is described in the literature [19, 20].

Element 5: Data acquisition and instrument control of a process analyzer is an essential part to integrate analyzer measurements with an automative control system. In the case of univariate analysis, implementation of automation control system is easy. However, when it comes to multivariate methods, communication between the process analytical instrument and the control system is challenging. There is a gap between these two types. The reasons are that the analyzer has different file formats and sometimes the control system has been implemented in a different file format in a different flat form. For example, in the analyzer, the data may be saved in csv file format and the control system implemented in MATLAB/LabVIEW interface needs data only from a wavelength range and needs data in txt or mat format as inputs.

3. An experiment on developing a full calibration model using Raman spectroscopy

The scope in this section is to present the methodology on how a process analytical instrument is implemented to replace traditional chemical analysis. The example described in this section is specific to CO_2 absorption process by amines, but a similar approach can be applied for any chemical analysis in laboratory or process plant. Analysis of CO_2 capture solvents is necessary almost in every R&D tasks and CO_2 process plants to optimize the absorption and desorption process. Some examples are investigating the effects of different types of solvents, blends, catalyzers, process parameters and equipment configuration on CO_2 absorption and desorption capacity.

In this example, it is shown how a Raman spectroscopy-based full spectrum calibration is performed using a laboratory experiment for four types of amines which are reacted with CO$_2$. Sample types are described in **Table 1**. Two primary and two tertiary amines were used for preparing four regression models. The primary amines are 2-aminoethanol (MEA) and 3-amino-1-propanol (3-AP). Tertiary amines have a different chemical mechanism than primary and secondary amines when absorbing CO$_2$ and they can reach CO$_2$ loading capacity up to 1 mol CO$_2$/mol amine. 3-dimethylamino-1-propanol (3DMA1P) and methyl diethanolamine (MDEA) are the two tertiary amines used in this experiment.

3.1. Sample preparation

For each model, a calibration and validation set was prepared to facilitate *test set validation* [21]. Number of samples in each calibration and validation set is given in **Table 1**. All the samples were prepared using analytical grade chemicals and Milli-Qwater (18.2 MΩ cm). Aqueous solutions and water were degassed using a rotavapor. First, two amine stock solutions having 30 w/w% (weight per total weight of solution) concentration were prepared and stirred in closed containers for 30 min using mechanical stirrers. Stirring helps to mix the two phases of water and solvent to get a homogeneous solution. CO$_2$ was bubbled into one stock solution until the whole amine sample was *maximum CO$_2$ loaded*. The meaning of *maximum CO$_2$ loaded* is that the solution is filled with equilibrium solubility of CO$_2$ at a given temperature and pressure. The time required to fully load the amine solution was calculated based on the data of volume of 30 w/w% amine sample, CO$_2$ bubbling flow rate, room temperature, pressure and equilibrium solubility. The CO$_2$ loaded amine solution was then stirred for 30 min in a closed vessel and left for 24 h at room temperature. The aim was to facilitate CO$_2$ gas dispersion homogeneously throughout the solution; to accelerate the reaction between gas and solvent and to reach equilibrated state. One gram from each stock solution was transferred to a beaker to titrate with 1 M hydrochloric acid (HCl) to determine amine
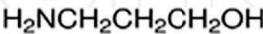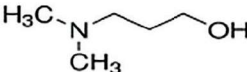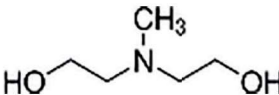
Name	Abbreviation	Chemical structure	Chemical category	Number of CO$_2$ loaded solutions	
				Calibration	Validation
2-Aminoethanol (monoethanolamine)	MEA	HO—CH$_2$CH$_2$—NH$_2$	Primary amine	19	18
3-Amino-1-propanol	3-AP	H$_2$NCH$_2$CH$_2$CH$_2$OH	Primary amine	22	20
3-dimethylamino-1-propanol	3DMA1P	H$_3$C—N(CH$_3$)—CH$_2$CH$_2$CH$_2$—OH	Tertiary amine	21	20
Methyl diethanolamine	MDEA	HO—CH$_2$CH$_2$—N(CH$_3$)—CH$_2$CH$_2$—OH	Tertiary amine	21	20

Table 1. Description of samples in the calibration and validation set.

concentration. By mixing different ratios of CO_2 loaded amine solution with the other amine stock solution (*CO_2 unloaded*), a series of 38–42 different CO_2 loaded samples were prepared in 10 mL glass reactors. After the solution in each glass reactor reached equilibrium, a titration method (refer Section 3.2) was carried out to measure its true CO_2 concentration in units of moles CO_2 per mole solvent.

3.2. Analysis of reference samples

Determination of true CO_2 concentration (CO_2 loading) in alkanolamine samples was carried out by the *$BaCl_2$ titration-precipitation method*. 0.1 M Sodium hydroxide (NaOH), 0.1 M HCl, 1 M HCl, barium chloride ($BaCl_2$) purchased from Merck (99%) and the titrator Mettler Toledo T50 were used for the experiment. The titration procedure is discussed in [22]. This titration is popular and a well-established method to analyze CO_2 loading in absorption processes both in laboratory and industrial applications. However, the method needs extensive chemical preparation; and it takes more than 2 h to analyze one sample and needs expertise and tedious manual work. The accuracy of the PLSR models is strongly affected by the accuracy and results of this analysis. All the sampling errors during sample extraction from stock solution, chemical preparation, weighing, transferring samples, dilution, filtering and titration were identified using a fish-bone analysis and addressed based on the knowledge from *Theory of Sampling* [16].

3.3. Raman spectroscopy

The Raman spectroscopy is a process analytical technique which can be used for batch-wise experiments where measurements are taken manually such as in laboratory tests, or for continuous operations such as in process plants where measurements can be taken continuously in each time interval. The instrument output is called a Raman spectrum which is a plot of intensity of scattered light (called Raman intensity) versus energy difference (given by wavenumber in cm^{-1}). If the objective is to measure the concentration of a chemical sample using Raman spectroscopy, then the peaks and their intensity in a Raman spectrum indicate information about the type of chemicals and their composition respectively for the measured sample. Kaiser RXN2 Analyzer (as shown in **Figure 2a**) with 785 nm laser wavelength, 400 mW laser power and 100–3425 cm^{-1} spectral range was the Raman spectrometer used in this experiment. An immersion optic probe was connected to the RXN2 Analyzer via a fiber optic cable (refer **Figure 2b**). During each measurement, the immersion probe was positioned vertically into the 10 mL glass reactor using a stand. The glass reactor was covered by a black box and aluminum foil to avoid interaction with fluorescence from external light sources (as shown in **Figure 2c**). Each scan was acquired as an average of six scans with 10 s over a total exposure time of 60 s to get a good signal-to-noise ratio.

3.4. Data processing

The aim of the data processing is to condition the measurement signal by removing as much as possible of unwanted structure from the data. Including noisy spectra in regression model
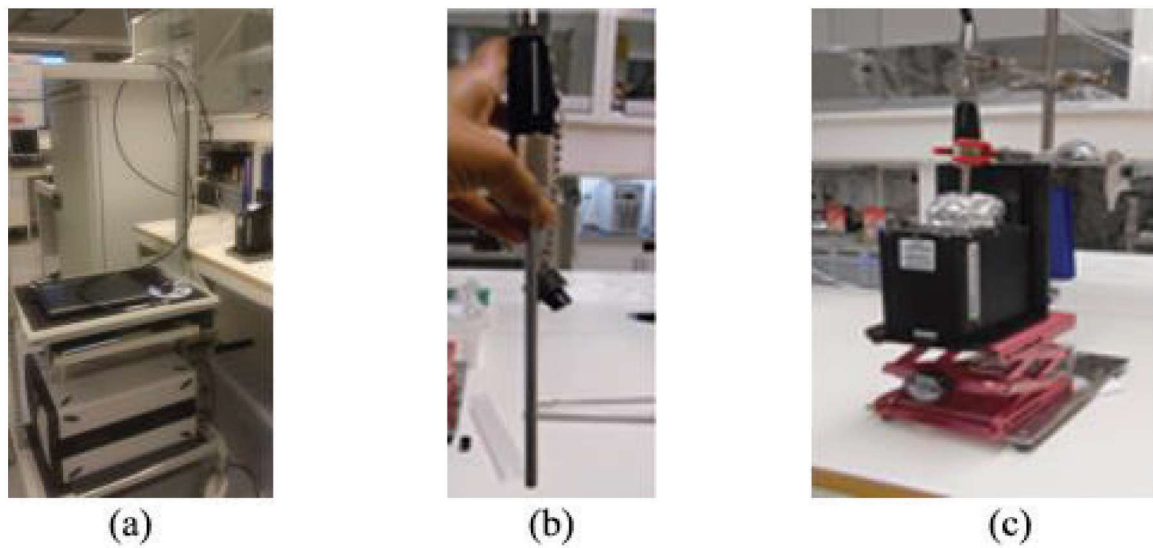
Figure 2. RXN2 analyzer; (a) Raman analyzer with exciting source and detector; (b) Raman immersion probe; (c) sample is in an enclosed sample compartment (black box) and probe, which is mounted vertically, takes measurements.
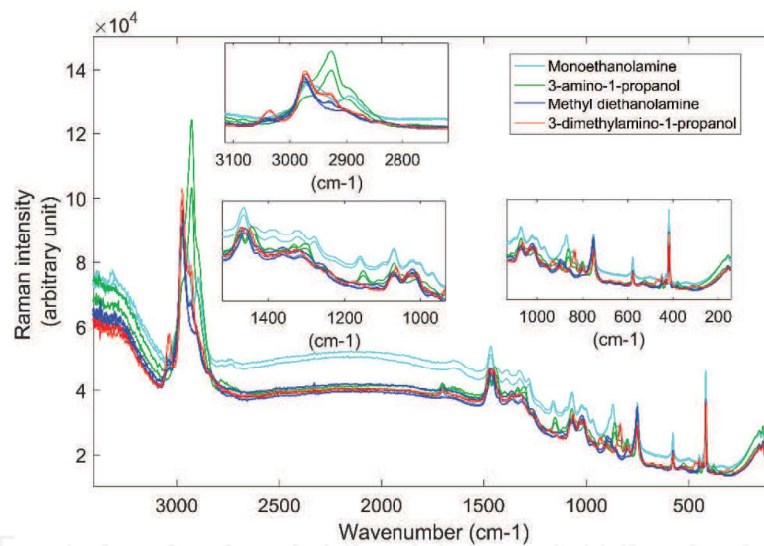
Figure 3. Unprocessed Raman spectrum for four types of CO_2 loaded amine solutions.

calibration results in poor correlation between property to be predicted and measured. The RXN2 analyzer was used to generate a data matrix of n × p where n is number of objects (e.g., different samples or measurements with time) and p is 3326 of Raman wavenumbers. This data matrix contains the chemical fingerprints of the objects and typically different types of noise. This noise comes from interference of other chemical components, laser input variations, noise from fiber optic cable or inadequate path length for the laser.

Figure 3 shows some raw spectra for four types of CO_2 loaded amines where normal features of Raman spectra are visible such as baseline shifts, scattering and peak overlaps. These features avoid the raw spectra to be used directly for the calibration model. Preprocessing of

raw spectra is recommended to improve the predictability of a regression model. There are several preprocessing methods available for PAT applications [23, 24]. The optimal choice of preprocessing method is specific to the application and instrument. In this analysis, the baseline correction based on the Whittaker filter [25] and mean centering was applied which provided the lowest prediction errors as presented by root mean square error of prediction.

3.4.1. Variable selection

When CO_2 is reacted with an amine, it is converted into different carbon ions as shown in Eqs. (1)–(10). The variables related to all these carbon species should be included as *x variables* for PLSR modeling. However, with reference to **Figure 3**, isolation of these variables from the rest of the spectra is not straightforward. The spectroscopy shows measurements in the wavelength range from 100 to 3425 cm^{-1}. In the model development, only a selected range of wavelength was included. The spectra for all the solvents (**Figure 3**) show noise which means unwanted variation, both in higher and lower frequency ranges. The middle frequency range shows a flat behavior with some offsets between measurements. The wavelength below 400 cm^{-1}, between 1600 and 2600 cm^{-1} and after 3100 cm^{-1} was excluded to remove this noise possibly arising either from the instrument, cables or measurement probe. Since these measurements are associated with a chemical reaction, there are frequencies which are assigned to vibrational mode of molecules. The reaction between alkanolamine and carbon dioxide produces carbonate, bicarbonate and carbamate ions for primary and secondary amines. Reaction between CO_2 and a tertiary amine does not form carbamate. For a CO_2-loaded amine solution, the vibrational modes from carbon species and amine species appear in the Raman spectra collectively which makes it more complex to study. One can understand what kind of chemical species present in a chemical system by observing peaks which vary with different concentrations. On the other hand, knowing what kind of chemical species present in the system helps to identify the peaks which should response differently when concentration changes. This fact is very important when selecting variables for modeling. Having a small number of variables makes the model easier to interpret.

There are disadvantages having unwanted variables in the model. The biggest challenge is overfitting, which makes the model correlates with the property to be predicted (*y* variable) during the model development stage, but future samples predict poorly. For instance, when developing a PLS model to predict total CO_2 loading in an aqueous MEA solution, important *x* variables are the vibrational modes coming from carbon species (i.e., carbonate, bicarbonate and carbamate ions). According to the vapor-liquid equilibrium in the system, the protonated MEA and free MEA concentrations correlate almost linearly with CO_2 loading less than 0.5 mol CO_2/mol MEA [9]. Therefore, by mistake, one can include the variables assigned to protonated MEA and free MEA to show a good correlation with CO_2 concentration. However, when this model is used for samples except those are in the calibration and validation sets, predictions will be unreliable.

When there is little or no knowledge on how the *x* variables relate to the *y* variable, variable selection becomes further critical. In principle, all combinations of *x* variables must be tried to

find the optimal choice which is not possible and practical. At such instances, variable selection methods such as iPLS (interval partial least squares regression), genetic algorithms (GA), selectivity ratio and jack-knife can be used [26]. Similar to finding the optimal preprocessing method, finding the optimal variable range is specific to the application and is an iterative procedure. In this example, the selection of the variable range for each model was performed which included vibrational modes of important carbon species available in literature [18]. Due to the overlapping of peaks, it was difficult to isolate the exact area for related vibrational modes and therefore 1000–1500 cm^{-1} and 1000–1164 cm^{-1} regions were selected for primary and tertiary amines respectively which made the models with the lowest RMSEPs.

3.5. Results

The calibration and validation results for each of the four respective PLSR models for CO$_2$ concentration in MEA, MDEA, 3-AP and 3-DMA1P solutions are presented in this section. Data preprocessing and model development were implemented in PLS Toolbox 8.21 in the MATLAB 2016a software (MathWorks Inc.).

The model behavior is presented using four graphs for each amine solution (from **Figures 4–11**) which are the score plot (t1–t2), regression coefficients, RMSEP and predicted CO$_2$ loading versus the measured loading. In the plots, c represents calibration samples and v represents validation samples. Samples are numbered as 1, 2, 3, 4 onwards with decreasing CO$_2$ concentration. The regression coefficient plot is an indication on what weight of each wavenumber contributes to the prediction. The higher the regression weight, the higher the importance of the assigned wavelength to the prediction. The regression plot can be mapped with the vibrational modes of carbon species which are chemically important to the total CO$_2$ loading.

The score plot gives the overview of the span of the calibration data and validation data. Even without knowing the value of CO$_2$ loading (y *variable*), by visualizing the sample location in the score plot, one can understand whether the sample is highly or less concentrated with CO$_2$. Score plot can also be used to identify outliers which mean samples that show nonrepresentative x *variables*. There can be various reasons for outliers such as impurities in samples, different sample type, instrument error and sampling errors. During the model development stage, if such outliers are identified, they should be carefully analyzed and removed from the model. When the model is used for process monitoring, visualization of such outliers helps in the quick identification of the abnormal behavior in the process. With the increasing number of PLS components, the prediction error of the models varies. A plot of RMSEP versus number of PLS components is used to conclude the required number of PLS components for the model. It is always preferable to select a small number of PLS components to avoid model complexities. An optimum number of PLS components avoids the risk of overfitting of the model. The aim of the model is to use the instrument for predicting CO$_2$ concentration. The predicted versus measured plots show how far the measured values deviate with respect to the predicted values for the validation set. This deviation is interpreted with statistical parameters such as r^2, RMSEP and offset. When *test set validation* is used, this plot gives an image on how the model will align with future data.

(a)

(b)
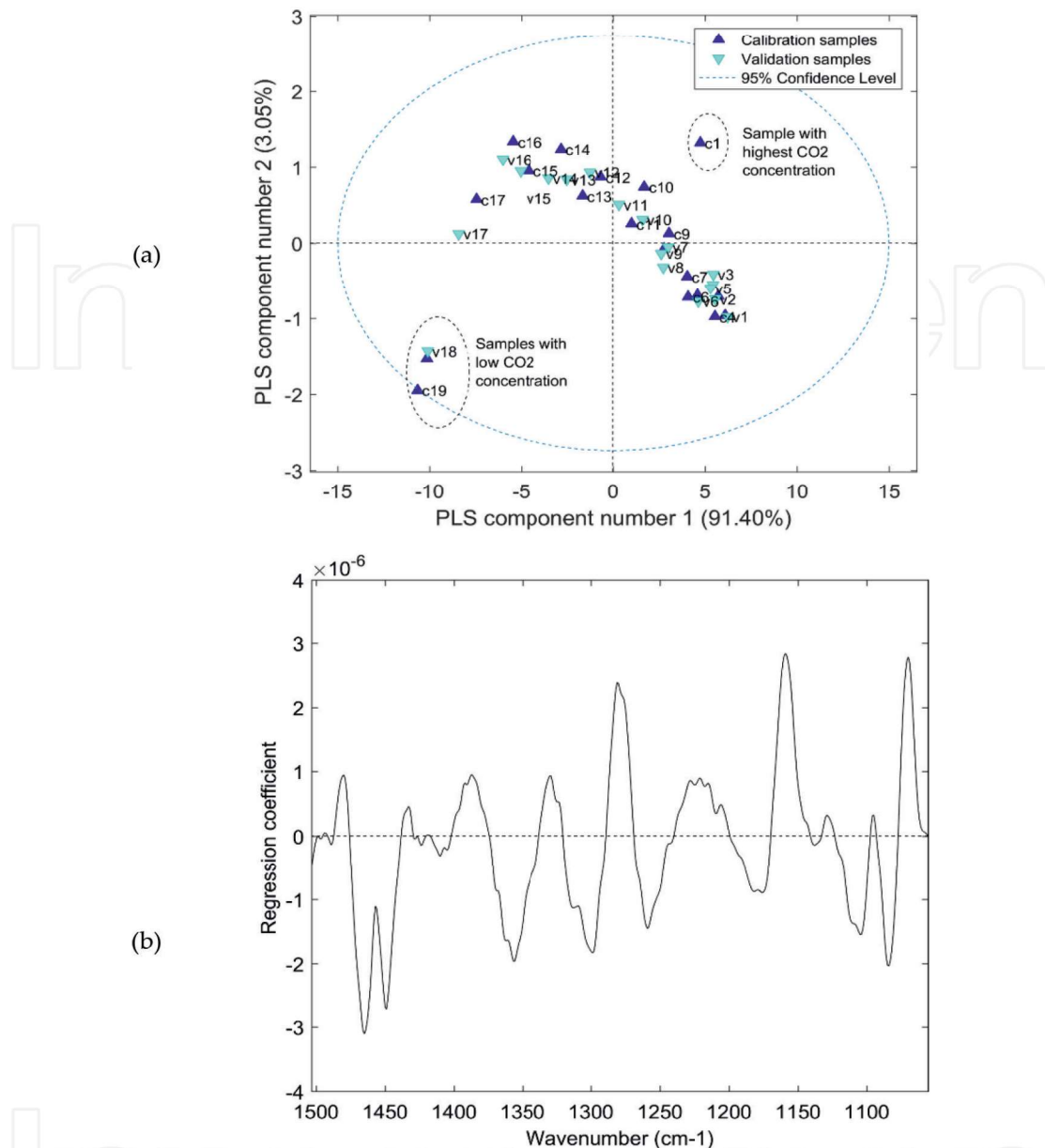
Figure 4. Results from PLSR model for MEA; (a) score plot of PLS components 1 vs. 2 showing calibration and validation samples; (b) regression coefficients based on a 2-component PLSR model.

Figure 4(a) is the score plot of PLS component 1 vs. 2 for MEA model. According to this plot, PLS component 1 describes more than 90% of variation of data while PLS component 2 describes around 3% of variation. The sample with the highest CO_2 concentration ($c1$) and that with the lowest CO_2 concentration ($c19$, $v18$) appear isolated in the score plot implying they have extreme concentration values. The samples are spread in the plot as a pattern where they move from right to left in the direction of PLS component 1 as the concentration decreases. When this model is used for new data, they will appear in the same data swarm area. Samples with high CO_2 concentration will appear in the positive side of PLS component 1 and when
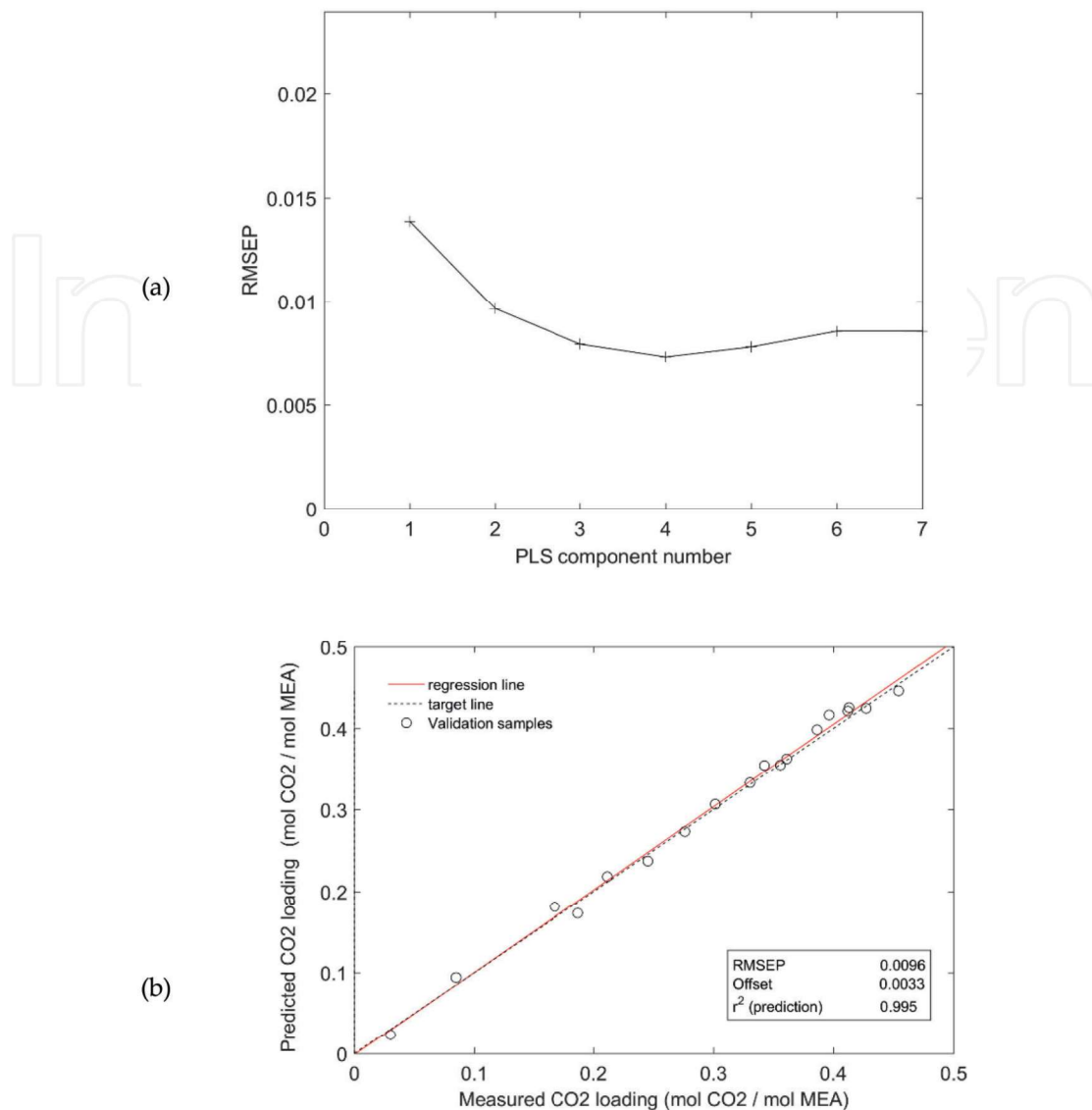
Figure 5. Results from PLSR model for MEA; (a) RMSEP with respect to number of PLS components and (b) predicted versus measured CO_2 loading.

their concentration increases, they move toward the negative side of PLS component 1. **Figure 4(b)** is the plot of regression coefficients between the wavenumber 1000–1500 cm^{-1}. Wavenumbers having positive and negative regression coefficients contribute positively and negatively respectively for the predicted property. **Figure 5(a)** shows the variation of RMSEP with increasing number of PLS component. According to this plot, RMSEP becomes the lowest at fourth PLS component. Having a higher number of PLS components in the model increases model complexity and include more noise to the model. There is not much difference in the prediction error between PLS component 2 and PLS component 4. Therefore, two PLS components were selected for the prediction model. **Figure 5(b)** shows how well the model fits when using for the validation data set to predict CO_2 concentration using their Raman spectra.

(a)

(b)
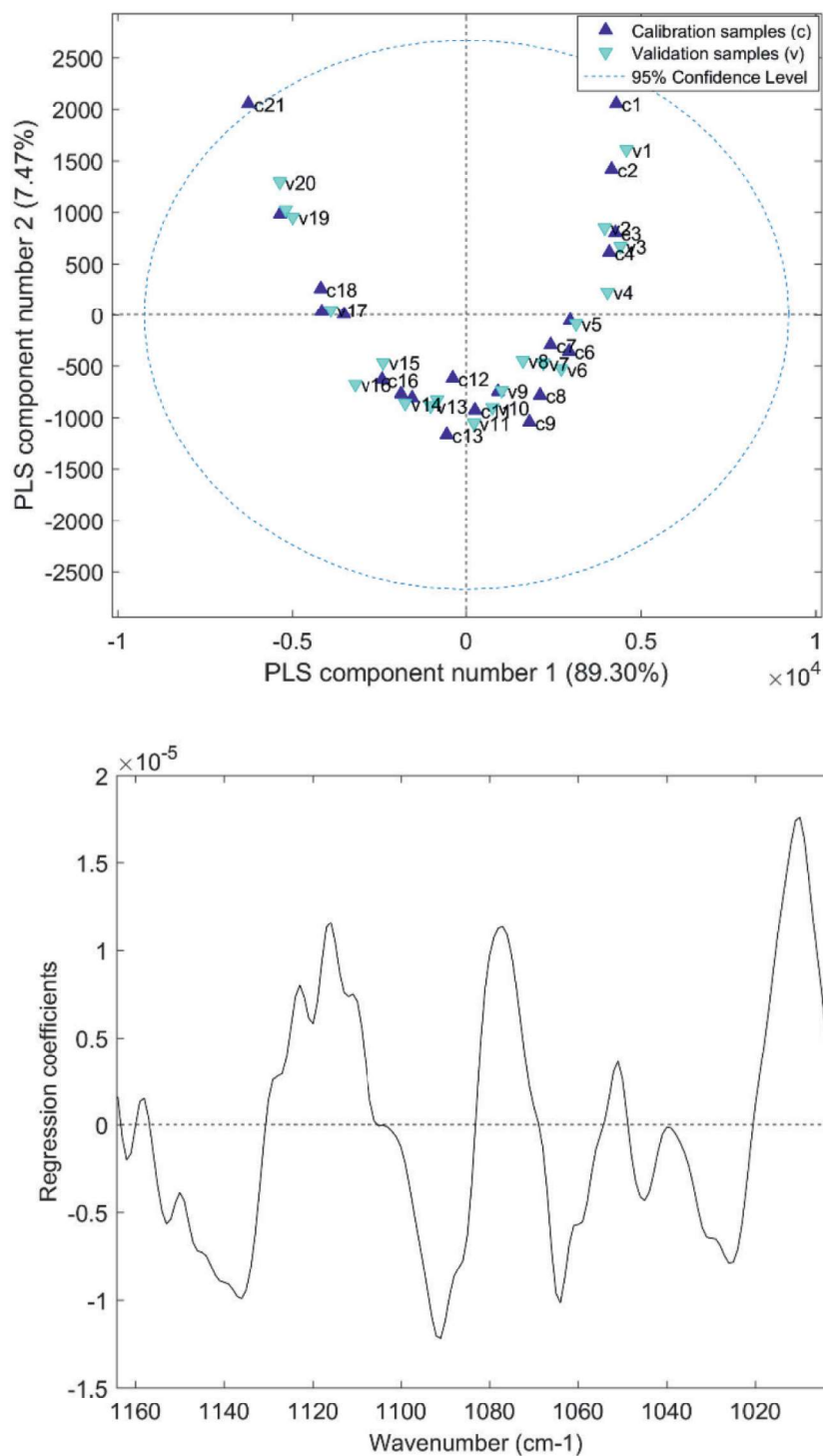
Figure 6. Results from PLSR model for MDEA; (a) score plot of PLS components 1 vs. 2 showing calibration and validation samples and (b) regression coefficients based on a 3-component PLSR model.

Similarly, in **Figure 6(a)**, score plot for the MDEA model shows a data swarm with a pattern moving from positive to negative side of PLS component 1 when the concentration decreases in MDEA samples. Plot of regression coefficients between wavenumber 1000 and 1164 cm^{-1} as shown in **Figure 6(b)** indicates that there are both positively and negatively correlated
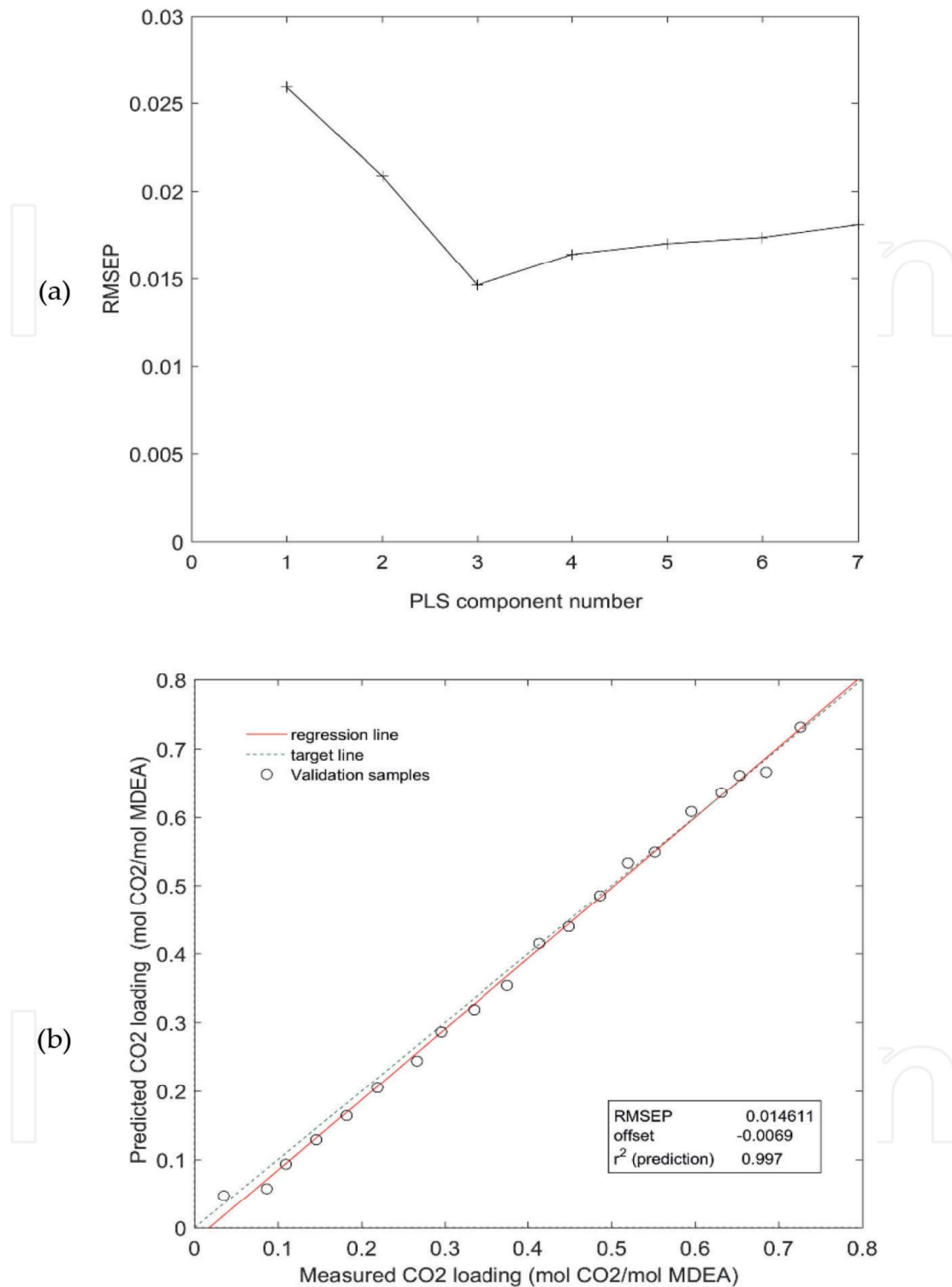
Figure 7. Results from PLSR model for MDEA; (a) RMSEP with respect to number of PLS components and (b) predicted versus measured CO$_2$ loading.

frequencies for the model in this range. Since the model shows the lowest RMSEP at PLS component 3 as given in **Figure 7(a)**, three components were selected for the model and model predictions for validation data set are shown in **Figure 7(b)** resulting an r^2 of 0.995.
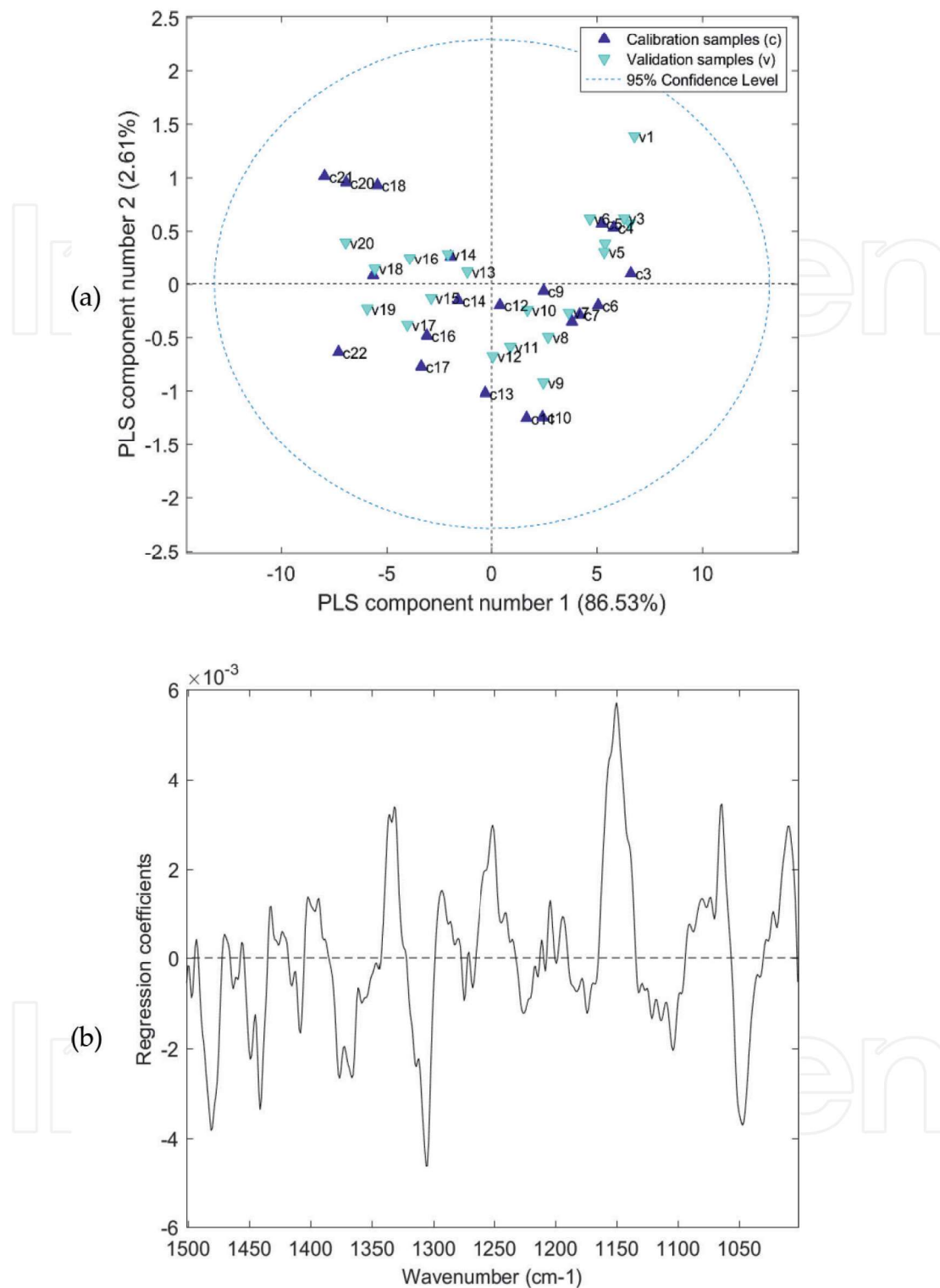
Figure 8. Results from PLSR model for 3-AP; (a) score plot of PLS components 1 vs. 2 showing calibration and validation samples and (b) regression coefficients based on a 2-component PLSR model.

Figure 8(a) shows the movement of samples from positive to negative side of PLS component 1 as the CO_2 concentration decreases in CO_2 loaded 3-AP solvent. The plot of regression coefficients between 1000 and 1500 cm^{-1} as given in **Figure 8(b)** shows negatively and positively
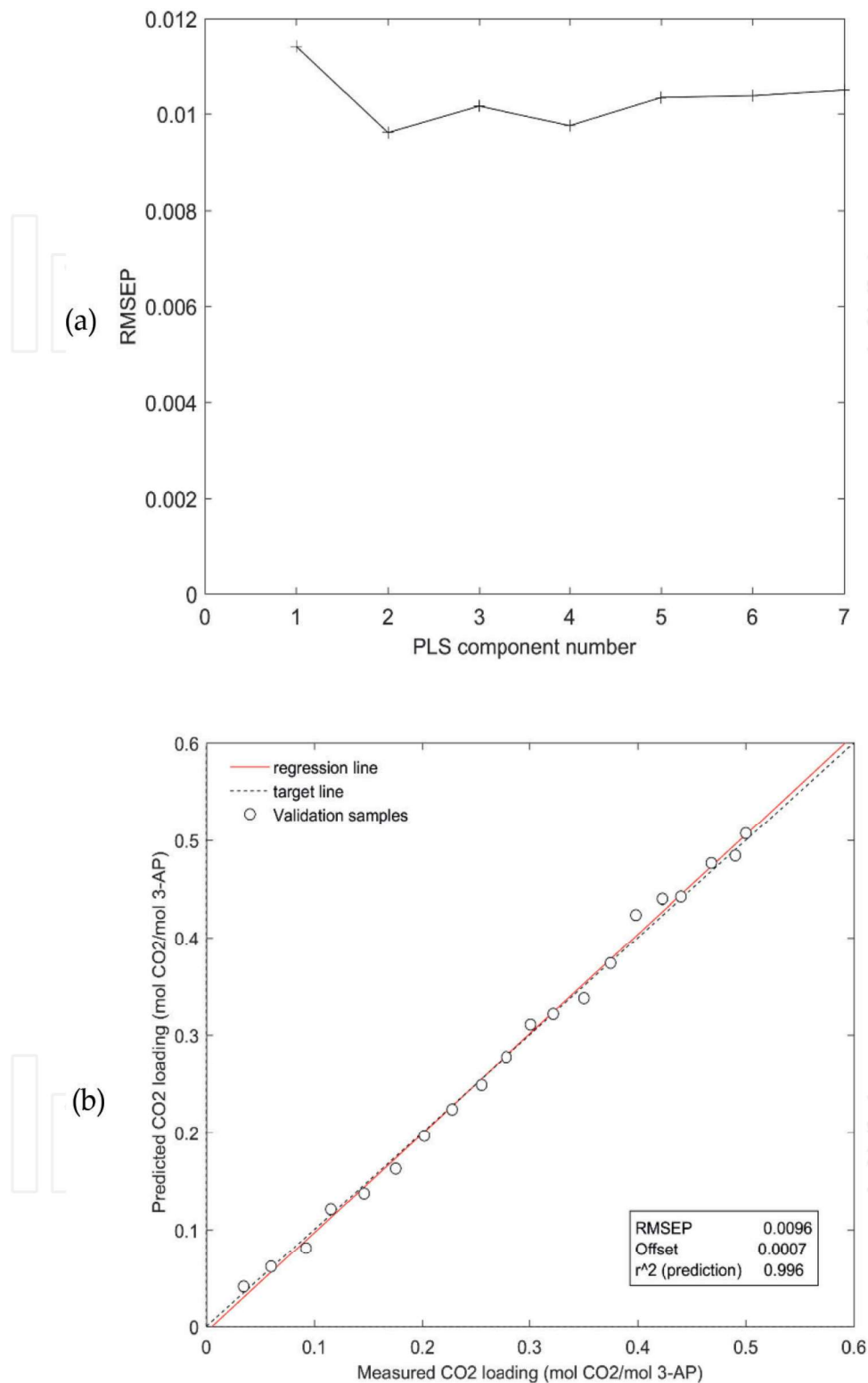
Figure 9. Results from PLSR model for 3-AP; (a) RMSEP with respect to number of PLS components and (b) predicted versus measured CO$_2$ loading.

correlated wavenumbers to the model predictions. According to RMSEP variation with respect to number of PLS components, two PLS components (**Figure 9(a)**) were selected for the model. **Figure 9(b)** shows how well model predicts for the test set samples. The model results
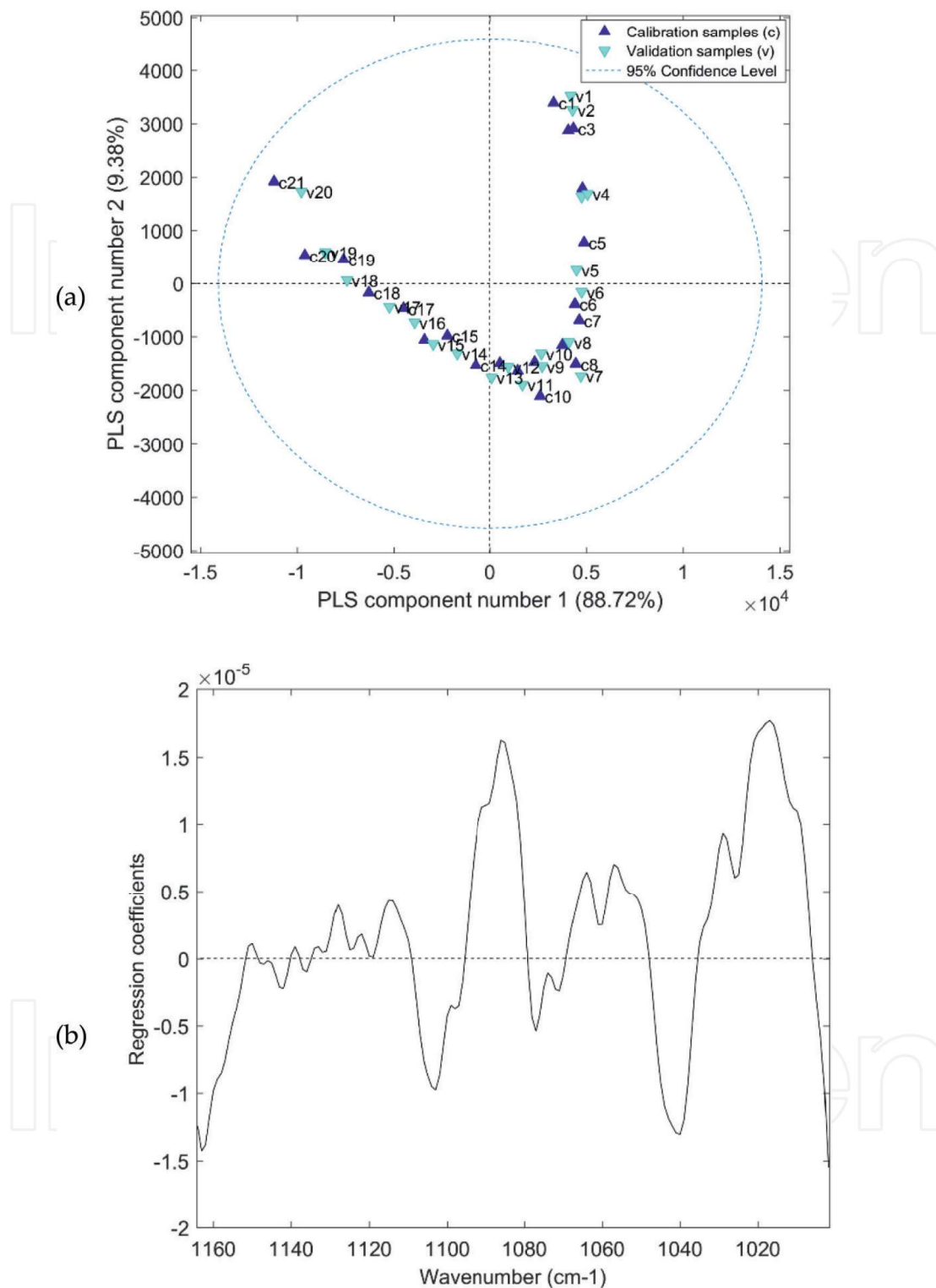
Figure 10. Results from PLSR model for 3DMA1P; (a) score plot of PLS components 1 vs. 2 showing calibration and validation samples and (b) regression coefficients based on a 3-component PLSR model.

for the tertiary amine 3DMA1P are shown in **Figures 10** and **11**. Similar to other solvents, the score plot shows a systematic variation of data swarm (**Figure 10(a)**) while **Figure 10(b)** shows the most and least important variables between 1000 and 1164 cm^{-1} wavenumbers. Three PLS
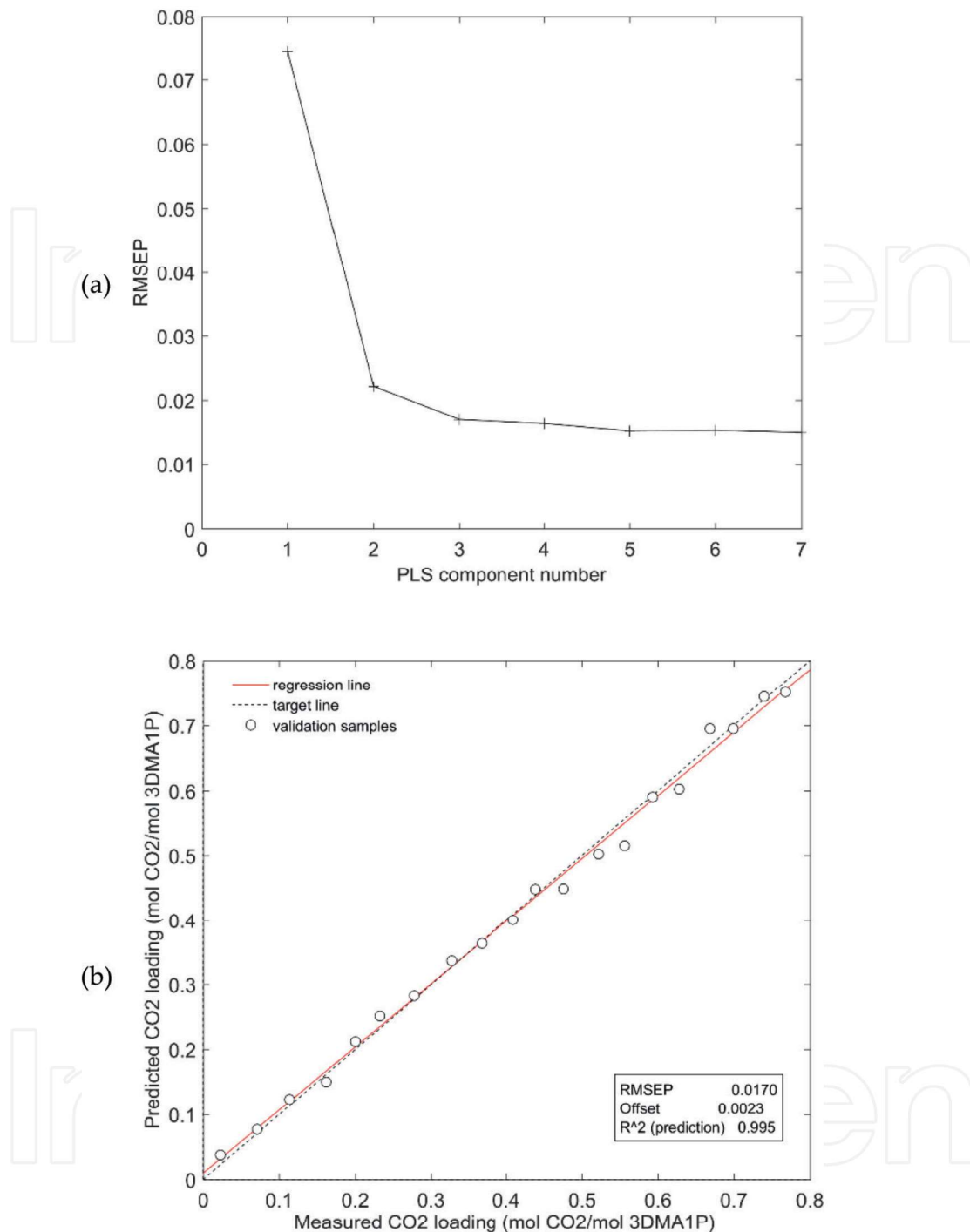
Figure 11. Results from PLSR model for 3DMA1P; (a) RMSEP with respect to number of PLS components and (b) predicted versus measured CO_2 loading.

components were selected (**Figure 11(a)**) for solvent 3DMA1P, and the model predicts the validation samples with r^2 of 0.995 (**Figure 11(b)**).

A summary of the model details for each amine solution is presented in **Table 2**. For all the predictions models, RMSEP percentages are less than 2.13% and r^2 is $\geq$0.995. Each PLSR model is valid only for the CO_2 loading range which is given in **Table 2**.

Model	CO_2 loading range (mol CO_2/mol amine)	Variable range (cm^{-1})	PLS components	RMSEP (RMSEP %)	r^2
MEA	0–0.4543	1000–1500	2	0.0096 (2.11)	0.995
3-AP	0–0.5149	1000–1500	2	0.0096 (1.86)	0.996
3DMA1P	0–0.7945	1000–1164	3	0.017 (2.13)	0.995
MDEA	0–0.7449	1000–1164	3	0.014 (1.88)	0.997

Table 2. Summary of PLSR models.

When these models are used for predictions of CO_2 loading in future samples, first their Raman spectra are preprocessed using Whittaker filter and mean centering. The required variable range is selected for each model and using the regression coefficient equation as shown in Eq. (11), the CO_2 loading is predicted.

$$Y = b_0 + b_1 X_1 + b_2 X_2 + b_3 X_3 + \ldots + b_n X_n \qquad (11)$$

In Eq. (11), Y is the predicted CO_2 concentration; b_0 is regression coefficient for the intercept, X_n is the preprocessed nth variable (Raman wavenumber) and b_n is the regression coefficient relevant to variable X_n.

In PAT, chemometric modeling does not end once a model is calibrated and validated to achieve a targeted prediction accuracy and precision. The model is needed to undergo continuous improvement or remodeling. Some suggestions are assessing the current model performance using new validation data, using additional calibration data to remodel the existing model, improving data preprocessing methods, improving sampling methods, moving to more accurate reference analysis, different x variable ranges and including calibration samples with more variations.

4. Conclusions

Implementation of PAT tools in CO_2 capture process is useful in many ways to accelerate laboratory analysis, R&D tasks and full-scale plant operations. One such example is using a Raman spectroscopy to determine CO_2 concentration in alkanolamine solutions real-time. During the process of implementation of a process analyzer for such an application, a chemometrics-based calibration model should be prepared. Four PLSR models were developed to predict CO_2 concentration in two primary amines and two tertiary amines solutions during CO_2 absorption process. The models predictions are satisfactory where RMSEP are 2.11, 1.86, 2.13 and 1.88% for MEA, 3-AP, 3DMA1P and MDEA, respectively. The target of the present experimental work was to show the PLSR calibration model development for reaction between CO_2 aqueous amine solutions. Primary amine and tertiary amine type was selected for the study because they have two different types of reaction mechanisms. Hence, work on secondary alkanolamines, and so on was out of scope. However, we expect that creating

a model for secondary amines would be similar to the reported case of primary amine since both primary and secondary amines produce carbamate when reacted with CO$_2$.

Acknowledgements

Conflict of interest

The authors in this paper declare no conflicts of interest.

Author details

M.H. Wathsala N. Jinadasa, Klaus-J. Jens and Maths Halstensen*

*Address all correspondence to: maths.halstensen@usn.no

Applied Chemometrics Research Group (ACRG), University College of Southeast Norway, Porsgrunn, Norway

References

[1] IPCC. Climate change: The physical science basis. Working Group I contribution to the IPCC Fifth Assessment Report. Cambridge, United Kingdom: Intergovernmental Panel on Climate Change; 2013

[2] Enaasen Flø N, Knuutila H, Kvamsdal HM, Hillestad M. Dynamic model validation of the post-combustion CO$_2$ absorption process. International Journal of Greenhouse Gas Control. 2015;**41**:127-141. DOI: https://doi.org/10.1016/j.ijggc.2015.07.003

[3] Garcia M, Knuutila HK, Gu S. ASPEN PLUS simulation model for CO$_2$ removal with MEA: Validation of desorption model with experimental data. Journal of Environmental Chemical Engineering. 2017;**5**(5):4693-4701. DOI: https://doi.org/10.1016/j.jece.2017.08.024

[4] Supap T, Idem R, Tontiwachwuthikul P, Saiwan C. Kinetics of sulfur dioxide- and oxygen-induced degradation of aqueous monoethanolamine solution during CO$_2$ absorption from power plant flue gas streams. International Journal of Greenhouse Gas Control. 2009;**3**(2):133-142. DOI: https://doi.org/10.1016/j.ijggc.2008.06.009

[5] Brigman N, Shah MI, Falk-Pedersen O, Cents T, Smith V, De Cazenove T, et al. Results of amine plant operations from 30 wt% and 40 wt% aqueous MEA testing at the CO$_2$ technology Centre Mongstad. Energy Procedia. 2014;**63**:6012-6022. DOI: https://doi.org/10.1016/j.egypro.2014.11.635

[6]   Kohl AL, Nielsen R. Gas Purification. 5th ed. Texas: Gulf Professional Publishing; 1997

[7]   IEA. Technology Roadmap Carbon Capture and Storage. International Energy Agency; 2013

[8]   Afkhamipour M, Mofarahi M. Comparison of rate-based and equilibrium-stage models of a packed column for post-combustion CO_2 capture using 2-amino-2-methyl-1-propanol (AMP) solution. International Journal of Greenhouse Gas Control. 2013;**15**(supplement C):186-99. DOI. https://doi.org/10.1016/j.ijggc.2013.02.022

[9]   Austgen DM, Rochelle GT, Peng X, Chen CC. Model of vapor-liquid equilibria for aqueous acid gas-alkanolamine systems using the electrolyte-NRTL equation. Industrial Engineerign Chemistry. 1989;**28**(7):1060-1073

[10] Sidi-Boumedine R, Horstmann S, Fischer K, Provost E, Fürst W, Gmehling J. Experimental determination of carbon dioxide solubility data in aqueous alkanolamine solutions. Fluid Phase Equilibria. 2004;**218**:85-94

[11] Tontiwachwuthikul P, Meisen A, Lim CJ. CO_2 absorption by NaOH, monoethanolamine and 2-amino-2-methyl-1-propanol solutions in a packed column. Chemical Engineering Science. 1992;**47**(2):381-390. DOI: https://doi.org/10.1016/0009-2509(92)80028-B

[12] Nwaoha C, Saiwan C, Supap T, Idem R, Tontiwachwuthikul P, Rongwong W, et al. Carbon dioxide (CO_2) capture performance of aqueous tri-solvent blends containing 2-amino-2-methyl-1-propanol (AMP) and methyldiethanolamine (MDEA) promoted by diethylenetriamine (DETA). International Journal of Greenhouse Gas Control. 2016;**53**:292-304. DOI: https://doi.org/10.1016/j.ijggc.2016.08.012

[13] Guenard R, Thurau G. Implementation of Process Analytical Technologies. In: Bakeev KA, editor. Process Analytical Technology: Spectroscopic Tools and Implementation Strategies for the Chemical and Pharmaceutical Industries. Chichester: John Wiley & Sons, Ltd.; 2010. p. 17-36

[14] FDA. FDA Guidance for Industry: PAT—A Framework for Innovative Pharmaceutical Development, Manufacturing and Quality Assurance Food and Drug Administration; 2004 [Available from: http://www.gmp-compliance.org/guidemgr/files/PAT-FDA-6419FNL.PDF [Accessed: 22/12/2017]

[15] Process Analytical Technology: Spectroscopic Tools and Implementation Strategies for the Chemical and Pharmaceutical Industries. 2nd ed. Bakeev KA, editor. Chichester: John Wiley & Sons, Ltd.; 2010

[16] Esbensen KH, Paasch-Mortensen, P. Process sampling: Theory of sampling—The missing link in process analytical technologies (PAT). In: Bakeev KA, editor. Process Analytical Technology: Spectroscopic Tools and Implementation Strategies for the Chemical and Pharmaceutical Industries. 2nd ed. Chichester, UK: John Wiley & Sons, Ltd; 2010

[17] Jinadasa MHWN, Jens K-J, Øi LE, Halstensen M. Raman spectroscopy as an online monitoring tool for CO_2 capture process: Demonstration using a laboratory rig. Energy Procedia. 2017;**114**:1179-1194. DOI: https://doi.org/10.1016/j.egypro.2017.03.1282

[18] Halstensen M, Jilvero H, Jinadasa WN, Jens K-J. Equilibrium measurements of the NH$_3$-CO$_2$-H$_2$O system: Speciation based on Raman spectroscopy and multivariate modeling. Journal of Chemistry. 2017;**2017**:13. DOI: 10.1155/2017/7590506

[19] Esbensen KH, Guyot D, Westad F, Houmoller LP. Multivariate Data Analysis: In Practice. CAMO Software; 2010

[20] Martens H, Tormod N. Multivariate calibration. Canada: John Wiley & Sons; 1989

[21] Esbensen KH, Geladi P. Principles of proper validation: Use and abuse of re-sampling for validation. Journal of Chemometrics. 2010;**24**(3-4):168-187. DOI: 10.1002/cem.1310

[22] Weiland RH, Trass O. Titrimetric determination of acid gases in alkali hydroxides and amines. Analytical Chemistry. 1969;**41**(12):1709-1710. DOI: 10.1021/ac60281a024

[23] Liland KH, Almøy T, Mevik B-H. Optimal choice of baseline correction for multivariate calibration of spectra. Applied Spectroscopy. 2010;**64**(9):1007-1016. DOI: 10.1366/000370210792434350

[24] Rinnan Å, Berg F, Engelsen S. Review of the Most Common pre-Processing Techniques for Near-Infrared Spectra. TRAC—Trends in Analytical Chemistry. 2009;**28**(10):1201-1222

[25] Eilers PHC. A perfect smoother. Analytical Chemistry. 2003;**75**(14):3631-3636

[26] Andersen CM, Bro R. Variable selection in regression—A Tutorial. Journal of Chemometrics. 2010;**24**(11-12):728-737

Paper D

Principal Component Analysis Applied to CO$_2$ Absorption by Propylene Oxide and Amines

Principal Component Analysis Applied to CO₂ Absorption by Propylene Oxide and Amines

M. H. Wathsala N. Jinadasa[1], Klaus J-Jens[1], Carlos F. Pfeiffer[1], Sara Ronasi[2], Carlos Barreto Soler[2], Maths Halstensen[1]

[1]Faculty of Technology, Natural Sciences and Maritime Sciences – University College of Southeast Norway, Post box 235, N-3603 Kongsberg, Norway, {Wathsala.jinadasa, Klaus.J.Jens, carlos.pfeiffer, Maths.Halstensen}@usn.no

[2]Norner Research, Asdalstrand 291, N-3962, Stathelle, Norway, {sara.ronasi, carlos.barreto}@norner.no

Abstract

Carbon dioxide absorption by mixtures of propylene oxide / polypropylene carbonate at 60⁰C was monitored by Raman spectroscopy at 20, 40 and 60 bar in a 2 L autoclave reactor. Multivariate preprocessing techniques were used to process raw Raman spectra and Principal Component Analysis was performed. Simulation data from the Peng- Robinson equation of state were used to model the absorbed CO₂ amount and spectroscopic signals. Results showed that Principal Component Analysis can be used to explore the dynamics of the system at different pressure levels and to track the CO₂ absorption. A similar analysis was carried out to monitor CO₂ absorption by four different amines at room temperature and pressure in a batch reactors. The CO₂ content was determined from titration and was used to model the spectroscopic data. Principal Component Analysis proved to be able to identify CO₂ absorption capacity in the amines. This feasibility study confirms that Raman spectroscopy together with multivariate analysis can effectively report chemical information and dynamics in these CO₂ absorption systems and hence can be used for developing regression models for online monitoring and control.

Keywords: principal component analysis, CO₂ absorption, propylene oxide, amines

1 Introduction

Carbon dioxide (CO₂) is known to be the primary greenhouse gas contributing more than 60% of global warming. Capturing CO₂ from power plants and industrial sources and utilization them to produce usable products is of paramount importance from a standpoint of "waste to money". Absorption of CO₂ by amines is one of the most popular technologies for CO₂ capture. Amines are categorized as primary, secondary or tertiary amine based on their chemical structure. The reaction between amines and CO₂ is complex (McCann *et al*, 2009). However, when considering the CO₂ mass balance, it can be seen that once absorbed by a primary amine, CO₂ will remain in the form of carbonate,

bicarbonate, carbamate or molecular CO₂ as given in (1). When it is a tertiary amine, there is no carbamate formation (2).

Synthesis of polypropylene carbonate (PPC) by reaction of CO₂ and propylene oxide (PO) in the

presence of a catalyst has become a fascinating research area as a CO₂ utilization technique to produce a polymer out of a waste greenhouse gas (Jiang *et al*, 2014). In the presence of a catalyst, the chemical reaction of PPC synthesis takes place as given in (3).

CO₂ absorption capacity by an amine or by in the liquid phase PO is a key performance criteria in industrial scale CO₂ capture and polymerization processes. However, the measurement of CO₂ absorption in these mixtures are challenging and require proper understanding of the chemistry behind reaction (1), (2) and (3). Several offline analytical instruments and chemical methods are available such as titration, Nuclear Magnetic Resonance spectroscopy and gas chromatography to determine the CO₂ absorption in both applications above. Most of these methods are time consuming. A fast, online method to detect CO₂ absorption is important in process monitoring and control. Considering the in-situ performance, Raman spectroscopy can be suggested as a competitive approach for this purpose. It gives chemical information of a sample as a function of Raman wavenumber and scattered light intensity. When converting the information given by a Raman spectroscopy, multivariate calibration is required to transform the spectroscopic measurement into informative output. Raman spectra contain several wavenumbers or group of wavenumbers which are chemically important and needed to be included in the multivariate regression models. However, it is often misleading to use

traditional multilinear methods such as ordinary least square for calibration, when a single wavenumber (X variable) is not sufficient to predict the useful quantity (y variable); when X variables are highly correlated or when there is no adequate information to understand which X variables are correlated to the y variable. In such instances, multivariate analysis gives the advantage of overcoming the collinearity problems while preserving useful information hidden in collinear data. In this study, Principal Component Analysis (PCA) which is a fundamental multivariate analysis tool, has been used as a data compression and exploratory method to investigate the feasibility of Raman spectroscopy as a viable analytical technology to quantify CO_2 absorption by amines and propylene oxide. Eight experimental cases have been used in this analysis. Four of them are related to CO_2 absorption by PO and a mixture of PO and PPC. These experiments were meant to compare CO_2 absorption in the CO_2-PO system with respect to the CO_2-PO-PPC system at some selected process conditions. The other 4 experiments were used to identify CO_2 uptake by four liquid amine solvents. These solvents are currently in research interest to capture CO_2 from flue gas in power plants and industries (Leung *et al*, 2014).

2 Methods

Experimental description of 8 test cases are presented in Table 1. Six organic chemicals were used in the experiments and they are given in Table 2. Case 1-4 were carried out in a closed 2L steam jacketed autoclave reactor equipped with a stirrer while the pressure was increased gradually by adding CO_2 to the reactor. Case

Table 1: Description of test cases.

Case Number	CO_2 loaded solution	Description
1	PO in non-stirred condition	Each case has one sample in a 2L reactor at 60^{0}C. Tested pressure levels :20, 40 and 60 bar Stirrer speed = 400 rpm
2	PO in stirred condition	
3	PO+PPC in non-stirred condition	
4	PO+ PPC in stirred condition	
5	MEA 37 samples	Each sample in 10 mL glass reactor. Reaction between CO_2 and amine took place at room temperature and pressure
6	3AP 42 samples	
7	3DMA1P 41 samples	
8	MDEA 41 samples	

1 and 2 were PO-CO_2 binary mixtures while Case 3 and 4 were PO-PPC-CO_2 ternary mixtures. A Raman immersion probe was connected through the bottom of the reactor and signals were acquired continuously with time. In case 5-8, CO_2 absorption on liquid amines was observed under equilibrium condition at room temperature and pressure. Raman signals were recorded by immersing the Raman probe into sample reactors after allowing each sample to reach equilibrium.
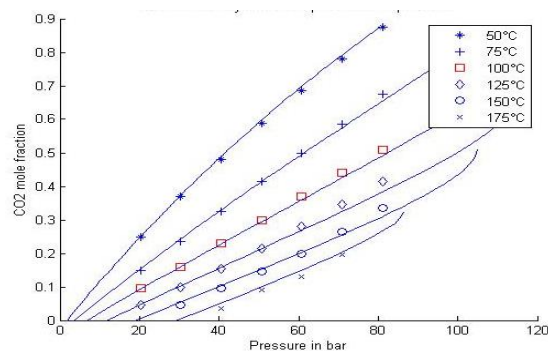
Figure 1. CO_2 mole fraction of PO-CO_2 system at different pressures and temperatures (Peng-Robinson model with binary interaction parameter equal to 0.281).

Table 2. Description of materials.

Name	Abbreviation	Chemical structure	Chemical category
Propylene oxide	PO		epoxide
Polypropylene carbonate	PPC		a copolymer of CO2 and PO
2- Aminoethanol	MEA		Primary amine
3-Amino-1-propanol	3-AP	$H_2NCH_2CH_2CH_2OH$	Primary amine
3-dimethylamino-1-propanol	3DMA1P		Tertiary amine
Methyl diethanolamine	MDEA		tertiary amine

2.1 CO_2 in polymer solutions – from thermodynamic models

In this study, Raman signals (X variables), were calibrated with the absorbed CO_2 content (y variable). Reliable measurement of y variable in Case 1-4 using an analytical method is challenging as CO_2 quickly desorbs if a sample is taken out from the reactor for analysis. Therefore, the CO_2 content data at required pressure and temperature were calculated from the vapour-liquid equilibrium (VLE) data of CO_2-PO system generated using the Peng-Robinson equation of state. The Peng-Robinson model was fitted using experimental data reported in (Chen *et al*, 1994; Shakhova *et al*, 1973). Figure 1 shows predictions of the CO_2 mole fraction in PO-CO_2 system using Peng-Robinson model simulated in Aspen Plus V7.2 software which shows that the absorption of CO_2 at a constant temperature gives a linear behavior with pressure. This linear relationship was taken to model the CO_2 mole fraction at 60^{0}C at which the experimental cases of 1-4 were carried out.

2.2 CO_2 in amine solutions – from titrations

In experiments from case 5-8, each sample contained 30 % of solvent (solvent weight/total weight of water and solvent) but different amounts of CO_2 added. They were prepared in 10 mL glass reactors and after reaching equilibrium a titration method was carried out to measure its true CO_2 content in units of moles CO_2 per mole solvent.

a) Case 1

(b) Case 3
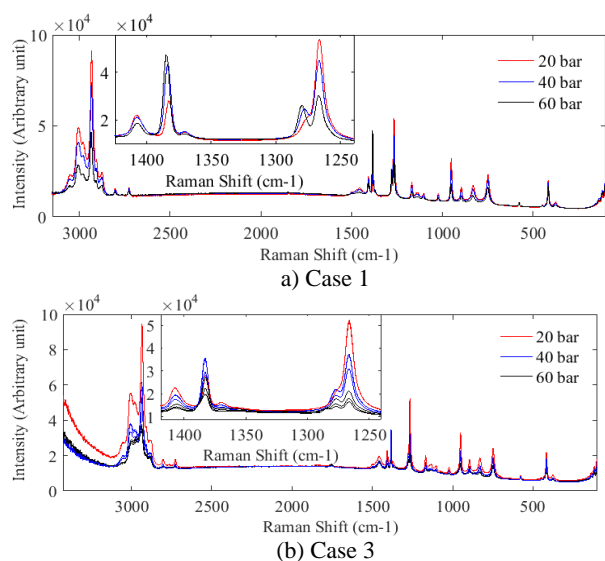
Figure 2. Raman signals of CO_2 loaded polymer samples.

(a) 100-3325 cm^{-1} (b) 950-1550 cm^{-1}

Figure 3. Raw spectra of CO_2 loaded samples (Case 5-8).

Figure 4. Raw spectra of CO2 loaded MEA samples (Case 5).

2.3 Raman Spectroscopy

Raman spectroscopy used in this study was Kaiser RXN2 Analyser of 785 nm laser wavelength, 400 mW laser power and 100-3425 cm^{-1} spectral range. An immersion optic probe which is connected to the RXN2 Analyser via a fibre optic cable, carries the laser light to the sample and in-elastically scattered Raman light is conveyed back to the instrument. The instrument output is a plot of intensity of scattered light versus energy difference (given by wavenumber in cm-1) which is called a Raman spectrum. Peaks and their intensity in a Raman spectrum carry information about the chemicals and their composition respectively.

2.4 Data Processing

For a set of n objects (eg: different samples or signals with time), a Raman spectroscopy measurement generates a data matrix of n x p where p is 3326 Raman wavenumbers. This data matrix contains useful information about the chemical fingerprint of objects as well as noise. They are also called residuals which can be due to the interference of other chemical components, laser input variations or instrument noise. Unless any data conditioning method is applied to remove this unwanted structure from the data matrix, calibration of spectroscopic signals will not be reliable and do not really generate a model which really represent the variation of analyte of interest.

Three data pre-processing techniques were applied for raw Raman data. These were baseline-whittaker filter, standard normal variate (SNV) and mean centering. The baseline-whittaker filter available in PLS toolbox in Matlab is an extended version of (Eilers, 2003) where a weighted least square method is applied to remove background noise and baseline variations. A detailed description of the algorithm can be found in the original work (Eilers, 2003) and (Atzberger et al, 2010). Some
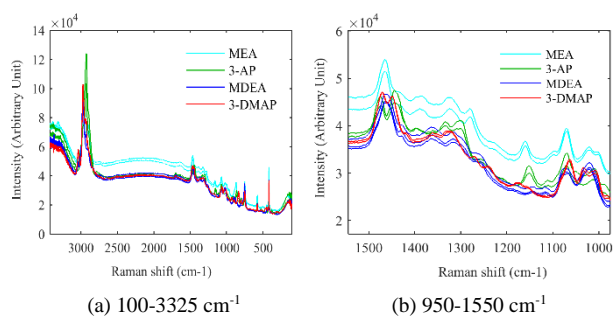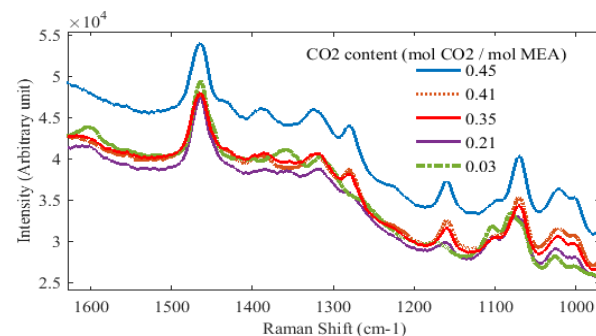
spectra which should be otherwise identical, become different due to baseline and pathlength changes. SNV was applied to remove these scatter effects in the spectra which were specially observed in case 1-4. The algorithm is similar to autoscaling row wise and hence corrects each spectrum individually (Barnes et al, 1989). By mean centering of data, each column in the data matrix is centered by subtracting the mean. It is reported that by mean centering, rank of the model is reduced, data fitting accuracy is increased and offset is removed (Bro et al, 2013).

2.5 Principal Component Analysis (PCA)

Principal component analysis is one of the most important data analysis methods providing a platform for advanced chemometrics methods. As stated in (S. Wold et al, 1987) PCA can have many goals; simplification, data reduction, modelling, outlier detection, variable selection, classification, prediction and unmixing. It can be used to understand general characteristics of data set and guide further investigation through more refined techniques (Wentzell et al, 2012). PCA reduces the dimension of data by calculating principal components (PCs) which reflect the structure of data corresponding to maximum variance. These PCs can then be plotted to visualize the relationship between samples and variables through the use of scores and loading plots. A tutorial review on PCA can be found in (Bro et al, 2014). Decomposing a data matrix X into a structure part which consists of a score matrix (T) and a

loading matrix (P) and noise part or residual matrix (E), is shown in (4) and (5).

$$X = TP^T + E \qquad (4)$$
$$X = t_1P_1{}^T + t_2P_2{}^T + t_3P_3{}^T + \cdots + t_AP_A{}^T + E \quad (5)$$

Case 1

Case 2

Case 3

Case 4
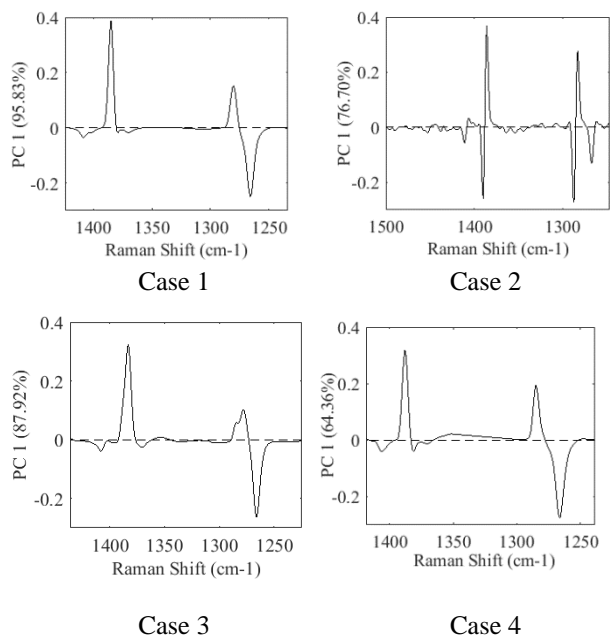
Figure 5. Loading plots of the first principal component for case 1-4 (Region : 1225 – 1450 cm-1).

t_A and P_A are score vector and loading vector for PCA respectively. PC1 is the first principal component which relates to the maximum variance of the data, and PC2 is the second principal component which corresponds to the second largest variance etc. Score values provide information about sample variations while loading value explains the relationship between variables. Residuals provides information as to what spectral variations have not been explained. There are different ways to decompose a matrix to score and loading vectors. NIPALS (*Non-linear Iterative Partial Least Squares*) algorithm (H. Wold, 1966) uses iterative sequence of ordinary least square regression to calculate PCs and was used in this study.

2.6 Important variables related to CO₂ absorption

CO_2 absorbed PO, PPC and amine mixtures exhibit several sharp overlapping peaks in the region of 300 to 1500 cm-1 and 2700 to 3250 cm-1. The focal point in this study is to investigate CO_2 absorption and hence only the peaks related to absorbed CO_2 are considered in the model development. In case 3-4, the monomer PO and the polymer PPC were added into the autoclave reactor and the CO_2 was absorbed into this mixture. Therefore, CO2 bands related to dissolved CO_2 in the PO or PO/PPC mixture were followed in this study.

Case 1

Case 2

Case 3

Case 4
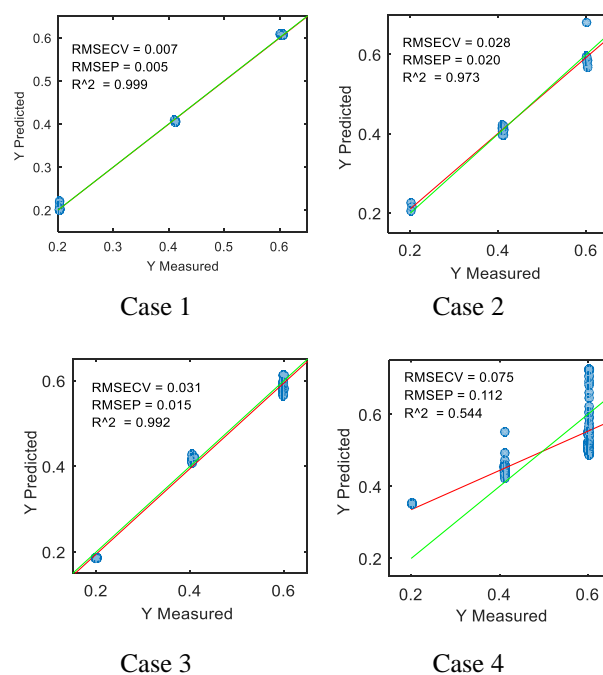
Figure 6. Development of linear regression model using PC1 score values and thermodynamic model data.

(Y measured = CO_2 mole fraction predicted by VLE data; Y predicted = CO_2 mole fraction predicted by PC1 scores; red line= best fitted line based on calibration points; green line=1:1 target line; RMSE (CV/P)= root mean square error of (cross validation/prediction)

Case 1

Case 2

Case 3

Case 4
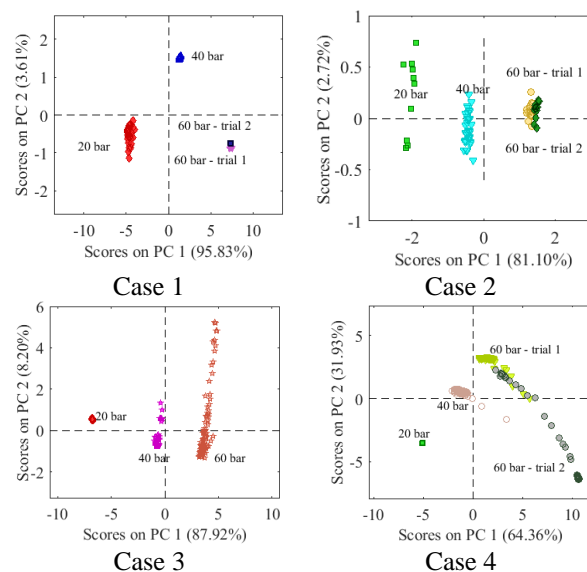
Figure 7. Score plots – PC1 vs PC2 for case 1-4.

Literature reports such Raman wavenumbers of 1264, 1284, 1369, 1387, 1408 cm-1 (Hanf *et al*, 2014). In case 5-8, peaks related to carbonate, bicarbonate, carbamate and dissolved CO_2 fall in the region of 1000-1500 cm-1 ((Vogt *et al*, 2011), (Wong *et al*, 2015)). Therefore, for development of PCA models, the region between 1000-1500 cm-1 and 1225-1450 cm^{-1} were selected for case 1-4 and case 5-8 respectively.
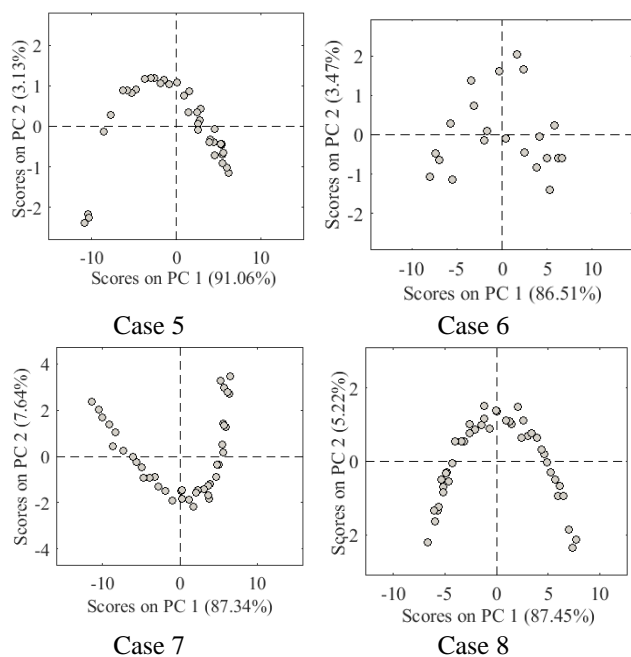
Figure 8. Score plots for case 5-8.

3 Results and Discussion

Figure 2 (a) and (b) show raw spectra for case 1 and 3 respectively highlighting spectral variation with
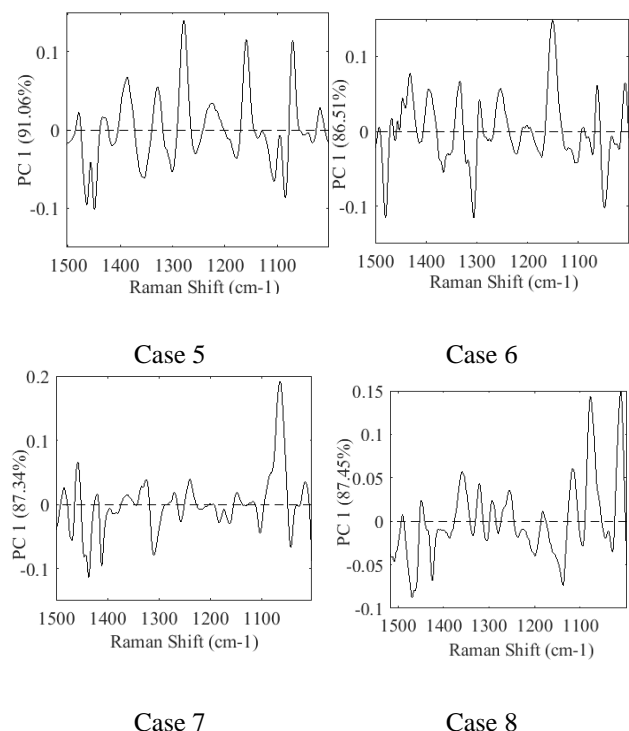
Figure 9. Loading plots of the first principal component for case 5-8.

increasing pressure in the region of 1225 to 1450 cm^{-1}. CO_2 peaks at 1264, 1284, 1369, 1387, 1408 cm-1 can be identified in this figure. A similar spectral behavior was observed for case 2 and 4 in the same region. Figure 3
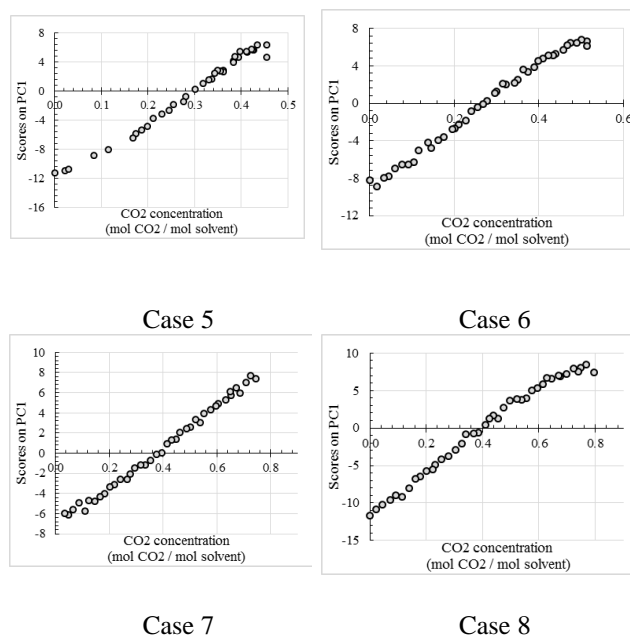
Figure 10. Development of linear regression model using PC1 score values and CO_2 content given by titration data.

gives raw Raman signals observed for CO_2 loaded 4 different amine solvents. Only two spectra from each solvent are shown. Figure 4 shows how the intensity of Raman bands varies with the CO_2 content for MEA samples (Case 5). Both Figure 3 and Figure 4 claim that spectral evolution in the region between 1000 to 1500 cm-1, for case 5-8 with respect to case 1-4 is complex due to curved baseline, baseline offsets and overlapping bands. The reason is that the chemical products when CO_2 is reacted with the solvent appear with overlapping peaks in this region. Therefore, when quantifying the total amount of CO_2 absorbed in solvent, all these peaks are needed.

All the Raman signals under each case were first smoothed using baseline-whittaker smoother, then SNV and finally mean centered. PCA was performed for processed data. First principal component was identified as the dimension explaining the largest variance of data in each case. Finally, score values of PC1, were compared with the mole fraction of CO_2 predicted by thermodynamic models for case 1-4 and CO_2 amount determined from titration for case 5-8. Loading plot, score plot and comparison of PC1 score value with CO_2 content under each case were used to explain characteristics in each system.

3.1 Case 1-4

With reference to Figure 5 loading plots of case 1, 3 and 4 almost give similar information about important variables (Raman shifts) while case 2 is different. This is caused by exposing the Raman sensor to both gas and liquid phases as a result of high stirrer speed and

development of vortex in case 2. There is also low viscosity in the medium at low pressures, which creates high turbulence. Score plots of PC1 vs. PC2 as given in Figure 7, show clear distinguish of recorded signals between the three pressure values of 20, 40 and 60 bar. PC2 direction explains only a small variation of data for case 1-3. Experiments for 60 bar, were conducted in replicates and their overlap in score values could be observed in case 1 and 2.

Figure 6 shows how closely PC1 score values are related to VLE data. Plots in this figure were derived by linear regression between PC1 score values as X variables and predicted CO_2 content from VLE data as y variables. From VLE data, CO_2 mole fractions at 20, 40 and 40 bar are 0.202, 0.411 and 0.601 respectively. These values are represented as 'Y measured' in Figure 6. PC1 score values at 3 pressure conditions follow the linear trend given by the mole fraction of CO_2 predicted by thermodynamic models at case 1 and 2. In the presence of PPC (case 3-4), even though pressure and temperature were maintained constant, a significant time was needed to achieve equilibrium condition of CO_2 absorption by the solvent especially at higher pressure region. For example, at 40 bar and 60 bar, PC1 score value of the initial spectra is less than the final recorded spectra at that condition. Therefore, although the reactor is maintained at the required pressure, the score plot gives the hint whether the equilibrium condition has been achieved or not. The significance of the above fact can be clearly understood when examining the score plot for case 4 (Figure 7). In this trial, we see that only 20 bar condition shows a compressed data swarm while at 40 bar, PC1 score values increases with time and this variation is more significant for 60 bar. This is further assured by Figure 6 (case 4) where the thermodynamic model satisfies the trend of final recorded data for 60 bar condition, but highly deviate from the initial recorded data at this condition. PC1 score values positively correlate with the amount of absorbed CO_2 by PO-CO_2 and PO-PPC-CO_2 systems.

3.2 Case 5-8

Absorption of CO_2 by amines (case 5-8), features several important variables in the region 1000-1500 cm-1 as given by loading plots in Figure 9 and this is the result of several parallel equilibrium reactions happening in each system. Each sample carries different information which mean different amount of CO_2 absorption and hence the concentration of chemical species produced during these reactions are different. Therefore, a data spread in score plot of PC1 vs PC2 can be observed in the score plots in each case as presented in Figure 8. However, similar to polymer-CO2 system, PC1 explains the largest variation of data structure and therefore PC1 score values were compared with total CO_2 absorbed by the system. Results are shown in

Figure 10. With the increasing amount of CO_2, there is a gradual increase of PC1 score value highlighting that PC1 score value is an indication of the level of CO_2 absorbed by the sample.

4 Conclusions

Monitoring CO_2 in liquid phase of PO-CO_2 system or PO-PPC-CO_2 system by analytical techniques is challenging as the CO_2 quickly desorbs if the pressure is lowered in sample taking. Therefore, online analysis such as spectroscopy is more favorable For CO_2-amine systems, an in situ characterization of CO_2 absorption gives credits to process monitoring and control ability. Based on this study, combination of Raman spectroscopy and PCA claims that PC1 score value explains variation of data structure corresponded to absorbed CO_2 amount. PCA plots give an indication of CO_2 composition, process dynamics and equilibrium conditions in these two chemical systems and hence can be used as an efficient tool to analyse collinear process data. Further investigation of PCA model development under different process parameters is recommended to validate the findings from this feasibility study. Experiments to develop advanced chemometrics tools such as partial least square regression can now be recommended for both polymer-CO_2 system and amine-CO_2 system.

References

C. Atzberger and P. H. C. Eilers. Evaluating the effectiveness of smoothing algorithms in the absence of ground reference measurements *International Journal of Remote Sensing,* 32(13): 3689–3709, 2010. doi:10.1080/01431161003762405

R. J. Barnes, M. S. Dhanoa, and S. J. Lister. Standard normal variate transformation and de-trending of near-infrared diffuse reflectance spectra. *Applied Spectroscopy,* 43(5): 772-777, 1989. doi:10.1366/0003702894202201

R. Bro and A. K. Smilde. Centering and scaling in component analysis. *Journal of Chemometrics,* 17(1): 16–33, 2013. doi:10.1002/cem.773

R. Bro and A. K. Smilde. Principal component analysis. *Anal. Methods,* 6: 2812-2831, 2014. doi:10.1039/C3AY41907J

L. B. Chen and X. G. Fang. Phase equilibria and CO2 distribution in the CO2-epoxide-toluene systems. *Natural Gas Chemical Industry,* 3: 255-266, 1994.

P. H. C. Eilers. A Perfect smoother. *Analytical Chemistry,* 75(14): 3631-3636, 2003. doi:10.1021/ac034173t

S. Hanf, R. Keiner, D. Yan, J. Popp, and T. Frosch. Fiber-enhanced Raman multigas spectroscopy: A versatile tool for environmental gas sensing and breath analysis. *Analytical Chemistry,* 86(11): 5278-5285, 2014. doi:10.1021/ac404162w

X. Jiang, F. Gou, and H. Jing. Alternating copolymerization of CO2 and propylene oxide catalyzed by C2v-porphyrin cobalt: Selectivity control and a kinetic study. *Journal of Catalysis,* 313: 159-167, 2014. doi:10.1016/j.jcat.2014.03.008

D. Y. C. Leung, G. Caramanna, and M. M. Maroto-Valer. An overview of current status of carbon dioxide capture

and storage technologies. *Renewable and Sustainable Energy Reviews,* 39: 426-443, 2014. doi:10.1016/j.rser.2014.07.093

N. McCann, D. Phan, X. Wang, W. Conway, R. Burns, M. Attalla, G. Puxty, and M. Maeder. Kinetics and mechanism of carbamate formation from CO2(aq), carbonate species, and monoethanolamine in aqueous solution. *The Journal of Physical Chemistry A,* 113(17): 5022–5029, 2009. doi:10.1021/jp810564z

S. F. Shakhova, O. L. Rutenberg, and M. N. Targanskaya. Liquid-gas equilibrium in the epoxypropane–carbon dioxide system. *Russ. J. Phys. Chem,* 47(6), 1973.

M. Vogt, C. Pasel, and D. Bathen. Characterisation of CO2 absorption in various solvents for PCC applications by Raman spectroscopy. *Energy Procedia,* 4: 1520-1525, 2011. doi:10.1016/j.egypro.2011.02.020

P. D. Wentzell and S. Hou. Exploratory data analysis with noisy measurements. *Journal of Chemometrics,* 26(6): 264–281, 2012. doi:10.1002/cem.2428

H. Wold. Estimation of principal components and related models by iterative least squares. *Journal of Multivariate Analysis* 1: 391-420, 1966.

S. Wold, K. H. Esbensen, and P. Geladi. Principal component analysis. *Chemometrics and Intelligent Laboratory Systems,* 2(1): 37-52, 1987. doi:10.1016/0169-7439(87)80084-9

M. K. Wong, M. A. Bustam, and A. M. Shariff. Chemical speciation of CO2 absorption in aqueous monoethanolamine investigated by in situ Raman spectroscopy. *International Journal of Greenhouse Gas Control,* 39: 139–147, 2015. doi:10.1016/j.ijggc.2015.05.016

Paper F

System Development for On-line Monitoring using Raman Spectroscopy for CO_2 Absorption by MEA

System Development for On-line Monitoring using Raman Spectroscopy for CO₂ Absorption by MEA

M. H. Wathsala N. Jinadasa, K. Amila Chandra, Maths Halstensen

Faculty of Technology, Natural Sciences and Maritime Sciences – University of South-eastern Norway, Post box 235, N-3603 Kongsberg, Norway, (Eigenvector Research)@usn.no

Abstract

Among various kinds of technologies available, carbon dioxide (CO_2) capture by monoethanolamine (MEA) is considered to be the most technically and scientifically matured technology which can be tested in industrial scale. When CO_2 is absorbed by an MEA, a chemical reaction takes place which results to form different carbon and amine species in the system. In this work, Raman spectroscopy has been used to measure those concentrations in-situ. Since the instrument does not provide direct measurements, multivariate analysis has been used to develop models and predictions are made using these models for future measurements. This study presents the methodology of acquiring measurements by the Raman spectroscopy for MEA-CO_2-H_2O system, transferring the measurement data into Matlab/Labview, converting data into concentration values and presenting the results in a graphical user interface. This software based platform makes the Raman spectroscopy to be accessed as a real-time instrument in CO_2 capture plants.

Keywords: CO_2 absorption by MEA, real-time monitoring, Raman spectroscopy, chemometrics, Labview

1 Introduction

68% of global anthropogenic greenhouse gas emissions comes from energy production and 90% of these greenhouse gases are carbon dioxide (IEA, 2017). Therefore capturing CO_2 emissions from energy production is a mandatory task under the climate change mitigation actions. As stated in (IEA, 2017) from 1870 to 2015, CO_2 emission by fossil fuels dramatically increased from near zero to over 33 Gt CO_2 which resulted fossil fuel power sector to be the largest source of greenhouse gas emissions. Greenhouse gases are responsible for increasing the world atmospheric temperature causing threatening impacts of climate change. While switching towards renewable and non-fossil fuel sources, the immediate action to reduce further CO_2 emission to the atmosphere is CO_2 capturing and storage from current emission sources.

After several studies on CO_2 capturing, the so-called 'monoethanolamine technology' or in other words, absorbing CO_2 chemically to an MEA solution is considered to be the most promising technology which can be tested in industrial level. Some examples for MEA based commercial plants are Boundary Dam CO_2 capture pant and Cansolv CO_2 capture system in Canada. When a CO_2 molecule bounds to an MEA molecule, they are converted chemically into different reaction intermediates. Among them carbonate (CO_3^{2-}), bicarbonate (HCO_3^-), carbamate ($MEACOO^-$) and protonated MEA ($MEAH^+$) are prime important. There can also be free MEA and dissolved CO_2 (unreacted) in the system. In an overall perspective, if one wants to get an overview about the chemical concentration of an MEA-CO_2-H_2O system, concentrations of above-mentioned chemical intermediates should be presented. Knowing the concentrations of intermediates gives the benefit to understand reaction path, impact of process parameters to the CO_2 absorption, inputs to thermodynamic modelling and thus help to design and optimize the process.

Raman spectroscopy is a process analytical instrument. Fundamentally, it gives information on molecular vibrations and crystal structures in a chemical system. This information can be mapped with other properties of the system such as concentration of a chemical specie. Multivariate regression models can be developed to estimate those properties using the instrument. In the CO_2 capture field, the use of such types of instruments are gradually becoming popular due to their fast response, ability to locate in-situ and facility to integrate with process automatic control systems. The Applied Chemometrics and Research Group (ACRG) at University of South-Eastern Norway (USN) has developed a method using Raman spectroscopy to determine concentration profiles in an MEA-CO_2-H_2O system based on multivariate analysis (Jinadasa, Jens, Øi, & Halstensen, 2017). The developed method can be used for laboratory experiments, R&D tasks, pilot plant operations and commercial applications of the CO_2 absorption process. It features over the traditional offline analyses due to the fast response. We use two software packages to operate the Raman instrument. The iC Raman 4.1 software which comes together with Raman analyzer is used to configure instrument and acquire measurements while Matlab is used to convert these measurements to concentration values. So far, these steps are carried out manually. Although it takes a couple of minutes to take a measurement from the system, file transferring

https://doi.org/10.3384/ecp18153328

328

Proceedings of The 59th Conference on Simulation and Modelling (SIMS 59), 26-28 September 2018, Oslo Metropolitan University, Norway

between the two software packages and giving commands for data processing and calculations takes time. Therefore the current approach is time consuming.

This paper describes a system development that can join the two software packages into one platform and enables the Raman spectroscopy as a real time analyzer for measuring concentrations of chemical species of the MEA-CO_2-H_2O system. It is also compatible to use by plant operators who have no/less knowledge on working with the data processing and calculations by Matlab.

2 Problem Identification

Several offline analytical instruments and chemical methods are available such as titration, nuclear magnetic resonance (NMR) spectroscopy and chromatography to determine chemical concentration in MEA-CO_2-H_2O system. All these methods are time consuming. Titration by $BaCl_2$ is common and a well-established method but it needs massive chemical preparation and the analysis takes around 2 hours per sample. NMR spectroscopy and chromatography are mostly limited to laboratory because they do not fit well in plant operations. Spectroscopic methods need prior calibration according to application and are expensive. Some of the spectroscopic instruments cannot be located in an industrial environment.

A fast, online method to monitor CO_2 absorption is important in process control and optimization. Maintaining the chemical concentration of the process streams at required levels is important for getting the target output from the plant. After several feasibility studies, Raman spectroscopy was selected as one of preferable solutions to monitor concentrations in this process. Several studies have been performed using Raman spectroscopy to investigate the concentration profiles in CO_2 capture process by amines. The method developed by USN using Raman spectroscopy was tested and validated at a mini-pilot CO_2 capture plant in Porsgrunn (Jinadasa et al., 2017). In this method, multivariate regression models have been calibrated and validated using test set validation. The raw Raman signals from the instrument was pretreated using techniques available in chemometrics and the regression models are based on partial least squares regression (PLSR) which is a powerful multivariate modelling approach.

However, there is a weak point in this approach as we move between two software platforms to transfer data and calculate the concentration value for each measurement. This operation is carried out manually and prevent the analyzer from being an in-situ monitoring application eventhough the Raman analyzer can take measurements continuously within a few seconds.

2.1 Existing method vs proposed method

When the Raman instrument is used to measure the chemical information in MEA-CO_2-H_2O system, first the Raman probe is fixed into the system. A new file is open in iC Raman 4.1 software and suitable number of scans and laser exposure time is selected. (Kaiser, 2018) A file saving path and a file type (either .spc or .csv) for auto export is configured. When the command to measure the chemical system is given through the software, laser light is sent through the fibre optic cable to the Raman probe to go through the sample. After a scan is finished, a plot of Raman intensity vs Raman wavenumber is shown in the computer connected to the Raman instrument. The software simultaneously saves the data to a data file. To convert such a Raman measurement into a concentration value, the following steps are carried out:

1). Taking measurements from the process by running the iC Raman software – the measurements can be batch or continuous-wise

2). Saving the data in iC Raman software

3). Importing the data file into Matlab

4). Start PLS toolbox in Matlab (Eigenvector Research, 2018a)

5). Preprocessing the Raman data file using preprocessing methods in PLS toolbox

5). Input the data file to a PLS model which has been previously calibrated and validated

6). Run the PLS model to get the predicted concentration value

7). Showing the resulting concentration value

The disadvantage with this approach is that this system does not give the concentration value at the same time as the measurement is taken. It takes time to import the data from iC Raman software to Matlab and follow the preprocessing step. There should be always an operator to carry out the steps from 3 to 6. It requires knowledge and experience in operation of the mentioned software.

The proposed system aims at removing the barrier of manual file transferring and data processing steps between the two software to save time. In the proposed system there is no need of importing data from iC Raman software to Matlab interface. The user should first open the iC Raman software and Labview interface. After setting the data saving locations, number of scans per measurement and laser exposure time, both software can be started. The readings from the Raman instrument automatically transfers to the labview from iC Raman software. In the Matlab/Labview interface, this data is preprocessed and concentrations are predicted based on the PLS model automatically. Anyone who is not experienced with the software or analysis method can operate the instrument and read the required concentration profiles with time both as numerically and graphically. The predicted concentration data are also saved in an excel file. Figure 1 shows how the software

https://doi.org/10.3384/ecp18153328

329

Proceedings of The 59th Conference on Simulation and Modelling (SIMS 59), 26-28 September 2018, Oslo Metropolitan University, Norway

and hardware link together to get a concentration value using the Raman measurement and the proposed system.
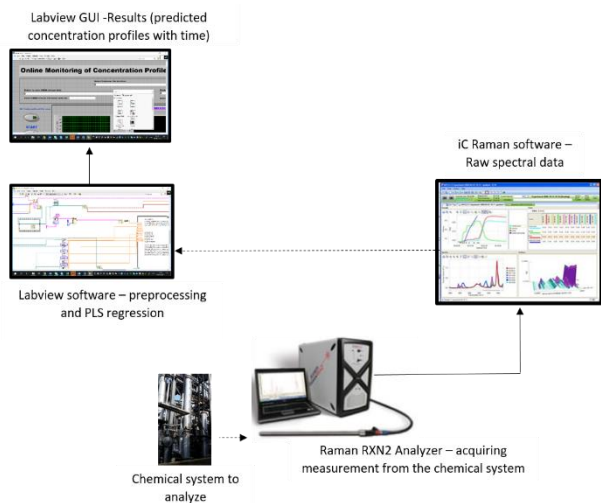
Figure 1. Schematic of Raman spectroscopy measurement showing hardware and software links

3   System development

3.1   Instrumentation

The Raman spectrometer available at USN is the Kaiser RXN2 Analyzer with 785 nm laser wavelength, 400 mW maximum laser power and 100-3425 cm^{-1} spectral range. An immersion optic probe is connected to the RXN2 Analyzer via a fibre optic cable. When the analyzer is switched on to take a measurement, the laser light reaches the molecules in the sample, scattered and the Raman scattered light is filtered by the analyzer. The output display is a plot of Raman intensity (y-axis) which is the Raman scattered radiation and Raman wavenumber (x-axis) which is the frequency difference from the incident radiation (Kaiser, 2018). Peaks and their intensity which appear in this plot carry information about the chemicals present in the system and their composition respectively.

3.2   Process description

The process of CO_2 capture by amine using an absorption column is shown in Figure 2. Flue gas which contains CO_2 is fed upward to the absorber. The CO_2 free flue gas goes out from the top plate of the absorber. The absorbing agent, which is an amine solvent is fed to the top plate of the absorber. This stream is called the 'lean amine' stream. While it flows through the absorber it absorbs CO_2 in the flue gas. The CO_2 rich amine flows out from the absorber bottom plate and this stream is called the 'rich amine' stream. In industry, the difference between CO_2 concentrations in the lean and rich streams is used as an important indicator to know

how much CO_2 is absorbed by the amine. The concentration of other species are also important to yield the maximum process efficiency. The Raman RXN2 analyzer comes with four channels with facility to connect four Raman immersion probes to one analyzer thus providing to measure four streams simultaneously. The aim of this study was to optimize the absorption process in a CO_2 capture process and hence configuration was set for two Raman probes to take measurements from both lean and rich streams.
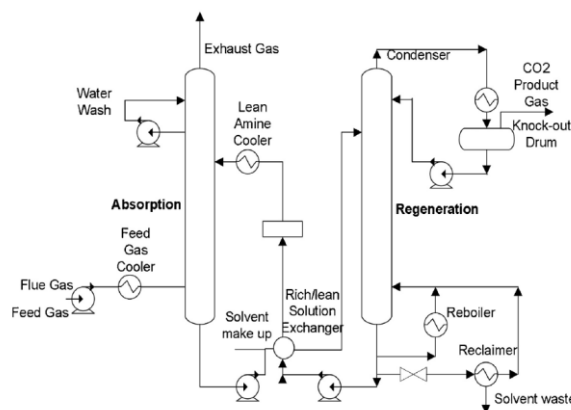
Figure 2. Process flow diagram of CO_2 capture absorption by amine (T. Li & Keener, 2016)

3.3   Data treatment

The outcome of a measurement series using RXN2 Analyzer is a data matrix of n x p where n is number of objects (eg: it can be different samples or signals with time) and p is 3326 Raman wavenumbers. Since this data matrix contains noise, preprocessing is needed before a model can be calibrated based on the PLSR algorithm. By performing such a data treatment, the noise generated due to interference of other chemical components, laser input variations or instrument noise can be minimized and the model predictability can be improved. There are different preprocessing techniques available in multivariate data analysis. The choice of which pre-processing method depends on many factors such as the instrument type, sample, impurities in the sample, environmental factors and properties of interest to measure. Based on our previous experience in developing PLS models for Raman measurements in MEA-CO_2-H_2O systems, three combinations of multivariate data processing methods showed lowest prediction error. They were scripted as Matlab codes which were the baseline-whittaker filter, standard normal variate (SNV) and mean centering.

3.4 Estimation of concentrations using the Partial Least Square Regression (PLSR) algorithm

There are different algorithms to develop a PLS model (Andersson, 2009) . PLS is available in many commercial software packages, such as The Unscrambler, PLS Toolbox, ProSensus and SIMCA-P. To be independent from using commercial software packages except Matlab/Labview, Matlab codes were used in this study. PLS calibration and validation using the so-called 'test set' method and data pretreatment were coded in Matlab. Procedures mentioned in pls.m, pretreat.m available at libPLS package was used for PLS regression and mean centering (H.-D. Li, Xu, & Liang, 2018). snv.m file and wlsbaseline.m file available at PLS toolbox were referred for SNV and whittaker filter coding (Eigenvector Research, 2018b). The values for regression coefficients for each specie was stored in an m-file called regcon.m file and after data pretreatment, prediction was performed using the equation of regression coefficient values.

Figure 3 shows the flow path when the proposed system is in operation. After launching the iC Raman software the user selects a location to save Raman files in csv format for rich and lean stream. Each measurement is saved according to the format of "name_date_time_sample name" and hence each file is uniquely distinguished. Then the user should move to the Labview GUI and enter the input variables. These variables are the locations of Labview file, location where Raman measurements from lean and rich stream are saved by iC Raman software and location where the predicted concentrations from matlab/labview system for lean and rich stream should be saved as excel files. After entering these inputs, both iC Raman software and labview are started. As shown in Figure 3, after setting the Raman data saving folder path (for lean and rich stream) and locating a location to save predicted concentrations (excel files), the Labview file start searching for a new Raman measurement file. When such a file is found, it is fed as an input to the PLS model. This is the only input variable to the PLS model. Output variable from the PLS model is concentration of specie. For each specie, there is a specific PLS model. Each PLS model gives the output value at the same time.

4 Results and Discussion

4.1 LabVIEW-based software platform

According to Figure 4, the GUI of the Labview based system shows the total CO_2 concentration and five concentrations of chemical species present in both lean and rich amine streams in a CO_2 capture process. The first graph in Figure 4 shows CO_2 concentration in units

of mol per mol MEA. The second graph shows concentration of free (unreacted MEA) and protonated MEA in units of mol per kg of H_2O. The third graph shows concentration of carbonate, bicarbonate and carbamate in units of mols per kg H_2O.
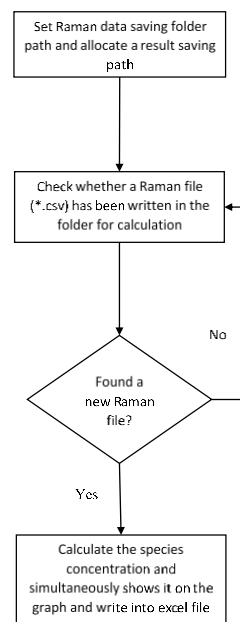
Figure 3. System flow sheet

To show how the online predicted concentration of CO_2 loading matches with offline titration Table 1 provides results of a CO_2 loaded process stream with decreasing CO_2 concentration and prediction error. During this experiment, the Raman spectroscopy was connected to the process stream

Table 1. Validation of the online monitoring system with offline measurements

Time	CO2 loading (mol CO2 / mols MEA)	
	Raman spectroscopy-predictions from online system ± prediction error	Offline titration results
15:15:56	0.491672 ± 0.0150	0.484216
15:35:41	0.481887 ± 0.0150	0.463091
15:55:26	0.489647 ± 0.0148	0.462196
16:16:21	0.44994 ± 0.0145	0.42835
16.35.08	0.350732 ± 0.0146	0.331385
16.56.04	0.262569 ± 0.0144	0.28351
17.15.53	0.196636 ± 0.0150	0.191744

The concentrations recorded by the Raman system closely match with the offline measurements for CO2 loading. The average prediction error for Raman measurement is 0.015 mol CO_2 / mol MEA.

https://doi.org/10.3384/ecp18153328

331

Proceedings of The 59th Conference on Simulation and Modelling (SIMS 59), 26-28 September 2018, Oslo Metropolitan University, Norway
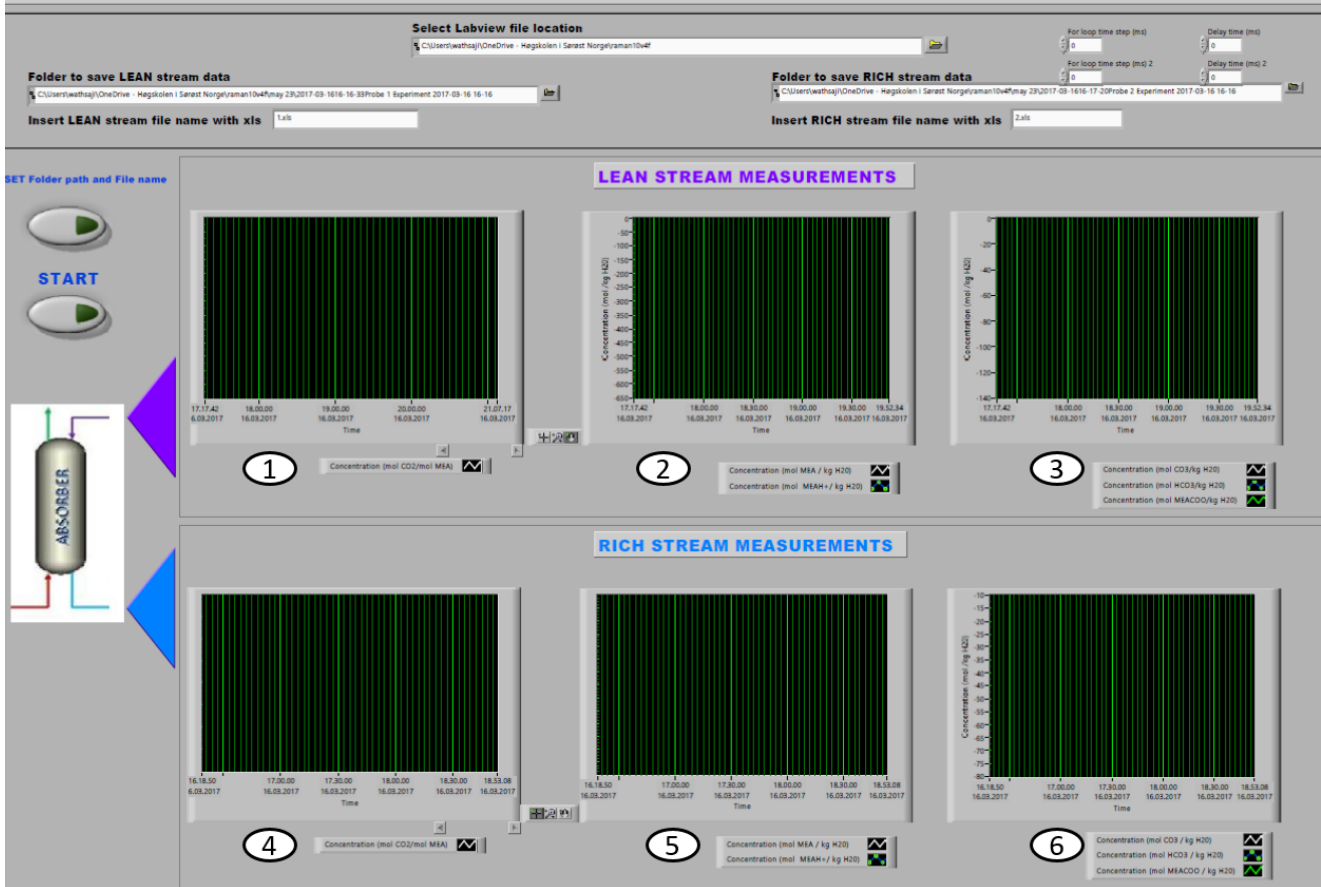
Figure 4. Graphical user interface for concentration profiles; plot 1, plot 2 and plot 3 are CO_2 loading, MEA/MEAH+ concentrations and CO_3^{2-}/HCO_3^-/MEACOO$^-$ for lean stream ; plot 4, plot 5 and plot 6 are CO_2 loading, MEA/MEAH+ concentrations and CO_3^{2-}/HCO_3^-/MEACOO$^-$ for rich stream
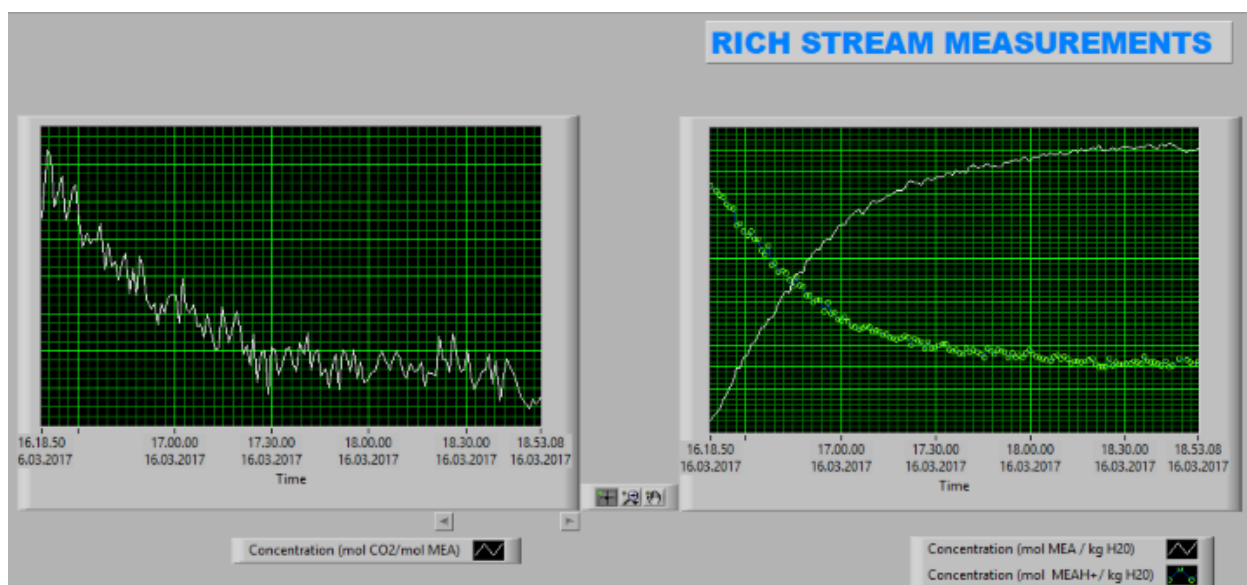
Figure 5. Example for recording real-time measurement for CO_2 loading and MEA/MEAH+ concentration in rich stream for two and half hour continuous operation of CO_2 desorption process

5 Conclusion and future work

Determining CO_2 absorption in liquid phase of MEA-CO_2-H_2O system by an analytical technique is useful in many aspects. It saves time and gives access to online monitoring of the system. The accuracy of laboratory methods is based on the skill of the analyst, demand time, labour and resource. Offline laboratory methods cannot be used for process automation. Eventhough, these traditional methods are still used to control the process parameters in CO_2 plants due to the non-availability of in-situ analysis methods.

In this paper, we present the development of Labview/Matlab based software platform which is connected to iC Raman software in Raman RXN2 Analyzer. The platform provides concentration profiles of different chemical species present in an MEA-CO_2-H_2O system. These concentration values are calculated indirectly from measurements from Raman analyzer. The calculation is based on partial least square regression method. PLS and data pretreatment algorithms were written as matlab scripts.

If a calibration and validation data set is available, this system can be easily modified to another amine based CO_2 capture system without extensive effort. For instance, there are other amines which have the ability to absorb CO_2 and Raman instrument can be used to determine the total CO_2 absorbed and the concentration of other chemical species. If the user needs to use this GUI for such amines, he can input new calibration and validation data set into PLS script and change the preprocessing script in Matlab accordingly. The developed system can also be used to monitor how the reaction between an amine and CO_2 evolves with time in a batch reaction.

It is also recommended to take the use of the data to perform other chemometric analysis such as principle component analysis, outlier detection and multivariate curve resolution to better understand the chemical system. The plots related to these analysis can be implemented in the developed GUI similar to the concentration plots.

References

Andersson, M. (2009). A comparison of nine PLS1 algorithms. *Journal of Chemometrics, 23*(10), 518-529. doi:https://doi.org/10.1002/cem.1248

Eigenvector Research, I. (29 March 2013). Advanced preprocessing: Noise, offset, and baseline filtering.

Eigenvector Research, I. (2018a). PLS toolbox. Retrieved from http://www.eigenvector.com/software/pls_toolbox.htm

Eigenvector Research, I. (2018b). PLS_Toolbox 8.2.1 software Manson, WA USA 98831. Retrieved from http://www.eigenvector.com

IEA. (2017). CO2 emissions from fuel combustion: Overview Retrieved from http://www.iea.org/publications/freepublications/publi cation/CO2EmissionsFromFuelCombustion2017Over view.pdf

Jinadasa, M. H. W. N., Jens, K.-J., Øi, L. E., & Halstensen, M. (2017). Raman Spectroscopy as an Online Monitoring Tool for CO2 Capture Process: Demonstration Using a Laboratory Rig. *Energy Procedia, 114*, 1179-1194. doi:https://doi.org/10.1016/j.egypro.2017.03.1282

Kaiser. (2018). iC Raman™ 4.1 Software. Retrieved from http://www.kosi.com/na_en/products/raman-spectroscopy/raman-software/ic-raman-4.1.php

Li, H.-D., Xu, Q.-S., & Liang, Y.-Z. (2018). libPLS: An integrated library for partial least squares regression and linear discriminant analysis. *Chemometrics and Intelligent Laboratory Systems, 176*, 34-43. doi:https://doi.org/10.1016/j.chemolab.2018.03.003

Li, T., & Keener, T. (2016). *A review: Desorption of CO2 from rich solutions in chemical absorption processes* (Vol. 51).

Paper G

Equilibrium Measurements of the NH$_3$-CO$_2$-H$_2$O System: Speciation Based on Raman Spectroscopy and Multivariate Modeling

Research Article

Equilibrium Measurements of the NH_3-CO_2-H_2O System: Speciation Based on Raman Spectroscopy and Multivariate Modeling

Maths Halstensen,[1] Henrik Jilvero,[2] Wathsala N. Jinadasa,[1] and Klaus-J. Jens[1]

[1]*Applied Chemometrics Research Group (ACRG), University College of Southeast Norway, Porsgrunn, Norway*
[2]*Department of Energy and Environment, Chalmers University of Technology, 412 96 Göteborg, Sweden*

Correspondence should be addressed to Maths Halstensen; maths.halstensen@usn.no

Liquid speciation is important for reliable process design and optimization of gas-liquid absorption process. Liquid-phase speciation methods are currently available, although they involve tedious and time-consuming laboratory work. Raman spectroscopy is well suited for in situ monitoring of aqueous chemical reactions. Here, we report on the development of a method for speciation of the CO_2-NH_3-H_2O equilibrium using Raman spectroscopy and PLS-R modeling. The quantification methodology presented here offers a novel approach to provide rapid and reliable predictions of the carbon distribution of the CO_2-NH_3-H_2O system, which may be used for process control and optimization. Validation of the reported speciation method which is based on independent, known, NH_3-CO_2-H_2O solutions shows estimated prediction uncertainties for carbonate, bicarbonate, and carbamate of 6.45 mmol/kg H_2O, 34.39 mmol/kg H_2O, and 100.9 mmol/kg H_2O, respectively.

1. Introduction

The rapid increase in the level of CO_2 in the earth's atmosphere is recognized as the single most important environmental challenge facing our global society [1]. All climate change mitigation plans rely on carbon dioxide capture and storage as a near-term "immediate response" technology [2]. Despite the various global CO_2 capture research and development initiatives, the well-established gas-liquid absorption process is expected to be the technology of choice for early, large-scale deployment [3], with the chilled ammonia process (CAP) [4] being one of the currently demonstrated technologies.

Out of several postcombustion techniques available to capture CO_2 from coal power plants, amine solutions have been commonly tested and used. The disadvantages of amine technology are that it requires large amount of energy in the stripping process and has thermal and oxidative degradation and corrosion problems [5]. Ammonia technology is an alternative to overcome these drawbacks. This process requires

less energy for stripping and the heat of reaction is much lower than amine process. There is less maintenance cost than amine process as there are no degradation or corrosion issues. CO_2 reacted ammonia can be used to produce fertilizer. The process of CO_2 capture by ammonia can be twofold depending on the temperature of CO_2 absorption. If the absorption is performed under 2–10°C, which is called the chilled ammonia process, there can be precipitations of ammonium carbonate compounds while if the absorption is increased to 25–40°C, the precipitation problem is eliminated [6].

If chemical speciation data could be generated concomitant with the determination of the physical and chemical solvent properties, the development and accuracy of the thermodynamic process model would be greatly facilitated. Improvement and optimization of commercial processes that target needed cost reductions require access to rigorous thermodynamic models that build on liquid-phase speciation data. Such data are currently acquired through tedious and time-consuming laboratory work. The standard

wet chemistry titration to determine liquid phase is the most popular method. This method takes time and errors can be propagated during sampling, chemical preparation, weighing, and titration [7]. Various analytical techniques can be used to determine the species present in CO_2 reacted ammonia solution. ^{13}C nuclear magnetic resonance (NMR) spectroscopy has been used [8] to determine ionic species in a range of ammonia concentration from 0.69 to 8.95 mol/L and CO_2 loading (total CO_2 moles/initial solvent moles) concentrations from 0.33 to 0.72. Fourier transform infrared spectroscopy (FT-IR) and X-ray diffraction (XRD) were used to qualitatively distinguish ammonium bicarbonate from ammonium carbonate and ammonium carbamate, while CHN elemental analysis and near-infrared (NIR) spectroscopy were used to quantify ammonium bicarbonate based on multivariate regression methods as reported in [9]. Wen and Brooker [10], Zhao et al. [11], and Kim et al. [12] suggested methods to determine carbon species in CO_2-NH_3-H_2O system based on factor analysis where they assumed that the corresponding Raman intensities were directly related to the concentrations of species.

This work reports on a method that combines Raman spectroscopy and partial least-squares regression (PLS-R) for in situ solvent speciation in the chilled ammonia process and which does not rely on calibration by an independent analysis method [13], for example, NMR. It describes the development, validation, and application of the method for determination of the liquid phase composition of the NH_3-CO_2-H_2O system, while comparisons of the speciation results obtained here and those from established CO_2-NH_3-H_2O thermodynamic equilibrium models are described in a separate publication [14].

In the thermodynamic modeling of the CO_2-NH_3-H_2O system, a vapor-liquid equilibrium (VLE) is assumed to exist for water, ammonia, and CO_2. The liquid phase can be described by reactions (1)–(5). The chemical composition of aqueous ammonia solution is described by

$$NH_3 + H_2O \rightleftharpoons NH_4{}^+ + OH^- \tag{1}$$
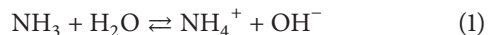
The reactions of dissolved CO_2 in aqueous ammonia solution are given by reactions (2)–(5). Within the present system, CO_2 is bound as the anion species of carbonate [$CO_3{}^{2-}$], bicarbonate [$HCO_3{}^-$], and carbamate [NH_2COO^-].

$$CO_{2(aq)} + H_2O \rightleftharpoons H^+ + HCO_3{}^- \tag{2}$$

$$HCO_3{}^- \rightleftharpoons H^+ + CO_3{}^{2-} \tag{3}$$

$$CO_{2(aq)} + 2NH_3 \rightleftharpoons NH_4{}^+ + NH_2COO^- \tag{4}$$

$$NH_4{}^+ + NH_2COO^- + H_2O$$
$$\rightleftharpoons NH_4{}^+ + HCO_3{}^- + NH_3 \tag{5}$$
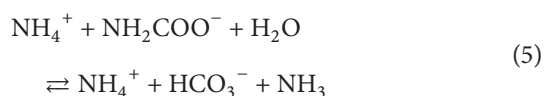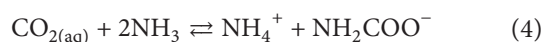
During CO_2 absorption by the aqueous NH_3 solution, reactions (1)–(5) will equilibrate according to the CO_2 concentration, pressure, and temperature; the carbon distribution in the solvent is given by the concentrations of the anions in reactions (2)–(5). In addition to these reactions and depending on the reaction conditions, various other compounds may precipitate, such as ammonium bicarbonate (NH_4HCO_3), ammonium carbonate [$(NH_4)_2CO_3$], ammonium carbamate ($NH_4NH_2CO_2$), and ammonium sesquicarbonate [$(NH4)_2CO_3 \cdot NH_4HCO_3$]. Even though the precipitation is promoted by low temperature, the high water content in the solvent reduces much of this possibility.

Spectroscopy, Raman spectroscopy in particular, is well known for in situ monitoring of the chemical reactions of aqueous solutions [16, 17]. The water molecule shows only weak Raman scattering; hence Raman spectroscopy has potential advantage over IR spectroscopy [18] for aqueous phase analysis such as required for the aqueous chilled ammonia CO_2 capture solvent. The Raman band envelopes of aqueous solutions of ammonium carbonate, ammonium bicarbonate, and ammonium carbamate have been identified and analyzed [10] and form the basis for the previously reported speciation studies of the CO_2-NH_3-H_2O system [11, 12]. However, evaluation of the Raman spectra in these previous studies was based on univariate, single-band analysis. The use of superior multivariate partial least-squares regression (PLS-R) [19] methods, which exploit the multivariate information in the spectra, has, to the best of our knowledge, not been reported previously. Furthermore, the method developed in the present study is not limited to laboratory applications but can also be used to monitor continuously a reactive process, which presents an opportunity for its implementation as an on-line process analytical technology (PAT) [20] in carbon capture plants for optimization and efficient operation.

2. Materials and Methods

The development of the Raman spectroscopy-based method for speciation of the CO_2-NH_3-H_2O system is based on PLS-R analysis of a series of samples of known composition. The procedure involves

(1) preparation of aqueous solutions that contain known concentrations of [$CO_3{}^{2-}$], [$HCO_3{}^-$], and [NH_2COO^-]: one set of solutions was prepared for PLS-R model calibration and a second independent set of solutions was used for validation;

(2) determination of the Raman spectrum of each sample solution;

(3) preprocessing of the Raman spectra by cropping each spectrum to cover the range 450–2300 cm^{-1}, with subsequent elimination of the inconsistently varying baseline from spectrum-to-spectrum and centering of each wavelength by subtraction of the mean;

(4) calibration of the PLS-R models for the anionic species [$CO_3{}^{2-}$], [$HCO_3{}^-$], and [NH_2COO^-] using the Raman spectra of the solutions prepared for model calibration in the previous step (Step (3));

(5) validation of the PLS-R models using the Raman spectra of the solutions prepared for model validation in Step (3).
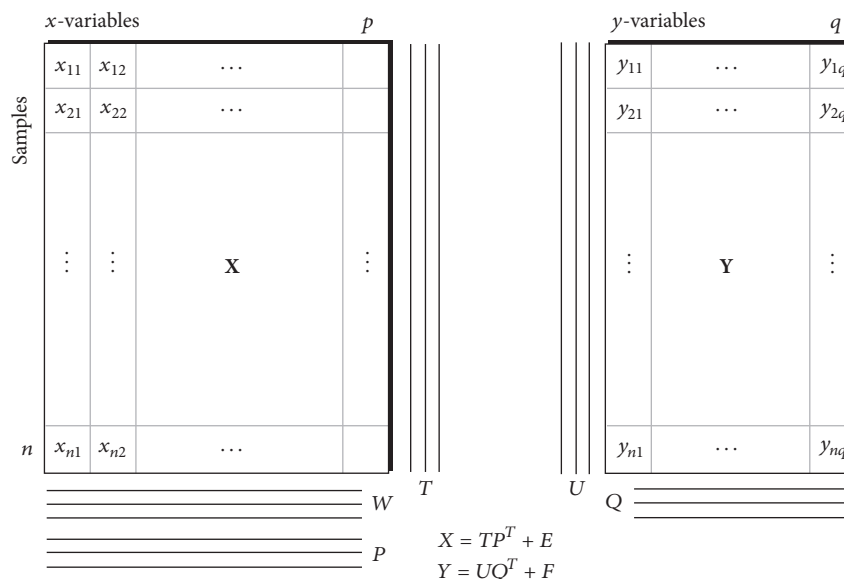
FIGURE 1: X-Y data and models in the PLS-R modeling approach [15]. The parameters that emanate from PLS-R calibration include P (X loadings); W (X loading weights); T (X scores); U (Y scores); and Q (Y loadings). E and F are the residuals for X and Y, respectively.

The procedures required to achieve reliable speciation using the proposed method are described in the following sections.

2.1. Raman Spectroscopy.

The Raman phenomenon is based on quantized vibrational changes that are associated with electromagnetic radiation absorption. An important advantage of Raman spectroscopy over infrared spectroscopy is that the water molecule shows very weak Raman scattering, whereas, in infrared spectroscopy, the water molecule shows strong absorption across an important part of the infrared spectrum.

The Raman instrument used in the investigations reported in the present paper was the RXN2 portable multichannel Raman spectrometer (Kaiser Optical Systems Inc.). Four fiber optic probes can be connected and utilized through an automatic sequential scanning system that is integrated into the instrument. The specifications of the RXN2 Raman spectrometer are listed in Table 1.

Raman spectra of aqueous solutions can be acquired using either a noncontact probe optic, whereby the sample solutions are not in direct contact with the probe optic, or an immersion probe optic, whereby the sample solution is in direct contact with the probe optic. The Raman spectra were acquired using a short-focus (200 μm), sapphire window, Hastelloy immersion probe (Kaiser Optical Systems Inc.).

2.2. Partial Least-Squares Regression Modeling.

PLS-R is an empirical data-driven modeling approach that requires both representative input data (X) and output data (Y). A detailed description of PLS-R and validation can be found in literature [15, 19, 21]. In this study PLS-R is used in combination with Raman spectroscopy. The X matrix contains Raman spectra that represent different concentrations and the Y vector contains known reference concentrations from the sample

TABLE 1: Specifications of the RXN2 Raman spectrometer.

Name	Description
Excitation laser wavelength (nm)	785
Spectral range (cm^{-1})	100–3425
Spectral resolution (cm^{-1})	4
Operating temperature range (°C)	15–30
Number of channels	4
Laser type	Invictus™ NIR diode laser
Spectrograph	f/1.8 Holographic imaging spectrograph
Grating	Holographic transmission grating
Detector	TE cooled, 1024 CCD Detector
Multichannel scanning	4-Channel sequential operation
Cal-Check™	Automatic analyzer monitor
Auto-Cal™	Automated calibration of axis and laser wavelength
Immersion probe optic	200 μm (short focus)/Hastelloy/sapphire window

preparation step. All models reported in this article are validated based on independent test data (test set validation) [21].

The concentration range spanned by X and Y should reflect the concentrations to be predicted. The overall aim of PLS-R is to model simultaneously the multivariate input data (X) and the output response (Y) (Figure 1). PLS-R avoids many of the problems associated with the traditional multiple

linear regression (MLR) and principal component regression (PCR) [15] methods. PLS-R is advantageous in cases where the X matrix contains collinear data. Colinearity is in most cases unavoidable in spectroscopy, as there are significantly more variables (waveshifts) than samples (observations). When the number of variables is significantly higher than the number of samples, colinearity is guaranteed. When collinear data are used, MLR fails or becomes unstable. Although PCR can deal with colinearity, it has other issues related to the way in which the X-matrix is decomposed without utilizing information on Y, often leading to models with a higher number of components than the PLS-R case. Another advantage of applying PLS-R is that the feature parameters that emerge from the model calibration stage, that is, X scores (T), X loadings (P), X loading weights (W), and Y scores (U), can be plotted and interpreted to support the calibration procedure (see Figure 1).

An important aspect of PLS-R modeling is model validation [21], which is important to determine the complexity of the model. The correct complexity of a PLS-R model is defined as the optimal number of PLS components, which can only be determined by proper validation of the model using an independent dataset that is acquired and used exclusively for this purpose. To determine the optimal number of components in a PLS-R model, a criterion based on the so-called root mean square error of prediction (RMSEP) [15] is calculated and minimized. RMSEP is based on predictions of Y, for example, concentrations from the validation dataset. Using several models with different numbers of components, the predictions are compared to the reference values of Y in the RMSEP calculation. The model that has the optimal number of components is defined as the one that ends up with the lowest RMSEP value. The RMSEP values are derived using (6):

$$ \text{RMSEP} = \sqrt{\frac{\sum_{i=1}^{I} \left(\mathbf{y}_{\text{predicted}} - \mathbf{y}_{\text{reference}} \right)^2}{I}}, \qquad (6) $$

where $\mathbf{y}_{\text{predicted}}$ is the predicted value from the PLS-R model, which is compared to the reference value $\mathbf{y}_{\text{reference}}$. The sum of the squared prediction errors is divided by I, which is the number of samples in the validation dataset.

2.3. Preparation of the Calibration and Validation Samples.

The ranges of concentrations, expressed in moles of each anion per kilogram of H_2O (molality), of the calibration and validation set were predetermined to reflect the concentrations expected in samples that would in the future be subjected to the developed speciation method. The calibration and validation sets covered the same concentration range. Analytical grade chemicals and Milli-Q water (18.2 MΩ·cm) were used to prepare the samples. The ammonia solution (25 wt%) was supplied by Merck KGaA (Darmstadt, Germany). Sodium hydrogen bicarbonate (99.7%), sodium carbonate (99.9%), and ammonium carbamate (98%) were supplied by Sigma-Aldrich (Steinheim, Germany). All chemicals were used as received. All solutions were prepared gravimetrically using a Mettler Toledo balance (±0.1 mg). Forty

solutions of each of Na_2CO_3, $NaHCO_3$, and $NH_4NH_2CO_2$, spanning the concentration ranges of 0–0.7 mol/kg H_2O, 0–0.96 mol/kg H_2O, and 0–2.56 mol/kg H_2O, respectively, were prepared for calibration and validation purposes.

The selection of concentration range for calibration and validation range is important especially when the model is used for analyzing future samples. Three factors were considered during this selection which are the solubility of the chemicals, expected species concentrations, and Raman instrument performance. As reported in [22], solubility of Na_2CO_3 is 0.7 g at 0°C and 1.25 g at 10°C per kg H_2O. $NaHCO_3$ solubility in water is 0.69 g at 0°C and 0.815 g at 10°C per kg H_2O. Ammonium carbamate is freely soluble in water. Holmes et al. [8] report a comparison of equilibrium measurements of ionic system in CO_2-NH_3-H_2O systems for different initial concentrations of CO_2 loading. The comparison is based on his experimental work on ^{13}C NMR measurements with three thermodynamic models of Pitzer model [23], NRTL model [24], and TIDES model [25]. This comparison gives an indication of expected species concentration for a given CO_2 loading and NH_3 concentration. For the demonstration of the proposed method in this study, different samples prepared using 5 wt% ammonia in the CO_2 loading range from 0 to 0.6 mol CO_2/mol NH_3 were used and the expected species concentration reasonably falls in the calibration and validation range based on the reported work by Holmes et al. [8]. The limitation of the Raman instrument was also considered when selecting the concentration range. An overview of the sample solutions used for the calibration and validation of the PLS-R models, including the respective concentrations, can be found in Appendix.

2.4. Acquisition of Raman Spectra.

The Raman spectra were measured with the Kaiser RXN2 Raman spectrometer using a laser power of 400 mW and a total exposure time of 60 seconds with six scans of 10 seconds each being applied to achieve a good signal-to-noise ratio. To maintain a consistent temperature in the spectrometer, the instrument was stabilized for 30 minutes before each measurement series. The short-focus immersion optic was fitted onto the fiber optic probe head and cleaned with acetone. The immersion probe was then positioned vertically using a stand, with the optical window facing down. A glass container that contained the sample solution was positioned under the immersion optic, which was then carefully immersed in the solution. The tip of the optic was positioned in the center of the solution, approximately 20 mm from the bottom of the glass container. The sample and probe optic were protected from external light sources (such as fluorescent light) using aluminum foil. The Raman spectrum was obtained by initiating a scan in the instrument software. In the intervals between sample measurements, the probe was cleaned in acetone to avoid cross-contamination of sample solutions.

2.5. Preprocessing of Raman Spectra.

Figure 2 presents an example of the preprocessing of the Raman spectra (calibration and validation samples for bicarbonate). During preprocessing, all the Raman spectra were cropped so as to cover the range of 450–2300 cm^{-1}, since wavelengths outside

(a)

(b)

(c)

(d)
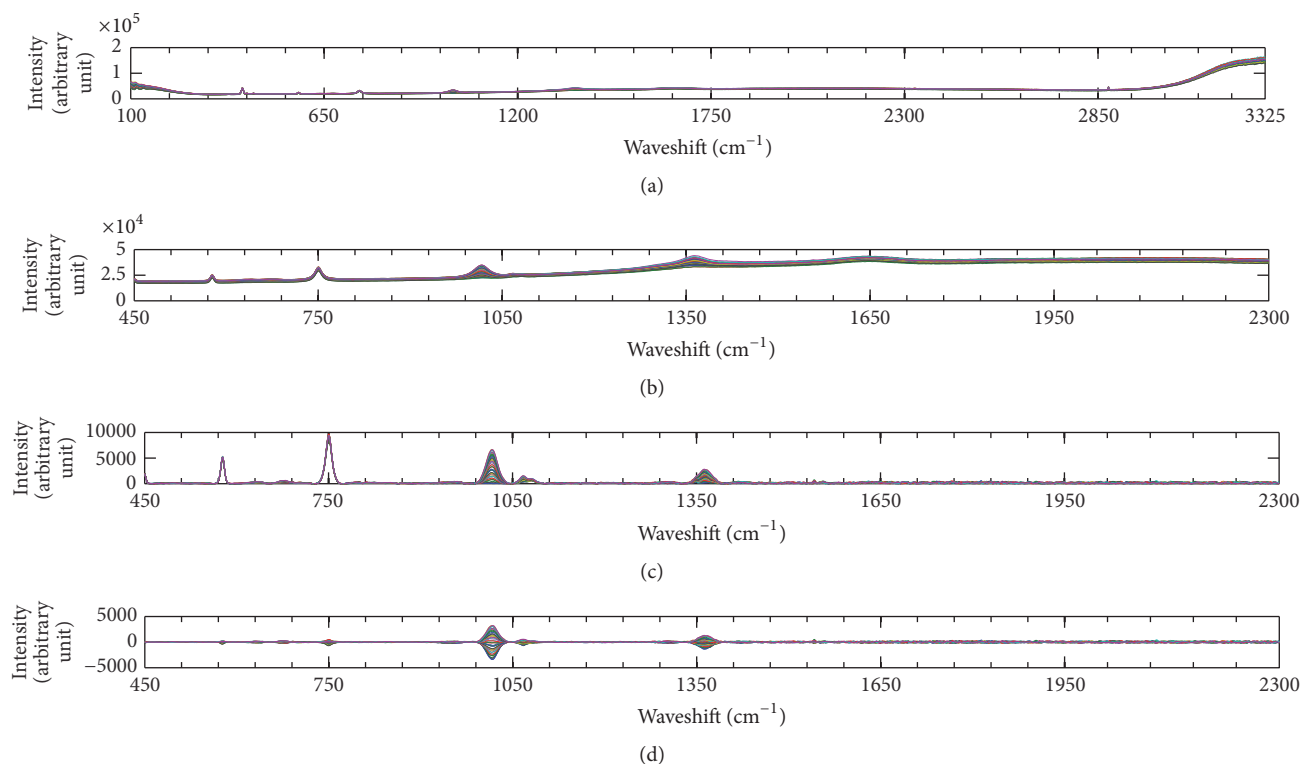
FIGURE 2: Preprocessing steps of the calibration and validation Raman spectra of bicarbonate. (a) Raw spectra for the range of 100–3325 cm^{-1}. (b) Spectra cropped to cover the range of 450–2300 cm^{-1}. (c) Spectra baseline corrected using the Whittaker filter (lambda = 100; P = 0.001). (d) Mean-centered spectra for PLS-R model calibration.

this range were not useful for the PLS-R analysis. Figures 2(a) and 2(b) show the bicarbonate spectra before and after cropping, respectively. In this range, the Raman spectra show an inconsistent baseline, which is particularly evident at the highest Raman shifts (above 2000 cm^{-1}). Raman spectra with variable baselines often generate regression models that have a higher number of components than is necessary, since the model also needs to model the baseline drift. To ensure a less complex model, a baseline correction is performed to decrease or remove the baseline drift in each Raman spectrum. Several baseline correction methods are available [26]. Spectroscopic data from a Raman spectrometer can be decomposed into three parts: (1) the analytical signal; (2) the baseline; and (3) noise. Noise was not a problem in the present study, whereas the baseline required some attention. The goal of all the baseline correction methods is to estimate the baseline in order to remove it. The MATLAB® 2012b software (MathWorks Inc.) in combination with PLS Toolbox 7.31 (Eigenvector Research Inc.) was used to find a suitable baseline correction in the present case. The lowest RMSEP was gained using the Whittaker filtering method [27] included in PLS Toolbox 7.31, which preserves the original shape of the signal part of the Raman spectrum. The Whittaker filter was applied with the following parameters: lambda = 100 and P = 0.001. The lambda parameter defines how much curvature is allowed, while the P parameter holds information about asymmetry in the spectra. Figure 2(c) shows the Raman spectra of bicarbonate after

baseline correction using the Whittaker filter. Finally, the spectra were centered by subtracting the mean from each variable (waveshift) in the Raman spectra. Centering [19] is applied prior to PLS-R calibration to avoid the need for an additional PLS-component to describe the mean of the data, which would entail a more complex model. Figure 2(d) shows the data after mean-centering. To summarize, the spectra were cropped to lie within the range of 450–2300 cm^{-1}, the baseline was corrected using the Whittaker filter with lambda value of 100 and P value of 0.001, and the spectra were centered on the mean prior to calibration of the PLS-R models of the three species (carbonate, bicarbonate, and carbamate).

2.6. PLS-R Modeling of Carbonate, Bicarbonate, and Carbamate. Individual models for carbonate, bicarbonate, and carbamate were calibrated based on the obtained Raman spectra of aqueous solutions that contained known concentrations in the ranges of 0–0.7 mol/kg, 0–0.96 mol/kg, and 0–2.56 mol/kg, respectively. Since the aim was to develop PLS-R models that could be used for speciation of a real CO_2-NH_3-H_2O system, a selection of variables (waveshifts) to be included in each model was carried out. The waveshifts to be included in the model of each respective anion were chosen based on backward selection, whereby only the wavelengths related to ammonia and the other two CO_2 anion species were omitted. In the model for the prediction of carbonate, the Raman wavelengths associated with ammonia,

TABLE 2: Vibrational assignments of $(NH_4)_2CO_3$, NH_4HCO_3, and $H_2NCOONH_4$ aqueous solutions, and omitted frequencies in the respective PLS-R models. Adapted from the data of Wen and Brooker [10].

Frequency [cm^{-1}]	Assignment	Omitted frequencies for the PLS-R anion model		
		Carbonate	Bicarbonate	Carbamate
3390	Antisymmetric N-H stretch of NH_3	X	X	X
3310	Symmetric N-H stretch of NH_3	X	X	X
3220	Fermi resonance with N-H symmetry stretch of NH_3	X	X	X
3050	Symmetric N-H stretch of NH_4^+	X	X	X
2850	A combination of fundamentals of NH_4^+	X	X	X
1690	NH_2 deformation of NH_4^+	X	X	X
1645	Antisymmetric deformation of NH_3			X
1630	C-O antisymmetric stretch of HCO_3^-			X
1550	Antisymmetric CO_2 stretch of H_2NCOO^-			X
1436, 1380	CO antisymmetric stretch of CO_3^{2-}	X, X	X, X	X, X
1430	Antisymmetric NH_2 deformation of NH_4^+	X	X	X
1405	Symmetric CO_2 stretch of H_2NCOO^-	X	X	
1360	CO symmetric stretch of HCO_3^-	X		X
1302	C-OH bend of HCO_3^-	X	X	X
1120	CN stretch of H_2NCOO^-	X	X	X
1065	CO symmetric stretch of CO_3^{2-}		X	X
1034	NH_2 wag of H_2NCOO^-	X	X	
1017	C-OH stretch of HCO_3^-	X	X	X
680	CO_2 antisymmetric deformation of CO_3^{2-}	X	X	X
640	(OH)-CO bend of HCO_3^-	X	X	X
570	Torsion about CO_2 skeleton of H_2NCOO^-	X	X	X

bicarbonate, and carbamate were omitted. The wavelength ranges used in the modeling of bicarbonate analysis were selected based on the same principle, while the carbamate model was based on a more limited range of wavelengths. Since PLS-R modeling of carbamate is more challenging than modeling of the other two species, forward selection was used to define the wavelength ranges in this model. Fine-tuning of the wavelength selection was made based on prediction results, in which the model with a combination of variables that resulted in the lowest prediction uncertainty was used. The carbonate, bicarbonate, and carbamate models were based on the respective frequency ranges of [450–520, 750–950, 1062–1100, 1140–1200, 1520–1650 and 1760–2300] cm^{-1}; [450–520, 750–950, 1140–1200, 1350–1390, 1520–1650 and 1760–2300] cm^{-1}; and [1033–1043] cm^{-1}. Table 2 lists the frequencies omitted from each PLS-R anion model.

The PLS-R models for carbonate, bicarbonate, and carbamate were all based on 20 calibration spectra, in addition to the 20 independent spectra that were used exclusively for the validation. Figure 3 shows the spectra used to calibrate and validate the carbonate, bicarbonate, and carbamate prediction models.

Dissolution of carbonate in water will lead to the following equilibrium state as given in reaction (7).

$$CO_3^{2-} + H_2O \rightleftarrows OH^- + HCO_3^- \tag{7}$$
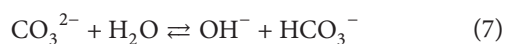
However, given the detection limit of the Raman spectrometer, only the carbonate band was observed. Therefore, this reaction was neglected in the carbonate PLS-R model development. However, in the cases of bicarbonate dissolution, reaction (8) and for carbamate dissolution reactions (7)–(13) were observed.

$$HCO_3^- \rightleftarrows H^+ + CO_3^{2-} \tag{8}$$

$$CO_3^{2-}{}_{(aq)} + NH_4^+{}_{(aq)} \rightleftarrows HCO_3^-{}_{(aq)} + NH_{3(aq)} \tag{9}$$

$$NH_3 + H_2O \rightleftarrows NH_4^+ + OH^- \tag{10}$$

$$NH_4^+ \rightleftarrows H^+ + NH_3 \tag{11}$$

$$HCO_3^-{}_{(aq)} + NH_{3(aq)} \rightleftarrows H_2NCOO^-{}_{(aq)} + H_2O \tag{12}$$

$$H_2NCOO^-{}_{(aq)} + H_2O \rightleftarrows CO_3^{2-}{}_{(aq)} + NH_4^+{}_{(aq)} \tag{13}$$
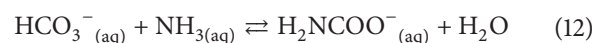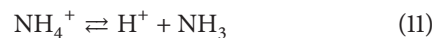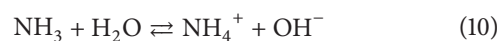
Thus, the quantitative PLS-R models were developed according to the following steps:

(1) Calibrate and validate the carbonate model.

(2) Predict carbonate in the bicarbonate calibration and validation datasets, and correct the bicarbonate references accordingly.

(3) Calibrate and validate the bicarbonate model based on the corrected dataset obtained in Step (2).

(a)

(b)

(c)
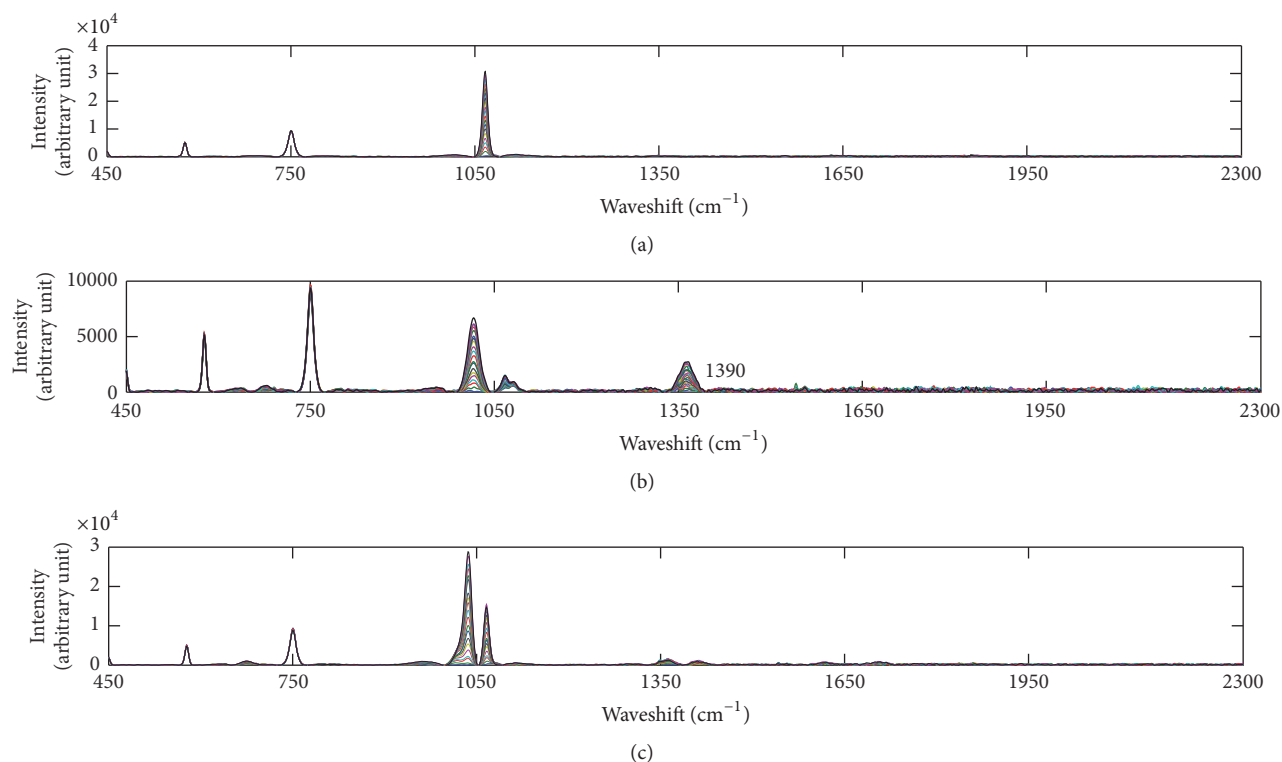
Figure 3: Raman spectra used in the PLS-R model calibration and validation. (a) Raman spectra of carbonate; (b) Raman spectra of bicarbonate; (c) Raman spectra of carbamate.

(4) Apply the carbonate model from Step (1) and bicarbonate model from Step (3) to predict carbonate and bicarbonate in the carbamate calibration and validation datasets.

(5) Correct the carbamate references in the calibration and validation datasets based on the predictions of carbonate and bicarbonate made in Step (4).

(6) Calibrate and validate the carbamate model.

All the PLS-R models developed in the present study were developed using the Unscrambler X ver. 10.3 software. Finally, the speciation method was demonstrated based on realistic aqueous solutions that contained 5 wt% ammonia loaded with CO_2. Since reference concentrations for carbonate, bicarbonate, and carbamate are not available for these datasets, the prediction results were assessed based on the calculated prediction uncertainties provided by Unscrambler X ver. 10.3.

3. Results and Discussion

The calibration and validation results for each of the respective PLS-R models for carbonate, bicarbonate, and carbamate are presented in the respective subsections below. Outliers were detected in the validation and calibration sets for carbonate using the $t_1 - u_1$ scatter plots (data not shown). An outlier may result from an air bubble sticking to the sapphire window in the tip of the probe optic or from the

probe optic being inserted so far down into the solution that the measurement is influenced by the glass container.

3.1. PLS-R Validation Results for Carbonate, Bicarbonate, and Carbamate. Figures 4–6 show the validation results for the PLS-R models of carbonate, bicarbonate, and carbamate, respectively. The results include plots of the scores ($t_1 - t_2$), regression coefficients (*B*), residual validation variances, and predicted concentrations versus the reference concentrations. The score plots are used to visualize how the calibration spectra compare to the validation spectra. The regression coefficients show the weight that each wavelength is assigned in the prediction. The residual validation variance plot shows the size of the residual for models with an increasing number of components. The predicted versus measured plots show how the predicted concentrations from the validation dataset in comparison with the references calculated from the sample preparation stage. Prediction performance is evaluated from an interpretation of the statistical parameters of merit, which include r^2, RMSEP, and the slope of the regression line.

For the carbonate series, one outlier, identified according to the definition provided previously [19], was removed from the validation dataset. No outliers were detected in the calibration dataset. The outlier was not considered thereafter. Figure 4 shows selected plots from the calibration and validation of the PLS-R model for carbonate. In bicarbonate series no outliers were detected in the calibration and validation datasets. Figure 5 shows selected plots from the calibration

(a)

(b)

(c)

(d)

Figure 4: PLS-R model for carbonate. (a) Score plot of PLS components 1 versus 2 showing the calibration samples and validation samples. (b) Regression coefficients based on a one-component PLS-R model. (c) The residual validation variance shows that one PLS-component is optimal. (d) Predicted carbonate concentrations based on the one-component PLS-R model versus the reference concentrations obtained from the solute ion preparation stage.

Table 3: PLS-R modeling of carbonate, bicarbonate, and carbamate.

Model	Carbonate model	Bicarbonate model	Carbamate model
Wavelength ranges included [cm^{-1}]	450–520, 750–950, 1062–1100, 1140–1200, 1520–1650 and 1760–2300	450–520, 750–950, 1140–1200, 1350–1390, 1520–1650 and 1760–2300	1033–1043
Slope	0.9898	0.9636	1.0246
r^2	0.9995	0.9932	0.9968
RMSEP [mmol/kg]	4.3	24.1	49.9
Number of components	1	1	1
Number of outliers	1 (in the validation set)	0	0

and validation of the PLS-R model for bicarbonate. For carbamate series also no outliers were detected in the calibration or validation datasets. Figure 6 shows selected plots from the calibration and validation of the PLS-R model for carbamate.

The wavelength ranges used in the PLS-R models for the predictions of carbonate, bicarbonate, and carbamate are presented in Table 3. Some variables (waveshifts) with regression coefficients close to zero were also included, as

it was found that the prediction uncertainties were slightly improved when these wavelengths were included. The values for the slope, r^2, RMSEP, the number of PLS components, and outliers in all three models are listed in Table 3.

Multivariate analysis has been proven to overcome many challenges in univariate method. Univariate method is simple and samples for calibration can be prepared using one chemical when there are no interferences from other constituents. There are many instances when the property of interest

(a)

(b)

(c)

(d)

Figure 5: PLS-R model for bicarbonate. (a) Score plot of PLS components 1 versus 2 showing the calibration samples and validation samples. (b) Regression coefficients based on a one-component PLS-R model. (c) The residual validation variance shows that one PLS-component is optimal. (d) Predicted bicarbonate concentrations based on the one-component PLS-R model versus the reference concentrations obtained from the solution preparation stage.

cannot be described by one peak. According to Table 2, vibrational modes assigned to carbonate, bicarbonate, and carbamate fall closer to each other in the finger print area from 1000 to 1420 cm^{-1}. The NH_3-CO_2-H_2O system consists of several equilibrium reactions and the compositions of carbonate, bicarbonate, and carbamate are influenced by the concentrations of each other. It can be seen from the calibration spectrum that there are completely visible, independent nicely shaped peak assigned to each other; however this may be not true when it comes to the real CO_2 loaded ammonia system. Two scenarios of misuse of the multivariate regression in spectroscopic applications have been explained by Esbensen et al. [28]. They are assigning individual peaks for regression which are identified by the preprocessed data or by regression coefficients. The regression coefficients are used to calculate the response value from the X-measurements. The size of the coefficients gives an indication of which variables have an important impact on the response variables. Assigning wavelengths selected during calibration development for regression must be done with caution because more than one wavelengths are associated with the functional group to some degree [28]. Many factors including scatter effect affect the

wavelength position and only by using a wavelength region can the robustness of the calibration model be increased.

The score plots shown in Figures 4–6 reveal that the calibration and validation datasets in all three cases span the same score space, which indicates similarity of the datasets. The most important wavelengths are those with regression coefficients that show the largest deviation from zero. The regression coefficients listed in Figure 4 (carbonate), Figure 5 (bicarbonate), and Figure 6 (carbamate) show that the most important wavelength ranges are 1060–1070 cm^{-1}, 1350–1380 cm^{-1}, and 1033–1043 cm^{-1}, respectively. In all three models, only a small contribution is gained from wavelengths outside these ranges. The residual validation variance plot shows that one-component PLS-R is sufficient for all three models. The slope of the regression line is 0.96–1.02 and the r^2 is 0.0.993–0.999, which is close to the optimal value of 1.0. The average prediction errors, that is, RMSEP values, for carbonate, bicarbonate, and carbamate, were 4.3 mmol/kg H_2O, 24.1 mmol/kg H_2O, and 49.9 mmol/kg H_2O, respectively.

3.2. Demonstration of the Method. The proposed speciation method was demonstrated using aqueous solutions of 5 wt% ammonia loaded with CO_2. Since reference concentrations
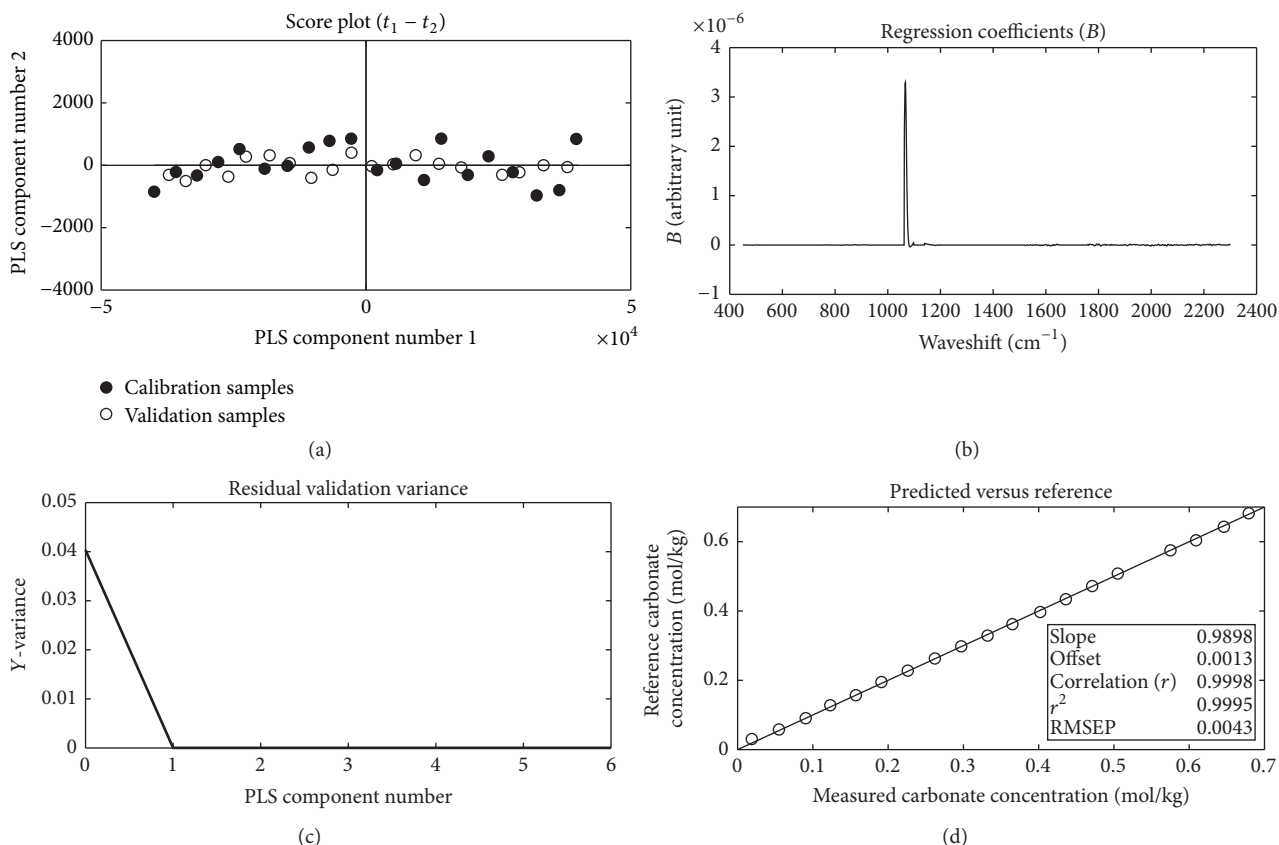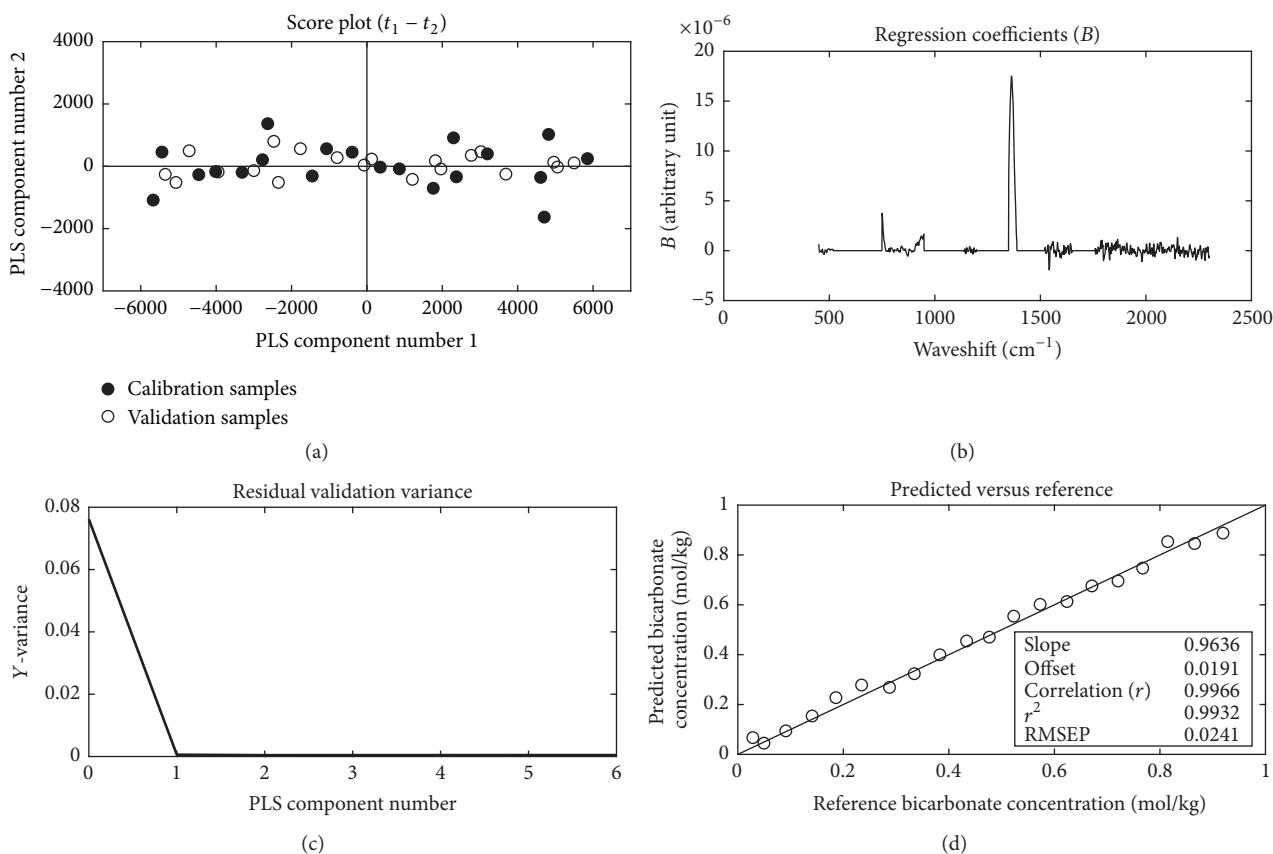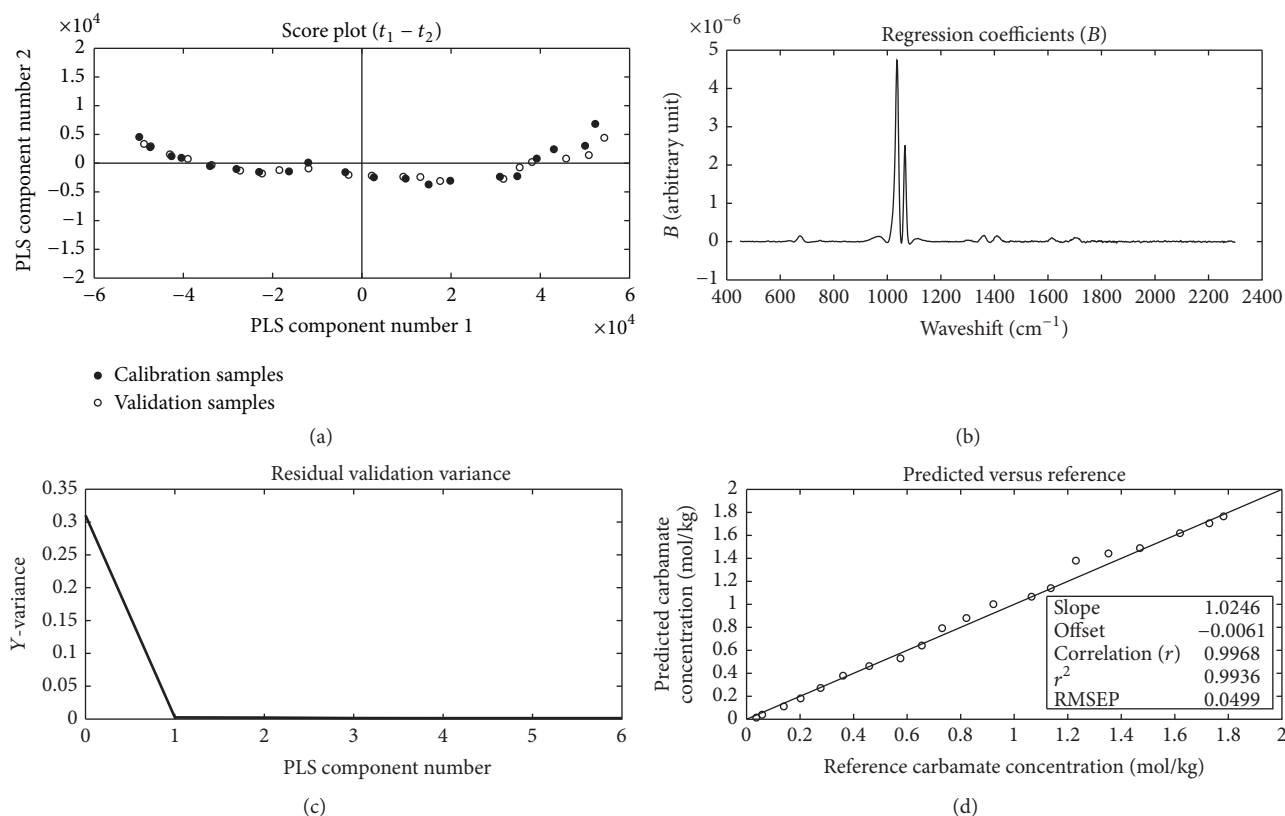
FIGURE 6: PLS-R model for carbamate. (a) Score plot of PLS components 1 versus 2 showing the calibration samples (filled circles) and validation samples (open circles). (b) Regression coefficients based on a one-component PLS-R model. (c) The residual validation variance shows that one PLS-component is optimal. (d) Predicted carbamate concentrations based on the one-component PLS-R model versus the reference concentrations obtained from the solution preparation stage.

of carbonate, bicarbonate, and carbamate were not available, the prediction performance level of each model was assessed based on the calculated prediction uncertainties, as defined previously [29]. The demonstration dataset was based on 14 solutions with different loadings (mole-ratio CO_2/NH_3) of CO_2, which were measured three times (42 samples in total). The solvent CO_2 loading is one of the primary process parameters in the operation of systems for the chemical absorption of CO_2.

Figure 7 shows the predicted concentrations of the measured species. The average prediction uncertainties for carbonate, bicarbonate, and carbamate were 6.45 mmol/kg H_2O, 34.39 mmol/kg H_2O, and 100.9 mmol/kg H_2O, respectively. Overall, the predictions of the sample solutions with corresponding uncertainties give a satisfactory outcome regarding speciation of all the anions. The last three predictions for carbamate shown in Figure 7(c) reveal greater uncertainties than those noted for the other predictions. This is due to either the precipitation of solids or the presence of a slightly higher concentration of ammonia in this sample. While a precipitate was not visible in this sample, the conditions were close to those for which precipitation is expected. Thus, the influence of precipitation could not be ruled out. In the accompanying report [14], the method presented here is

compared to the experimental data of the same samples with the precipitation-titration method, with good agreement. In the present study, the difference observed between the demonstration dataset and the carbamate calibration is that even though all the same species are present, the CO_2 loading differs (see reactions (12) and (13)). In the demonstration dataset, the amounts of ammonia and water are roughly constant, and the amount of CO_2 increases continuously with increasing sample number. In the demonstration dataset, the CO_2 loading is increased from 0 to 0.6. Thus, the present method can relate the CO_2 loading to the liquid carbon distribution through reactions (2)–(5).

3.3. Comparison of the Model with Literature.

Three models developed in this study have been used in the study of VLE data of chilled ammonia system [14]. This study shows the model predictability which has been compared with two thermodynamic models of Darde et al. [6] and Que and Chen [24] and experimental work carried out by Wen and Brooker [10], Holmes et al. [8], Zhao et al. [11], and Ahn et al. [30]. The composition analysis performed by Zhao et al. [11] for CO_2-NH_3-H_2O system is based on univariate analysis of Raman measurements. They record results for different initial ammonia concentrations in the
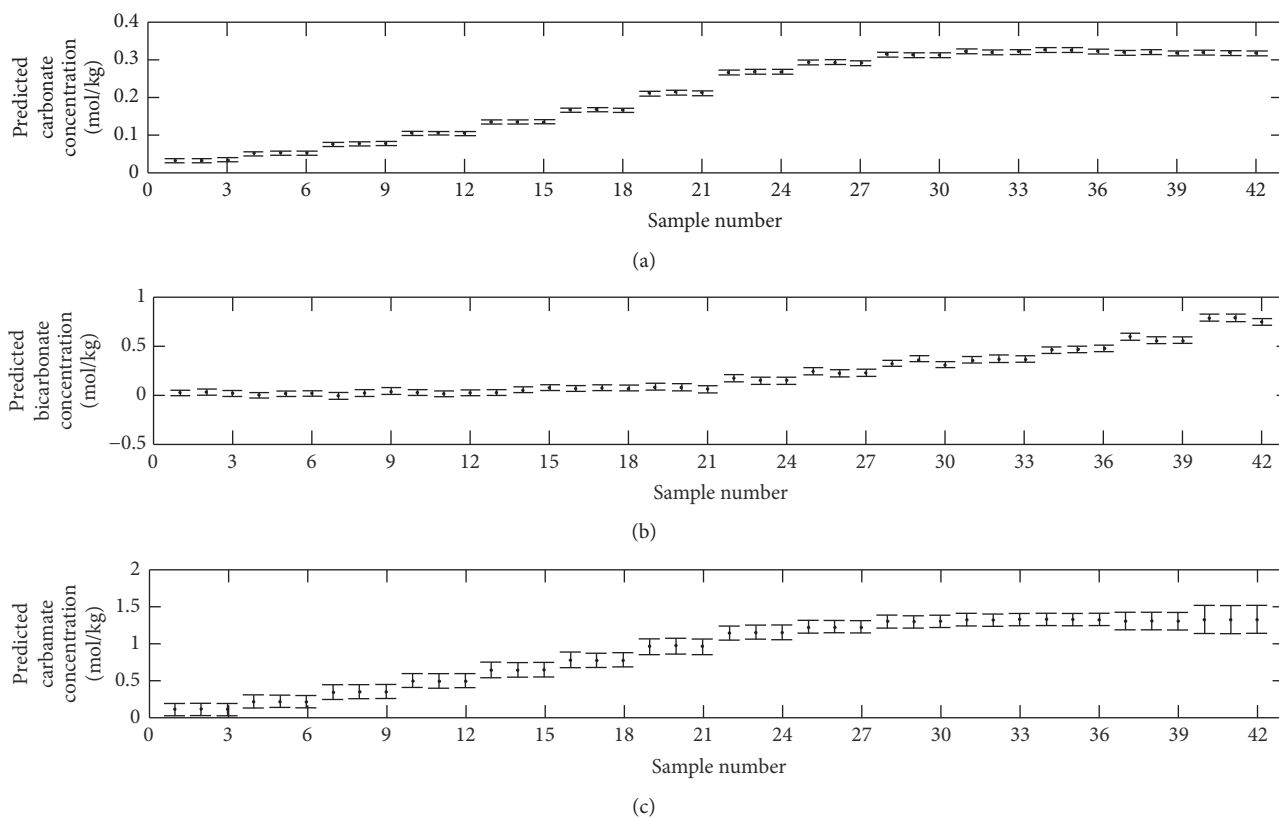
Figure 7: Predicted concentrations [mol/kg] of (a) carbonate; (b) bicarbonate; and (c) carbamate.

range of 0.69 mol/L to 2.10 mol/L and CO_2 concentration range from 0.18 to 0.67 mol/L. The work is related to low concentrations of ammonia. The proposed method in this study is independent of ammonia concentration and is based on three calibration sets each with 20 measurements which were followed by validation using independent data set spanning in the calibration range for each species. Zhao's method includes calculating molar scattering intensity (J) of each carbon species by preparation of series of solutions of sodium carbonate and sodium bicarbonate to calculate J of carbonate and bicarbonate while J of carbamate was calculated by carbon conservation balance. Therefore the molar scattering intensity of carbamate was dependent on those of other 2 components.

4. Conclusion

A method for speciation of the CO_2-NH_3-H_2O system is proposed. The proposed method can be applied without the need for additional analytical calibration methods. Speciation is achieved based on a combination of Raman spectroscopy and multivariate PLS-R modeling, wherein the so-called full spectrum calibration method is applied to extract information from the entire spectrum. The concentrations of carbonate, bicarbonate, and carbamate were predicted with an average prediction error (RMSEP) as being 4.3 mmol/kg H_2O, 24.1 mmol/kg H_2O, and 49.9 mmol/kg H_2O, respectively.

For the method demonstration case, which lacked reference concentrations, the prediction uncertainties for carbonate, bicarbonate, and carbamate were 6.45 mmol/kg H_2O, 34.39 mmol/kg H_2O, and 100.9 mmol/kg H_2O, respectively.

Appendix

Concentrations of the Carbonate, Bicarbonate, and Carbamate Species in the Solutions Used for Model Calibration and Validation

See Table 4.

Conflicts of Interest

The authors declare no conflicts of interest regarding the publication of this research paper.

Acknowledgments

TABLE 4: Overview of sample solutions reported as mol/kg H_2O.

Sample number	Carbonate [mol/kg H_2O]		Bicarbonate [mol/kg H_2O]		Carbamate [mol/kg H_2O]	
	Calibration	Validation	Calibration	Validation	Calibration	Validation
(1)	0.00000	0.01974	0.00000	0.03441	0.00000	0.07923
(2)	0.03840	0.05585	0.05671	0.05704	0.14939	0.14652
(3)	0.07280	0.09137	0.10508	0.10159	0.29518	0.27757
(4)	0.11073	0.12401	0.15180	0.15504	0.39826	0.40627
(5)	0.14710	0.15777	0.20941	0.20138	0.53542	0.55145
(6)	0.18544	0.19187	0.25647	0.25214	0.67098	0.67585
(7)	0.22126	0.22658	0.30250	0.30090	0.80054	0.80525
(8)	0.25856	0.26310	0.35346	0.35263	0.93483	0.94422
(9)	0.29493	0.29814	0.40131	0.40289	1.08200	1.05871
(10)	0.33113	0.33291	0.46320	0.45270	1.21012	1.21201
(11)	0.36895	0.36560	0.49901	0.49946	1.33941	1.33618
(12)	0.39913	0.40255	0.54737	0.54932	1.47757	1.47498
(13)	0.44205	0.43683	0.59693	0.60006	1.61910	1.60257
(14)	0.47772	0.47227	0.65191	0.65196	1.73472	1.73898
(15)	0.51599	0.50607	0.70127	0.70248	1.87207	1.87232
(16)	0.55162	0.54010	0.74870	0.75143	2.02088	2.01094
(17)	0.59048	0.57554	0.79937	0.79809	2.12369	2.13626
(18)	0.62521	0.61002	0.84721	0.84682	2.27083	2.28208
(19)	0.66210	0.64656	0.90173	0.89758	2.41909	2.41723
(20)	0.69948	0.68035	0.95353	0.94859	2.55658	2.44528

References

[1] S. Solomon, D. Qin, M. Manning et al., "Climate Change 2007: The Physical Science Basis," Contribution of Working Group I to the Fourth Assessment Report of the Intergovernmental Panel on Climate Change, Cambridge University Press, Cambridge, UK, 2007.

[2] IEA, *Technology Roadmap: Carbon Capture and Storage*, International Energy Agency, Paris, France, 2013.

[3] G. T. Rochelle, "amine scrubbing for CO2 capture," *Science*, vol. 325, no. 5948, pp. 1652–1654, 2009.

[4] G. d. Koeijer, Y. O. Enge, C. Thebault, S. Berg, J. Lindland, and S. J. Overå, "European CO2 test centre mongstad–testing, verification and demonstration of post-combustion technologies," *Energy Procedia*, vol. 1, no. 1, pp. 1321–1326, 2009.

[5] O. Lawal, A. Bello, and R. Idem, "The role of methyl diethanolamine (MDEA) in preventing the oxidative degradation of CO2 loaded and concentrated aqueous monoethanolamine (MEA)-MDEA blends during CO2 absorption from flue gases," *Industrial and Engineering Chemistry Research*, vol. 44, no. 6, pp. 1874–1896, 2005.

[6] V. Darde, K. Thomsen, W. J. M. van Well, and E. H. Stenby, "Chilled ammonia process for CO2 capture," *International Journal of Greenhouse Gas Control*, vol. 4, no. 2, pp. 131–136, 2010.

[7] J. T. Yeh, H. W. Pennline, K. P. Resnik, and K. Rygle, *Absorption And Regeneration Studies for CO2 Capture by Aqueous Ammonia*, Pittsburgh, PA, USA, 2004.

[8] P. E. Holmes, M. Naaz, and B. E. Poling, "Ion concentrations in the CO2-NH3-H2O system from 13C NMR spectroscopy," *Industrial and Engineering Chemistry Research*, vol. 37, no. 8, pp. 3281–3287, 1998.

[9] L. Meng, S. Burris, H. Bui, and W.-P. Pan, "Development of an analytical method for distinguishing ammonium bicarbonate from the products of an aqueous ammonia CO2 scrubber," *Analytical Chemistry*, vol. 77, no. 18, pp. 5947–5952, 2005.

[10] N. Wen and M. H. Brooker, "Ammonium carbonate, ammonium bicarbonate, and ammonium carbamate equilibria: a raman study," *Journal of Physical Chemistry®*, vol. 99, no. 1, pp. 359–368, 1995.

[11] Q. Zhao, S. Wang, F. Qin, and C. Chen, "Composition analysis of CO2-NH3-H2O system based on Raman spectra," *Industrial and Engineering Chemistry Research*, vol. 50, no. 9, pp. 5316–5325, 2011.

[12] Y. J. Kim, J. K. You, W. H. Hong, K. B. Yi, C. H. Ko, and J.-N. Kim, "Characteristics of CO2 absorption into aqueous ammonia," *Separation Science and Technology*, vol. 43, no. 4, pp. 766–777, 2008.

[13] P. A. G. L. Samarakoon, N. H. Andersen, C. Perinu, and K.-J. Jens, "Equilibria of MEA, DEA and AMP with bicarbonate and carbamate: a Raman study," *Energy Procedia*, vol. 37, pp. 2002–2010, 2013.

[14] H. Jilvero, K.-J. Jens, F. Normann et al., "Equilibrium measurements of the NH3-CO2-H2O system - measurement and evaluation of vapor-liquid equilibrium data at low temperatures," *Fluid Phase Equilibria*, vol. 385, pp. 237–247, 2015.

[15] K. H. Esbensen, D. Guyot, F. Westad, and L. P. Houmoller, *Multivariate Data Analysis: in Practice*, CAMO Software, Oslo, Norway, 2010.

[16] U. Lichtfers and B. Rumpf, "Infrared spectroscopic studies of the determination of species concentrations in aqueous solutions containing ammonia and carbon dioxide," *Chemie Ingenieur Technik*, vol. 72, pp. 1526–1530, 2000.

[17] U. Lichtfers and B. Rumpf, "An infrared spectroscopic investigation on the species distribution in the system NH3 + CO2 + H2O," *Thermodynamic Properties of Complex Fluid Mixtures*, pp. 92–119, 2004.

[18] J. R. Ferraro, K. Nakamoto, and C. W. Brown, *Introductory Raman Spectroscopy*, Academic Press, San Diego , Calif, USA, 2 edition, 2008.

[19] H. Martens and T. Naes, *Multivariate calibration*, John Wiley & Sons, London, UK, 1989.

[20] K. A. Bakeev, *Process analytical technology: spectroscopic tools and implementation strategies for the chemical and pharmaceutical industries*, John Wiley & Sons, 2010.

[21] K. H. Esbensen and P. Geladi, "Principles of proper validation: use and abuse of re-sampling for validation," *Journal of Chemometrics*, vol. 24, no. 3-4, pp. 168–187, 2010.

[22] A. Seidell, *Solubilities of inorganic and organic compounds; a compilation of quantitative solubility data from the periodical literature*, D. Van Nostrand Company, New York, NY, USA, 2 edition, 1919.

[23] K. S. Pitzer, "Thermodynamics of electrolytes. I. theoretical basis and general equations," *Journal of Physical Chemistry*, vol. 77, no. 2, pp. 268–277, 1973.

[24] H. Que and C.-C. Chen, "Thermodynamic modeling of the NH3-CO2-H2O system with electrolyte NRTL model," *Industrial and Engineering Chemistry Research*, vol. 50, no. 19, pp. 11406–11421, 2011.

[25] E. M. Pawlikowski, J. Newman, and J. M. Prausnitz, "Phase equilibria for aqueous solutions of ammonia and carbon dioxide," *Industrial Engineering Chemistry Research Process Design and Development*, vol. 21, pp. 764–770, 1982.

[26] K. H. Liland, T. Almøy, and B.-H. Mevik, "Optimal choice of baseline correction for multivariate calibration of spectra," *Applied Spectroscopy*, vol. 64, no. 9, pp. 1007–1016, 2010.

[27] P. H. C. Eilers, "A perfect smoother," *Analytical Chemistry*, vol. 75, no. 14, pp. 3631–3636, 2003.

[28] K. Esbensen, P. Geladi, A. Larsen, and P. Williams, "Mythbusters: one can always assign a wavelength/wavelength region specific for one's application," *NIR News*, vol. 26, no. 4, pp. 15–17, 2015.

[29] M. Høy, K. Steen, and H. Martens, "Review of partial least squares regression prediction error in Unscrambler," *Chemometrics and Intelligent Laboratory Systems*, vol. 44, no. 1-2, pp. 123–133, 1998.

[30] C. K. Ahn, H. W. Lee, Y. S. Chang et al., "Characterization of ammonia-based CO2 capture process using ion speciation," *International Journal of Greenhouse Gas Control*, vol. 5, no. 6, pp. 1606–1613, 2011.

International Journal of
Medicinal Chemistry
Hindawi Publishing Corporation
http://www.hindawi.com
Volume 2014

Organic Chemistry
International
Hindawi Publishing Corporation
http://www.hindawi.com
Volume 2014

International Journal of
Photoenergy
Hindawi Publishing Corporation
http://www.hindawi.com
Volume 2014

International Journal of
Analytical Chemistry
Hindawi Publishing Corporation
http://www.hindawi.com
Volume 2014

Advances in
Physical Chemistry
Hindawi Publishing Corporation
http://www.hindawi.com
Volume 2014

International Journal of
Carbohydrate
Chemistry
Hindawi Publishing Corporation
http://www.hindawi.com
Volume 2014

Journal of
Quantum Chemistry
Hindawi Publishing Corporation
http://www.hindawi.com
Volume 2014

The Scientific
World Journal
Hindawi Publishing Corporation
http://www.hindawi.com
Volume 2014

Submit your manuscripts at
https://www.hindawi.com

Hindawi

Journal of
Analytical Methods
in Chemistry
Hindawi Publishing Corporation
http://www.hindawi.com
Volume 2014

Journal of
Spectroscopy
Hindawi Publishing Corporation
http://www.hindawi.com
Volume 2014

International Journal of
Inorganic Chemistry
Hindawi Publishing Corporation
http://www.hindawi.com
Volume 2014

International Journal of
Electrochemistry
Hindawi Publishing Corporation
http://www.hindawi.com
Volume 2014

Journal of
Applied Chemistry
Hindawi Publishing Corporation
http://www.hindawi.com
Volume 2014

Bioinorganic Chemistry
and Applications
Hindawi Publishing Corporation
http://www.hindawi.com
Volume 2014

Journal of
Theoretical Chemistry
Hindawi Publishing Corporation
http://www.hindawi.com
Volume 2014

Chromatography
Research International
Hindawi Publishing Corporation
http://www.hindawi.com
Volume 2014

Journal of
Catalysts
Hindawi Publishing Corporation
http://www.hindawi.com
Volume 2014

Journal of
Chemistry
Hindawi Publishing Corporation
http://www.hindawi.com
Volume 2014

International Journal of
Spectroscopy
Hindawi Publishing Corporation
http://www.hindawi.com
Volume 2014

Appendix

Table A- 1. Comparison of CO₂ loading from titration and Raman spectroscopy in rich amine stream during PACT campaign (Uc = uncertainty values calculated by the Raman models)

Day#	time	CO$_2$ loading (mol/mol MEA) – rich stream		
		Titration	Raman predictions	
			Time of acquiring Raman spectra	Value	± Uc
1	13:15	0.153373	13:10:55	0.141957153	0.0102
			13:12:36	0.1447069	0.0104
			13:21:55	0.151084033	0.0101
1	13:45	0.37699	13:44:52	0.367931778	0.0091
			13:45:58	0.378113074	0.0088
			13:47:04	0.386933479	0.0088
1	14:05	0.439896	14:04:38	0.447304464	0.0092
			14:05:44	0.44871423	0.0097
			14:06:50	0.447404157	0.0095
1	14:25	0.486367	14:24:25	0.480229869	0.0094
			14:25:30	0.475508568	0.0094
			14:26:36	0.481497733	0.0095
1	14:45	0.475426	14:44:10	0.490212364	0.0093
			14:45:16	0.494240943	0.0094
			14:46:22	0.49839744	0.0095
1	15:15	0.484216	15:14:55	0.494205368	0.0097
			15:16:01	0.499282562	0.0096
			15:17:07	0.500604884	0.0097
1	15:35	0.463091	15:34:41	0.482200133	0.0096
			15:35:46	0.484946962	0.0094
			15:36:52	0.486532812	0.0096
1	15:55	0.462196	15:54:26	0.47736251	0.0095
			15:55:32	0.478879968	0.0094
			15:56:38	0.482785583	0.0093
1	16:15	0.42835	16:14:12	0.469110204	0.0095
			16:15:18	0.465763094	0.0094
			16:17:40	0.458682739	0.0095
1	16:35	0.331385	16:34:17	0.388741446	0.0088
			16:35:23	0.380634396	0.0088
			16:36:29	0.380228	0.0088
1	16:55	0.28351	16:54:06	0.284643762	0.0088
			16:55:12	0.277759863	0.0087

			16:56:18	0.280339032	0.0088
1	17:15	0.191744	17:13:55	0.209449384	0.0090
			17:15:02	0.204762528	0.0090
			17:16:08	0.208032136	0.0091
2	10:25	0.114649	10:24:49	0.125993496	0.0116
			10:25:55	0.122851742	0.0112
			10:27:01	0.123547155	0.0118
2	11:05	0.267122	11:04:29	0.252611434	0.0088
			11:05:35	0.250383702	0.0089
			11:06:41	0.254343467	0.0088
2	11:30	0.304644	11:29:50	0.294803578	0.0088
			11:30:56	0.303768031	0.0087
			11:32:03	0.303887257	0.0088
2	12:00	0.322018	11:59:35	0.332978564	0.0089
			12:00:42	0.34293726	0.0089
			12:01:48	0.33638242	0.0088
2	12:30	0.302003	12:29:21	0.302485721	0.0088
			12:30:27	0.301098831	0.0089
			12:31:33	0.306824078	0.0088
2	13:00	0.271299	12:59:07	0.272222532	0.0088
			13:00:13	0.27163003	0.0088
			13:01:19	0.269202593	0.0088
2	13:30	0.420024	13:29:04	0.411547716	0.0098
			13:30:10	0.418867868	0.0093
			13:31:16	0.417852231	0.0098
2	13:45	0.430781	13:44:28	0.433254377	0.0093
			13:45:34	0.433927146	0.0094
			13:46:40	0.437507076	0.0090
2	14:00	0.434504	13:59:52	0.427955286	0.0098
			14:00:58	0.4393602	0.0094
			14:02:04	0.429513089	0.0093
2	14:15	0.434618	14:14:09	0.430510688	0.0093
			14:15:15	0.433922169	0.0092
			14:16:20	0.435372677	0.0094
2	14:45	0.338655	14:44:24	0.354791444	0.0089
			14:45:46	0.348097677	0.0088
			14:48:52	0.353694855	0.0091
2	15:00	0.366251	14:54:52	0.367527565	0.0089
			15:01:05	0.369625796	0.0090
			15:05:14	0.370164045	0.0095
2	15:15	0.35636	15:13:22	0.370965167	0.0090
			15:16:47	0.378373176	0.0089
			15:17:53	0.37620467	0.0089

2	15:30	0.334543	15:28:58	0.37677801	0.0090
			15:30:04	0.36946285	0.0090
			15:31:18	0.350117017	0.0091
2	15:45	0.334663	15:42:54	0.346655728	0.0090
			15:49:59	0.355378132	0.0089
			15:51:14	0.354349837	0.0090
2	16:00	0.344137	15:57:10	0.352775152	0.0090
			16:02:28	0.350552832	0.0092
			16:04:13	0.353206889	0.0091
2	16:15	0.33803	16:14:38	0.359639092	0.0089
			16:16:00	0.354106172	0.0090
			16:17:06	0.349247599	0.0092
2	16:30	0.320904	16:29:22	0.35663223	0.0090
			16:30:29	0.363648563	0.0092
			16:31:34	0.365390265	0.0089
2	16:45	0.313799	16:44:46	0.325853667	0.0091
			16:45:52	0.332053055	0.0091
			16:46:58	0.330559537	0.0090
2	17:00	0.325545	16:59:06	0.343278441	0.0090
			17:00:12	0.344637883	0.0090
			17:01:18	0.340977086	0.0091
2	17:15	0.335603	17:14:29	0.331061971	0.0089
			17:15:35	0.341110003	0.0091
			17:16:41	0.342035572	0.0090
2	17:30	0.358162	17:29:53	0.342276761	0.0090
			17:30:59	0.341600561	0.0093
			17:32:05	0.34463627	0.0090
3	10:00	0.256941	-	-	
			-	-	
			--	-	
3	10:30	0.231785	10:29:52	0.214266241	0.0091
			10:30:58	0.207547164	0.0094
			10:32:04	0.213588688	0.0091
3	11:00	0.389	10:59:36	0.281570228	0.0089
			11:00:42	0.274333882	0.0090
			11:01:48	0.280203489	0.0090
3	11:30	0.401722	11:29:20	0.400819487	0.0093
			11:30:26	0.403340651	0.0096
			11:31:32	0.400379391	0.0094
3	12:00	0.374217	11:59:04	0.391524224	0.0096
			12:00:11	0.392784068	0.0094
			12:01:17	0.393253291	0.0095
3	12:30	0.402764	12:28:53	0.408097382	0.0093

			12:30:00	0.406810964	0.0093
			12:31:06	0.398636687	0.0095
3	13:00	0.393799	12:59:45	0.400823292	0.0095
			13:00:52	0.396912156	0.0097
			13:01:58	0.395801834	0.0097
3	13:30	0.406388	13:29:33	0.397989108	0.0096
			13:30:39	0.391442516	0.0097
			13:31:45	0.387454983	0.0098
3	14:00	0.395441	13:59:19	0.39162306	0.0097
			14:00:25	0.387641176	0.0100
			14:01:15	0.39536585	0.0099
3	14:30	0.307216	14:30:06	0.479030787	0.0672
			14:31:12	0.371598659	0.0093
			14:32:19	0.308242633	0.0093
3	15:00	0.392325	14:59:53	0.406833947	0.0097
			15:00:59	0.409090194	0.0094
			15:02:06	0.400881175	0.0095
3	15:30	0.381261	15:29:40	0.397011952	0.0096
			15:30:46	0.396438519	0.0096
			15:31:52	0.396391107	0.0095
3	16:00	0.395945	15:59:26	0.399773716	0.0093
			16:00:32	0.399041368	0.0095
			16:01:38	0.391031302	0.0096
3	16:30	0.386963	16:29:38	0.387827803	0.0095
			16:30:50	0.387331172	0.0095
			16:32:01	0.379534424	0.0095

Table A- 2. Comparison of CO₂ loading from titration and Raman spectroscopy in lean amine stream during PACT campaign (Uc = uncertainty values calculated by the Raman models)

Day#	time	CO₂ loading (mol/mol MEA) – lean stream			
		Titration	Raman predictions		
			Time of acquiring Raman spectra	Value	± Uc
1	13:15	0.141858	13:14:33	0.15136	0.0096
			13:15:05	0.14908	0.0097
			13:16:17	0.14806	0.0103
1	13:45	0.219616	13:43:58	0.19482	0.0091
			13:45:04	0.20091	0.0091
			13:46:10	0.20419	0.0091
1	14:05	0.330098	14:04:50	0.31584	0.0091
			14:05:56	0.32381	0.0092
			14:07:02	0.32723	0.0093
1	14:25	0.394555	14:24:37	0.40590	0.0093
			14:25:43	0.40962	0.0091
			14:26:48	0.40930	0.0093
1	14:45	0.428106	14:44:22	0.45216	0.0094
			14:45:28	0.45636	0.0094
			14:46:34	0.45825	0.0094
1	15:15	0.472425	15:14:01	0.48647	0.0095
			15:15:07	0.48698	0.0094
			15:16:13	0.49063	0.0095
1	15:35	0.464507	15:34:53	0.49819	0.0101
			15:35:59	0.50100	0.0103
			15:37:04	0.49934	0.0101
1	15:55	0.455322	15:54:38	0.49207	0.0107
			15:55:44	0.48674	0.0104
			15:56:50	0.48919	0.0105
1	16:15	0.391166	16:14:24	0.45594	0.0101
			16:15:30	0.44763	0.0098
			16:16:36	0.44372	0.0100
1	16:35	0.290897	16:34:03	0.34486	0.0097
			16:35:10	0.33739	0.0096
			16:36:16	0.33494	0.0098
2	16:55	0.238621	16:54:59	0.24760	0.0096
			16:56:05	0.24354	0.0095

			16:57:11	0.23842	0.0093
2	10:25	0.119086	10:24:31	0.12563	0.0110
			10:25:37	0.12927	0.0107
			10:26:43	0.13104	0.0106
2	11:05	0.121516	11:04:11	0.13141	0.0106
			11:05:17	0.13602	0.0104
			11:06:23	0.13963	0.0101
2	11:30	0.180569	11:29:32	0.17908	0.0094
			11:30:38	0.17988	0.0095
			11:31:44	0.18605	0.0094
2	12:00	0.163864	11:59:17	0.18578	0.0094
			12:00:24	0.18410	0.0094
			12:01:30	0.17967	0.0094
2	12:30	0.146731	12:29:03	0.15940	0.0098
			12:30:09	0.16054	0.0097
			12:31:15	0.15540	0.0097
2	13:00	0.121293	12:59:55	0.14773	0.0099
			13:01:01	0.14614	0.0100
			13:02:07	0.14896	0.0100
2	13:30	0.123048	13:29:52	0.14417	0.0100
			13:30:58	0.14575	0.0100
			13:32:04	0.14399	0.0100
2	13:45	0.133961	13:44:10	0.14829	0.0099
			13:45:16	0.14480	0.0102
			13:46:22	0.14953	0.0099
2	14:00	0.14378	13:59:34	0.14543	0.0100
			14:00:40	0.14569	0.0099
			14:01:46	0.15034	0.0099
2	14:15	0.130527	14:14:57	0.14506	0.0099
			14:16:03	0.14706	0.0099
			14:17:08	0.14790	0.0100
2	14:30	0.13583	14:29:14	0.14557	0.0101
			14:30:20	0.14680	0.0099
			14:31:26	0.14642	0.0100
2	14:45	0.149866	14:40:13	0.16082	0.0096
			14:41:19	0.16307	0.0097
			14:49:42	0.17868	0.0096
2	15:00	0.166645	14:49:42	0.16307	0.0097
			15:03:52	0.17868	0.0096
			15:06:02	0.18333	0.0094
2	15:15	0.173953	15:14:12	0.18864	0.0095
			15:16:29	0.18516	0.0095
			15:17:35	0.19110	0.0095

2	15:30	0.183956	15:28:40	0.19605	0.0096
			15:29:46	0.19276	0.0094
			15:32:12	0.19745	0.0095
2	15:45	0.182665	15:29:46	0.19276	0.0094
			15:32:12	0.19745	0.0095
			16:05:03	0.19483	0.0095
2	16:00	0.181365	16:05:03	0.19483	0.0095
			16:08:09	0.19673	0.0094
			16:09:14	0.19542	0.0095
2	16:15	0.183677	16:14:19	0.19177	0.0094
			16:16:48	0.19914	0.0095
			16:19:11	0.19793	0.0096
2	16:30	0.183041	16:29:05	0.20147	0.0095
			16:30:11	0.19946	0.0094
			16:31:17	0.20029	0.0094
2	16:45	0.183306	16:44:28	0.20149	0.0095
			16:45:34	0.20111	0.0095
			16:46:40	0.20227	0.0095
2	17:00	0.192209	16:59:54	0.21336	0.0095
			17:01:00	0.20995	0.0095
			17:02:06	0.21265	0.0095
2	17:15	0.230232	17:14:11	0.21354	0.0096
			17:15:18	0.21778	0.0096
			17:16:23	0.21498	0.0095
2	17:30	0.205829	17:29:35	0.21927	0.0096
			17:30:41	0.21802	0.0096
			17:31:47	0.21787	0.0097
3	10:00	0.247776	-	-	-
3	10:30	0.206119	10:29:15	0.20615	0.0091
			10:34:57	0.20411	0.0092
			10:36:03	0.20366	0.0092
3	11:00	0.183217	10:59:11	0.18459	0.0096
			11:00:17	0.18235	0.0096
			11:01:23	0.18229	0.0096
3	11:30	0.187808	11:28:54	0.19849	0.0097
			11:30:01	0.19658	0.0096
			11:31:07	0.19567	0.0096
3	12:00	0.201553	11:59:45	0.20372	0.0097
			12:00:51	0.20589	0.0097
			12:01:57	0.20328	0.0097
3	12:30	0.191495	12:29:34	0.19989	0.0097

			12:30:40	0.20076	0.0097
			12:31:46	0.20254	0.0098
3	13:00	0.199085	12:59:19	0.20041	0.0097
			13:00:26	0.20094	0.0098
			13:01:32	0.20461	0.0097
3	13:30	0.197129	13:29:07	0.19943	0.0097
			13:30:13	0.19982	0.0097
			13:31:20	0.20003	0.0098
3	14:00	0.20011	13:58:54	0.19782	0.0098
			14:00:00	0.20080	0.0098
			14:01:06	0.19886	0.0098
3	14:30	0.201948	14:29:18	0.21019	0.0095
			14:30:25	0.20743	0.0096
			14:31:36	0.21693	0.0096
3	15:00	0.16243	14:59:27	0.18507	0.0098
			15:00:33	0.18822	0.0098
			15:01:39	0.18765	0.0097
3	15:30	0.189119	15:29:14	0.19547	0.0097
			15:30:20	0.20075	0.0097
			15:31:26	0.19918	0.0098
3	16:00	0.181443	15:59:00	0.19867	0.0098
			16:00:06	0.19880	0.0097
			16:01:12	0.19628	0.0098
3	16:30	0.18593	16:29:58	0.20130	0.0097
			16:31:09	0.19755	0.0097
			16:34:49	0.19733	0.0097

—

usn.no